ISSN: 0009-7411

CIRUGÍA Y CIRUJANOS

ÓRGANO DE DIFUSIÓN CIENTÍFICA DE LA ACADEMIA MEXICANA DE CIRUGÍA

FUNDADA EN 1933

Contenido

Artículos originales

PERMANYER MÉXICO
www.permanyer.com

Volumen 92, No. 5, Septiembre-Octubre 2024

Indexada en WoS Core Collection/SCIETM; MEDLINE/PubMed

10109AMEX245

ARTÍCULO ORIGINAL

Evolución clínica de los pacientes con infección asociada a dispositivos ortopédicos en tratamiento con presión negativa continua

Clinical evolution of patients with infection associated with orthopedic devices in treatment with continuous negative pressure

Jorge Quiroz-Williams[1], José R. Viveros-Encarnación[1], Suemmy Gaytán-Fernández[1], Rodolfo G. Barragán-Hervella[1], Carlos R. Rueda-Alvarado[1], América Ramírez-Polanco[1], M. Paloma Martínez-Senda[2] y Andrea M. Palma-Jaimes[2]*

[1]Unidad Médica de Alta Especialidad, Hospital de Traumatología y Ortopedia Manuel Ávila Camacho, Instituto Mexicano del Seguro Social; [2]Facultad de Medicina, Universidad Popular Autónoma del Estado de Puebla. Puebla, Puebla, México

Resumen

Objetivo: *Describir el uso de la terapia de presión negativa con (TPNi) y sin instilación (TPNs) como tratamiento adyuvante en el manejo de infecciones asociadas a dispositivo ortopédico (IADO).* **Método:** *Estudio observacional analítico de expedientes de pacientes con IADO manejados con TPNi y TPNs con solución salina al 0.9%, mayores de 18 años, operados en el periodo 2018-2021. Se evaluaron las características clínicas de infección, el agente infeccioso y las variables sociodemográficas. La TPN se realizó con sistema V.A.C.VERAFLO™. Para los análisis se emplearon las pruebas χ^2, Fisher y t de Student. Valor estadísticamente aceptado: p < 0.05.* **Resultados:** *La muestra fue de 40 pacientes, el 75% masculinos. Fracturas: 42.5% expuestas y 57.5% cerradas. En el 92.5% se aplicó antibiótico profiláctico (30-120 min). Implantes: 35% placas, 12.5% clavo centromedular, 10% prótesis de rodilla y 12.5% cadera. El 47.5% con sangrado < 500 ml. En el 72.5% un tiempo quirúrgico de 2-4 horas. Tiempo de hospitalización previa: TPNs 3 semanas 55.9% y 4 semanas 26.5%; TPNi 3 semanas 50% y 4 semanas 33.3%. Conservación del implante: 73.5% TPNs y 50% TPNi (p = 0.341). Cierre de herida: 91.2% con TPNs y 100% con TPNi (p = 1.000).* **Conclusiones:** *El uso de TPNs y TPNi fue útil como tratamiento adyuvante en IADO, y además permitieron conservar el implante y el cierre de la herida en la mayoría de los pacientes.*

Palabras clave: *Fijación interna. Infecciones periprotésicas. Complicaciones posquirúrgicas. Implantes ortopédicos.*

Abstract

Objective: *To describe the use of negative pressure therapy with (TPNi) and without instillation (TPNs) as adjuvant treatment in the management of orthopedic device-associated infections (IADO).* **Method:** *Analytic observational study of records of patients with IADO managed with TPNi and TPNs with 0.9% saline solution, in patients > 18 years, operated on in 2018-2021. Clinical characteristics of infection, infectious agent as well as sociodemographic variables were evaluated. TPN was performed with the V.A.C. VERAFLO™ system. Analysis with χ^2, Fisher and t-Student. Statistically accepted value p < 0.05.* **Results:** *Sample 40 patients. 75% male. Fractures 42.5% exposed and 57.5% closed. 92.5% applied prophylactic antibiotic (30-120 min). 35% plate implants, 12.5% centromedullary nail, 10% knee prosthesis and 12.5% hip. 47.5% bleeding < 500 ml. 72.5% surgical*

***Correspondencia:**
Rodolfo G. Barragán-Herevella
E-mail: rodolfo68@icloud.com;
rodolfobarraganh@gmail.com

Fecha de recepción: 08-05-2023
Fecha de aceptación: 14-07-2023
DOI: 10.24875/CIRU.23000248

Cir Cir. 2024;92(5):559-566
Contents available at PubMed
www.cirugiaycirujanos.com

time of 2-4 hours. Previous hospitalization time, TPNs 3 weeks 55.9% and 4 weeks 26.5%; TPNi, 3 weeks 50% and 4 weeks 33.3%. Conservation of the implant 73.5% TPNs and 50% TPNi (p = 0.341). Wound closure 91.2% with TPNs and 100% with TPNi (p = 1.000). **Conclusions:** *The use of TPNs and TPNi were useful as adjuvant treatments in the management of IADO, in addition they allowed to preserve the implant and wound closure in a large part of the patients.*

Keywords: *Orthopedic fixation devices. Prothesis-related infections. Postoperative complications. Orthopedic equipment.*

Introducción

Las infecciones asociadas a la atención en salud son consideradas como un problema de salud pública, tanto en los países desarrollados como en aquellos en vías de desarrollo. Las infecciones del sitio quirúrgico, entre ellas las asociadas a dispositivos ortopédicos (IADO)[1,2], se incluyen en las infecciones asociadas a la atención en salud. Las IADO son poco frecuentes, pero cuando se presentan lo hacen de manera grave, con evolución tórpida y ocasionando discapacidad prolongada, alto costo de atención y pérdida de bienestar. Las IADO pueden tener diversas causas, pero la principal es la contaminación durante el acto quirúrgico[3-7]. También depende del daño causado en las partes blandas, sobre todo en la cirugía traumática ortopédica[5,8,9].

La incidencia de IADO varia de país en país, así como según el procedimiento quirúrgico realizado. Argüelles Martínez et al.[4] encuentran en su estudio que la infección periprotésica más frecuente fue la de rodilla. Carvajal y Londoño[10] hallaron que las infecciones del sitio quirúrgico secundarias a implantes ortopédicos tenían frecuencias más elevadas en cirugías de rótula, tibia y peroné, pero más bajas en cirugía de antebrazo y reemplazos articulares.

En general, el tratamiento de las IADO consiste en un aseo y un desbridamiento enérgico. Desde hace más de 30 años se realiza la terapia con presión subatmosférica como adyuvante en el tratamiento de las infecciones de heridas, así como de infecciones profundas[8,11-14]. La terapia con presión negativa (TPN) tiene dos modalidades: con presión permanente o intermitente[14,15].

La TPN no es la panacea del tratamiento en las infecciones de heridas tanto profundas como superficiales. Su éxito depende del seguimiento y del cuidado de la infección, del tiempo de uso y del manejo aunado con un tratamiento enérgico quirúrgico con lavados seriados y antibioticoterapia[12,16,17].

El éxito en el tratamiento de las infecciones del sitio quirúrgico en cirugía ortopédica se observa en aquellas en las que se coloca material de osteosíntesis o reemplazo articular. Con la introducción de la TPN, en diversos estudios se observa el éxito, ya que más del 43% de los casos conservan el implante y la erradicación de la infección arriba al 76-83% cuando se combina con una instilación a permanencia[18,19].

Debido a que con el uso de la TPN con instilación (TPNi) con antiséptico a permanencia los tiempos de tratamiento son menores que en los pacientes que solo se manejan con lavado quirúrgico y antibiótico sistémico, disminuyendo tanto costos como insumos, el objetivo de este estudio fue describir el uso de la TPN con y sin instilación como tratamiento adyuvante en el manejo de infecciones asociadas a implante ortopédico, además de describir la experiencia del hospital en el manejo de esta terapia, la evolución clínica y la caracterización microbiológica de los pacientes con este tipo de infección.

Método

Se realizó un estudio observacional analítico, transversal y retrospectivo en pacientes con IADO a quienes se agregó al tratamiento el uso de TPNi y de TPN sin instilación (TPNs) con solución salina. Este estudio, previo a su realización, fue sometido a revisión y autorización por los comités de investigación en salud y ética en investigación en salud, con el número de registro R-2019-2105-046.

La técnica de muestreo fue no probabilística a criterio del investigador, pero no se realizó una determinación del tamaño de muestra ya que se consideraron todos los pacientes que cumplieran los criterios de inclusión en el periodo de enero de 2018 a mayo de 2021. Se incluyeron pacientes mayores de 18 años que presentaron infección de herida quirúrgica y recibieron TPN como adyuvante para el tratamiento de IADO, sin distinción de sexo, y que contaran con expediente clínico completo. Se excluyeron los pacientes con expediente clínico incompleto y los que no recibieron TPN como tratamiento adyuvante. Se eliminaron los pacientes que abandonaron la TPN antes de la curación del cuadro clínico y aquellos a los que la TPN no se les aplicó de manera adecuada.

Los datos fueron recabados de la base de datos de los servicios clínicos del hospital, donde se identifican aquellos que presentaron infección de herida quirúrgica. Las variables que se recabaron de los expedientes clínicos fueron edad, sexo, comorbilidad, tabaquismo e índice de masa corporal (IMC), así como también signos clínicos (fiebre, fístula, induración y enrojecimiento de la herida) y valores de laboratorio indicativos de infección (conteo de leucocitos, hemoglobina, hematocrito, proteína C reactiva [PCR], velocidad de sedimentación globular y proteínas), antecedentes de manejo previo (fractura expuesta, implante colocado, antibiótico profiláctico en la cirugía inicial, sangrado transquirúrgico y tipo de procedimiento), tiempo de cirugía inicial, tiempo de evolución de la infección y datos bacteriológicos (agente etiológico, resistencia antibiótica, sensibilidad antibiótica). Las fracturas expuestas fueron categorizadas de acuerdo con la clasificación de Gustillo-Anderson.

La decisión de colocar TPNi fue a criterio del cirujano. Los procedimientos quirúrgicos fueron realizados por los médicos adscritos con experiencia en el manejo de infecciones óseas, los cuales contaban con capacitación previa en la colocación del sistema de presión negativa.

A todos los pacientes se les realizó, antes de colocar la TPN, un desbridamiento quirúrgico agresivo, y predominantemente se buscó la conservación del implante, siempre y cuando no se observara aflojamiento de este. Una vez preparado el lecho de la herida, se colocaba una esponja de poliuretano reticulada de celdas abiertas (V.A.C.® GranuFoam™). Para la oclusión de la herida se utilizó un recubrimiento adhesivo acrílico, el cual se conecta al tubo de succión del sistema V.A.C. VERAFLO™. La instilación se llevó a cabo con solución salina al 0.9% con un tiempo de instilación de 3 horas, 30 minutos de succión y 15 minutos de retención de instilación. La succión se establece a una presión continua de 125 mmHg.

El recambio de la TPN se realizó cada 7 días, con cambio de esponja y contenedor. En cada cambio de esponja se tomaba cultivo del lecho de la herida. El criterio para el retiro definitivo de la TPN fue tener dos cultivos negativos, así como presencia de tejido de granulación y ausencia de exudado purulento.

En el análisis estadístico se expresaron las variables cualitativas en frecuencias y porcentajes, mientras que las variables numéricas se expresaron en media y desviación estándar (DE). En el análisis inferencial se utilizaron la prueba χ^2 para la asociación de variables politómicas y la prueba exacta de Fisher para variables dicotómicas. Para la asociación de variables cuantitativas se utilizó la prueba t de Student. Se tomó como estadísticamente significativo un valor de $p < 0.05$.

Tabla 1. Variables sociodemográficas (n = 40)

Variables	n (%)
Sexo	
Masculino	30 (75)
Femenino	10 (25)
Peso	
Bajo peso	5 (12.5)
Peso normal	12 (30)
Sobrepeso	20 (50)
Obesidad grado I	3 (7.5)
Comorbilidad	
Diabetes *mellitus*	12 (30)
Hipertensión arterial sistémica	6 (15)
Ninguna	22 (55)

Tabla 2. Diagnósticos ortopédicos (n = 40)

Diagnósticos	n (%)
Fractura expuesta	
IIIA	4 (10)
IIIB	9 (22.5)
IIIC	4 (10)
Fractura cerrada	23 (57.5)
Gonartrosis	2 (5)
Coxartrosis	4 (10)

Resultados

En el periodo de estudio presentaron fracturas 2033 pacientes, y se realizó reemplazo articular de cadera o rodilla a 1503 pacientes, de los cuales solo se identifican 60 con IADO que usaron la TPN como tratamiento adyuvante, pero hubo que eliminar a 20 ya que no se les aplicó de manera adecuada la TPN, quedando una muestra de 40 pacientes. De la muestra final, el 75% fueron de sexo masculino. La media de edad fue de 43.2 años (DE: 16.8; rango: 19-76). El 55% no presentaban comorbilidad. Presentaron sobrepeso el 50%, peso normal el 30% y bajo peso el 12.5% (Tabla 1); el IMC tuvo una media de 25 (DE: 0.8; rango: 10-40). Entre los diagnósticos ortopédicos, el 42.5% de la muestra presentaron fractura expuesta (Gustilo y Anderson) y el 57.5% cerrada. El 11.8% tenían padecimientos crónicos degenerativos (Tabla 2).

Tabla 3. Antecedentes quirúrgicos en los pacientes con infecciones asociadas a dispositivo ortopédico (n = 40)

Antecedentes	n (%)
Riesgo quirúrgico	
ASA II	33 (82.5)
ASA III	7 (17.5)
Tiempo de profilaxis antibiótica	
30-120 min	37 (92.5)
> 120 min	3 (7.5)
Antibiótico profiláctico	
Cefalexina	21 (52.5)
Cefalotina	9 (22.5)
Ceftriaxona	10 (25)
Implante ortopédico	
Placa	14 (35)
Clavo centromedular	5 (12.5)
Osteosíntesis mínima	5 (12.5)
Prótesis de rodilla	4 (10)
Prótesis de cadera	5 (12.5)
Tornillos pediculares	2 (5)
Sangrado quirúrgico	
< 500 ml	19 (47.5)
500-999 ml	20 (50)
1000-1400 ml	1 (2.5)
Tiempo quirúrgico	
< 2 h	10 (25)
2-4 h	29 (72.5)
> 4 h	1 (2.5)

Tabla 4. Signos clínicos, valores de laboratorio y hallazgos radiológicos iniciales en los pacientes con infecciones asociadas a dispositivo ortopédico (n = 40)

Variables	n (%)
Tiempo de inicio de la infección	
< 3 meses	29 (72.5)
3-24 meses	7 (17.5)
> 24 meses	4 (10)
Induración	
Sí	33 (82.5)
No	7 (17.5)
Temperatura	
< 37°C	14 (35)
37-37.9°C	9 (22.5)
38-38.5°C	16 (40)
> 38.5°C	1 (2.5)
Enrojecimiento	
Sí	38 (95)
No	2 (5)
Fístula	
Sí	10 (25)
No	30 (75)
Radiografías	
Sin signos radiográficos	32 (80)
Interfase segmento-hueso	3 (7.5)
Osteólisis	5 (12.5)
Proteína C reactiva	
5-10 mg/dl	14 (35)
11-20 mg/dl	24 (60)
21-50 mg/dl	2 (5)
Proteínas totales	
Alteradas	23 (57.5)
Sin alteración	17 (42.5)

Al describir los antecedentes de manejo quirúrgico en los pacientes que presentaron IADO, en cuanto al riesgo quirúrgico de acuerdo con la clasificación ASA (American Society of Anesthesiologists) se encontró que el 92.5% eran ASA II y el 17.5% eran ASA III. El tiempo de administración del antibiótico profiláctico fue de 30 a 120 minutos previos al evento quirúrgico en el 92.5%. El antibiótico más frecuentemente administrado fue cefalexina (52.5%). Los implantes ortopédicos más usados fueron placa (35%), clavo centromedular (12.5%) y osteosíntesis mínima (12.5%). Se reportó sangrado quirúrgico < 500 ml en el 47.5% y > 500 ml en el 50%. El tiempo quirúrgico fue < 2 horas en el 25%, de 2 a 4 horas en el 72.5% y > 4 horas en el 2.5% (Tabla 3).

En cuanto a los signos clínicos de los pacientes con IADO, se encontraron induración (17.5%), enrojecimiento (95%), fístula (25%) y fiebre (42.5%). El tiempo de inicio de la infección fue < 3 meses en el 72.5%, de 3 a 24 meses en el 17.5% y más de 24 meses en el 10% (Tabla 4).

Entre los valores de laboratorio iniciales se encontró que la PCR estaba en valores de 5 a 10 mg/dl en el 35%, de 11 a 20 mg/dl en el 60% y de 21 a 50 mg/dl en el 5%. Las cifras de proteínas totales estaban alteradas en el 57.5% de los pacientes (Tabla 4).

En las radiografías iniciales se observaron interfase segmento-hueso en el 7.5% y osteólisis en el 12.5% (Tabla 4).

En cuanto al tiempo de hospitalización previa al uso de TPN y el tipo de esta, para la TPNs fue 1 semana en el 2.9%, 2 semanas en el 5.9%, 3 semanas en el 14.7%, 4 semanas en el 41.2%, 5 semanas en el 20.6%, 6 semanas en el 8.8% y 7 semanas en el 5.9%; para la TPNi fue 4 semanas en el 50%, 5 semanas en el 33.3% y 6 semanas en el 16.7% (p = 0.864) (Tabla 5).

En cuanto a la TPN utilizada, en el 85% fue TPNs y en el 15% fue TPNi. Y en relación al tiempo de uso, para la TPNs, el 14.7% la usó 2 semanas, el 55.9% 3 semanas, el 26.5% 4 semanas y el 2.9% 5 semanas; para la TPNi, el 16.7% la usó 2 semanas, el 50%

Tabla 5. Asociación de tipo de terapia de presión negativa con tiempo de uso, la conservación del implante, el cierre de la herida y el tiempo de hospitalización (n = 40)

	TPNs n = 34 (85%) n (%)	TPNi n = 6 (15%) n (%)	Total n (%)	Significancia*
Tiempo de uso				
2 sem	5 (14.7)	1 (16.7)	6 (15)	
3 sem	19 (55.9)	3 (50)	22 (55)	0.958
4 sem	9 (26.5)	2 (33.3)	11 (27.5)	
5 sem	1 (2.9)	0	1 (2.5)	
Conservación del implante ortopédico				
Sí	25 (73.5)	3 (50)	28 (70)	0.341
No	9 (26.5)	3 (50)	12 (30)	
Cierre de la herida				
Sí	31 (91.2)	6 (100)	37 (92.5)	1.000
No	3 (8.8)	0	3 (7.5)	
Tiempo de hospitalización previa				
1 sem	1 (2.9)	0	1 (2.5)	
2 sem	2 (5.9)	0	2 (5)	
3 sem	5 (14.7)	0	5 (12.5)	0.864
4 sem	14 (41.2)	3 (50)	17 (42.5)	
5 sem	7 (20.6)	2 (33.3)	9 (22.5)	
6 sem	3 (8.8)	1 (16.7)	4 (10)	
7 sem	2 (5.9)	0	2 (5)	

*$p < 0.05$.
TPNi: terapia de presión negativa con instilación; TPNs: terapia de presión negativa sin instilación.

3 semanas y el 33.3% 4 semanas. La conservación del implante se observó en el 73.5% con TPNs y el 50% con TPNi, mientras que hubo que retirar el implante en el 26.5% con TPNs y el 50% con TPNi (p = 0.341). Se realizó cierre de la herida en el 91.2% con TPNs y el 100% con TPNi (p = 1.000) (Tabla 5).

Al asociarse los valores de laboratorio iniciales y finales con el tipo de TPN, con la TPNs la hemoglobina inicial tuvo una media de 11.35 ± 3.4 mg/dl y con TPNi de 9.2 ± 1.9 mg/dl (p = 0.042), y la final tuvo una media de 13.1 ± 1.4 mg/dl con TNPs y de 12.3 ± 1.5 mg/dl con TPNi (p = 0.251). El conteo de leucocitos inicial fue de 13,097 ± 4641.7 por campo con TPNs y de 13,133.3 ± 4195.6 por campo con TPNi (p = 0.985), y el final fue de 7758.8 ± 1578.6 por campo con TPNs y de 7966.7 ± 242.2 por campo con TPNi (p = 0.475). La PCR inicial fue de 2.7 ± 0.6 con TPNs y de 2.7 ± 0.5 con TPNi, y la final fue de 1.1 ± 0.4 con TPNs y 1.2 ± 0.4 con TPNi (p = 0.915). Las proteínas totales iniciales fueron de 5.9 ± 0.9 con TPNs y de 6.3 ± 1.0 con TPNi (p = 0.366), y las finales fueron de 6.5 ± 0.7 con TPNs y de 6.2 ± 0.4 con TPNi (p = 0.258) (Tabla 6).

Discusión

Las IADO son un reto para el cirujano ortopedista; los costos relacionados con su tratamiento son seis a siete veces más en comparación con los procedimientos no infectados[20]. En la presente investigación se observó que el uso de TPN en IADO permite la conservación del implante ortopédico en un gran porcentaje de pacientes. La mayoría de los autores que han utilizado la TPN para el tratamiento de IADO, en un gran porcentaje (75-85%) retienen el implante ortopédico[16,17,21,22]. En contraste con la literatura, el porcentaje de conservación del implante en esta investigación fue similar a lo reportado, pero solo con TPNs (73.5%), mientras que de los pacientes que se trataron con TPNi solo la mitad conservaron el implante, pero sin significancia estadística, posiblemente por la heterogeneidad de los grupos. Webb[23] argumenta que el uso de TPNi presenta resultados favorables, pero faltan estudios de calidad para garantizar la eficacia de esta terapia. West et al.[24] refieren que la instilación puede erradicar la infección en sitios quirúrgicos con alto riesgo de infección, facilitando la conservación del implante, pero podría presentar daño a largo plazo de los tejidos debido a la toxicidad de la solución de instilación utilizada. En la presente investigación, la instilación solo se realizó con solución salina para evitar toxicidad en los tejidos circundantes.

El uso de TPNs y TPNi debe ser como tratamiento adyuvante, por periodos limitados y en pacientes

Tabla 6. Valores de laboratorio iniciales y finales de los pacientes con infecciones asociadas a dispositivo ortopédico tratados con terapia de presión negativa (n = 40)

Parámetros	TPNs	TPNi	Significancia*
Hemoglobina inicial	11.35 ± 3.4	9.2 ± 1.9	0.042
Hemoglobina final	13.1 ± 1.4	12.3 ± 1.5	0.251
Leucocitos iniciales	13,097.1 ± 4641.7	13,133.3 ± 4195.6	0.985
Leucocitos finales	7758.8 ± 1578.6	7966.7 ± 242.2	0.475
Proteína C reactiva inicial	2.7 ± 0.6	2.7 ± 0.5	0.871
Proteína C reactiva final	1.1 ± 0.4	1.2 ± 0.4	0.915
Proteínas totales iniciales	5.9 ± 0.9	6.3 ± 1.0	0.366
Proteínas totales finales	6.5 ± 0.7	6.2 ± 0.4	0.258

*p < 0.05.
TPNi: terapia de presión negativa con instilación; TPNs: terapia de presión negativa sin instilación.

cuidadosamente seleccionados[11,12]. En esta investigación, la TPN se aplicó a los pacientes que presentaron persistencia de la IADO posterior a un tratamiento inicial y que no presentaban mejoría clínica. El tiempo de hospitalización de los pacientes varió dependiendo de los factores asociados encontrados. Cabe señalar que en la población a la cual se aplicó tanto TPNs como TPNi presentaba en un gran porcentaje una estancia hospitalaria > 4 semanas antes de la aplicación de la TPN. Este tipo de terapias han mostrado su efectividad para el manejo de las infecciones profundas[13]. Falci et al.[25] identifican como variables potenciales de contaminación de la herida quirúrgica las condiciones clínicas de los pacientes (ASA), el tipo de procedimiento quirúrgico y la duración de la cirugía. Ángeles-Garay et al.[9] reportan como factores de riesgo de desarrollo de infección del sitio quirúrgico el índice tabáquico, el bajo peso, una técnica inadecuada de lavado de manos, la transfusión sanguínea durante la cirugía, la cirugía contaminada, la estancia hospitalaria de 8 a 14 días, la permanencia con venoclisis de 1 a 3 días y la permanencia con sonda vesical de 1 a 3 días. Este estudio no tenía como objetivo principal estudiar los factores de riesgo para el desarrollo de IADO, pero como comorbilidad la mitad de los pacientes estudiados presentaban diabetes *mellitus* o hipertensión arterial sistémica; y la mayor parte de los pacientes presentaban peso normal o sobrepeso, mientras que unos bajos porcentajes tenían obesidad o bajo peso. Más de la mitad de los pacientes presentaron una fractura cerrada y en menor proporción una fractura expuesta (Gustillo-Anderson III). En cuanto al riesgo quirúrgico, el 82.5% de los pacientes fueron ASA II. El tiempo quirúrgico en la cirugía primaria fue de 2 a 4 horas en el 72.5%, y en más de la mitad el sangrado transquirúrgico fue < 1000 ml.

Respecto a los valores de laboratorio de control posterior a la aplicación de TPNs e TPNi, mostraron una importante reducción el conteo de leucocitos (p = 0.475), la PCR (p = 0.915) y las proteínas totales (p = 0.258).

Izadpanah et al.[17] establecen que los factores que contribuyen al fracaso de la TPN en pacientes con infecciones posquirúrgicas tras una osteosíntesis son las manifestaciones tardías de infección (> 4 semanas), así como una mezcla bacteriana y una lesión importante de tejidos blandos, además de unos valores altos de PCR (> 20 mg/l). En la investigación se mostraron solo los valores de laboratorio al final de la TPN, en los que sí se observó una disminución de la PCR, pero no fue significativa, posiblemente por el tamaño de la muestra de pacientes.

La fortaleza de este estudio es la comparación de dos técnicas de TPN, y además se demostró la efectividad de estas terapias como adyuvantes del tratamiento de IADO, permitiendo la conservación del implante en un gran porcentaje de pacientes. Las debilidades del estudio son la heterogeneidad entre los grupos y la escasa cantidad de pacientes estudiados, motivo por el cual los valores estadísticos no fueron significativos. Además, a los pacientes no se

les dio seguimiento, pero se contempla para un estudio futuro, así como realizar un estudio de costos y con una cantidad mayor de pacientes, con un seguimiento a 12 meses. También es importante señalar que esta terapia se administró posterior a haber realizado un manejo con desbridamiento quirúrgico y antibioticoterapia, por lo que no se realiza un contraste en la reducción de tiempos de estancia hospitalaria, sugiriendo el uso de la TPN desde un inicio para el manejo de IADO sin comparar con pacientes manejados sin TPN.

Conclusiones

El uso de TPNs y TPNi fue útil como tratamiento adyuvante en el manejo de la IADO, y además permitieron conservar el implante ortopédico y el cierre de la herida quirúrgica de manera definitiva en una gran parte de los pacientes. En este estudio no hubo una diferencia significativa en los resultados al comparar ambas técnicas de TPN. La elección de TPNs y TPNi se deja a consideración del cirujano. Se requiere realizar más ensayos clínicos aleatorizados, con una mayor cantidad de pacientes y con un seguimiento más largo, además de aplicar la TPN en un inicio del tratamiento, para demostrar la efectividad en la erradicación de IADO y así poder demostrar qué técnica de TPN es mejor.

Agradecimientos

Los autores agradecen a los servicios clínicos de extremidades y columna y cadera de la Unidad Médica de Alta Especialidad Hospital de Traumatología y Ortopedia Manuel Ávila Camacho por su apoyo.

Financiamiento

Los autores declaran no haber recibido financiamiento para este estudio.

Conflicto de intereses

Los autores declaran no tener conflicto de intereses.

Responsabilidades éticas

Protección de personas y animales. Los autores declaran que para esta investigación no se han realizado experimentos en seres humanos ni en animales.

Confidencialidad de los datos. Los autores declaran que han seguido los protocolos de su centro de trabajo sobre la publicación de datos de pacientes.

Derecho a la privacidad y consentimiento informado. Los autores han obtenido la aprobación del Comité de Ética para el análisis y publicación de datos clínicos obtenidos de forma rutinaria. El consentimiento informado de los pacientes no fue requerido por tratarse de un estudio observacional retrospectivo.

Uso de inteligencia artificial para generar textos. Los autores declaran que no han utilizado ningún tipo de inteligencia artificial generativa en la redacción de este manuscrito ni para la creación de figuras, gráficos, tablas o sus correspondientes pies o leyendas.

Bibliografía

1. Berriós-Torres SI, Umscheid CA, Bratzler DW, Leas B, Stone EC, Kelz RR, et al. Centers for disease control and prevention guideline for the prevention of surgical site infection. JAMA Surg. 2017;152:784-91.
2. Ducel G, Fabry J, Nicolle L, Girard R, Perraud M, Prüss A, et al. Guía práctica. Prevención de las infecciones nosocomiales. WHO/CDS/CSR/EPH; 2009.
3. Instituto Mexicano del Seguro Social. Diagnóstico y tratamiento de las infecciones asociadas a dispositivos ortopédicos, prótesis y/o material de osteosíntesis. 2013. Disponible en: http://www.imss.gob.mx/profesionales/guiasclinicas/Pages/guias.aspx.
4. Argüelles-Martínez O, Rivera-Villa A, Miguel-Pérez A, Torres-González R, Pérez-Atanasio JM, Mata-Huerta A, et al. Agentes etiológicos más frecuentes en infecciones periprotésicas de artroplastia primaria de rodilla y cadera en adultos mayores. Acta Ortop Mex. 2016;30:116-8.
5. García-Aldeco M, Martínez-Hernández A, González-Gámez M. Infección asociada a implantes ortopédicos. Lux Médica. 2019;41:59-66.
6. Suárez-Ahedo C, Obil-Chavarría C, Gil-Orbezo F, García-Felix Díaz G. Prevención de infecciones en el perioperatorio de la artroplastia primaria de cadera y rodilla. Acta Ortop Mex. 2011;25:4-11.
7. Muñoz-Mahamud E, García S, Bori G, Martínez-Pastor JC, Zumbado JA, Riba J, et al. Comparison of a low-pressure and a high-pressure pulsatile lavage during debridement for orthopaedic implant infection. Arch Orthop Trauma Surg. 2011;131:1233-8.
8. Nam D, Sershon RA, Levine BR, Della Valle CJ. The use of closed incision negative-pressure wound therapy in orthopaedic surgery. J. Am Acad Orthop Surg. 2018;26:295-302.
9. Ángeles-Garay U, Morales-Márquez LI, Sandoval-Balanzarios MA, Velázquez-García JA, Méndez-Cano AF. Factores de riesgo relacionados con infección del sitio quirúrgico en cirugía electiva. Cir Cir. 2014;82:48-62.
10. Carvajal R, Londoño A. Factores de riesgo e infección del sitio quirúrgico en procedimientos de cirugía ortopédica con prótesis. Rev Chil Infectol. 2012;29:395-400.
11. Robert N. Negative pressure wound therapy in orthopaedic surgery. Orthop Traumatol Surg Res. 2017;103(1S):S99-103.
12. Cid N, García Ruano F, Athenea Luanco Gracia A, Jiménez Martín M, Sicre González A. Terapia por presión negativa en el manejo de heridas complejas en traumatología. Innovación e indicación. Rev S And Traum y Ort. 2014;31:17-23.
13. Aceves-Pérez A, Medina-Romero P, Ávila-Jiménez MJ. Terapia de presión negativa como alternativa en el manejo de la infección en cirugía de columna. Columna. 2013;12:330-3.
14. Kurra S, Rashid A, Yirenkyi H, Castle P, Lavelle WF. Outcomes of negative pressure wound therapies in the management of spine surgical site wound infections. Int J Spine Surg. 2020;14:772-7.
15. Kelm J, Schmitt E, Anagnostakos K. Vacuum-assisted closure in the treatment of early hip joint infections. Int J Med Sci. 2009;6:241-6.
16. Lehner B, Fleischmann W, Becker R, Jukema GN. First experiences with negative pressure wound therapy and instillation in the treatment of infected orthopaedic implants: a clinical observational study. Int Orthop. 2011;35:1415-20.
17. Izadpanah K, Hansen S, Six-Merker J, Helwig P, Südkamp NP, Schmal H. Factors influencing treatment success of negative pressure wound therapy in patients with postoperative infections after osteosynthetic fracture fixation. BMC Musculoskelet Disord. 2017;18:247.

18. Beckmann NA, Hanslmeier MG, Omlor GW, Feisst M, Maier MW, Lehner B. Is negative pressure wound therapy with instillation suitable for the treatment of acute periprosthetic hip joint infection? J Clin Med. 2021;10:3246.
19. Ene R, Panti Z, Albu E, Ene P, Cirstoiu MM, Cirstoiu FC. Negative pressure, a "solution" in the treatment of infected knee prosthesis? Maedica (Bucur). 2015;10:5-9.
20. Depypere M, Kuehl R, Metsemakers WJ, Senneville E, McNally MA, Obremskey WT, et al. Recommendations for systemic antimicrobial therapy in fracture-related infection: a consensus from an international expert group. J Orthop Trauma. 2020;34:30-41.
21. Chang CW, Chan HZ, Lim SW, Khoo E, Zulkiflee O. Negative pressure wound therapy in infected wound following posterior spinal instrumentation using simple self-assembled system: a case report. Malays Orthop J. 2014;8:49-51.
22. Pelham FR, Kubiak EN, Sathappan SS, Di Cesare PE. Topical negative pressure in the treatment of infected wounds with exposed orthopaedic implants. J Wound Care. 2006;15:111-6.
23. Webb LX. The impact of negative pressure wound therapy on orthopaedic infection. Orthop Clin North Am. 2017;48:167-79.
24. West JM, Jordan SW, Mendel E, Khan SN, Chandawarkar RY, Valerio IL. Instillation negative pressure wound therapy: an effective tool for complex spine wounds. Adv Wound Care (New Rochelle). 2018;7: 333-8.
25. Falci Ercole F, Castro Franco LM, Rezende Macieira TG, Crespo Wenceslau LC, Nascimento de Resende HI, Machado Chianca TC. Riesgo para infección de sitio quirúrgico en pacientes sometidos a cirugías ortopédicas. Rev Latino-Am Enfermagem. 2011;19: 1-8.

ORIGINAL ARTICLE

Role of contrast agent in evaluation of periprostatic invasion in prostate cancer

Papel del agente de contraste en la evaluación de la invasión periprostática en el cáncer de próstata

Hüseyin A. Kızıloğlu[1], Murat Beyhan[1], Erkan Gökçe[1], Yaşar Birişik[1], Çiğdem S. Salbaş[2], and Mustafa Yeşilyurt[3]*

[1]Department of Radiology, Tokat Gaziosmanpaşa University Faculty of Medicine, Tokat; [2]Department of Radiology, Bandırma Training and Research Hospital, Balıkesir; [3]Department of Radiology, Erzurum Training and Research Hospital, Erzurum. Türkiye

Abstract

Objective: *Our study aims to demonstrate the detection of invasion by biparametric prostate MRI (bpMRI).* **Materials and methods:** *The cases whose histopathological diagnosis was prostate cancer (PCa) and whose mpMRI report was reported as PIRADS 4 and 5 were evaluated retrospectively by two radiologists with different prostate imaging experiences. The images were grouped into two data sets. Dataset-1 was bpMRI, and dataset-2 was mpMRI. Two radiologists first evaluated dataset-1 independently of each other, and 1 month later, dataset-2. They recorded whether there was an invasion and where it was seen in the patients. Then, the results were compared.* **Results:** *A total of 75 patients were included in the study. Periprostatic invasion was detected in 33 of the patients. Both the 1st reader and the 2nd reader image detected all the cases with invasion (100%) separately between dataset-1 and set-2. Compatibility for image dataset-1 and dataset-2 between both readers was observed to be excellent.* **Conclusions:** *There is no need to use contrast agent to evaluate periprostatic invasion and to have an idea about local staging in PCa patients.*

Keywords: *Periprostatic invasion. Contrast agent. Prostate. Multiparametric. Biparametric.*

Resumen

Objetivo: *Nuestro estudio tiene como objetivo demostrar la detección de la invasión por resonancia magnética biparamétrica de próstata (BPMRI).* **Material y métodos:** *Los casos cuyo diagnóstico histopatológico fue PCA y cuyo informe MPMRI se informó como Pirads 4 y 5 fueron evaluados retrospectivamente por dos radiólogos con diferentes experiencias de imágenes de próstata. Las imágenes se agruparon en dos conjuntos de datos. DataSet-1 fue BPMRI, DataSet-2 fue MPMRI. Dos radiólogos evaluaron por primera vez el conjunto de datos 1 independientemente el uno del otro, y 1 mes después, el conjunto de datos-2. Registraron si había una invasión y dónde se vio en los pacientes. Luego se compararon los resultados.* **Resultados:** *Se incluyeron un total de 75 pacientes en el estudio. La invasión periprostática se detectó en 33 de los pacientes. Tanto el primer lector como la imagen del segundo lector detectaron todos los casos con invasión (100%) por separado entre el conjunto de datos-1 y el set-2. Se observó que la compatibilidad para el conjunto de datos de imágenes-1 y el conjunto de datos entre ambos lectores era excelente.* **Conclusiones:** *No es necesario usar el agente de contraste para evaluar la invasión periprostática y tener una idea sobre la puesta en escena local en pacientes con PCA.*

Palabras clave: *Invasión periprostática. Agente de contraste. Próstata. Multiparamétrico. Biparamétrico.*

***Correspondence:**
Hüseyin A. Kızıloğlu
E-mail: alperkzloglu@hotmail.com

Date of reception: 10-03-2023
Date of acceptance: 15-09-2023
DOI: 10.24875/CIRU.23000131

Cir Cir. 2024;92(5):567-573
Contents available at PubMed
www.cirugiaycirujanos.com

Introduction

Prostate cancer (PCa) is one of the most diagnosed and leading causes of cancer-related death in men[1,2]. Prostate cancer is suspected in the presence of a positive digital rectal examination and/or elevated prostate-specific antigen (PSA). This antigen, which is widely used in PCa screening in the clinic, is secreted from both normal prostate epithelium and malignant cells[2]. Conventional radiological evaluations such as ultrasonography (US), computed tomography (CT), and contrast-enhanced lower abdomen magnetic resonance imaging (MRI) are insufficient in detecting and staging prostate cancer. Therefore, with the publication of Prostate Imaging Reporting Data System version 1 (PIRADS v1) in 2012, multiparametric prostate MRI (mpMRI) was brought into the literature and routine practice, and the reporting system was simplified with PIRADS v2 in 2015[3]. PIRADS v2.1 was published in 2019 by the PIRADS committee due to the feedback of the uncertainties and limitations of PIRADS v2 in many studies[4]. The use of mpMRI in the diagnosis of PCa has been increasing in recent years, and mpMRI is also used for treatment planning, local staging, determination of biopsy localization, and estimation of tumor aggressiveness[5]. According to the PIRADS guideline published by the European Society of Urogenital Radiology (ESUR) in 2012, the mpMRI protocol consists of multiplanar T1-weighted (T1W) and T2-weighted (T2W) images, diffusion-weighted images (DWI), and dynamic contrast-enhanced (DCE) sequences[3]. In local staging, which is an important step after the diagnosis of PCa, the specificity of MRI is high, but the specificity is low in demonstrating microscopic extraprostatic extension. The current method used to determine whether the tumor has exceeded the prostate border is PSA, Gleason score, positive core percentage, and digital rectal evaluation[6]. These data are combined with the patient's clinic to predict possible extraprostatic extension, seminal vesicle invasion, lymph node involvement, and distant metastasis. Prostate MRI directly visualizes the extraprostatic extension instead of these evaluations. Although MRI has relatively low sensitivity (38%) in demonstrating extraprostatic extension in early studies, it is highly specific[7].

In PIRADS v2 published by ESUR, the level of contribution of DCE to diagnosis was reduced. In the differentiation of clinically significant PCa, DWI was used for the peripheral zone (PZ) and T2W images were used as the dominant sequence for the transitional zone (TZ). It was also suggested that the contribution of DCE to the diagnosis in PCa is minimal for PZ lesions and is useless for TZ lesions[8]. According to PIRADS v2, DCE only elevates PZ lesions from the PIRADS-3 category to the PIRADS-4 category. In some studies, it is argued that DCE does not contribute significantly to the diagnosis of clinically significant PCa, and it is suggested that only T2-weighted images and DWI images are sufficient[9-11]. In this situation, the place of contrast series in diagnosing clinically significant PCa has become controversial. Accordingly, biparametric prostate MRI (bpMRI), in which only T2-weighted images and DWI images are considered, has been discussed. There are many studies in the literature comparing mpMRI and bpMRI in detecting clinically significant PCa[12-14]. However, bpMRI studies focusing on detecting extraprostatic invasion used in local staging are very limited in the literature.

The main purpose of this study is to demonstrate the diagnostic accuracy of bpMRI in detecting extraprostatic invasion, which is especially important in local staging. In addition, in this study, we aimed to show the agreement of two radiologists with different experiences in the evaluation of extraprostatic invasion with bpMRI.

Materials and method

The study was carried out retrospectively and the study was started after the approval of the local ethics committee dated 28 July 2022 and numbered 22-KAEK-155. Our study was carried out according to the "Helsinki Declaration".

Case selection

In our study, patients diagnosed with PCa histopathologically between January 2019 and June 2022 were examined. Inclusion criteria for the study were patients with elevated PSA and/or positive digital rectal examination findings, patients with mpMRI examination before and within 6 months of prostate biopsy, patients with mpMRI examination within 6 months before prostatectomy, mpMRI report PIRADS 4 and 5 according to PIRADS v2.1 reported patients. Apart from the two readers who performed the study, the PIRADS score was performed by a genitourinary system radiologist with 5 years of prostate MRI reading experience. Exclusion criteria were history of previous

surgery for the prostate, incomplete histopathological data, inadequate mpMRI image quality (artifactual image due to patient movement, presence of magnetic susceptibility artifact due to pelvic surgery such as total hip replacement, presence of artifact on DWI images due to full rectum and inability to comment on the presence of invasion due to collapsed seminal vesicles), and hormonal therapy before mpMRI.

MRI protocol

All patients underwent MRI examination on a 1.5 T device (SIGNA™ Explorer-60 cm GE Healthcare) without using an endorectal coil. MRI sequences used axial fast-spin echo T1W without fat suppression, axial, coronal, and sagittal turbo-spin echo T2W without fat suppression, axial single-shot spin echo-planar DWI images, and T1 Lava three-dimensional spoiled gradient echo pulse sequences without fat suppression. The technical parameters of the sequences are T1W; TR/TE 817/11; slice thickness 3 mm; no slice gap; matrix 256 × 256, and field of view (FOV) 200 × 200 mm for axial images. T2W; TR/TE 8590/108; slice thickness 3 mm; no slice gap; matrix 256 × 256 and FOV 200 × 200 mm for axial images. For DWI, TR/TE 7100/66, slice thickness 3 mm, no slice gap, matrix 256 × 256 and FOV 200 × 200 mm for axial images and b values are 0, 500, and 1500 s/mm^2. The apparent diffusion coefficient map was calculated for each patient and T1 Lava; TR/TE 4/1, slice thickness 3 mm, no slice gap, matrix 256 × 256 and FOV 200 × 200 mm for axial images. Gadolinium-based contrast agents 0.1 mmol/kg were used for contrast images. Dynamic images were acquired with 30 phases every 7 s. The examination time for the patients lasted approximately 40–45 min.

Before the examination, the patients were advised to sexual abstinence for 3 days. During the examination, care was taken to ensure that the rectum of the patients was empty. Buscopan 20 mg/kg intravenous injection was administered to reduce intestinal peristalsis if there were no contraindications during the examination.

Image analysis

The images were evaluated by two radiologists (1st reader 5-year prostate MRI reading experience and 2nd reader 2-year prostate MRI reading experience) with different experiences on evaluating prostate MRI. Images were evaluated from a 21.3 inch 3MP IPS Screen medical monitor through Sectra IDS 7 Picture Archiving and Communication Systems. The images were divided into two sets. It was classified as image set-1 bpMRI (T2W, T1W, and DWI sequences) and image set-2 mpMRI (T2W, T1W, DWI, and DCE sequences). While evaluating patients in the study, readers did not look at contrast-enhanced images for bpMRI. Contrast-enhanced images were eliminated in the computer environment, and readers only viewed bpMRI images of the same patients. First, image set-1 was evaluated by both readers. After 1 month, in the second session, evaluation of the same patients, the image set-2 was examined by both readers. Readers evaluated the images independently of each other. At the end of the evaluation, periprostatic invasion was recorded for each patient as present/absent. Invasion sites; it was localized as extraprostatic (extension beyond the prostatic capsule to the fat planes), seminal vesicle invasion, and bladder invasion. In addition, protrusions and irregularities in the prostate contour, obliteration of the rectoprostatic angle, tumor-capsule interface larger than 1 cm, and neurovascular bundle involvement, defined as invasion criteria according to PIRADS v.2.1, were also recorded in the extraprostatic extension. The presence of invasion for image set-1 was accepted in cases where an extraprostatic soft-tissue lesion extending to the seminal vesicle and bladder and causing restriction in diffusion was detected. For image set-2, the presence of invasion was accepted when extraprostatic, seminal vesicle, and a contrasting soft-tissue lesion extending to the bladder were detected. Then, the obtained data were compared in terms of the presence and localization of invasion between readers and between image sets.

Statistical analysis

The SPSS 24 statistical software package (IBM Corp., Armonk, NY, USA) was used for all data analysis. Categorical measurements were summarized as numbers and percentages, and continuous measurements as mean, deviation, and minimum-maximum. Normality of distributions was evaluated using the Kolmogorov–Smirnov and Shapiro–Wilk W tests. Independent samples *t*-test was used as our data showed a normal distribution. $p < 0.05$ was considered statistically significant. The Cohen's kappa test was used to determine the level of compatibility among readers. Kappa coefficient; If it is < 0, weak

agreement, 0-0.20 agreement insignificant, 0.21-0.4 low agreement, 0.41-0.6 medium agreement, 0.61-0.8 high agreement, and 0.61-0.8 agreement. 0.81-1 was evaluated as a perfect agreement.

Results

A total of 75 male patients were included in the study. The mean age of these patients was calculated as 66.49 ± 7.57 (48-86 years). On mpMRI, 35 (46.7%) of the patients were reported as PIRADS 4 and 40 (53.3%) as PIRADS 5. The mean PSA of the patients was 16.17 ± 13.95 ng/mL (3.58-66 ng/mL). The histopathological report of all patients was reported as adenocancer. The mean age of the patients reported as PIRADS 4 was 65.46 ± 8.69 years and the mean PSA of these patients was 9.05 ± 5.89 ng/mL. The mean age of the patients reported as PIRADS 5 was 67.4 ± 6.4 years and the mean PSA of these patients was 22.4 ± 15.94 ng/mL (Table 1). There was no statistically significant difference between PSA values and age for patients reported as PIRADS 4 and 5.

Periprostatic invasion was detected in 33 (44%) of the patients. All of the patients with invasion were reported as PIRADS 5. The mean age of the patients with invasion was 67.97 ± 6.35 years and the mean PSA of these patients was 24.95 ± 16.32 ng/mL. The mean age of the patients without invasion was 65.33 ± 8.29, and the mean PSA of these patients was 9.27 ± 5.74 ng/mL (Table 1). A statistically significant difference was found between PSA values for patients with and without invasion ($p < 0.001$). The most common invasion was extraprostatic (extension beyond the prostatic capsule into the fat planes) in 14 patients (42.4%) (Figs. 1 and 2). Seminal vesicle invasion was detected in 13 patients (39.4%), both seminal vesicle and bladder invasion were detected in 3 patients (9.1%), and both seminal vesicle and extraprostatic invasion were detected in 3 patients (9.1%).

Both the 1st and 2nd reader image data set-1 (bpMRI) and set-2 (mpMRI) detected all the cases with invasion (100%) separately. The compatibility between both readers for image data set-1 and set-2 was observed to be excellent (Kappa value +1) (Table 2).

Table 1. Descriptive data of the patients

Radiopathological data	Number/ Percent	Age ± SD (year)	PSA ± SD (ng/mL)
PIRADS 4	35/46.7%	65.46 ± 8.69	9.05 ± 5.89
PIRADS 5	40/53.3%	67.4 ± 6.4	22.4 ± 15.94
Cases with invasion	33/44%	67.97 ± 6.35	24.95 ± 16.32
Cases with no invasion	42/56%	65.33 ± 8.29	9.27 ± 5.74
Total	75/100%	66.49 ± 7.57	16.17 ± 13.95

SD: standard deviation; PSA: prostate-specific antigen; PIRADS: prostate imaging reporting data system.

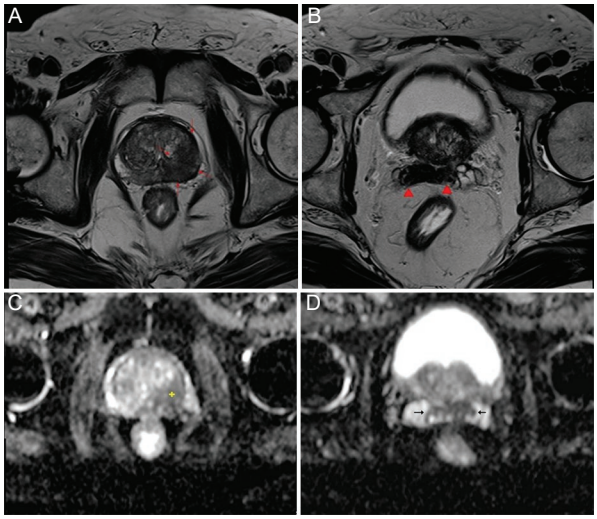

Figure 1. A-D: *a 68-year-old male patient. PIRADS 5 lesion involving the anterior and posterior compartments of the middle peripheral zone on the left and involving the transitional zone anterior and posterior zone. The lesion extends to the base of the prostate in more superior sections and invades both seminal vesicles from there.* **A:** *T2-weighted image shows signal loss at the described location of the lesion (between the red arrows).* **B:** *T2-weighted image, it is observed that the lesion has invaded both seminal vesicles (red arrowheads).* **C:** *the apparent diffusion coefficient map, lesion appears hypointense (yellow mark).* **D:** *the apparent diffusion coefficient map shows that the lesion has invaded both seminal vesicles (between black arrows).*

Discussion

In our study, since all cases with invasion detected on mpMRI could be detected with bpMRI and excellent agreement was observed between two radiologists with different prostate imaging experiences in the detection of invasion on bpMRI, gross local staging of PCa could be performed by showing periprostatic invasion by bpMRI.

With the change on prostate imaging over the years, the areas of use of contrast media are narrowing. Because, besides its minimal contribution to diagnostic accuracy, it has disadvantages that cannot be ignored. There are three major advantages to removing DCE from the protocol. These shorten the examination time, reducing the cost of the examination, and eliminating the possible undesirable effects of the contrast agent. Some known side effects linked to the use of gadolinium-based contrast agents include:

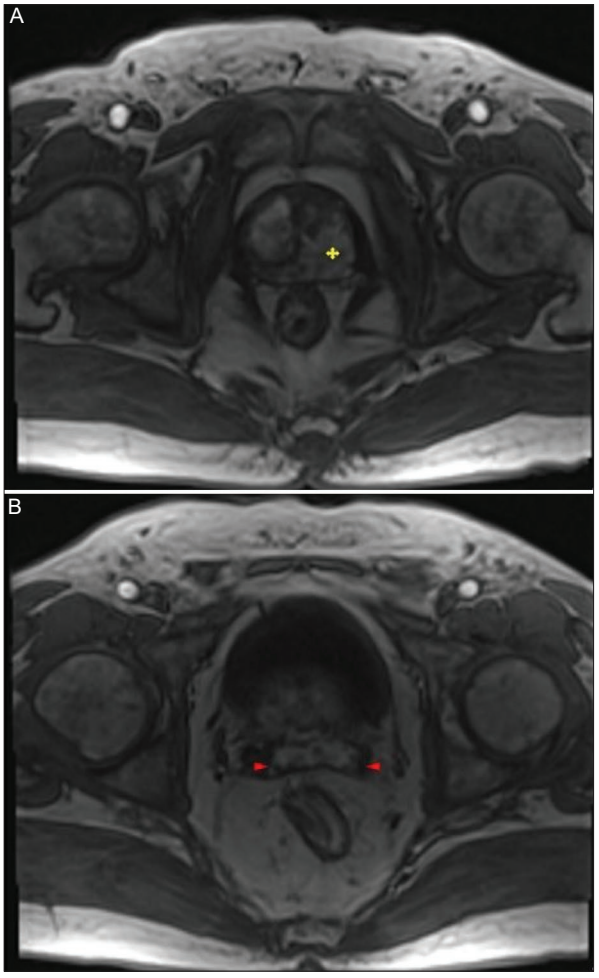

Figure 2. A and **B:** *post-contrast T1-weighted image of the same patient without fat suppression.* **A:** *the lesion has heterogeneous contrast (yellow mark).* **B:** *seminal vesicle invasion is seen as a contrasting space-occupying formation (between the red arrowheads).*

Table 2. Compatibility among readers

Observers	Invasion detection (number/percent)		Kappa
	Data set-1 (bpMRI)	Data set-2 (mpMRI)	
Reader I	33/100%	33/100%	1
Reader II	33/100%	33/100%	

bpMRI: biparametric prostate magnetic resonance imaging; mpMRI: multiparametric prostate magnetic resonance imaging.

Table 3. bpMRI and mpMRI advantages

bpMRI (T2W, DWI) advantages	mpMRI (T2W, DWI, DCE) advantages
Examination time is short	Diagnostic accuracy increases if T2W and DWI image quality is poor
Possible side effects of the contrast agent are eliminated	Diagnostic accuracy increases in the presence of inexperienced radiologist
Cost is lower	Detection of small lesions becomes easier
Evaluation is easier	Contributes to diagnostic accuracy in uncertain cases

bpMRI: biparametric prostate magnetic resonance imaging; mpMRI: multiparametric prostate magnetic resonance imaging; T2W: T2 weighted; DWI: diffusion-weighted imaging; DCE: dynamic contrast enhanced.

development of allergic reaction, systemic nephrogenic fibrosis and accumulation of contrast agent in the brain[15]. Other side effects are seen at a rate of 0.004-0.7% and include coldness or warmth at the injection site, pain at the injection site, nausea, vomiting, headache, paresthesia, and dizziness[16]. DCE is still included in clinical use and in the PIRADS v2.1 guideline. Because DCE has advantages such as detecting small PCa and following patients after radical prostatectomy[11,17]. In addition, the use of contrast agent has additional advantages such as increasing the diagnostic accuracy of some inexperienced radiologists and supporting the correct diagnosis if the image quality of DWI and/or T2W sequences is low[16]. However, it has also been shown that the use of DCE causes false positives in some benign conditions such as prostatitis and fibrosis[18]. The role of DCE in diagnosis and staging is controversial. One advantage of using the bpMRI protocol is that it is easier to evaluate images than mpMRI. The comparison of mpMRI and bpMRI in terms of advantages is shown in table 3.

Studies on the use of bpMRI in local staging, which is the focus of our study, are limited. Although the specificity of prostate MRI is high in local staging, the sensitivity is low due to the inability of MRI to show microscopic extraprostatic extension[4]. In this instance, we think that imaging with DCE will not be of additional benefit in showing the microscopic extension. Our results also detected periprostatic invasion at the same rate in contrast-enhanced and non-contrast series, regardless of microscopic extension.

There are some studies showing that bpMRI has the same diagnostic accuracy as mpMRI in detecting clinically significant PCa according to PIRADS v2[14,19-21]. In a study that divided patients with suspected PCa into low-risk, intermediate-high-risk, and very high-risk patients, it was reported that only bpMRI evaluation would be sufficient in the very high-risk patient group (having a very high PSA and positive digital rectal examination finding)[22]. According to this study, our patient group

falls into the very high-risk category, and we argue that bpMRI will be sufficient to evaluate patients in this category. Recent evidence has revealed that the bpMRI protocol may be sufficient in the diagnosis for PCa of 10 mm and above[11]. In another study, the bpMRI protocol for clinically significant PCa was shown to have the same diagnostic accuracy as mpMRI[20]. In a similar study, bpMRI focused on the detection of cancer in the anterior fibromuscular stroma and TZ, and they showed that the rates of clinically significant PCa detection by bpMRI were not lower than mpMRI[23].

Detection of periprostatic invasion (extraprostatic extension, seminal vesicle invasion, bladder invasion) is an important step in treatment planning. Our findings contribute to local staging with bpMRI at this stage. This stage will be more advantageous than mpMRI in shortening the examination time, reducing the cost, and eliminating possible side effects.

Ga68 Prostate Specific Membrane Antigen (Ga68-PSMA) is a new monitoring agent used on PET. Ga68 PSMA-positron emission tomography-computed tomography (PET/CT) is used in the diagnosis, evaluation of the extent of prostate cancer, and treatment follow-up. Ga68 PSMA-PET/CT examination was accepted as the gold standard for demonstrating the presence of invasion. However, this method has some limitations in diagnosis and staging. Ga68 PSMA-PET/CT is confusing and false-positive in conditions such as benign prostatic hypertrophy that increases PSA levels and in conditions such as prostatitis. In this case, Ga68 PSMA-PET/CT can provide additional diagnostic benefits in demonstrating periprostatic invasion of bpMRI, and it can also be used instead of Ga68 PSMA-PET/CT.

The limitations of our study are the fact that the study is retrospective and single center, and the number of patients is low, which is in the first place. The second limitation is that the endorectal coil is not used on MRI sequences. The third limitation is that the images were obtained with a 1.5 T MRI device. Since the second and third limitations will reduce the signal-to-noise ratio, the image quality is low. Another limitation of our study is that the Galium-68 PSMA-PET/CT examination, which is used in routine practice in demonstrating invasion and metastasis, was not included in the study.

Conclusion

There is no need to use contrast agent to evaluate periprostatic invasion and to have an idea about local staging in PCa patients. With this method, prolongation of dynamic contrast sequence-based examination, increase in cost, and undesirable side effects of contrast agent are eliminated. With adequate image quality, T2W and DWI images, radiologists experienced on prostate imaging will not need contrast-enhanced series in the evaluation of periprostatic invasion. We hope that more comprehensive studies will be conducted with images in which the contrast agent is eliminated.

Funding

The authors declare that they have not received funding.

Conflicts of interest

The authors declare no conflicts of interest.

Ethical disclosures

Protection of human and animal subjects. The authors declare that no experiments were performed on humans or animals for this study.

Confidentiality of data. The authors declare that they have followed the protocols of their work center on the publication of patient data.

Right to privacy and informed consent. The authors have obtained approval from the Ethics Committee for analysis and publication of routinely acquired clinical data and informed consent was not required for this retrospective observational study.

References

1. Bjurlin MA, Mendhiratta N, Wysock JS, Taneja SS. Multiparametric MRI and targeted prostate biopsy: improvements in cancer detection, localization, and risk assessment. Cent European J Urol. 2016;69:9-18.
2. Stenman UH, Leinonen J, Zhang WM, Finne P. Prostate-specific antigen. Semin Cancer Biol. 1999;9:83-93.
3. Barentsz JO, Richenberg J, Clements R, Choyke P, Verma S, Villeirs G, et al. ESUR prostate MR guidelines 2012. Eur Radiol. 2012;22:746-57.
4. Turkbey B, Rosenkrantz AB, Haider MA, Padhani AR, Villeirs G, Macura KJ, et al. Prostate imaging reporting and data system version 2.1: 2019 update of prostate imaging reporting and data system version 2. Eur Urol. 2019;76:340-51.
5. Rosenkrantz AB, Shanbhogue AK, Wang A, Kong MX, Babb JS, Taneja SS. Length of capsular contact for diagnosing extraprostatic extension on prostate MRI: assessment at an optimal threshold. J Magn Reson Imaging. 2016;43:990-7.
6. Ravery V, Boccon-Gibod L. T3 prostate cancer: how reliable is clinical staging? Semin Urol Oncol. 1997;15:202-6.
7. Yu KK, Hricak H, Alagappan R, Chernoff DM, Bacchetti P, Zaloudek CJ. Detection of extracapsular extension of prostate carcinoma with endorectal and phased-array coil MR imaging: multivariate feature analysis. Radiology. 1997;202:697-702.
8. Vargas HA, Hötker AM, Goldman DA, Moskowitz CS, Gondo T, Matsumoto K, et al. Updated prostate imaging reporting and data system (PIRADS v2) recommendations for the detection of clinically significant prostate cancer using multiparametric MRI: critical evaluation using whole-mount pathology as standard of reference. Eur Radiol. 2016;26:1606-12.

9. Stanzione A, Imbriaco M, Cocozza S, Fusco F, Rusconi G, Nappi C, et al. Erratum to "Biparametric 3t magnetic resonance imaging for prostatic cancer detection in a biopsy-naïve patient population: a further improvement of PI-RADS v2? [Eur J Radiol. 2016;85:2269-74], Eur J Radiol. 2017;87:125.
10. Hansford BG, Peng Y, Jiang Y, Vannier MW, Antic T, Thomas S, et al. Dynamic contrast-enhanced MR imaging curve-type analysis: is it helpful in the differentiation of prostate cancer from healthy peripheral zone? Radiology. 2015;275:448-57.
11. Scialpi M, Prosperi E, D'Andrea A, Martorana E, Malaspina C, Palumbo B, et al. Biparametric versus multiparametric MRI with non-endorectal coil at 3T in the detection and localization of prostate cancer. Anticancer Res. 2017;37:1263-71.
12. Tamada T, Kido A, Yamamoto A, Takeuchi M, Miyaji Y, Moriya T, et al. Comparison of biparametric and multiparametric MRI for clinically significant prostate cancer detection With PI-RADS version 2.1. J Magn Reson Imaging. 2021;53:283-91.
13. Zhang J, Xu L, Zhang G, Zhang X, Bai X, Ji Z, et al. Comparison between biparametric and multiparametric MRI diagnosis strategy for prostate cancer in the peripheral zone using PI-RADS version 2.1. Abdom Radiol (NY). 2022;47:2905-16.
14. Xu L, Zhang G, Shi B, Liu Y, Zou T, Yan W, et al. Comparison of biparametric and multiparametric MRI in the diagnosis of prostate cancer. Cancer Imaging. 2019;19:90.
15. Barth BK, De Visschere PJ, Cornelius A, Nicolau C, Vargas HA, Eberli D, et al. Detection of clinically significant prostate cancer: short dual-pulse sequence versus standard multiparametric MR imaging-a multireader study. Radiology. 2017;284:725-36.
16. ACR Committee on Drugs and Contrast Media. ACR Manual on Contrast Media Version 10.3; 2018. Available from: https://www.acr.org/clinical-resources/contrast-manual [Last accessed on 2019 Jan 08].
17. Verma S, Turkbey B, Muradyan N, Rajesh A, Cornud F, Haider MA, et al. Overview of dynamic contrast-enhanced MRI in prostate cancer diagnosis and management. AJR Am J Roentgenol. 2012;198:1277-88.
18. Kitzing YX, Prando A, Varol C, Karczmar GS, Maclean F, Oto A. Benign conditions that mimic prostate carcinoma: MR imaging features with histopathologic correlation. Radiographics. 2016;36:162-75.
19. Di Campli E, Delli Pizzi A, Seccia B, Cianci R, d'Annibale M, Colasante A, et al. Diagnostic accuracy of biparametric vs multiparametric MRI in clinically significant prostate cancer: comparison between readers with different experience. Eur J Radiol. 2018;101:17-23.
20. Choi MH, Kim CK, Lee YJ, Jung SE. Prebiopsy biparametric MRI for clinically significant prostate cancer detection with PI-RADS version 2: a multicenter study. AJR Am J Roentgenol. 2019;212:839-46.
21. Junker D, Steinkohl F, Fritz V, Bektic J, Tokas T, Aigner F, et al. Comparison of multiparametric and biparametric MRI of the prostate: are gadolinium-based contrast agents needed for routine examinations? World J Urol. 2019;37:691-9.
22. Schoots IG, Barentsz JO, Bittencourt LK, Haider MA, Macura KJ, Margolis DJ, et al. PI-RADS committee position on MRI without contrast medium in biopsy-naive men with suspected prostate cancer: narrative review. AJR Am J Roentgenol. 2021;216:3-19.
23. Radtke JP, Boxler S, Kuru TH, Wolf MB, Alt CD, Popeneciu IV, et al. Improved detection of anterior fibromuscular stroma and transition zone prostate cancer using biparametric and multiparametric MRI with MRI-targeted biopsy and MRI-US fusion guidance. Prostate Cancer Prostatic Dis. 2015;18:288-96.

ORIGINAL ARTICLE

Beneficial effects of IVIG treatment on experimental-induced osteoporosis

Efectos beneficiosos del tratamiento con IVIG en la osteoporosis inducida experimentalmente

Savaş Özdemir[1] and Oytun Erbas[2]*

[1]Department of Gynecology and Obstetrics, Istanbul Prof. Dr. Cemil Taşçıoğlu City Hospital; [2]Department of Physiology, Demiroglu Bilim University. Istanbul, Turkey

Abstract

Objective: *Estrogen (E2) plays a significant role in postmenopausal osteoporosis, and its deficiency is related to chronic low-grade inflammation. Intravenous immunoglobulin (IVIG) is composed of immunoglobulins derived from the plasma of healthy donors. Numerous anti-inflammatory pathways are responsible for IVIG's anti-inflammatory action The aim of this study is to investigate the effects of IVIG on experimental-induced osteoporosis.* **Materials and methods:** *Forty adult female Wistar rats were included in the study. Thirty rats underwent bilateral dorsal ovariectomy. Rats were grouped as Group 1 (n = 10, ovariectomy and saline); Group 2 (n = 10, ovariectomy and E2); Group 3 (n = 10, ovariectomy and IVIG), and Control group (n = 10, no oophorectomy). Histopathological examination of bone tissue, and biochemical analysis for beta-catenin, plasma Tumor Necrosis Factor-α, IL-6, receptor activator of nuclear-κB ligand (RANKL), and osteoprotegerin (OPG) levels were made.* **Results:** *The IVIG group had increased trabecular number, area, and thickness with increased bone mineral density as well as decreased trabecular separation compared with the saline group. IVIG group had lower serum RANKL and higher serum OPG levels when compared with the saline group. The bone marrow beta-catenin level was significantly higher in the control and ovariectomy + IVIG groups.* **Conclusion:** *IVIG has beneficial effects on experimentally induced osteoporosis with a possible action on inflammation and RANKL-β-catenin pathway.*

Keywords: *β-catenin. IVIG. RANKL. Osteoporosis.*

Resumen

Objetivo: *El estrógeno juega un papel importante en la osteoporosis posmenopáusica y su deficiencia está relacionada con la inflamación crónica de bajo grado. La inmunoglobulina intravenosa (IGIV) está compuesta por inmunoglobulinas derivadas del plasma de donantes sanos. El objetivo de este estudio es investigar los efectos de IVIG en la osteoporosis inducida experimentalmente.* **Materiales y métodos:** *30 ratas se sometieron a ovariectomía dorsal bilateral. las ratas se agruparon como: Grupo 1 (n = 10, ovariectomía y solución salina); Grupo 2 (n = 10, ovariectomía y estrógeno); Grupo 3 (n = 10, ovariectomía e IVIG) y Grupo Control (n = 10, sin ovariectomía). Se realizó un examen histopatológico del tejido óseo y un análisis bioquímico de los niveles de beta-catenina, factor de necrosis tumoral α (TNF-α), IL-6, RANKL y osteoprotegerina (OPG) en plasma.* **Resultados:** *El grupo IVIG había aumentado el número, el área y el grosor trabecular con una mayor densidad mineral ósea, así como una menor separación trabecular en comparación con el grupo de solución salina. El nivel de beta-catenina en la médula ósea fue significativamente mayor en los grupos de control y de ovariectomía + IVIG.* **Conclusión:** *IVIG tiene efectos beneficiosos sobre la osteoporosis inducida experimentalmente con una posible acción sobre la inflamación y la vía RANKL-β-catenina.*

Palabras clave: *β-catenina. IVIG. RANKL. Osteoporosis.*

***Correspondence:**
Savaş Özdemir
E-mail: savasozdemirdr@hotmail.com

Date of reception: 27-04-2023
Date of acceptance: 08-11-2023
DOI: 10.24875/CIRU.23000219

Cir Cir. 2024;92(5):574-580
Contents available at PubMed
www.cirugiaycirujanos.com

Introduction

Uncoupling of bone resorption and production in the same bone region characterizes postmenopausal osteoporosis (PMO). Hormones and bone-derived substances in the bloodstream regulate osteoblastogenesis and osteoclastogenesis[1]. By promoting osteogenic differentiation and decreasing osteoclastogenesis, estrogen (E2) plays a significant role in this process. During PMO, the number of osteoclasts (OC) in the bone may increase by up to 70%, but bone formation may increase to a lower degree, remain steady, or decrease, depending on the stage of menopause[2]. Therefore, PMO is characterized by an increase in bone turnover and a remodeling balance shift toward resorption[3].

E2 has been demonstrated to interact with a number of immune cells, resulting in chronic low-grade pro-inflammation in individuals lacking in E2[4].

Chronic inflammatory disorders mediated by immune complexes are often associated with bone loss. These conditions also increase the uncoupling of osteoclast and osteoblast activities, resulting in excessive and pathologic bone resorption[5].

Intravenous immunoglobulin (IVIG) is a medication composed of immunoglobulins derived from the plasma of thousands of healthy donors. It has been shown to be beneficial in the treatment of a number of autoimmune and chronic inflammatory illnesses. Fc gamma receptors, which bind immunoglobulin G Fc component, and CD209 are two receptors that transmit IVIG signals (also known as DC-SIGN, dendritic cell-specific intercellular adhesion molecule-3-Grabbing Non-integrin)[6,7]. Numerous well-established anti-inflammatory pathways are responsible for IVIG's anti-inflammatory action. However, the precise mechanisms behind the immunomodulatory and anti-inflammatory effects of IVIG therapy remain unknown.

Despite extensive studies of the beneficial effects of IVIG on inflammatory diseases, the effects of IVIG on osteoclastogenesis and osteoblastic functions in a sub-inflammatory state like post-menopausal osteoporosis are not known.

Regarding the inflammatory condition in post-menopausal osteoporosis, the aim of this study is to determine the effect of IVIG on bone structure and the markers of osteoblast, osteoclast, and osteocyte functions.

Materials and methods

Animals

In this study, 40 female Wistar albino mature rats at weighing 200-250 g, were used. The present study was approved by the Animal Ethics Committee (Science University, Ethical number: 03220201). The rats used in the experiment were obtained from the Experimental Animal Laboratory of Science University. Rats were fed ad libitum and housed impairs in steel cages having a temperature-controlled environment (22 ± 2°C) with 12-h light/dark cycles.

Experimental protocol

In the present study, 40 adult female Wistar rats were used. Thirty rats underwent bilateral dorsal ovariectomy. Ten rats did not undergo oophorectomy. For the surgical procedure, rats were anesthetized by intraperitoneal injection of a combination of ketamine hydrochloride at a dose of 50 mg/kg and 10 mg/kg xylazine hydrochloric.

Rats were kept at the postmenopausal period for 3 weeks and were ovariectomy rats divided into three groups. Normal control group rats have no ovariectomy and no any therapy. Group 1 (n = 10, ovariectomy and saline) rats were given 1 mL/kg/day saline (0.9% NaCl) by intraperitoneally; Group 2 (n = 10, ovariectomy and E2) rats were given 17-beta-estradiol (E2) 0.5 mg/kg dissolved in sesame oil daily orally by gavage; and Group 3 (n = 10, ovariectomy and IVIG) rats were given IVIG 250 mg/kg/day by intraperitoneally. All treatments were given for 12 weeks.

Twelve weeks later, bone mineral density (BMD) of experimental animals under ketamin anesthesia (50 mg/kg) was measured by Hologic QDR-4500A (DEXA Scan) and a "small animal" program. Measurements were taken with high resolution in two different regions: the left extremity proximal femoral diaphysis and the lumbar vertebrae. Blood samples were collected by cardiac puncture for biochemical analysis and the removal of femurs was performed for histopathological and biochemical examination.

Histopathological examination of bone tissue

For histological and immunohistochemical studies, all animals were anesthetized by an i.p. of ketamin (40 mg/kg, (40 mg/kg, Alfamine®, Ege Vet, Alfasan International B.V., Holland)/xylazine (4 mg/kg, Alfazyne®, Ege Vet, Alfasan International B.V., Holland) and perfused with 200 mL of 4% formaldehyde in 0.1 M phosphate-buffer saline (PBS).

Following the perfusion procedure, the left femurs of the animals were dissected and kept at room temperature in a 10% formaldehyde fixative for 24 h for histomorphometric analysis. Following fixation, specimens

were placed in 10% formic acid. After decalcification was completed within 28 days, they were taken into routine light microscope follow-up. From the prepared paraffin blocks, transverse sections were obtained in 3-micron thicknesses with a Leica MR 2145 microtome. For morphometric analysis, hematoxylenen-eosin dyed preparations were used[8].

Morphometric analyses

For each animal, five cross-sections were obtained, from the left hind extremity proximal femoral metaphysis in the paraffine blocks serially, for morphometric analyses. Sections were stained with hematoxylin-eosin, and 20× zoomed digital pictures were taken by an Olympus microscope. To measure trabecular count, trabecular thickness, trabecular area, and trabecular separation, the semi-automatic digital system UTHSCSA Image Tool for Windows Version 1.28 was used. Trabecular measurements were performed at 0.46 mm proximal of the epiphysis plaque and at equal distances from both sides of the cortex in femur preparations. The lengths were calculated as pixels using the program (1 pixel=128 × 10-8 mm)[8]. All measurements were implemented in accordance with the article by Parfitt et al.[9]

Morphometric measurements

For trabecular thickness (μm), measurements were taken at a minimum of 50 different points for every trabecula, and measurements continued to be taken until the mean values became constant. The trabecular count was obtained by counting all trabeculae and each trabecula parallel to each other at 0.46 mm distal to the epiphysis plaque at equal distances from both sides of the cortex. The trabecular area (mm^2) was calculated by determining the borders of the trabeculae in the region where the trabecular count was determined. Cortical thickness (μm) was calculated by mean values of fifty measurements from 3-micron sections in digital pictures of each preparation. Osteoblast and osteoclast counts were calculated in hematoxylene-eosin dyed preparations with 40× objective zoomed digital pictures using an image analysis program and counting cells around trabeculae 0.5 mm under the epiphysis plaque[8].

Bone marrow biochemical analysis for beta-catenin

The material obtained was homogenized with a glass homogenizer in 5 volumes of PBS that was 5 times the volume of the obtained tissue (pH 7.4) and centrifuged at 5.000 g for 15 minutes. Beta-catenin the bone marrow supernatants was measured using commercially available rat enzyme-linked immunosorbent assay (ELISA) kits.

Plasma TNF-α, IL-6, RANKL, and OPG levels were measured using commercially available ELISA kits.

Results

The mean trabecular numbers (number/mm^2) were significantly higher in the control group compared with ovariectomy + saline, ovariectomy + E2, and ovariectomy + IVIG groups (respectively; $p < 0.01$, $p < 0.01$ and $p < 0.05$). The mean trabecular number was also significantly higher in the ovariectomy + IVIG group compared with ovariectomy + saline, and ovariectomy + E2 groups (respectively, $p < 0.01$ and $p < 0.05$). Trabecular area (μm^2) was significantly higher in the control group compared with ovariectomy + saline, ovariectomy + E2, and ovariectomy + IVIG groups (respectively; $p < 0.001$, $p < 0.001$ and $p < 0.05$). It was also significantly higher in the ovariectomy + IVIG group compared with ovariectomy + saline and ovariectomy + E2 groups (respectively; $p < 0.001$ and $p < 0.05$). Trabecular separation was significantly lower in control and IVIG groups compared with ovariectomy + saline and ovariectomy + E2 groups (respectively; $p < 0.001$, and $p < 0.001$; $p < 0.05$ and $p < 0.001$). The mean trabecular thickness (μm) was significantly higher in control group compared with with ovariectomy + saline and ovariectomy + E2 groups (respectively; $p < 0.01$ and $p < 0.01$). Similarly, it was found to be higher in the IVIG group compared with ovariectomy + saline and ovariectomy + E2 groups (respectively; $p < 0.01$ and $p < 0.05$). Femoral BMD (g/cm^2) was significantly higher in the control and IVIG groups compared with the saline group ($p < 0.01$ and $p < 0.05$). The mean values of lomber vertebra BMD (g/cm^2) were found to be significantly higher in the control and IVIG groups compared with saline group ($p < 0.01$ and $p < 0.05$). The data are presented at table 1 (Figs. 1 and 2).

The mean value of plasma TNF-α level (pg/mL) was significantly lower in the control group compared with ovariectomy + saline, ovariectomy + E2, and ovariectomy + IVIG groups (respectively; $p < 0.001$, $p < 0.001$, and $p < 0.01$). The mean plasma IL-6 level was significantly lower in the control group compared with ovariectomy + saline, ovariectomy + E2, and ovariectomy + IVIG groups (respectively; $p < 0.001$, $p < 0.001$, and $p < 0.05$). The IVIG group had a significantly lower

Table 1. Comparison of bone morphometric analyses and measurements between groups

Analysis results	Normal control (n = 10)	Ovariectomy + saline (n = 10)	Ovariectomy + E2 (n = 10)	Ovariectomy + IVIG (n = 10)
Trabecular number (number/mm^2)	12.21 ± 1.03	7.25 ± 0.9*	9.37 ± 1.2†	10.8 ± 0.7†
Trabecular area (μm^2)	24345.5 ± 2854.2	11457.8 ± 1021.2‡	17365.2 ± 985.7†	20215.3 ± 854.1§
Trabecular separation (μm)	121.3 ± 10.9	244.6 ± 12.8‡	198.5 ± 9.9§	155.8 ± 11.3§
Trabecular thickness (μm)	305.3 ± 24.9	168.2 ± 19.5*	202.1 ± 17.6†	288.5 ± 13.01§
Femoral BMD (g/cm^2)	0.48 ± 0.11	0.29 ± 0.08*	0.32 ± 0.15	0.35 ± 0.07†
Lomber vertebra BMD (g/cm^2)	0.30 ± 0.09	0.18 ± 0.12*	0.20 ± 0.05	0.22 ± 0.04†

*p < 0.05.
†p < 0.01.
‡p < 0.001 (different from the control group).
§p < 0.001 (different from ovariectomy and saline group).
Results were presented as mean ± SEM. Statistical analyses were performed by one-way ANOVA test.

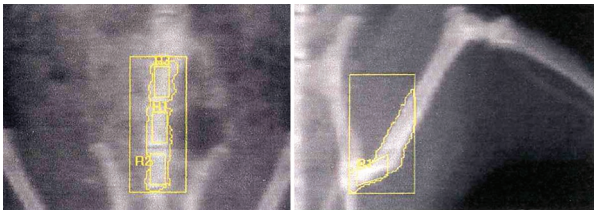

Figure 1. *Rat DEXA scan.*

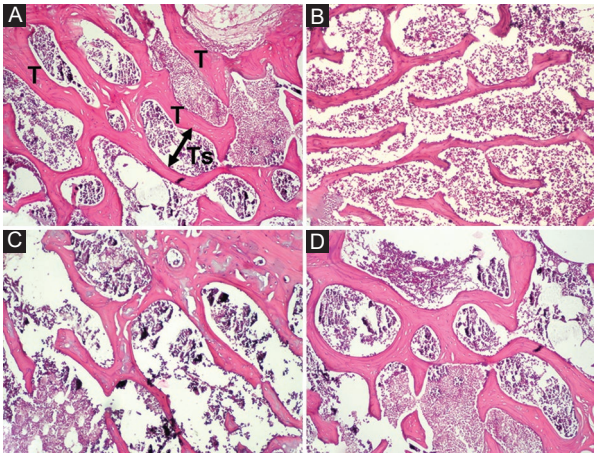

Figure 2. *Bone trabeculae (Tb) of rat femur with H&E stain ×20.* **A:** *normal control group.* **B:** *ovariectomized group trabecular thinning and widening of trabecular space 15 weeks after ovariectomy.* **C:** *ovariectomized and estradiol (E2) group restoration of the trabecular thickness.* **D:** *ovariectomized and IVIG group restoration of the trabecular thickness. T: trabeculae; Ts: trabecular separation.*

level of plasma IL-6 compared with the ovariectomy + saline group (p < 0.01). The mean plasma RANKL level was significantly lower in the control group compared with ovariectomy + saline, ovariectomy + E2, and ovariectomy + IVIG groups (respectively; p < 0.001, p < 0.001, and p < 0.01). It was also significantly lower in ovariectomy + IVIG group and ovariectomy + E2 group compared with ovariectomy + saline group (p < 0.01 and p < 0.05). The mean plasma OPG level was significantly higher in the control group compared with ovariectomy + saline, ovariectomy + E2, and ovariectomy + IVIG groups (p < 0.01). It was also significantly higher in the ovariectomy + IVIG group and ovariectomy + E2 group compared with the ovariectomy + saline group (p < 0.01 and p < 0.05). The mean levels of bone marrow beta-catenin level (pg/mg protein) were significantly higher in control and ovariectomy + IVIG groups compared with ovariectomy + saline and ovariectomy + E2 groups (respectively; p < 0.01, and p < 0.01; p < 0.01 and p < 0.01) (Table 2).

Discussion

In the current study, the administration of IVIG was shown to have favorable benefits, including an increase in trabecular number, trabecular area, trabecular thickness, femoral BMD, and lomber vertebra BMD, and a decrease in trabecular separation. In the current investigation, it was shown that IVIG is equally efficient as E2 in treating experimentally induced osteoporosis. Moreover, IVIG therapy has been demonstrated to be better in various osteoporosis-related parameters.

Osteoporosis is the most frequent metabolic bone disease, affecting 50% of women and 30% of men in their sixth and seventh decades of life[10]. Osteoporosis is characterized by uncoupled bone resorption, which results in a loss of bone mass. Continuous bone remodeling is

Table 2. Comparison of immune parameters, RANKL, OPG, and bone marrow beta-catenin between groups

Parameters	Normal control (n = 10)	Ovariectomy + saline (n = 10)	Ovariectomy + E2 (n = 10)	Ovariectomy + IVIG (n = 10)
Plasma TNF-α level (pg/mL)	30.1 ± 9.5	97.4 ± 14.8*	65.6 ± 12.9†	55.7 ± 9.8‡
Plasma IL-6 level (pg/mL)	405.5 ± 28.5	644.1 ± 11.3*	542.7 ± 8.8†	487.5 ± 13.5‡
Plasma RANKL level (pg/mL)	60.3 ± 2.24	145.4 ± 4.95§	114.1 ± 5.67†	108.03 ± 6.4†
Plasma OPG level (pg/mL)	20.5 ± 1.09	9.8 ± 1.1*	14.3 ± 0.8†	13.2 ± 1.5†
Bone Marrow Beta-catenin level (pg/mg protein)	21.4 ± 5.5	11.6 ± 2.9*	19.5 ± 1.5†	25.8 ± 2.3‡

*p < 0.05.
†p < 0.01.
‡p < 0.001 (different from ovariectomy and saline group).
§p < 0.001 (different from the control group).
Results were presented as mean ± SEM. Statistical analyses were performed by one-way ANOVA test.

a coordinated procedure for repairing microfractures and maintaining bone mass.

The two primary cell types involved in bone remodeling are bone-resorbing OC and bone-forming osteoblasts (OB). In the past 10 years, bone-embedded osteocytes have emerged as critical regulators. OC are multinucleated monocytic cells whose differentiation is controlled by the nuclear factor-kB receptor activator (RANK) and RANKL. Multiple signaling mechanisms, including WNT/b-catenin and BMP, govern OB formation from the mesenchymal stem cell lineage. During remodeling, the OC and OB form the bone remodeling unit[11].

E2 deficiency has been associated to a predictor of future osteoporosis in postmenopausal women for about eight decades. Despite extensive investigation, the mechanism behind E2 deficiency-induced accelerated bone resorption is unclear[12] Menopause and aging have been linked to reduced calcium absorption, deterioration of renal function, and changes in vitamin D metabolism[13].

In our study, TNF alpha and IL6 levels increased after oophorectomy. This elevation was greatest in the oopherectomy+ saline group and lower in the IVIG group.

The adaptive immune system has been shown in both human and animal models to have a critical role in the development of PMO. After detecting the influence of T-cell-derived cytokines on bone, Arron and Choi created the term osteoimmunology in 2000[14]. Proinflammatory cytokines produced by T cells, such as TNF and interleukin-17A, have proresorptive properties[15]. Chronic inflammation induced by an E2 deficiency may aggravate osteoporosis and lead to other complications[16].

Takayanagi et al. discovered that IFN-g generated by T cells may block RANKL signaling during OC formation[17]. Because Th1 cells produce a large amount of IFN-g, it was assumed that inflammatory bone loss was induced by Th1 cells.

IL-17A has been demonstrated to induce significant bone loss, especially in those with autoimmune disorders[17]. TNF has been shown to stimulate osteoclastogenesis by directly acting on OC[18]. Patients with rheumatoid arthritis, inflammatory bowel disease, and chronic lung disease are more likely to have osteoporosis[19]. An increase in local cytokines may accelerate bone resorption in these circumstances[20].

In the current study, the IVIG group had lower serum RANKL levels and higher serum OPG levels than the saline group.

RANKL is a cytokine that belongs to the TNF superfamily. The RANKL receptor, known as RANK, is strongly linked with CD40. It is well known that genetic deletion or mutation of RANKL causes severe osteoporosis, which is accompanied with a total deficiency on OC[21]. RANKL stimulation with RANK has a detrimental effect on OC development. TNF receptor-associated factors and kinases are activated when RANKL binds to RANK[22]. OPG is a RANKL receptor. While binding RANKL, OPG inhibits RANKL/RANK interaction and promotes bone resorption by blocking OC formation[23]. Experimental investigations have revealed that genetic deletion of OPG causes osteoporosis[24]. It is thought that an increase in RANKL and a concurrent reduction in OPG is a key risk factor for bone illnesses such as osteoporosis[25]. There have been two earlier studies that looked at the relationships between IVIG and RANKL. In addition to its immunosuppressive effects, Lee and colleagues revealed that IVIG directly suppressed osteoclastogenesis through a mechanism that included RANK signaling suppression[26]. Kim and colleagues discovered that IVIG reduced osteoclastogenesis when monocytes were cocultured with Th17 cells[27].

Although both studies demonstrated the effects of IVIG on RANKL in cell culture, they conceptually supported the positive benefits of IVIG in osteoporosis therapy.

In our research, bone marrow beta-catenin levels were higher in the IVIG group than in the saline group and Wnt signaling is widely known to have a function in bone remodeling and development. The Wnt/-catenin pathway is a key component of this signaling system[28]. As the quantity of -catenin grows, it translocates into the nucleus and activates the genes Lef1 and Tcf1[29]. Following this stimulation, osteoblastic differentiation and bone production ensue[30]. As a result, this route is crucial for bone. Furthermore, there has been therapeutic use of the Wnt pathway; sclerostin - which neutralizes antibodies[31]. These antibodies are currently accessible for clinical usage in the treatment of osteoporosis[32]. Nonetheless, these antibody medications are expensive, have a one-year shelf life, and have considerable vascular adverse effects. As a result, the application of these antibodies in clinical practice is thought to be restricted[33]. There is just one research in the literature that looks at the relationship between IVIG and -catenin. Kranam and colleagues demonstrated that therapeutic normal IgG IVIG treatment resulted in the activation of the -catenin pathway[34]. Our findings validated the previous work, and we also established for the first time that IVIG therapy had a beneficial impact on -catenin in experimentally generated osteoporosis.

In conclusion, this is the first study to demonstrate the protective benefits of IVIG on experimentally induced osteoporosis. Mechanism activities are linked to RANKL, anti-inflammation, and the -catenin pathway. Following more research, anti-inflammatory medicines impacting these pathways, such as IVIG, may be regarded a potential agent in the treatment of osteoporosis without major adverse effects.

Funding

The author declares no funding was received for this study.

Conflicts of interest

The author declares no conflicts of interest.

Ethical disclosures

Protection of human and animal subjects. The authors declare that the procedures followed were in accordance with the regulations of the relevant clinical research ethics committee and with those of the Code of Ethics of the World Medical Association (Declaration of Helsinki).

Confidentiality of data. The authors declare that no patient data appear in this article. Furthermore, they have acknowledged and followed the recommendations as per the SAGER guidelines depending on the type and nature of the study.

Right to privacy and informed consent. The authors declare that no patient data appear in this article.

Use of artificial intelligence for generating text. The authors declare that they have not used any type of generative artificial intelligence for the writing of this manuscript nor for the creation of images, graphics, tables, or their corresponding captions.

References

1. Romas E, Martin TJ. Cytokines in the pathogenesis of osteoporosis. Osteoporos Int. 1997;7:47-53.
2. Eriksen EF, Hodgson SF, Eastell R, Rıggs BL, Cedel SL, O'Fallon WM. Cancellous bone remodeling in type İ (postmenopausal) osteoporosis: quantitative assessment of rates of formation, resorption, and bone loss at tissue and cellular levels. J Bone Miner Res. 1990;5:311-9.
3. Garnero P, Sornay-Rendu E, Chapuy MC, Delmas PD. Increased bone turnover in late postmenopausal women is a major determinant of osteoporosis. J Bone Miner Res. 1996;11:337-49.
4. Ralston SH. Analysis of gene expression in human bone biopsies by polymerase chain reaction: evidence for enhanced cytokine expression in postmenopausal osteoporosis. J Bone Miner Res. 2009;9:883-90.
5. Schett G, Gravallese E. Bone erosion in rheumatoid arthritis: mechanisms, diagnosis and treatment. Nat Rev Rheumatol. 2012;8:656-64.
6. Schwab I, Nimmerjahn F. Intravenous immunoglobulin therapy: how does IgG modulate the immune system? Nat Rev Immunol. 2013;13:176-89.
7. Anthony RM, Kobayashi T, Wermeling F, Ravetch JV. Intravenous gammaglobulin suppresses inflammation through a novel TH2 pathway. Nature. 2011;475:110-3.
8. Eminov E, Hortu I, Akman L, Erbas O, Yavasoglu A, Cirpan T. Exenatide preserves trabecular bone microarchitecture in experimental ovariectomized rat model. Arch Gynecol Obstet. 2018;297:1587-93.
9. Parfitt AM, Drezner MK, Glorieux FH, Kanis JA, Malluche H, Meunier PJ, et al. Bone histomorphometry: standardization of nomenclature, symbols, and units: report of the ASBMR histomorphometry nomenclature committee. J Bone Miner Res. 2009;2:595-610.
10. Kenkre J, Bassett J. The bone remodelling cycle. Ann Clin Biochem. 2018;55:308-27.
11. Albright F, Smith PH, Richardson AM. Postmenopausal osteoprosis: its clinical feature. JAMA. 1941;116:2465-74.
12. Riggs BL, Khosla S, Melton LJ 3rd. A unitary model for involutional osteoporosis: estrogen deficiency causes both type I and type II osteoporosis in postmenopausal women and contributes to bone loss in aging men. J Bone Miner Res. 1998;13:763-73.
13. Eastell R, Yergey AL, Vieira NE, Cedel SL, Kumar R, Riggs BL. Interrelationship among vitamin D metabolism, true calcium absorption, parathyroid function, and age in women: Evidence of an age-related intestinal resistance to 1,25-dihydroxyvitamin D action. J Bone Miner Res. 2009;6:125-32.
14. Arron JR, Choi Y. Bone versus immune system. Nature. 2000;408:535-6.
15. Aurora R. Confounding factors in the effect of gut microbiota on bone density. Rheumatology (Oxford). 2019;58:2089-90.
16. Das M, Cronin O, Keohane DM, Cormac EM, Nugent H, Nugent M, et al. Gut microbiota alterations associated with reduced bone mineral density in older adults. Rheumatology. 2019;58:2295-304.
17. Takayanagi H, Ogasawara K, Hida S, Chiba T, Murata S, Sato K, et al. T-cell-mediated regulation of osteoclastogenesis by signalling cross-talk between RANKL and IFN-γ. Nature. 2000;408:600-5.
18. Zhao B, Grimes SN, Li S, Hu X, Ivashkiv LB. TNF-induced osteoclastogenesis and inflammatory bone resorption are inhibited by transcription factor RBP-J. J Exp Med. 2012;209:319-34.
19. Moran CA, Neale Weitzmann M, Ofotokun I. Bone loss in HIV infection. Curr Treat Options Infect Dis. 2017;9:52-67.
20. Tang M, Lu L, Yu X. Interleukin-17A interweaves the skeletal and immune systems. Front Immunol. 2021;11:625034.

21. Dougall WC, Glaccum M, Charrier K, Rohrbach K, Brasel K, De Smedt T, et al. RANK is essential for osteoclast and lymph node development. Genes Dev. 1999;13:2412-24.
22. Yao Z, Getting SJ, Locke IC. Regulation of TNF-induced osteoclast differentiation. Cells. 2021;11:132.
23. Boyce BF, Xing L. Biology of RANK, RANKL, and osteoprotegerin. Arthritis Res Ther. 2007;9:S1.
24. Bucay N, Sarosi I, Dunstan CR, Morony S, Tarpley J, Capparelli C, et al. Osteoprotegerin-deficient mice develop early onset osteoporosis and arterial calcification. Genes Dev. 1998;12:1260-8.
25. Hofbauer LC. Clinical implications of the osteoprotegerin/RANKL/RANK system for bone and vascular diseases. JAMA. 2004;292:490-5.
26. Lee MJ, Lim E, Mun S, Bae S, Murata K, Ivashkiv LB, et al. Intravenous immunoglobulin (IVIG) attenuates TNF-induced pathologic bone resorption and suppresses osteoclastogenesis by inducing A20 expression. J Cell Physiol. 2016;231:449-58.
27. Kim KW, Kim HR, Kim BM, Won JY, Lee KA, Lee SH. Intravenous immunoglobulin controls Th17 cell-mediated osteoclastogenesis. Immune Netw. 2019;19:e27.
28. Krishnan V, Bryant HU, MacDougald OA. Regulation of bone mass by Wnt signaling. J Clin Invest. 2006;116:1202-9.
29. Baron R, Kneissel M. WNT signaling in bone homeostasis and disease: from human mutations to treatments. Nat Med. 2013;19:179-92.
30. Leucht P, Minear S, Ten Berge D, Nusse R, Helms JA. Translating insights from development into regenerative medicine: the function of Wnts in bone biology. Semin Cell Dev Biol. 2008;19:434-43.
31. van Dinther M, Zhang J, Weidauer SE, Boschert V, Muth EM, Knappik A, et al. Anti-sclerostin antibody inhibits internalization of sclerostin and sclerostin-mediated antagonism of Wnt/LRP6 signaling. PLoS One. 2013;8:e62295.
32. Cosman F, Crittenden DB, Adachi JD, Binkley N, Czerwinski E, Ferrari S, et al. Romosozumab treatment in postmenopausal women with osteoporosis. N Engl J Med. 2016;375:1532-43.
33. Asadipooya K, Weinstock A. Cardiovascular outcomes of romosozumab and protective role of alendronate. Arterioscler Thromb Vasc Biol. 2019;39:1343-50.
34. Karnam A, Rambabu N, Das M, Bou-Jaoudeh M, Delignat S, Käsermann F, et al. Therapeutic normal IgG intravenous immunoglobulin activates Wnt-β-catenin pathway in dendritic cells. Commun Biol. 2020;3:96.

ARTÍCULO ORIGINAL

Efecto de la manga gástrica laparoscópica vs. el *bypass* gástrico laparoscópico en Y de Roux sobre la pérdida ponderal a largo plazo en población mexicana con obesidad

Effect of laparoscopic gastric sleeve vs. laparoscopic gastric bypass in Roux-Y on long-term weight loss in obese mexican population

David Lomeli-Reyes[1], Gonzalo M. Torres-Villalobos[2,3], José M. Correa-Rovelo[2], Alejandro Díaz Girón-Gidi[2], Amado J. Athié-Athié[2] y Perla X. López-Almanza[1]*

[1]Posgrado de Cirugía General, Hospital Médica Sur, Facultad Mexicana de Medicina, Universidad La Salle; [2]Departamento de Cirugía General, Hospital Médica Sur; [3]Departamento de Cirugía Experimental, Instituto Nacional de Ciencias Médicas y Nutrición Salvador Zubirán. Ciudad de México, México

Resumen

Objetivo: *Comparar los resultados de pérdida de peso con los procedimientos MGL y BGYRL a largo plazo (hasta 5 años) en pacientes mexicanos con obesidad y comorbilidad asociada. Son dos los procedimientos quirúrgicos bariátricos más frecuentes en todo el mundo: la manga gástrica lapa-roscópica (MGL) y el bypass gástrico en Y de Roux laparoscópico (BGYRL); ambos como tratamiento para pérdida ponderal y remisión de la comorbilidad asociadas a la obesidad. Sin embargo, se desconocen los resultados de pérdida de peso a largo plazo en la población mexicana.* **Método:** *Cohorte retrospectiva, observacional, de pacientes con obesidad sometidos a MGL o BGYRL en el hospital privado Médica Sur, de Ciudad de México, en el período de 2013 a 2021. Se utilizó el análisis de variables instrumentales y diferencias de medias estandarizadas para calcular los desenlaces hasta 5 años posquirúrgicos en cinco consultas de seguimiento (S1-S5) a los 7 días, 2 meses, 6 meses, 10 meses y 2-5 años posquirúrgicos, para comparar los resultados de los grupos.* **Resultados:** *Se incluyeron 104 pacientes en dos grupos: 31 (30.09%) con MG y 73 (70.87%) con BGYR. En el último seguimiento (S5), el grupo de MG registró media de EW 9.61 kg, EW% 12.72% y EWL% 73.50%, y el grupo BGYR tuvo EW 10.1 kg, EW% 14.72% y EWL% 70.41%.* **Conclusiones:** *No se encontró diferencia significativa entre grupos para pérdida de EW a largo plazo (p = 0.082); sin embargo, hay una mayor disminución de pérdida ponderal en los pacientes con BGYRL a los 6-12 meses en comparación con los tratados con MGL.*

Palabras clave: *Cirugía bariátrica. Cirugía metabólica. Obesidad. Gastrectomía en manga. Bypass gástrico en Y de Roux.*

Abstract

Objective: *Compare the weight loss results between long-term procedures up to 5 years, after undergoing MGL and RYGB in Mexican patients with obesity and associated comorbidity. The most common bariatric surgical procedures worldwide are, laparoscopic gastric sleeve (MGL) and laparoscopic Roux-en-Y gastric bypass (RYGB), as a treatment for weight loss and remission of comorbidity associated with obesity; however, they are the long-term weight loss results in the Mexican population are unknown.* **Method:** *Retrospective, observational cohort of patients with obesity undergoing MGL or RYGB in a private*

***Correspondencia:**
David Lomeli-Reyes
E-mail: dlomelirey@gmail.com

Fecha de recepción: 02-11-2023
Fecha de aceptación: 16-03-2024
DOI: 10.24875/CIRU.23000545

Cir Cir. 2024;92(5):581-587
Contents available at PubMed
www.cirugiaycirujanos.com

hospital Medica Sur, in Mexico City, in the period from 2013 to 2021. Instrumental variables analysis and standardized mean differences were used to calculate outcomes up to 5 years at 5 follow-up visits (S1-S5), at 7 days, 2 months, 6 months, 10 months and 2-5 years after surgery, to compare results of the groups. **Results:** *104 patients were included in two groups: 31 (30.09%) with MG and 73 (70.87%) with RYGB. The last follow-up (S5), the MG group recorded a mean EW 9.61 kg, EW% 12.72% and EWL% 73.50%, and the RYGB group EW 10.1 kg, EW% 14.72% and EWL% 70.41%.* **Conclusions:** *No significant difference was found between groups for long-term EW loss (p = 0.082); however, there is a greater decrease in weight loss in RYGB at 6-12 months compared to MGL.*

Keywords: *Bariatric surgery. Metabolic surgery. Obesity. Sleeve gastrectomy. Roux-en-Y gastric bypass.*

Introducción

Desde hace décadas, la obesidad se ha convertido en un problema de salud público y continúan en aumento su incidencia global y su prevalencia, así como los costos de su tratamiento y repercusiones crónicas. La acumulación excesiva de grasa corporal (usualmente un 20% por encima del peso ideal) terminará afectando la salud y conducirá a un daño que pudiera no ser reversible y que a largo plazo tendría como desenlace múltiple comorbilidad asociada[1], así como un gran deterioro en la calidad de vida[2]. Se estima que, para el año 2030, el 57.8% de la población mundial (3.3 billones de personas) presentarán sobrepeso u obesidad[3]. Se ha demostrado una marcada mejoría en la calidad de vida relacionada con la salud en pacientes sometidos a cirugía bariátrica[4].

La cirugía bariátrica laparoscópica es actualmente la opción quirúrgica de elección como tratamiento para la obesidad y la comorbilidad relacionada con ella, siendo la manga gástrica (MG) el procedimiento más realizado hoy en día, sobre el *bypass* gástrico (BGYR), como procedimientos mayormente realizados en todo el mundo[5].

En el seguimiento posquirúrgico es de suma importancia presentar los datos bajo un sistema de reporte de resultados estandarizado, como el que incluye y comparte la American Society for Metabolic and Bariatric Surgery (ASMBS), donde se determina como seguimiento a largo plazo al menos 5 años posteriores al procedimiento, así como las variables del campo bariátrico como son el exceso de peso (EW) y el porcentaje de pérdida de exceso de peso (EWL%)[6].

En un metaanálisis sobre manga gástrica laparoscópica (MGL) vs. *bypass* gástrico en Y de Roux laparoscópico (BGYRL), en pacientes con índice de masa corporal (IMC) > 50 kg/m^2, se demostró que el BGYR logró una mejor pérdida de peso después de 6 a 12 meses y una mayor resolución de la dislipidemia después de 1 año de la intervención[7].

Del seguimiento observacional SLEEVEPASS a 10 años, siendo ensayo clínico aleatorizado multicéntrico, se encontró un 8.4% más de EWL% en BGYR en comparación con MG. La pérdida de peso en un metaanálisis de 18 estudios no encontró significancia estadística entre pérdida de EW con MG vs. BGYR[8]. En un seguimiento a 4 años, la MG tuvo menos reintervenciones, hospitalizaciones y complicaciones, menor gasto general en atención médica y menos mortalidad[9], que los pacientes sometidos a BGYR[10]. Sin embargo, a los 2 años, la cirugía de revisión fue más frecuente con MG.

Existen diversas clases y grados de obesidad: grave, mórbida o grado III. Uno de los estudios que mayor seguimiento presenta, de 12 años para el 90% de su población inicial, demuestra que los pacientes sometidos a BGYR sostuvieron una pérdida de peso promedio de 35 kg en el seguimiento, frente a 0 a 2.9 kg perdidos en el grupo no quirúrgico[11]. El BGYRL es más efectivo en general que la MGL, con remisión total de la comorbilidad asociada a la obesidad[12]. La morbimortalidad a corto plazo con ambos procedimientos tiene una incidencia muy baja; si se presenta regularmente sería con complicaciones menores a 6 meses[13].

El éxito de la cirugía bariátrica radica en la alta tasa de remisión completa o parcial de la comorbilidad asociada a la obesidad, previniendo las complicaciones, los efectos tardíos y las enfermedades relacionadas, y con una mejora en la calidad de vida[14], al lograr una pérdida ponderal sostenida[15]. Es de suma importancia conocer los beneficios y los resultados a largo plazo de los procedimientos bariátricos por el gran impacto que tienen sobre la morbimortalidad asociada con el síndrome metabólico y la obesidad[16].

El objetivo del presente estudio fue comparar la pérdida ponderal hasta por 5 años en cinco seguimientos posquirúrgicos de pacientes mexicanos tras someterse a los principales procedimientos bariátricos.

Método

Estudio retrospectivo, observacional, de pacientes con obesidad sometidos a cirugía bariátrica laparoscópica en el período comprendido de marzo de 2013 a septiembre de 2021 en el hospital de tercer nivel Médica Sur, en Ciudad de México. Se realizó un muestreo no probabilístico a conveniencia, por casos consecutivos en el periodo de estudio, de acuerdo con los criterios de inclusión. Se utilizaron expedientes clínicos físicos y electrónicos empleando G*Power de la Universidad Heinrich Heine Düsseldorf, para el cálculo del análisis de potencia estadística, con una población de pacientes de 120, siendo posoperados de MGL y BGYRL, con un intervalo de confianza del 95%, con un tamaño de muestra ideal de 89 pacientes.

Todos los pacientes recibieron tromboprofilaxis mecánica previamente al abordaje quirúrgico y tromboprofilaxis farmacológica hasta el egreso hospitalario.

Se incluyeron pacientes (Fig. 1) con obesidad mórbida/grado III (IMC > 40 kg/m^2) y obesidad grado II (IMC > 35 kg/m^2) más comorbilidad asociada a obesidad (hipertensión arterial sistémica, diabetes *mellitus* tipo 2, síndrome de apnea obstructiva del sueño, dislipidemia), con valoración preoperatoria cardiológica sin contraindicaciones. Se excluyeron los pacientes que fueron sometidos a cirugía de revisión (procedimiento secundario), que contaban con antecedente quirúrgico intrabdominal, y con obesidad de grado II sin comorbilidad. Las variables consideradas fueron la edad, el sexo, el IMC y la comorbilidad, y las variables a comparar fueron EW, porcentaje de exceso de peso (EW%) y EWL% entre grupos.

Se realizó seguimiento de los pacientes por medio de cinco consultas posteriores al procedimiento, correspondiendo al primer seguimiento una media de 10 días (n = 104), al segundo seguimiento una media de 72 días (n = 97), al tercer seguimiento una media de 235 días (n = 79), al cuarto seguimiento una media de 317 días (n = 55) y al quinto seguimiento una media de 669 días (n = 38), tanto para el grupo de MG como el de BGYR, y se compararon en cada seguimiento. Todos los resultados se muestran como media, con desviación estándar (DE) e intervalo de confianza del 95% (IC95%). Se obtuvieron medidas antropométricas y parámetros bariátricos posquirúrgicos en todas las consultas de seguimiento.

En cuanto a la técnica quirúrgica de BGYRL, se realizó *pouch* gástrico de 20 cm^3 con asa biliar de 100 cm y asa alimentaria de 150 cm, y sonda de calibración de 36 Fr, con uso de endoscopia transoperatoria. En cuanto a la MGL, se realizó con antrectomía hasta 1 cm lateral al ángulo de His y calibración con sonda de 40 Fr con uso de endoscopia transoperatoria.

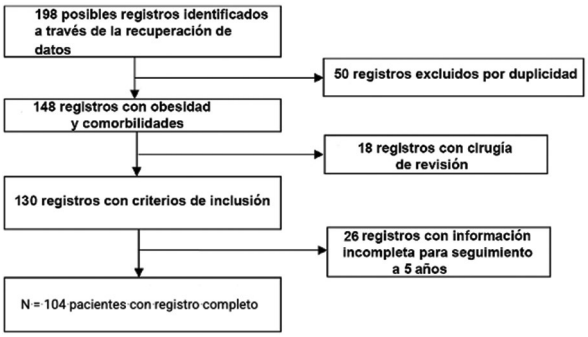

Figura 1. *Diagrama de flujo de la inclusión de pacientes.*

Para evitar los sesgos en la técnica quirúrgica, los procedimientos los habían realizado el mismo cirujano y el mismo equipo quirúrgico.

Para los análisis estadísticos se empleó el programa SPSS *(Statistical Package for the Social Sciences)* v.25.0. Las variables categóricas se presentan con frecuencias y porcentaje, y las numéricas con media y DE como medida de dispersión. Se realizaron la prueba de Kolmogórov-Smirnov para comprobar que los datos siguieran una distribución normal y la prueba de Levene para confirmar la homocedasticidad de los datos. Para el análisis de las variables numéricas en los diferentes grupos se utilizó una prueba t pareada para analizar los resultados dentro de un mismo grupo a lo largo del tiempo. Se empleó la prueba t de Student para explorar las diferencias entre grupos a lo largo del tiempo. Se utilizó un método de transformación de dos pasos en el caso de las variables que no se ajustaran a una distribución normal. Se consideran como significativos todos los valores con $p < 0.05$.

Resultados

Se incluyeron 104 pacientes, divididos en grupo BGYRL y grupo MGL. Los datos demográficos (Tabla 1) mostraron diferencia significativa entre grupos en las variables sexo femenino, presencia de dislipidemia y enfermedad por reflujo gastroesofágico ($p < 0.001$). En cuanto a EW, EW% y EWL%, no se obtuvo significancia estadística entre los grupos en los seguimientos registrados (Tabla 2).

Tabla 1. Características demográficas basales de la población incluida

Características	BGYRL (n = 73; 70.87%)	MGL (n = 31; 30.09%)	p
Mujeres	52 (71.2%)	16 (51.6%)	< 0.001
Hombres	21 (28.8%)	15 (48.4%)	0.472
Edad, años, media (DE)	43.6 (14.18)	43.25 (15.31)	0.914
Peso, kg, media (DE)	115.91 (26.71)	111.54 (22.02)	0.389
Talla, m, media (DE)	1.69 (0.19)	1.71 (0.16)	0.552
IMC, kg/m^2, media (DE)	43.03 (7.56)	39.24 (5.27)	0.004
Diabetes *mellitus* tipo II	22 (29.7)	11 (35.5)	0.136
Hipertensión arterial	21 (28.5)	11 (35.5)	0.171
Dislipidemia	25 (33.8)	5 (16.1)	< 0.001
SAOS	9 (12.2)	4 (12.9)	0.072
ERGE	3 (4.1)	0 (0.0)	< 0.001
Síndrome metabólico	49 (66.2)	21 (67.7)	0.057

BGYRL: *bypass* gástrico en Y de Roux laparoscópico; DE: desviación estándar; ERGE: enfermedad por reflujo gastroesofágico; IMC: índice de masa corporal; MGL: manga gástrica laparoscópica; SAOS: síndrome de apnea obstructiva del sueño.

Se demostró mayor pérdida de peso ponderal en BGYRL a los 6-12 meses en comparación con MGL; sin embargo, no se encontró diferencia significativa entre el peso, el exceso de peso ni la pérdida de exceso de peso en los seguimientos entre ambos grupos.

Con los datos antropométricos registrados durante el seguimento se graficaron las medias de peso (Fig. 2), EW (Fig. 3), EWL%, EW% (Fig. 4) e IMC, desde el inicio del protocolo prequirúrgico hasta el último seguimiento posquirúrgico (Fig. 5).

Discusión

Existen numerosos tratamientos para combatir la obesidad ante la creciente incidencia global, pero la cirugía bariátrica continúa siendo el método más efectivo. Se conoce que a largo plazo, en un período de hasta 10 años posquirúrgicos, el BGYRL es el procedimiento más efectivo; sin embargo, el más realizado en todo el mundo actualmente es la MGL, y de ahí la relevancia de generar resultados comparativos entre ambos procedimientos a largo plazo.

En diversos estudios se ha identificado una mayor pérdida de peso en los pacientes con BGYR en comparación con MG, siendo ensayos clínicos controlados, así como revisiones sistemáticas y metaanálisis.

Tabla 2. Seguimientos posquirúrgicos (S1-S5)

	S1 ($\bar{x}$ 10 días)			S2 ($\bar{x}$ 72 días)			S3 ($\bar{x}$ 235 días)			S4 ($\bar{x}$ 317 días)			S5 ($\bar{x}$ 669 días)		
	BGYRL	MGL	p	BGYRL	MGL	p	BGYRL	MGL	p	BGYRL	MGL	p	BGYRL	MGL	p
EW (kg)															
$\bar{x}$	40.44-48.75	32.28-40.79	0.083	31.94-40.43	26.09-33.05	0.185	23.35-32.83	16.76-25.98	0.417	16.98-25.66	13.32-17.62	0.141	10.13-17.03	9.61-14.75	0.082
DE	7.59	7.94		8.22	5.9		7.8	7.72		6.77	3.06		5.56	4.09	
IC 95%	6.99-9.06	7.43-9.58		6.06-11.01	4.72-9.21		7.39-11.56	6.74-11.68		6.69-10.66	2.45-6.16		4.85-8.94	3.49-7.77	
EW%															
$\bar{x}$	59.93-66.16	44.92-50.0	0.068	47.42-66.16	36.31-45.9	0.138	34.92-48.86	23.42-36.18	0.233	24.86-38.08	18.26-24.26	0.086	14.72-25.32	12.72-16.98	0.061
DE	6.85	4.02		16.02	7.69		11.81	10.23		10.85	4.4		8.43	3.81	
IC 95%	4.62-7.82	3.63-6.58		8.91-16.67	6.66-12.51		11.04-16.83	9.62-15.87		10.14-16.28	3.33-8.66		7.5-13.69	3.69-10.2	
EWL%															
$\bar{x}$	9.18-19.86	13.57-24.56	0.623	19.50-38.37	23.24- 39.90	0.401	38.66-56.84	39.63-65.32	0.883	53.06-70.89	67.75-78.98	0.129	14.72-70.41	12.72-73.50	0.161
DE	10.6	10.86		16.28	12.09		17.04	24.68		15.03	11.21		47.13	39.02	
IC 95%	7.5-13.84	6.63-15.34		15.41-22.32	12.07-21.24		13.65-22.7	18.20-33.16		14.07-21.58	10.92-20.14		42.06-69.30	33.93-87.61	

DE: desviación estándar; EW: exceso de peso; EW%: porcentaje de exceso de peso; EWL%: porcentaje de exceso de peso perdido; IC95%: intervalo de confianza del 95%.

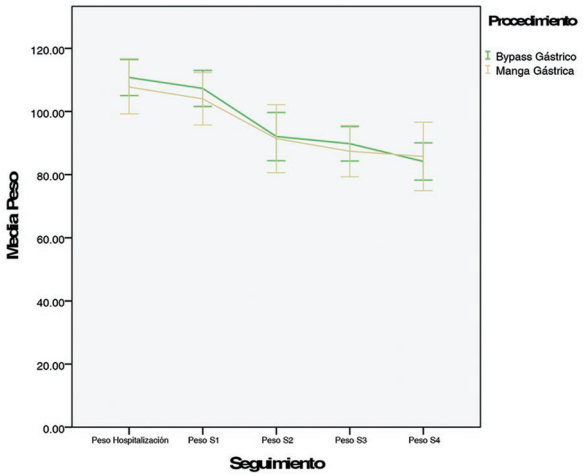

Figura 2. *Seguimiento posquirúrgico de la pérdida ponderal (media de peso).*

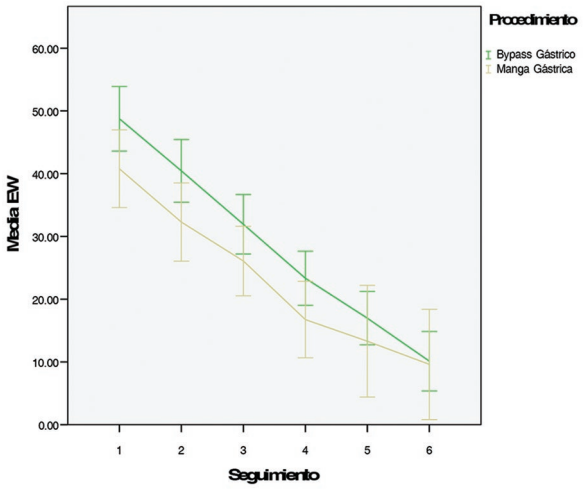

Figura 3. *Seguimiento posquirúrgico del exceso de peso.*

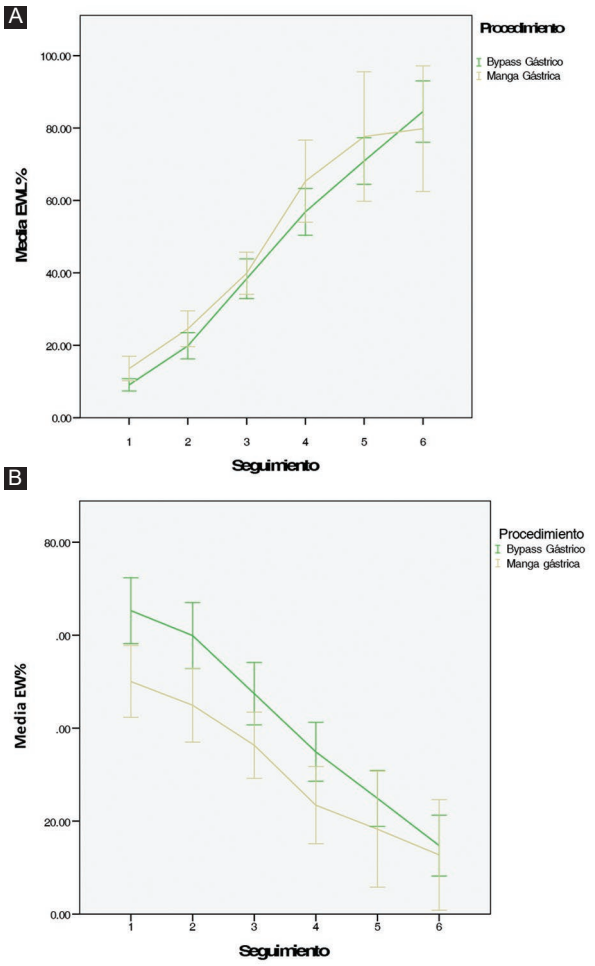

Figura 4. A: *seguimiento posquirúrgico del porcentaje de pérdida de exceso de peso (EWL%).* **B:** *seguimiento posquirúrgico del porcentaje de exceso de peso (EW%).*

En un metaanálisis[6] se identificó que no hay diferencia en la pérdida ponderal en el seguimiento > 5 años de ambos procedimientos.

En nuestro estudio, el número de procedimientos fue mayor para el grupo de BGYRL que para el de MGL, a diferencia de lo descrito en la literatura y la tendencia mundial actual, debido a los años iniciales en los que se sometió a los pacientes a cirugía bariátrica, siendo un volumen inicial mayor y posteriormente siguiendo la inversión de frecuencia, siendo ahora la MGL el procedimiento más realizado, sin variar en las técnicas quirúrgicas previamente descritas. Las variables demográficas fueron similares en ambos grupos, así como la comorbilidad, que no tuvieron diferencia significativa. Se presentaron tres complicaciones como sangrado posquirúrgico de la línea de grapeo en el grupo de MGL, resueltas en el mismo internamiento.

En nuestra cohorte retrospectiva se obtuvieron numerosas variables antropométricas en un seguimiento con cinco registros, con una media de 669 días posquirúrgicos en el último. La pérdida de peso fue similar en ambos grupos, pero se observó una mayor pérdida de peso en los primeros 6-12 meses posquirúrgicos en el grupo de BGYRL[6].

En el último seguimiento, en el grupo de MG se registró EW 9.61 kg, EW% 12.72% y EWL% 73.50%, y el grupo de BGYR se registró EW 10.1 kg, EW% 14.72% y EWL% 70.41%, sin diferencia significativa.

Se realizaron análisis entre los grupos en los diversos registros realizados, sin obtener una diferencia

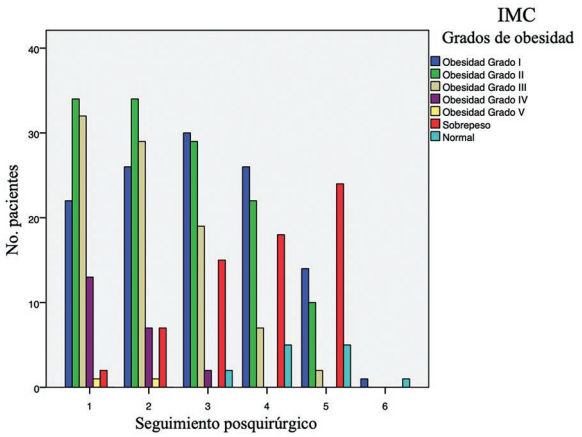

Figura 5. *Comparación del índice de masa corporal en el seguimiento posquirúrgico.*

estadística significativa en cuanto a la pérdida de peso ponderal en el seguimiento a 20 meses, con una tasa de seguimiento del 100%; posteriormente, la cantidad de pacientes que no continuaron con el seguimiento por consulta externa fue variable y con tendencia a abandonarlo.

Una de las debilidades de esta cohorte retrospectiva, por su naturaleza, es el seguimiento a largo plazo, con falta de información en los registros y, por tanto, con exclusión de pacientes. Además, el año de selección de los pacientes no fue el mismo y la cohorte no fue homogénea en ambos grupos; sin embargo, sí lo fue el seguimiento en cinco consultas posquirúrgicas. Es de suma relevancia destacar el distinto apego a las consultas de seguimiento por parte de los integrantes del estudio.

Conclusiones

La MG tuvo la misma pérdida de peso ponderal a largo plazo en población mexicana que el BGYR, siendo este último procedimiento más efectivo en la pérdida ponderal en los primeros 6-12 meses. No se encontró diferencia en cuanto a resolución de la comorbilidad entre los grupos, y tampoco hubo diferencia significativa en complicaciones y reintervenciones. Actualmente no existe una estrategia efectiva para pacientes posoperatorios a largo plazo, por lo que se deben implementar mejores medidas para el seguimiento de los pacientes con obesidad que se someten a cirugía bariátrica y así lograr un óptimo control y seguimiento posoperatorio para disponer de resultados más confiables a largo plazo, así como obtener una regulación en control de peso para mejorar la calidad de vida de los pacientes y continuar con la remisión total de la comorbilidad asociada a la obesidad.

Agradecimientos

Los autores agradecen a l Hospital Médica Sur, por ser mi nuestra casa, y a la Facultad Mexicana de Medicina de la Universidad La Salle, por el apoyo académico para la realización de este estudio.

Financiamiento

Los autores declaran no haber recibido financiamiento para este estudio.

Conflicto de intereses

Los autores declaran no tener conflicto de intereses.

Responsabilidades éticas

Protección de personas y animales. Los autores declaran que para esta investigación no se han realizado experimentos en seres humanos ni en animales.

Confidencialidad de los datos. Los autores declaran que han seguido los protocolos de su centro de trabajo sobre la publicación de datos de pacientes.

Derecho a la privacidad y consentimiento informado. Los autores han obtenido la aprobación del Comité de Ética para el análisis y publicación de datos clínicos obtenidos de forma rutinaria. El consentimiento informado de los pacientes no fue requerido por tratarse de un estudio observacional retrospectivo.

Uso de inteligencia artificial para generar textos. Los autores declaran que no han utilizado ningún tipo de inteligencia artificial generativa en la redacción de este manuscrito ni para la creación de figuras, gráficos, tablas o sus correspondientes pies o leyendas.

Bibliografía

1. Andersen JR, Aasprang A, Karlsen TI, Natvig GK, Våge V, Kolotkin RL. Health-related quality of life after bariatric surgery: a systematic review of prospective long-term studies. Surg Obes Relat Dis. 2015;11:466-73.
2. Grönroos S, Helmiö M, Juuti A, Tiusanen R, Hurme S, Löyttyniemi E, et al. Effect of laparoscopic sleeve gastrectomy vs Roux-en-Y gastric bypass on weight loss and quality of life at 7 years in patients with morbid obesity: the SLEEVEPASS randomized clinical trial. JAMA Surg. 2021;156:137-46.
3. Kelly T, Yang W, Chen CS, Reynolds K, He J. Global burden of obesity in 2005 and projections to 2030. Int J Obes. 2008;32:1431-7.
4. Agha M, Agha R. The rising prevalence of obesity: part A: impact on public health. Int J Surg Oncol (N Y). 2017;2:e17.
5. Kolotkin RL, Andersen JR. A systematic review of reviews: exploring the relationship between obesity, weight loss and health-related quality of life. Clin Obes. 2017;7:273-89.

6. Brethauer SA, Kim J, el Chaar M, Papasavas P, Eisenberg D, Rogers A, et al. Standardized outcomes reporting in metabolic and bariatric surgery. Surg Obes Relat Dis. 2015;11:489-506.
7. Blüher M. Obesity: global epidemiology and pathogenesis. Nat Rev Endocrinol. 2019;15:288-98.
8. Han Y, Jia Y, Wang H, Cao L, Zhao Y. Comparative analysis of weight loss and resolution of comorbidities between laparoscopic sleeve gastrectomy and Roux-en-Y gastric bypass: a systematic review and meta-analysis based on 18 studies. Int J Surg. 2020;76:101-10.
9. Howard R, Chao GF, Yang J, Thumma J, Chhabra K, Arterburn DE, et al. Comparative safety of sleeve gastrectomy and gastric bypass up to 5 years after surgery in patients with severe obesity. JAMA Surg. 2021;156:1160-9.
10. Courcoulas A, Coley RY, Clark JM, McBride CL, Cirelli E, McTigue K, et al. Interventions and operations 5 years after bariatric surgery in a cohort from the US National Patient-Centered Clinical Research Network Bariatric Study. JAMA Surg. 2020;155:194-204.
11. Adams TD, Davidson LE, Litwin SE, Kim J, Kolotkin RL, Nanjee MN, et al. Weight and metabolic outcomes 12 years after gastric bypass. N Engl J Med. 2017;377:1143-55.
12. Hu Z, Sun J, Li R, Wang Z, Ding H, Zhu T, et al. A comprehensive comparison of LRYGB and LSG in obese patients including the effects on QoL, comorbidities, weight loss, and complications: a systematic review and meta-analysis. Obes Surg. 2020;30: 819-27.
13. Helmiö M, Victorzon M, Ovaska J, Leivonen M, Juuti A, Peromaa-Haavisto P, et al. Comparison of short-term outcome of laparoscopic sleeve gastrectomy and gastric bypass in the treatment of morbid obesity: a prospective randomized controlled multicenter SLEEVE-PASS study with 6-month follow-up. Scand J Surg. 2014;103: 175-81.
14. Hachem A, Brennan L. Quality of life outcomes of bariatric surgery: a systematic review. Obes Surg. 2016;26:395-409.
15. Cooiman MI, Aarts EO, Janssen IMC, Hazebroek EJ, Berends FJ. Weight loss, remission of comorbidities, and quality of life after bariatric surgery in young adult patients. Obes Surg. 2019;29:1851-7.
16. Dawani S, Dawani A, Ahmed H, Rasul S. Effectiveness of metabolic weight loss surgery on type-II diabetes, hypertension and lipid disturbances: review of systemic analysis. Pak J Surg. 2018;34:84-8.

ORIGINAL ARTICLE

Finite element analysis evaluation of hypothetical alternative treatment scenarios for neglected developmental dysplasia of the hip

Evaluación mediante análisis de elementos finitos de escenarios hipotéticos de tratamiento alternativo para la displasia del desarrollo de cadera desatendida

Victor M. Araujo-Monsalvo[1,2], Marcos Martínez-Cruz[3], Lázaro Morales-Acosta[3], Víctor M. Domínguez-Hernández[1,2], Ramiro Cuevas-Olivo[4], Jesus A. Carrillo-Pelaes[3], Javier Perez-Orive[3,5], and Elisa Martinez-Coria[6]*

[1]Laboratorio de Biomecánica, Instituto Nacional de Rehabilitación "Luis Guillermo Ibarra Ibarra"; [2]Laboratorio Nacional Conahcyt en Biomecánica del Cuerpo Humano (LNC BiomeCH); [3]Facultad de Ingeniería, Universidad Nacional Autónoma de México; [4]Servicio de Ortopedia Pediátrica, Instituto Nacional de Rehabilitación "Luis Guillermo Ibarra Ibarra"; [5]Servicio de Neurociencias Básicas, Instituto Nacional de Rehabilitación "Luis Guillermo Ibarra Ibarra"; [6]Servicio de Tomografía Computada, Instituto Nacional de Rehabilitación "Luis Guillermo Ibarra Ibarra". Mexico City, Mexico

Abstract

Objective: *The study aimed to evaluate three different degrees of correction in the surgical treatment of neglected developmental dysplasia of the hip (DDH) using finite element models based on computed tomography.* **Method:** *Three tridimensional FEA models of hypothetical post-operative (PO) outcomes were developed, based on three tridimensional CT of a pediatric patient diagnosed with luxated neglected DDH: One with the acetabular index of the contralateral hip (CLAT); another based on a theoretical Bombelli biomechanical model (BMB); and another recreating the patient's actual PO.* **Results:** *The stresses in the affected hip were greater than those in the unaffected hip. CLAT showed the greatest stress and the smallest loading zone (LZ). In contrast, BMB showed the smallest stress and the biggest LZs.* **Conclusions:** *The approach based on the BMB gave the best results in terms of the distribution of the stresses over the hip, whereas the worst was CLAT. Qualitatively, estimating the stability and range of movement of the hip, the PO case was considered the best.*

Keywords: *Neglected developmental dysplasia of the hip. Dega acetabuloplasty. Finite element analysis. Biomechanics.*

Resumen

Objetivo: *Evaluar tres diferentes grados de corrección en el tratamiento quirúrgico de la displasia del desarrollo de la cadera (DDH) inveterada mediante modelos de elementos finitos basados en tomografía computarizada.* **Método:** *Se desarrollaron tres modelos tridimensionales de elementos finitos de resultados posoperatorios hipotéticos, basados en tres tomografías computarizadas tridimensionales de un paciente pediátrico diagnosticado de displasia del desarrollo de la cadera luxada inveterada: uno con el índice acetabular de la cadera contralateral (CLAT), otro basado en un modelo biomecánico teórico de Bombelli (BMB) y otro recreando el posoperatorio real (PO) del paciente.* **Resultados***: Los esfuerzos en la cadera afectada fueron mayores que en la cadera no afectada. El CLAT mostró el mayor esfuerzo y la menor zona de carga. Por el contrario, el BMB mostró el menor esfuerzo y las mayores zonas de carga.* **Conclusiones:** *La propuesta basada en el BMB dio los*

Correspondence:
Víctor M. Domínguez-Hernández
E-mail: vm_dominguez@yahoo.com.mx

Date of reception: 13-03-2023
Date of acceptance: 26-10-2023
DOI: 10.24875/CIRU.23000137

Cir Cir. 2024;92(5):588-593
Contents available at PubMed
www.cirugiaycirujanos.com

mejores resultados en cuanto a la distribución de los esfuerzos sobre la cadera, mientras que la peor fue el CLAT. Cualitativamente, estimando la estabilidad y la amplitud de movimiento de la cadera, el caso PO se consideró el mejor.

Palabras clave: *Displasia del desarrollo de la cadera inveterada. Acetabuloplastía tipo Dega. Análisis por elementos finitos. Biomecánica.*

Introduction

Developmental dysplasia of the hip (DDH) is one of the main afflictions in pediatric orthopedics and a common cause of disability[1,2]. Diagnosis and treatment during the first 9 months of age generally result in a very positive prognosis[3].

Neglected cases are those in which the condition has remained undiagnosed and untreated for a very long time, even years, which unfortunately is still prevalent in mid- and low-income countries. In such cases, the severity of the dysplasia is greater, the treatment is more aggressive, and the outcome is less predictable[4]. The consequences of neglected DDH include early joint degeneration during adulthood[5,6]. The relationship between clinical and biomechanical parameters is currently being investigated to predict the long-term performance of a DDH-affected hip[7-10].

Neglected DDH is treated with open reduction, pelvic, and femoral osteotomies to correct the characteristic deformities of the condition (complete luxation, shallow and steep acetabulum, femoral anteversion, and valgus) and to restore congruence and function to the joint. For a better outcome, the hip should be reduced and well-oriented with conservative treatment before the surgical procedure, but in neglected cases, the surgeon cannot wait for this pre-requisite, so the reduction and reorientation are carried out in a single surgical procedure. Pediatric pelvic osteotomies represent one of the most technically challenging surgeries. Despite this difficulty, on many occasions, the surgical planning and clinical follow-up are carried out using plain radiographies (RX), due to its low cost and radiation dose, compared to other types of imaging studies, such as computed tomography (CT)[3,11,12].

However, as some adult and older children hip dysplasia studies have shown[7,13], the 3D models built from CT images, and its integration with biomechanical finite element analysis (FEA), make this technology a better alternative to conventional RX for the study, planning, and evaluation of treatment of the dysplastic hip, regardless of the increased cost and radiation dose[3,12]. Although the majority of examples in the literature are about adult dysplasia, the treatment for pediatric neglected DDH patients could also benefit from the CT capacities for visualization and FEA integration.

Surgical planning assistance by means of biomechanical models could improve the neglected DDH treatment effectiveness, because it could allow predicting the behavior of the hip under different possible osteotomy approaches, each leading to a distinct post-operative (PO) outcome, and then choosing the scenario that offers the best biomechanical performance.

There exist different criteria for the ideal approach to dysplastic hip treatment. One criterion establishes as a PO goal an acetabular index (AI) value normal for the patient's age; for a unilateral DDH case, the contralateral control hip should have such a normal AI value (CLAT approach). In contrast, another criterion establishes that, for a unilateral, completely dislocated DDH case, the best option is to produce a configuration that avoids a re-dislocation, even if that implies an over-correction, this option corresponds to the real post-operatory outcome with the patient (PO)[4]. A third criterion developed by Bombelli and based on 2D biomechanical models, suggested that the best hip joint configuration is one that has a horizontal loading zone (LZ) in the acetabular roof, right above the femoral head (Bombelli biomechanical model [BMB])[14]. Each of these criteria is optimized by following each of the three different approaches (CLAT, PO, and BMB, respectively).

The objective of this study is to develop CT-based biomechanical finite element models from a single patient to determine which osteotomy approach, each optimizing one of the aforementioned criteria, is the one that produces the best outcome, in terms of the mechanical stresses and LZs over the joint surfaces, as well as how this relates with clinical practice.

Methods

This research work was approved by the research committee of our institute. The patient's parents signed the informed consent form.

The modeling was based on a 6-year-old female patient, diagnosed with unilateral neglected luxated

DDH on the right hip, and with no record of previous treatment. The contralateral hip was considered the control and the dislocated one was the case. A CT scan (LighSpeed® VCT 64, General Electric, Fairfield, CT, USA) of the patient was obtained with 0.625 mm slices from the vertebral body of L5 to the proximal third section of the femur. The modeling was based on this CT scan, and institutional guidelines for patient data protection and privacy were followed. The patient presented a complete hip dislocation and hip dysplasia grade IV for the DDH IHDI classification[15], with AI values of 43° and 28° on the affected and non-affected side, respectively, as well as severe deformity of the acetabulum and proximal femur. One month after the CT scan, the patient was treated with one-stage open reduction and a Dega acetabuloplasty, and a derotational and shortening femoral osteotomy, postoperatively immobilized with a fiberglass pelvic cast for 12 weeks and then managed with physical therapy and rehabilitation for a further 12 weeks. Diagnosis, CT scan, and treatment were performed in our institution following standard clinical practice.

3D models of the pelvis and femur were built after the segmentation of the CT images. Posteriorly, those 3D models were used to generate tetrahedral meshes. Segmentation and reconstruction of the models were done using the InVesalius 3.1.1 (CTI Renato Archer, Campinas, SP, Brazil) and Autodesk Meshmixer (Autodesk, Inc., San Rafael, CA, USA).

Three hypothetical models were generated: CLAT, with the same AI value (28°) that in the contralateral hip; BMB, with an AI value of 0°, based on the theoretical model of Bombelli; and PO, that reproduces the post-operatory outcome (AI = 7°), based on an AP RX projection taken at the end of the surgery (Fig. 1).

Since the starting position was a complete dislocation, the femur 3D model was translated and rotated to simulate the femoral derotational and shortening osteotomy. In all the scenarios, the inter-articular space was set to be the same as the one measured in the unaffected hip.

To transmit the loads during the FEA, similarly to the articular cartilage in the actual joints, interface volumes between the articular surfaces were generated. The generated meshes were composed of around 270,000 ten-noded tetrahedral elements (TET10). FEA was performed using ANSYS Mechanical APDL v14.5 (ANSYS Inc., Canonsburg, PA, USA).

All bones and interface volumes were considered to be linear elastic homogeneous isotropic solids, described by these mechanical properties: 17,000 MPa and 0.3 for the elastic modulus and Poisson coefficient of the bone, respectively; and 15 MPa and 0.45 for the elastic modulus and Poisson coefficient of the cartilage, respectively[13].

The finite element model was linear static, simulating a biped stance, applying the following loading conditions: 56% of the patient's body weight, in the vertical direction, over the S1 superior vertebral body surface, representing the body weight above the waistline; 63% of the patient's body weight over the greater trochanter and ilium wing (insertion zones of the abductor muscles), with force directions resembling the abductor muscle fibers; total movement restriction in the distal end of the proximal femur; rotational restriction on the pelvic bone. Loading conditions were formulated as previously described by other researchers[13,16].

Maximum von Mises stresses (SMAX) and LZs over the articular surfaces of the acetabular roofs were registered. A LZ was arbitrarily defined as that in which the top 20% of the stresses were concentrated. For clarity, the LZ is presented as a percentage of the total articular surface. Quantitative and qualitative comparisons of the stress distributions in the acetabular roofs were made. As is standard practice, we considered that the lesser the SMAX the better, and the greater the LZ the better. The qualitative assessment involved the evaluation of joint congruency, location of stress peak values and bone protuberances, and an impression of dislocation risk by the medical team.

Results

In the three analyzed alternatives, the stresses in the affected hip were greater than those in the unaffected hip. Stress magnitude and distribution in the control hip (SMAX of 30.3 MPa, and LZ of 20.7% of the total articular surface in the acetabular roof) did not seem affected by the configuration of the affected osteotomy-treated hip. Stress magnitude and distribution in the affected hip, however, did change considerably between scenarios (Fig. 2).

CLAT showed the greatest SMAX, 65.45 MPa, and an LZ of 9.9%, the smallest found (Figs. 3 and 4). Qualitatively, the instability of the setup and the disposition to redislocation were noticeable. Furthermore, the stresses are concentrated on the anterior flank, thereby increasing the risk of arthrosis.

In contrast, BMB showed the smallest SMAX of the affected hips, 33.99 MPa, and the biggest LZ, 62.7%. However, this scenario also showed a clear

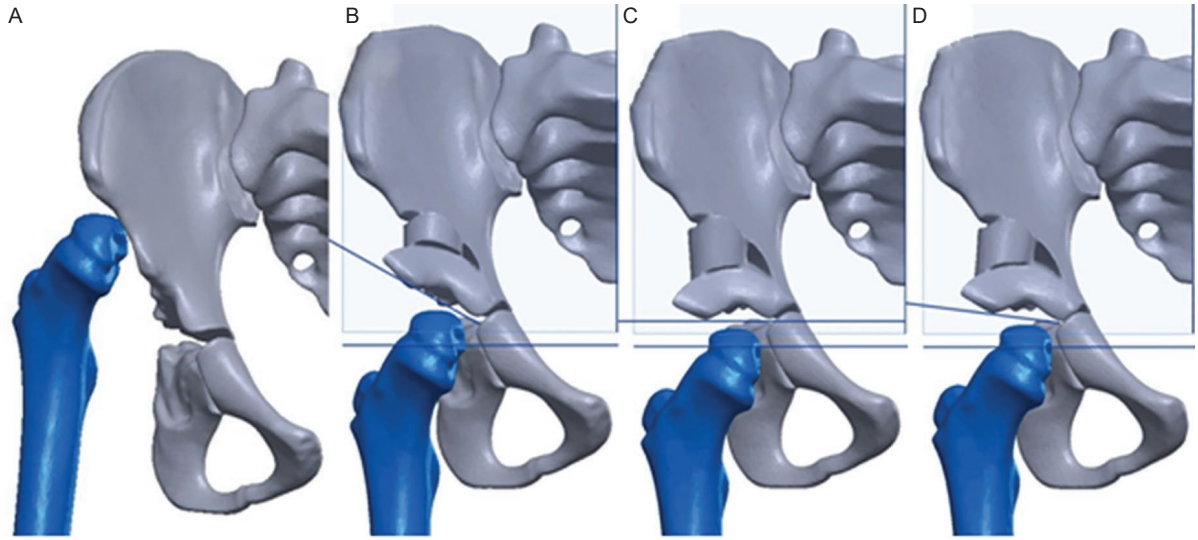

Figure 1. *CT 3D models of the neglected developmental dysplasia of the hip-affected hip.* **A:** *pre-operatory state showing an IHDI grade IV dysplasia.* **B:** *CLAT with acetabular index (AI) = 28°.* **C:** *bombelli biomechanical model scenario with AI = 0°.* **D:** *PO with AI = 7°.*

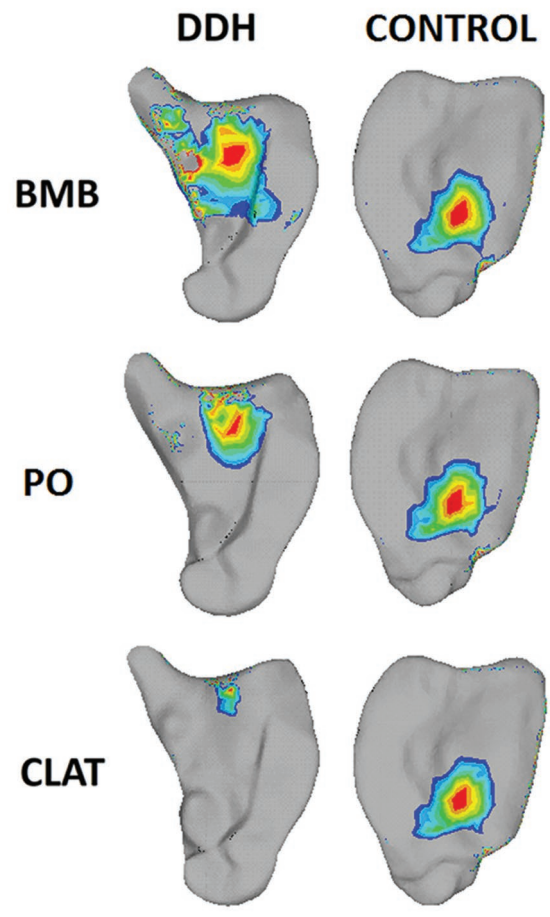

Figure 2. *Inferior view of the acetabular roofs showing loading zones on the simulated surgery analyzed both on control and affected hips. The scale was adjusted to show only the zones with von Mises stresses greater or equal to 80% of the maximum of each case.*

over-correction and limb shortening. On the contrary, it shows the best load distribution by concentrating the stresses in the central portion.

PO, a SMAX of 41.43 MPa and a LZ of 36% were found. It showed an apparent over-correction as well. In addition, the leading edge is tilted forward, which exerts excessive pressure on the femoral head.

Discussion

Based on our results, CLAT is the worst of the alternatives given that it showed considerable stress concentration on the articular surface and setup instability. Those characteristics, in an actual hip joint, are related to immediate post-operatory complications, such as avascular necrosis and re-dislocations[4,13,14].

Findings in CLAT also suggest that the AI, used on its own to evaluate a DDH-affected hip, could lead to an overestimation of the actual joint state. The AI offers only a measure of the steepness of the acetabular roof, and indirectly, assuming normal morphology, a measure of acetabular coverage or stability. Auxiliary radiological measurements, such as the Center-Edge or Wiberg angle, could help obtain a better estimate of acetabular coverage with RX images. Nevertheless, being plane projection measurements, it would be difficult to evaluate acetabular concavity, a determining characteristic of hip stability. Concavity is one of the most important reasons why the unaffected hip can be stable whereas the affected hip in the CLAT scenario is not, even if both hips have the same AI.

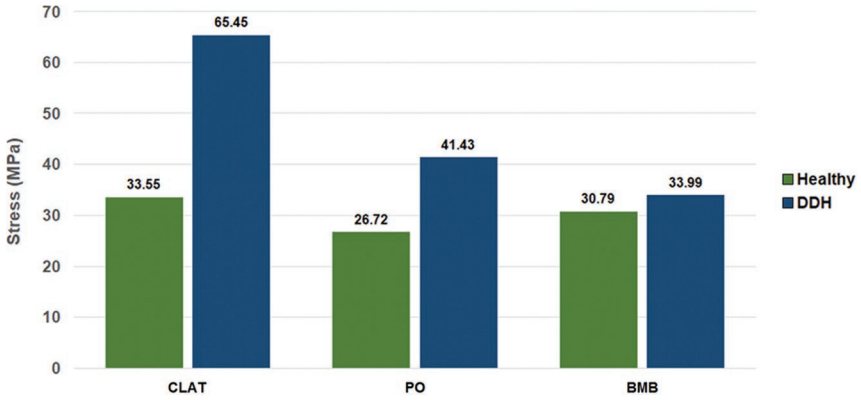

Figure 3. *Maximum stresses in the acetabular roof of control and developmental dysplasia of the hip affected hips, in the surgical simulation scenarios.*

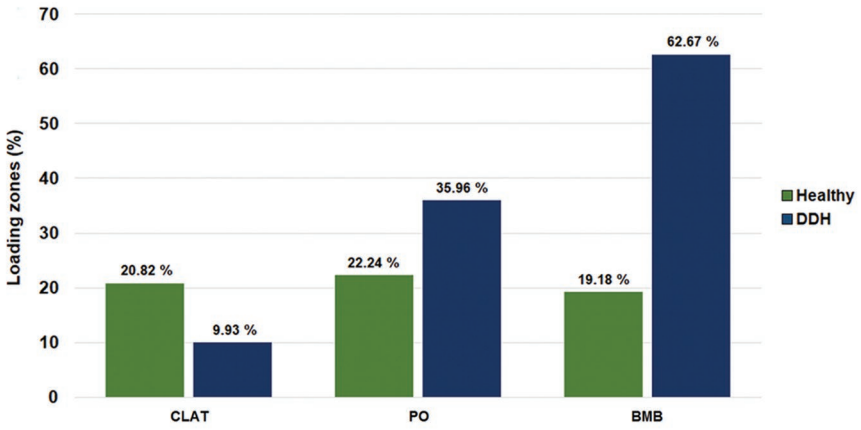

Figure 4. *Loading zones in the acetabular roof of control and developmental dysplasia of the hip affected hips, in terms of percentage of the total articular surface, on the surgical simulation scenarios.*

When comparing BMB and PO, it is clear that the quantitative results of BMB are better than those of PO, as suggested by Bombelli's theoretical point of view, both in terms of maximum stresses and in terms of LZs. Qualitatively, it can be seen that the results also favor BMB, given that the load is concentrated in the central region of the hip with DDH, as opposed to PO which locates the LZs at the anterior border, with the risk of redislocation. However, the overcorrection observed in BMB could have adverse consequences for the function of the hip joint, since its range of motion would be limited, producing a discrepancy in the length of the limb and possibly an impingement.

A limitation of this study is that the models do not consider the effect of bone remodeling. In an actual patient, the hip is immobilized for at least 3 months after surgery, before being allowed to be loaded with the body weight, and only then, the bone remodeling process is mechanically stimulated. Bone remodeling and resorption could generate concavity in shallow acetabular roofs and reduce bone protuberances that limit movement. It would be beneficial to perform a rigorous PO follow-up of neglected DDH patients to find out how the correction level achieved in the surgery and the bone remodeling relate to hip joint evolution in the short, medium, and long terms. Neglected DDH produces deformities that make each case unique, and so, it makes its treatment unique as well. Subsequent studies analogous to this one exploring additional patients would offer additional data.

The use of models similar to the ones used in this study could help achieve an optimal correction degree that maximizes stress distribution on joint surfaces and minimizes over-correction and its

consequences. Clinical implementation of such models could improve treatment effectiveness and patient life quality, and potentially delay or avoid adulthood DDH sequelae.

In conclusion, even though obtained biomechanical results seem to indicate that a hip would have a better stress distribution as the acetabular roof gets more horizontal, the morphologic characteristics of the hip should not be dismissed, as these factors could indicate overcorrections and its harmful consequences: impingement, limb length discrepancy, and limited range of movement.

Caution must be taken when using the AI to plan and evaluate treatment for neglected DDH; if auxiliary measurements and images, such as the Center-Edge angle or 3D visualizations, were not to be available or used to assess acetabular coverage and joint congruency, the sole AI value could be overestimating the actual state of the hip joint.

More studies are needed to determine the ideal correction degree for the surgical treatment of neglected DDH, to work out the best means to reproduce virtual surgery scenarios in the actual surgery, and to investigate the long-term consequences of the treatment and its planning procedures.

Acknowledgments

The authors gratefully acknowledge the work done by technician Martín Luna Méndez from the CT and Ultrasound Department, at the Instituto Nacional de Rehabilitación “Luis Guillermo Ibarra Ibarra”.

Funding

There were no funding sources.

Conflicts of interest

The authors declare no conflicts of interest related to the present manuscript.

Ethical disclosures

Protection of human and animal subjects. The authors declare that the procedures followed were in accordance with the regulations of the relevant clinical research ethics committee and with those of the Code of Ethics of the World Medical Association (Declaration of Helsinki).

Confidentiality of data. The authors declare that they have followed the protocols of their work center on the publication of patient data.

Right to privacy and informed consent. The authors have obtained the written informed consent of the patients or subjects mentioned in the article. The corresponding author is in possession of this document.

References

1. Weinstein SL, Mubarak SJ, Wenger DR. Developmental hip dysplasia and dislocation: part I. Instr Course Lect. 2004;53:523-30.
2. Dezateux C, Rosendahl K. Developmental dysplasia of the hip. Lancet. 2007;369:1541-52.
3. Grissom L, Harcke HT, Thacker M. Imaging in the surgical management of developmental dislocation of the hip. Clin Orthop Relat Res. 2008;466:791-801.
4. El-Tayeby HM. One-stage hip reconstruction in late neglected developmental dysplasia of the hip presenting in children above 8 years of age. J Child Orthop. 2009;3:11-20.
5. Terjesen T. Residual hip dysplasia as a risk factor for osteoarthritis in 45 years follow-up of late-detected hip dislocation. J Child Orthop. 2011;5:425-31.
6. Alcobía Díaz B, Luque Pérez R, García Bullón I, Moro Rodríguez LE, López-Durán Stern L. Long-term clinical and radiological outcomes in a serie of 26 cases of symptomatic adult developmental dysplasia of the hip managed with Bernese periacetabular osteotomy. Rev Esp Cir Ortop Traumatol. 2015;59:421-8.
7. Wang X, Peng J, Li D, Zhang L, Wang H, Jiang L, et al. Does the optimal position of the acetabular fragment should be within the radiological normal range for all developmental dysplasia of the hip? A patient-specific finite element analysis. J Orthop Surg Res. 2016;11:109.
8. Lee KJ, Park SJ, Lee SJ, Naito M, Kwon SY. Biomechanical study on the efficacy of the periacetabular osteotomy using patient-specific finite element analysis. Int J Precis Eng Manuf. 2015;16:823-9.
9. Ike H, Inaba Y, Kobayashi N, Yukizawa Y, Hirata Y, Tomioka M, et al. Effects of rotational acetabular osteotomy on the mechanical stress within the hip joint in patients with developmental dysplasia of the hip: a subject-specific finite element analysis. Bone Joint J. 2015;97-B:492-7.
10. Huayamave V, Rose C, Serra S, Jones B, Divo E, Moslehy F, et al. A patient-specific model of the biomechanics of hip reduction for neonatal developmental dysplasia of the hip: investigation of strategies for low to severe grades of developmental dysplasia of the hip. J Biomech. 2015;48:2026-33.
11. Clohisy JC, Carlisle JC, Trousdale R, Kim YJ, Beaule PE, Morgan P, et al. Radiographic evaluation of the hip has limited reliability. Clin Orthop Relat Res. 2009;467:666-75.
12. Pearce MS, Salotti JA, Little MP, McHugh K, Lee C, Kim KP, et al. Radiation exposure from CT scans in childhood and subsequent risk of leukaemia and brain tumours: a retrospective cohort study. Lancet. 2012;380:499-505.
13. Zhao X, Yan YB, Cao PC, Ma YS, Wu ZX, Zhang Y, et al. Surgical results of developmental dysplasia of the hip in older children based on using three-dimensional computed tomography. Surg Res. 2014;189:268-73.
14. Bombelli R. Osteoarthritis of the Hip. Berlin: Springer-Verlag; 1983.
15. Narayanan U, Mulpuri K, Sankar WN, Clarke NM, Hosalkar H, Price CT, et al. Reliability of a new radiographic classification for developmental dysplasia of the hip. J Pediatr Orthop. 2015;35:478-84.
16. De Leva P. Adjustments to zatsiorsky-seluyanov’s segment inertia parameters. J Biomech. 1996;29:1223-30.

ARTÍCULO ORIGINAL

Tabla de vida para derechohabientes del Instituto de Seguridad y Servicios Sociales de los Trabajadores del Estado (ISSSTE), México 2021

Table of life for beneficiaries of the Institute of Security and Social Services of State Workers (ISSSTE), Mexico 2021

*Judith E García-de-Alba-Verduzco[1], Javier E. García-de-Alba-Verduzco[2], Ramiro López-Elizalde[1] y Javier E. García-de-Alba-García[3]**

[1]Subdirección Médica, Instituto de Seguridad y Servicios Sociales de los Trabajadores del Estado, Ciudad de México; [2]Centro Universitario de Ciencias Biológicas, Universidad de Guadalajara, Guadalajara, Jalisco; [3]Cátedra García de Alba-Salcedo, Zapopan, Jalisco. México

Resumen

Objetivo: *Determinar la esperanza de vida en la población amparada del Instituto de Seguridad y Servicios Sociales de los Trabajadores del Estado en México para 2021.* **Método:** *Se utilizó el método abreviado de Reed-Merrel para calcular la esperanza de vida en grupos quinquenales de edad.* **Resultados:** *Para 2021, la esperanza de vida general fue de 79.51 años; de 81.40 años y 78.91 años para mujeres y para hombres, respectivamente.* **Conclusiones:** *La esperanza de vida calculada no presentó reducción después de la pandemia de COVID-19 para la población de empleados federales de México en 2021.*

Palabras clave: *Esperanza de vida. ISSSTE. México.*

Abstract

Objective: *Determine the life expectancy in the covered population of the Institute of Security and Social Services of State Workers in México for 2021.* **Method:** *We used the abrogated method from Reed-Merrel, for calculate the life expectancy in age groups.* **Results:** *By 2021, life expectancy general was 79.51 years; 81.40 years and 78.91 years for woman and men, respectively.* **Conclusions:** *The calculated life expectancy not show a reduction in the population of federal and State employees in Mexico.*

Keywords: *Life expectancy. ISSSTE. Mexico.*

Correspondencia:
Javier E. García-de-Alba-García
E-mail: javiereduardogarciadealba@gmail.com

Fecha de recepción: 21-06-2023
Fecha de aceptación: 26-10-2023
DOI: 10.24875/CIRU.23000321

Cir Cir. 2024;92(5):594-602
Contents available at PubMed
www.cirugiaycirujanos.com

Introducción

Contexto histórico

Dos hitos históricos de orden bioestadístico-epidemiológico en salud pública constituyen los antecedentes de las tablas de vida.

El primero es el trabajo pionero que el capitán John Graunt publicó en 1662 como *Natural and Political Observations Mentioned in a Following Index, and Made Upon the Bills of Mortality,* base para el cálculo de las tasas de mortalidad tal como las conocemos actualmente (defunciones de una población en un periodo de tiempo/población a la mitad de ese periodo de tiempo), por una constante poblacional (de 100, 1000 o 10,000) habitantes en ese tiempo y lugar. El trabajo se fundamentó en los registros parroquiales semanales de defunciones y de bautizos habidos de la ciudad de Londres, institucionalizados por la epidemia de la peste bubónica en Inglaterra.

Las defunciones solo se estimaban de forma genérica señalando el lugar y el tiempo, vgr.: «La viruela arribó a la Nueva España por el puerto de Veracruz en la primavera o verano de 1779 y se fue extendiendo a lo largo de los caminos entre los pueblos que conducían a Puebla y la ciudad de México, que fue alcanzada en el otoño de 1779, cuando se registraron al menos 45,000 casos en el último cuatrimestre del año, con más de 14,000 víctimas fatales. Desde la ciudad de México se propagó al occidente, llegando a Toluca en diciembre, a Michoacán al iniciar 1780 y a la Nueva Galicia en febrero, alcanzando la ciudad de Guadalajara, donde fallecieron 1268 habitantes entre marzo y mayo»[1].

El otro hito, basado en el cálculo matemático, teniendo como acicate el desarrollo mercantilista europeo, lo logró Edmund Halley (con apoyo de Godofredo Leibnitz y la recomendación de la Royal Society de Inglaterra) al estudiar los registros de nacimientos y muertes de Breslau (ciudad ubicada al suroeste de Polonia), entre 1687 y 1691. Sus resultados fueron publicados en una de las primeras revistas científicas europeas, *Philosophical Transactions,* en el año 1693, bajo el título *An Estimate of the Degrees of the Mortality of Mankind, Drawn from Curious Tables of the Births and Funerals at the City of Breslaw; with an Attempt to Ascertain the Price of Annuities upon Lives* («Una estimación de los grados de mortalidad humana, extraídos de las tablas de nacimiento y funerales en la ciudad de Breslavia; con un intento de determinar el precio de las rentas vitalicias»), que indudablemente iba dirigido a las compañías de seguros de ese tiempo para que calculasen el valor de las primas a cobrar y las pensiones individuales y mancomunadas a pagar en función de la edad de los adquirientes[2].

Como se puede colegir, el desarrollo del cálculo de las tablas de vida ha pasado del ámbito privado (cálculo de riesgos económicos) al público (cálculo de situaciones sanitarias), y desde el trabajo manual, en las llamadas «sábanas estadísticas», hasta los programas computarizados como Epidat, elaborado y distribuido gratuitamente por la Organización Panamericana de la Salud y la Consejería de Sanidad de la Junta de Galicia (España)[3].

Ahora, la tabla de vida es una tecnología de uso común, y de su aplicación destaca que actualmente, entre las naciones del mundo, las mujeres japonesas tienen la esperanza de vida más alta al nacer, por encima de los 87 años. Sin embargo, cabe señalar que hace más de 120 años, en 1840, el récord estaba en manos de las mujeres suecas, cuyo promedio de vida se estimaba en 46 años[4].

Contexto aplicativo

Las tablas de vida han ampliado la estrecha métrica de la mortalidad en edades tempranas de la vida, al captar el curso de vida de una población, al señalarnos el promedio de muerte de dicha población, convirtiéndose la esperanza de vida en una clave de la salud poblacional. Así, entonces, en el mundo premoderno de 1800, la esperanza de vida frisaba en los 30 años, y actualmente ningún país del mundo presenta tal expectativa de vida. Sin embargo, aunque la esperanza de vida actual se ha casi triplicado, la desigualdad entre los países sigue siendo importante; por ejemplo, antes de la pandemia en 2019, la República Centroafricana registraba 53 años, mientras que Japón tenía 30 años más[5].

Antecedentes técnicos

La tabla de vida es un constructo metodológico estadístico útil para analizar, mediante los datos de mortalidad y de la población respectiva, la probabilidad de sobrevivir de una población específica en un entorno ambiental de tiempo y espacio particularizados, donde se interactúa con ciertos agentes cuya

dinámica epidemiológica plantea la salud-enfermedad como proceso grupal.

La tabla de vida también se considera como una medida bioestadística de muerte prematura en una población; o sea, la edad promedio de muerte en la misma colectividad, cuyos resultados de sobrevida se ven obviamente mermados principalmente por las defunciones infantiles y preescolares.

Por su construcción, se consideran dos tipos de tablas de vida:

- De periodos estáticos: muestran la probabilidad actual de muerte año por año de edad o por edades agrupadas.
- De cohortes: muestran la probabilidad de muerte de las personas de una cohorte determinada (por ejemplo, el año de nacimiento) a lo largo de su vida.

Por su agrupación etárea, se tienen dos formas de tablas de vida:

- Año por año: desde el nacimiento hasta la última edad conocida.
- Abreviadas: los valores de los años de la tabla de vida se presentan acomodados por ciertos grupos de edad, en lugar de registrarse para cada año de edad. Por ejemplo, según las divisiones funcionales de la vida humana: menores de 1 año, de 1 a 4 años, de 5 a 9 años, y así de 5 en 5 años hasta 85 y más años.

En este caso usamos tablas de vida estáticas, aplicando el método de abreviado de Reed y Merrell, publicado en la antigua *American Journal of Hygiene* (actualmente *American Journal of Epidemiology*) en 1939 por el departamento de biometría y estadísticas vitales de la Universidad Johns Hopkins[6].

Las tablas se aplicaron en las personas protegidas por el Instituto de Seguridad y Servicios Sociales de los Trabajadores Estado (ISSSTE), población conformada por empleados y familiares de las Secretarías de Estado, que constituyen el aparato operativo del Gobierno Federal en el país[7].

Objetivo

Esta comunicación tiene como objetivo estimar la esperanza de vida de la segunda población de servidores públicos más grande en el país atendida por el ISSSTE y sus beneficiarios en el año 2021.

Método

El universo de estudio para este trabajo incluyó la población cubierta por el ISSSTE registrada en el Anuario del ISSSTE para 2021[7], y las defunciones registradas para derechohabientes del ISSSTE también de 2021, incluidas en el cubo dinámico de la Secretaría de Salud[8].

Los datos se agruparon por quinquenios de edad, con excepción de las poblaciones de menores de 1 año (población infantil), de 1 a 4 años (población preescolar), y de 85 y más años (población de adultos ancianos)[9].

El cálculo de la esperanza de vida se realizó de acuerdo con en el método abreviado de Reed y Merrel[6], y con las recomendaciones de Camel[10] para tablas de vida abreviadas.

Tabla 1. Especificaciones para la construcción de las tablas de vida

(a) = grupos de edad
(b) = Población ISSSTE Anuario 2021
(c) = Decesos registrados ISSSTE Anuario 2021
(d) = c/b
(e) = para -1 año = 2d/2+d; para 1-4 años = 4 (2d/2+d); para 5-9 años a 80-84 años = 5 (2d/2+d); para 85 y más años = 1.00
(f) = para -1 año = 100,000; para 1-4 años: (e -1 año) (f -1 año) – (f -1 año); para 5-14 años: (e 1-4 años) (f 1-4 años) – (f 1-4 años), continuar igual.
(g) = para todos los grupos = (e) (f)
(h) = para -1 año = [(0,25) (f -1 año) + (0,75) (f 1-4)]; para 1-4 años = [(1.9) (f 1-4 años) + (2.1); para 5-9 años = [(5) (f 5-9 años) + (f 10-14 años)/2], y así sucesivamente hasta 80-84 años = [(5) (f 80-84 años) + (5) (f 85 y más años)]/2]; para 85 años y más = [log 85 (f 85 años o más)]
(i) = para i 85 años o más = h (85 años o más); para i 80-84 años = (h 80-84 años) + (h 75-79 años); etc.; para i 1-4 años = (i 5-9 años) + (h 1-4 años); para i -1 año = (i 1-4 años) + (h -1 año)
(j) = (i) de cada grupo de edad)/(f) del mismo grupo de edad

Resultados

La construcción de una tabla de vida es laboriosa y requiere seguir una serie de especificaciones que se enlistan después de las tablas presentadas (Tabla 1), para cada columna, marcadas con una letra del alfabeto en la parte superior de las mismas.

Al efecto estimamos una esperanza de vida de 79.51 años para la población de ambos sexos cubierta por el ISSSTE en el país para el año 2021 (Tabla 2); de 81.40 años para las mujeres y de 78.91 años para los hombres (Tablas 3 y 4)

Discusión

Los resultados obtenidos en este estudio son válidos para para las tablas de vida de la población usuaria del

Tabla 2 . Tablas de vida ISSSTE 2021, población ambos sexos

Grupos de edad (a)	Población (1) (b)	Defunciones (2) (c)	Tasas especificas (d)	Probabilidad ajustada (e)	Población estándar (f)	Muertes teóricas (g)	Años de sobrevida a la mitad del periodo (h)	Años de vida restantes (i)	Esperanza de vida (j)
< 1 año	67,440	304	0.0045077	0.00449756	100,000	450	99,662	7,951,991	79,51
1 a 4 años	327,779	67	0.0002044	0.0008175	99,550	81	398,029	7,852,329	78.87
5 a 9 años	754,782	64	0.0000847	0.00042348	99,469	42	497,240	7,454,300	74.94
10 a 14 años	913,205	74	0.0000810	0.00040498	99,427	40	497,035	6,957,060	69.97
15 a 19 años	931,580	177	0.0001899	0.0009494	99,387	94	496,700	6,460,025	64.99
20-24 años	613,784	184	0.0002997	0.00149827	99,293	149	496,092	5,963,325	60.05
25 a 29 años	565,326	273	0.0004829	0.00241391	99,144	239	495,122	5,467,233	55.14
30 a 34 años	663,840	594	0.0008947	0.04471499	98,905	442	493,420	4,972,111	50.27
35 a 39 años	822,005	925	0.0011252	0.00562283	98,463	553	490,932	4,478,691	45.48
40 a 44 años	843,293	1,462	0.0017333	0.00865899	97,910	847	487,743	3,987,759	40.72
45 a 49 años	881,095	2,413	0.0027386	0.01367427	97,063	1,327	481,997	3,500,016	36.05
50 a 54 años	918,255	3,476	0.0037854	0.01889124	95,736	1808	474,160	3,018,019	31.52
55 a 59 años	1,067,404	6,332	0.0059321	0.02957278	93,928	2,778	462,695	2,543,859	27.08
60 a 64 años	1,108,627	8,383	0.0075616	0.03766559	91,150	3,433	447,167	2,081,164	22.83
65 a 69 años	936,458	9,610	0.0126207	0.06270779	87,717	5,500	424,835	1,633,997	18.62
70 a 74 años	726,816	10,225	0.0140682	0.06984967	82,217	5,743	396,727	1,209,162	14.70
75 a 79 años	546,759	10,043	0.0183682	0.09100519	76,474	6,959	364,972	812,435	10.62
80 a 84 años	405,867	9,127	0.0224876	0.11187826	69,515	7,729	328,252	447,463	6.43
85 y más	586,759	14,668	0.0249983	1.00000	61,786	61,786	119,211	119,211	1.92
No edad	0	2	NC	NC	NC	NC			
Total	13,681,077	78,403	0.00573076						

(1) ISSSTE: Anuarios Estadísticos 2021. Capítulo 1. Estadísticas de población. 1.4.
(b) Secretaría de Salud. DGIS. Cubos dinámicos.
NC: no calculable.

ISSSTE residente en México, en 2021. No obstante, como cualquier dato poblacional de natalidad y mortalidad, pueden presentar sesgos de registro no cuantificados, que limitan su generalización, ya que en ocasiones no se introduce el carácter de derechohabiente del ISSSTE en las personas que nacen o fallecen fuera del ámbito institucional, situación que no ocurre con los nacimientos y las muertes hospitalarias, y por lo tanto consideramos que la tabla debe tomarse como una aproximación razonable.

En nuestro caso, la esperanza de vida total calculada para ambos sexos fue de 79.51 años en las personas usuarias del ISSSTE de México en 2021, unas décimas menos que la esperanza de vida para el ISSSTE de Jalisco en 2016, que se calculó en 80.81 años[11].

La esperanza de vida estimada para el ISSSTE es mayor en relación con la esperanza de vida para el país, que en 2018 registró 75.0 años (72.2 años para los hombres y 77.9 años para las mujeres) y en 2022 fue de 75.32 años (72.62 años para los hombres y 78.38 años para las mujeres), con un leve incremento influido por el impacto de la pandemia de COVID-19 en los años anteriores[12].

Es importante señalar que, en nuestro medio, la esperanza de vida ha ido creciendo a través del tiempo, situación que se constata en varios grupos poblacionales, sobre todo donde se goza de seguridad social.

Tabla 3. Tablas de vida ISSSTE 2021, población nacional mujeres

Grupos de edad (a)	Población (1) (b)	Defunciones (2) (c)	Tasas especificas (d)	Probabilidad ajustada (e)	Población estándar (f)	Muertes teóricas (f)	Años de sobrevida a la mitad del periodo (h)	Años de vida restantes (i)	Esperanza de vida (j)
< 1 año	33,234	135	0.0040621	0.00405386	100,000	405	99,696	8,140,043	81.40
1 a 4 años	159,863	33	0.0002064	0.00082551	99,595	82	398,207	8.040,347	80.73
5 a 9 años	369,495	29	0.0000784	0.00039198	99,513	39	497,467	7,642,140	76.79
10 a 14 años	447,219	30	0.0000670	0.00033498	99,474	33	497,287	7,144,673	71.82
15 a 19 años	456,472	62	0.0001358	0.00067895	99,441	67	497,037	6,647,386	66.84
20-24 años	310,169	58	0.0001869	0.00093441	99,374	92	496,640	6,150,349	61.89
25 a 29 años	332,693	97	0.0002915	0.00145728	99,282	144	496,050	5,653,709	56.94
30 a 34 años	399,509	194	0.0004855	0.00242691	99,138	240	497,590	5,157,590	52.02
35 a 39 años	473,837	315	0.0006647	0.00332239	98,898	328	493,670	4,660,069	47.11
40 a 44 años	468,520	542	0.0011568	0.00578065	98,570	569	491,427	4,166,399	42.26
45 a 49 años	495,645	939	0.0018945	0.00946000	98,001	927	487,687	3,674,972	37.49
50 a 54 años	536,675	1418	0.0026421	0.01319307	97,074	1280	482,170	3,187,285	32.83
55 a 59 años	633,379	2707	0.0042739	0.02132393	95,794	2,042	473,865	2,705,115	28.23
60 a 64 años	640,165	3545	0.0055376	0.02761154	93,752	2588	462,290	2,231,250	23.79
65 a 69 años	527,823	4191	0.0079401	0.03954351	91,164	3604	445,818	1,768,960	19.40
70 a 74 años	406,988	4455	0.0109462	0.05443308	87,560	4766	425,885	1,323,142	15.11
75 a 79 años	312,018	4580	0.0146786	0.07285827	82,794	6032	398,890	897,257	10.83
80 a 84 años	234,796	4680	0.0199321	0.0 986770	76,762	7,574	364,875	498,367	6.49
85 y más	333,157	8426	0.0252913	1.00000	69,188	69,188	133,492	133,492	1.92
No edad	NA	2	NC						
Total	7,571,657	36,438	0.0048124						

(1) ISSSTE: Anuarios Estadísticos 2021. Capítulo 1. Estadísticas de población. 1.4.
(2) Secretaría de Salud. DGIS. Cubos dinámicos.
NA: no aplica; NC: no calculable.

Por ejemplo, para la ciudad de Guadalajara, en 1974, la esperanza de vida total era de 67.80 años[13], y la de derechohabientes del Instituto Mexicano del Seguro Social (IMSS) en Jalisco para 1983 era de 74.97 años para ambos sexos (73.38 para los hombres y 76.40 años para las mujeres)[14]. En 2015, la población de asegurados del IMSS en Jalisco, que incluía al 81% de cobertura de la población laboral del Estado[15], registraba una esperanza de vida total de 79.22 años[16]. Proceso acorde con el aumento general de la esperanza de vida humana moderna, atribuible al paso de una transición demográfica con alta natalidad y alta mortalidad a un régimen transicional de baja natalidad y baja mortalidad, dinámica donde la seguridad social influye en un mejoramiento de la duración de la vida, resultado de salvar vidas y prevenir muertes en edades tempranas, provocando que las poblaciones humanas vivan más tiempo y alcancen altas edades de fallecimiento como sociedades desarrolladas[4].

Este incremento de la edad a la muerte es insumo y producto de determinantes sociales que nos obligan a mantener tendencias positivas en la esperanza de vida de la población, en este caso, a incrementar la cobertura y reducir las barreras a la seguridad social poblacional[17], por su evidente impacto en la duración de la vida[4], pues una población que carece de seguridad social acentúa y evidencia los tipos fundamentales de desigualdad humana (de clase, de género, étnica, urbana, etc.) a lo largo de su trayectoria vital, acortando o lentificando su longitud, o variando la distribución interna de la esperanza de vida humana

Tabla 4. Tablas de vida ISSTE 2021, población nacional hombres

Grupos de edad (a)	Población (1) (b)	Defunciones (2) (c)	Tasas especificas (d)	Probabilidad ajustada (e)	Población estándar (f)	Muertes teóricas (f)	Años de sobrevida a la mitad del periodo (h)	Años de vida restantes (i)	Esperanza de vida (j)
< 1 año	34,206	169	0.0049406	0.004928425	100,000	494	99,629	7,891,349	78.91
1 a 4 años	167,916	34	0.0002024	0.000809518	99,506	20	397,982	7,791,720	78.30
5 a 9 años	385,287	35	0.0000908	0.000453979	99,486	45	497,317	7,393,738	74.31
10 a 14 años	465,986	44	0.0000944	0.000471978	99.441	46	497,090	6,896,421	69.35
15 a 19 años	475,108	115	0.0002420	0.001209854	99,395	120	496,675	6,399,331	64.38
20-24 años	303,618	126	0.0004149	0.00207407	99,275	205	495,862	5,902,656	59.45
25 a 29 años	232,633	176	0.0007565	0.00378107	99,070	374	494,415	5,406,794	54.57
30 a 34 años	264,331	400	0.0015132	0.00756028	98,696	746	491,615	4,912,379	49.77
35 a 39 años	348,168	610	0.0017520	0.00875233	97,950	857	487,607	4,420,764	45.13
40 a 44 años	374,773	920	0.0024548	0.01225895	97,093	1,190	482,490	3,933,157	40.50
45 a 49 años	385,450	1474	0.0038241	0.01908401	95,903	1,830	474,940	3,450,667	35.98
50 a 54 años	381,580	2058	0.0053933	0.02689397	94,073	2,529	464,042	2,975,727	31.63
55 a 59 años	434,025	3625	0.0083520	0.04158633	91,544	3,806	448,292	2,511,685	27.43
60 a 64 años	468,462	4838	0.0103274	0.05137173	87,773	4,507	427,597	2,063,393	23.50
65 a 69 años	408,635	5419	0.0132612	0.06586936	83,266	5,484	401,620	1,635,796	19.54
70 a 74 años	319,828	5770	0.0180408	0.08939759	77,382	6,917	369,617	1,234,176	15.94
75 a 79 años	234,741	5463	0.0232724	0.11502356	70465	8,105	334,562	864,559	12.26
80 a 84 años	171,071	4447	0.0259950	0.12830732	63,360	8,129	368,132	529,997	8.36
85 y más	253,602	6242	0.0246133	1.00000	83,893	83,893	161,865	161,865	1.92
Total	6,109,420	41,965	0.0068689						

(1) ISSSTE: Anuarios Estadísticos 2021. Capítulo 1. Estadísticas de población. 1.4.
(2) Secretaría de Salud. DGIS. Cubos dinámicos.

en la estructura poblacional, desigualdades que no se han observado en los primates no humanos por millones de años[4].

En el caso de la seguridad social en México (ISSSTE e IMSS), se ha logrado una trayectoria operativa de tres cuartos de siglo, donde al avanzar, la frontera de la supervivencia hacia edades más avanzadas y la esperanza de vida individual son cada vez menos diferenciales, como se puede observar en nuestros datos, lo cual plantea un escenario optimista que, de fomentarse el actual ritmo de progreso en la esperanza de vida, una buena cantidad de las niñas y los niños nacidos en este milenio podrían celebrar su cumpleaños número 100.

Sin embargo, la incertidumbre ligada a la persistencia de la desigualdad y de la inequidad poblacional en nuestro medio opaca el optimismo, pues en la realidad, la esperanza de vida pudiera aumentar muy poco, a pesar de que en las últimas tres décadas se han logrado avances sustanciales en la profundización de la comprensión de cuánto tiempo han vivido los humanos y cuánto tiempo podrían vivir. Pensar entonces en una esperanza de vida poblacionalmente igualitaria radica en acciones sociales, económicas, de salud, culturales y políticas para aumentar la calidad de vida en la longevidad, requiriendo el desarrollo de métodos sociodemográficos más poderosos para el pronóstico y la evaluación de la vitalidad poblacional[18].

Tocante a la metodología, Dowd y Hamoud[19] señalan que se pueden prevenir sesgos en el cálculo de la esperanza de vida observando las siguientes precauciones:

- Siempre que sea posible, identificar tendencias mediante el seguimiento de la misma población.
- Cuando se comparen diferentes poblaciones, estratificar las características que han sido estables durante al menos una generación humana que no inciden efectivamente en un punto temprano del curso de la vida. De esta manera es metodológicamente posible calcular medidas de la esperanza de vida a lo largo del tiempo para subgrupos, y aun así, al hacerlo no hay certeza de interpretar válidamente las diferencias observadas.
- Estratificar poblaciones con referencia explícita a su historia social, con un marco teórico-conceptual claro y articulado en ciencias tanto sociales como biológicas.

Si un resultado se mide en poblaciones no comparables, entonces el mero hecho de que las medidas se calculen en dos «circunstancias» diferentes no hace que la discrepancia entre ellas sea una «tendencia», y el uso no responsable de palabras como «caída» o «declive» es probable que haga más daño que bien para el público[19].

En lo que toca a la dimensión cualitativa, se continúan encontrando resultados variados en la esperanza de vida. Por ejemplo, la encontrada por nosotros entre sexos, con un diferencial mayor a favor de las mujeres. Aspecto corroborado en el país desde los registros de 1930, que indicaban una esperanza de vida para las mujeres de 34.7 años y para los hombres de 33.0; o la variabilidad espacial evidenciada en 2019, cuando se registraban las mayores esperanzas de vida para la Ciudad de México (antes Distrito Federal), con 76.5 años, y para Baja California, con 75.9 años, mientras que las más bajas eran para Guerrero, 73.2 años, y para Oaxaca, con 74.0 años[12].

Otros ejemplos no nacionales de que la esperanza de vida no es pareja para todas las poblaciones, en este caso según la etnia, son los Estados Unidos de América, donde las poblaciones de indios americanos y de nativos de Alaska tienen la esperanza de vida más baja de todas las poblaciones que integran esa nación, además de que experimentaron una reducción de sus indicadores de expectativa de vida en la mayoría de sus condados, con una brecha de más de 21 años[20]. O como sucede en España, donde la esperanza de vida total aumentó de 2010 a 2018 en 1.17 años, pero proporcionalmente no aumentó igual en los hombres que en las mujeres, pues en los primeros se incrementó en 1.41 años mientras que en las mujeres lo hizo en 0.82 años, con lo que la diferencia relativa en esperanza de vida de las mujeres respecto a los hombres se redujo entre 2010 y 2018 en 0.5 años, aunque de manera absoluta continuó existiendo una mayor esperanza de vida a favor de las mujeres (5.39 años en 2018)[21].

La complejidad de la esperanza de vida se observa desde la tasa de mortalidad general (por 1000 habitantes), que puede presentar una gran dispersión, por el mayor envejecimiento poblacional o por una mayor letalidad debida a padecimientos específicos, así como por el descenso de las tasas de mortalidad infantil (que se están igualando entre niños y niñas), hasta los determinantes sociales que hacen los grandes contrastes entre zonas geográficas, grupos étnicos y niveles socioeconómicos[22], donde ocupa un lugar destacado la relación entre pobreza y peores indicadores de salud, relación ligada a peores viviendas, problemas de acceso a una dieta saludable, desempleo y subempleo, peores condiciones de trabajo con mayores riesgos para la salud, mayor consumo de sustancias toxicas (alcohol, tabaco, drogas), peor nivel educativo, hábitos menos saludables y problemas de acceso a muchas prestaciones sanitarias.

En cuanto a los cambios en la esperanza de vida en el ISSSTE según los datos de 2016[11] y los de esta presentación (2021), cuya escasa magnitud puede ser atribuida a la epidemia de COVID-19, su sustentabilidad puede ser también atribuida al amparo que otorga la seguridad social. Aunque consideramos que posiblemente estos aumentos serán cada vez menores en relación con los observados para Guadalajara y el IMSSS de Jalisco en décadas anteriores[13,14], que paradójicamente serán provocados por el incremento de la cobertura de la seguridad social y la compensación entre las causas de muerte entre los grupos analizados[23], así como el impacto de nuevos eventos epidémicos, merced a la creciente globalización que afecta a nuestro país, sin dejar de considerar la existencia o la permanencia de «archipiélagos o bolsones intrapoblacionales» que pueda sufrir la heterogénea población usuaria de empleados que atiende la seguridad social, en este caso los federales del ISSSTE.

Así pues, el aumento de la longevidad poblacional institucional nos debe hacer pensar:

- Si nuestra esperanza de vida saludable y sin discapacidad podrá realmente aumentar tanto como la esperanza de vida total[24].
- Si estos cambios demográficos son fundamentalmente cuantitativos, sin cambios en el contexto social de la longevidad humana, o sea, sin un verdadero florecimiento humano[25].

Conclusiones

Aunque la esperanza de vida de un país aumenta con el ingreso nacional, también se ha evidenciado que se hacen indispensables políticas y estrategias fundadas en la comunidad, como igualdad y equidad en el acceso a bienes y servicios, educación (sobre todo a mujeres), empoderamiento de género, asociaciones de desarrollo comunitario real y participación política poblacional, y no con economía de consumo masivo, seguridad social limitada, atención de salud basada en el mercado, promoción y protección de salud limitada, desigualdades de género, etnia, etarias, etc.[26].

Desgraciadamente, hay pocos estudios nacionales que permitan evaluar las desigualdades en esperanza de vida y que hagan un análisis según dimensiones sociales, económicas y culturales, para ayudar a desarrollar instrumentos que tengan como eje doctrinal la unidad de servicio, la prevención y un enfoque multidisciplinario en el abordaje de la salud-enfermedad entendida como proceso, que pueden ayudar a reducir diferenciales.

Habrá entonces que destacar que el tener derechohabiencia propicia una mayor esperanza de vida (79.51 años en las personas usuarias del ISSSTE de México para 2021), por lo que es urgente avanzar en materia de seguridad social[27], aprovechando los avances teóricos y la evidencia recogida sobre la influencia de la estructura social en el estado de salud de los grupos sociales. El estudio de la esperanza de vida aún es un campo en construcción, todavía no suficientemente delimitado, que no debe revolverse con el tradicional enfoque de factores de riesgo[28].

Financiamiento

Los autores declaran no haber recibido financiamiento para este trabajo.

Conflicto de intereses

Los autores declaran no tener ningún conflicto de intereses.

Responsabilidades éticas

Protección de personas y animales. Los autores declaran que en este artículo no aparecen datos de pacientes. Además, los autores han reconocido y seguido las recomendaciones según las guías SAGER dependiendo del tipo y naturaleza del estudio.

Confidencialidad de los datos. Los autores declaran que han seguido los protocolos de su centro de trabajo sobre la publicación de datos de pacientes.

Derecho a la privacidad y consentimiento informado. Los autores declaran que en este artículo no aparecen datos de pacientes.

Uso de inteligencia artificial para generar textos. Los autores declaran que no han utilizado ningún tipo de inteligencia artificial generativa en la redacción de este manuscrito ni para la creación de figuras, gráficos, tablas o sus correspondientes pies o leyendas.

Bibliografía

1. Méndez Main S. Xalapa, Jilotepec y Naolinco: una ruta de contagio en el camino Veracruz-México, 1765-1820. En: Magaña-Mancilla MA, coordinador. Epidemias y rutas de propagación en la Nueva España y México (siglos XVIII y XIX). México: Universidad Autónoma de Baja California-Instituto de Investigaciones Culturales-Museo; 2013. p. 13-24.
2. Robles Villane A. Más allá de las estrellas: aportes de Edmond Halley a la demografía. Otros Diálogos. 2022;18. Disponible en: https://otrosdialogos.colmex.mx/mas-alla-de-las-estrellas-aportes-de-edmond-halley-a-la-demografia
3. Epidat 3.1. Consellería de Sanidade. SERGAS. Disponible en: https://www.sergas.es/Saude-publica/Epidat-3-1-descargar-Epidat-3-1-(espanol)?idioma=es
4. Aburto JM. Dynamics of life expectancy and life span equality. PNAS. 2020;117:5250-9.
5. Roser M, Ortiz-Espina E, Ritchie H. Life expectancy. Our World in Data. 2013. (Consultado el 22-03-2022.) Disponible en: https://ourworldindata.org/life-expectancy
6. Reed LJ, Merrel MA. Short method for constructing and abridged life table. The American Journal of Hygiene. 1939:30:33-62.
7. Anuario Estadístico. ISSSTE. 2021. Disponible en: http://www.issste.gob.mx/datosabiertos/anuarios/anuarios2021.html.
8. Secretaría de Salud. Cubos dinámicos. Mortalidad. 2021. (Consultado el 22-03-2022.) Disponible en: http://www.dgis.salud.gob.mx/contenidos/basesdedatos/bdc_defunciones_gobmx.html
9. García Pulgarín LV, García Ortiz LH. El adulto mayor maduro: condiciones actuales de vida. Rev Med Risaralda. 2005;11(2). (Consultado el 22-03-2022.) Disponible en: https://revistas.utp.edu.co/index.php/revistamedica/article/view/1189
10. Camel Vargas F. Estadísticas médicas y de salud pública. La Habana, Cuba: Unidad Andrés Voisin; 1968. p. 371-81.
11. García de Alba García J.E, López Elizalde R, García de Alba Verduzco J.E. 2023. Tabla de Vida Abreviada, para la población amparada del ISSSTE-Jalisco. 2016. Salud Jalisco. En: Valdez Zepeda A, Salazar Estrada JG y Barragan Bautista E. Las tecnologías en y para la salud pública. Universidad de Guadalajara. CUSUR. México. pp 537-552.
12. CONAPO. La situación demográfica de México. (Consultado el 01-05-2023.) Disponible en: http://www.gob.mx/conapo y
13. García de Alba García JE, Espinoza Hernández J, Morán González R. Tablas de vida para la ciudad de Guadalajara 1974-1975. Salud Publica de México. 2014;18:1005-9.
14. García de Alba García JE, Barba Marabel O. Tablas de vida para la población derechohabiente del Instituto Mexicano del Seguro Social, delegación estatal en Jalisco 1983. Salud Publica de México. 1976; 27:155-160.
15. MIDE Jalisco. Monitoreo de indicadores del desarrollo de Jalisco. (Consultado el 12-05-2023.) Disponible en: https://mide.jalisco.gob.mx.
16. García de Alba García JE, Salcedo Rocha AL, Milke Najar ME, Reynoso C, García de Alba Verduzco JE, De Celis Carrillo R. Tablas de vida 2015, población usuaria del Instituto Mexicano del Seguro Social - Jalisco. Revista Médica del IMSS. 2018;56:261-73.
17. Olshansky J, Passaro DJ, Hershow RC, Layden J, Carnes BA, Brody J, et al. Potential decline in life expectancy in the United States in the 21st Century. New Engl J Med. 2005;352:1138-45.
18. Vaupel JW, Villavicencio F, Bergeron-Boucher MP. Demographic perspectives on the rise of longevity. Proc Natl Acad Sci U S A. 2021; 118:e2019536118.

19. Dowd JB, Hamoud A. Is life expectancy really falling for groups of low socio-economic status? Lagged selection bias and artefactual trends in mortality. Int J Epidemiol. 2014;43:983-8.
20. NIH: News Releases. Thursday, June 16, 2022: Life expectancy in the U.S. increased between 2000-2019, but widespread gaps among racial and ethnic groups exist. (Consultado el 21-03-2023.) Disponible en: https://www.nih.gov/news-events/news-releases/life-expectancy-us-increased-between-2000-2019-widespread-gaps-among-racial-ethnic-groups-exist
21. Carlos Sánchez y Sergio Fernández 2020 . En: Menor esperanza de vida en los grupos sociales con menos ingresos https://www.consumidor.es,2020/08/13,menor-esp (consultado el 18/06/2024).
22. Lustig N. Salud y desarrollo económico. El caso de México. El Trimestre Econ. 2007;74:793-822.
23. Heuveline P. Global and national declines in life expectancy: an end-of-2021 assessment. Popul Dev Rev. 2022;48:31-50.
24. Robine JM. Ageing populations: we are living longer lives, but are we healthier?| UN DESA Publications. United Nations. (Consultado el 22-05-2022.) Disponible en: https://desapublications.un.org/working-papers/ageing-populations-we-are-living-longer-lives-are-we-healthier
25. Dieterlen P. Cuatro enfoques sobre la idea del florecimiento humano. Desacatos. 2007; (23):147-58.
26. Freeman T, Gesesew HA, Bambra C, Giugliani ERJ, Popay J, Sanders D, et al. Why do some countries do better or worse in life expectancy relative to income? An analysis of Brazil, Ethiopia, and the United States of America. Int J Equity Health. 2020;19:202.
27. Soria Romero Z, Montoya Arce BJ. Envejecimiento y factores asociados a la calidad de vida de los adultos mayores en el Estado de México. Pap Poblac. 2017;23:59-93.
28. Álvarez Castaño LS. Los determinantes sociales de la salud: más allá de los factores de riesgo. Revista Gerencia y Políticas de Salud. 2009; 8:69-79.

ORIGINAL ARTICLE

Association of Vitamin D and magnesium levels with severity and mortality in patients with COVID-19

Asociación de los niveles de vitamina D y magnesio con la gravedad y la mortalidad en pacientes con COVID-19

*Mariela M. García-Zendejas[1], Edgar A. Cano-Torres[2], and Luis E. Simental-Mendía[3]**

[1]Servicio de Urgencias, Hospital General Salvador Zubirán Anchondo, Chihuahua, Chihuahua; [2]Department of Internal Medicine, Hospital Rebren, Durango, Durango; [3]Unidad de Investigación Biomédica, Delegación Durango, Instituto Mexicano del Seguro Social, Durango, Durango. México

Abstract

Objective: *The study aimed to determine the association between serum magnesium and Vitamin D levels with the severity and mortality by coronavirus disease 19 (COVID-19) in hospitalized patients.* **Method:** *Men and women over 18 years of age with probable COVID-19 were enrolled in a case–control study. Patients with a positive or negative test for Severe acute respiratory syndrome coronavirus 2 (SARS-CoV-2) were allocated into case or control groups, respectively. Vitamin D deficiency was defined by concentrations < 20 ng/mL and hypomagnesemia by serum levels < 1.8 mg/dL.* **Results:** *A total of 54 patients, 30 women and 24 men, were enrolled and allocated into the groups with (n = 27) and without (n = 27) COVID-19. The logistic regression analysis showed that Vitamin D deficiency (odds ratio [OR] = 6.13; 95% confidence intervals [CI]: 1.32-28.34) and insufficiency (OR = 0.12; 95% CI: 0.02-0.60) are significantly associated with hospitalization. However, Vitamin D disorders and hypomagnesemia were not associated with mortality.* **Conclusions:** *The results of the present study revealed that Vitamin D disturbances, but not hypomagnesemia, are associated with the severity of SARS-CoV-2.*

Keywords: *Coronavirus disease 19. Magnesium. Mortality. Severity. Vitamin D.*

Resumen

Objetivo: *Determinar la asociación entre los niveles séricos de vitamina D y de magnesio con la gravedad y la mortalidad de la COVID-19 en pacientes hospitalizados.* **Método:** *Hombres y mujeres mayores de 18 años con probable COVID-19 fueron enrolados en un estudio de casos y controles. Los pacientes con una prueba positiva o negativa para SARS-CoV-2 fueron asignados en los grupos de casos y de controles, respectivamente.* **Resultados:** *Un total de 54 pacientes, 30 mujeres y 24 hombres, fueron enrolados y asignados a los grupos COVID-19 (n = 27) y control (n = 27). El análisis de regresión logística mostró que la deficiencia de vitamina D (odds ratio [OR]: 6.13; intervalo de confianza del 95% [IC95%]: 1.32-28.34) y la insuficiencia de vitamina D (OR: 0.12; IC95%: 0.02-0.60) se asocian significativamente con hospitalización. Sin embargo, las alteraciones de la vitamina D y la hipomagnesemia no se asociaron con mortalidad.* **Conclusiones:** *Los resultados del presente estudio revelaron que las alteraciones de la vitamina D, pero no la hipomagnesemia, se asocian con la gravedad de la COVID-19.*

Palabras clave: *COVID-19. Magnesio. Mortalidad. Gravedad. Vitamina D.*

Correspondence:
Luis E. Simental-Mendía
E-mail: luis_simental81@hotmail.com

Date of reception: 10-12-2023
Date of acceptance: 30-12-2023
DOI: 10.24875/CIRU.23000514

Cir Cir. 2024;92(5):603-607
Contents available at PubMed
www.cirugiaycirujanos.com

Introduction

Severe acute respiratory syndrome coronavirus 2 (SARS-CoV-2) is a multiorgan disease with inflammatory and prothrombotic characteristics[1,2]. The number of SARS-CoV-2 cases increased rapidly worldwide and, in Mexico, hospitals and emergency services were modified for the specialized treatment of coronavirus disease 19 (COVID-19) patients[3,4]. Through the angiotensin-converting enzyme 2 (ACE-2) receptor, this virus infects lung epithelial cells and macrophages, leading to the activation of macrophages, neutrophils, and T cells, causing sustained elevations of pro-inflammatory cytokines such as interleukin-1, 6 and tumor necrosis factor alpha. In this context, the "cytokine storm," a hyperinflammatory state triggered by SARS-CoV-2, is responsible for some of the most severe complications of COVID-19, including acute respiratory distress syndrome (ARDS). Although the inflammatory response initially helps to eliminate pathogens, it also damages the alveolar endothelial-epithelial barrier, resulting in edema and thrombosis, which in turn causes apoptosis of Type 2 pneumocytes and, in some patients, ARDS[2].

Magnesium is an essential mineral for basic biochemical reaction, physiological functions and metabolism in the human body[5-8]. In addition, this element has anti-inflammatory, antioxidant, anti-spasm, vasodilation, and neuroprotection effects[9] and plays an important role in the regulation of the immune response through immunoglobulin synthesis, immune cell adherence, antibody-dependent cytolysis, immunoglobulin M lymphocyte binding, macrophage response to lymphokines, and T helper-B cell adherence, especially in viral infections[10]. Therefore, it has been hypothesized that subjects with hypomagnesemia are at higher risk of developing respiratory tract infections[11].

Magnesium is fundamental in the synthesis, transport, and activation of Vitamin D, since acts as a cofactor for the enzymes involved in its metabolism[12]. Vitamin D confers a protective effect against respiratory tract infections by inhibiting the hyperinflammatory response through the regulation of cytokines and differentiation of T cells[12-14]. Furthermore, some authors have suggested that Vitamin D may downregulate ACE-2 receptors, resulting in a protective effect against fibrosis of COVID-19 by accelerating the healing process in the lung tissue[15]. Thus, the objective of this study was to determine the association between serum Vitamin D and magnesium levels with severity and mortality in hospitalized patients diagnosed with COVID-19.

Materials and methods

With prior approval by the Ethics and Research Committee of the Hospital Salvador Zubirán Anchondo from Chihuahua, México (registration number 0294), and following the principles of the Helsinki Declaration, a cross-sectional and longitudinal study was conducted. Men and women over 18 years of age with probable pulmonary infection were considered to participate in this study after acceptance of the informed consent. After admission in the emergency service, patients were assessed through standardized interviews, clinical examination, and laboratory tests including reverse transcriptase-polymerase chain reaction test for SARS-CoV-2. According to the result of this last test, participants were assigned into the groups with (positive test) or without (negative test) COVID-19. Exclusion criteria were pregnancy, chronic diarrhea, chronic kidney disease, heart failure, cancer, and the supplement intake during the last 4 weeks before the study. Hospitalized patients were followed until discharge due to recovery or death, including the admission to the intensive care unit (ICU).

Definitions

Hypomagnesemia was defined by serum levels < 1.8 mg/dL and Vitamin D deficiency by concentrations < 20 ng/mL, and Vitamin D insufficiency for concentrations 20 and < 30 ng/mL. Finally, hospitalization and admission to the ICU were considered for severity.

Assays

The venous blood samples were obtained following 8-10 h overnight fasting. The serum levels of 25-hydroxyvitamin D were determined by electroluminescence method with a coefficient of variation of 6.7 using a COBAS 6000 analyzer (Roche Diagnostics, Germany). The serum magnesium concentrations were measured with quantitative photometric biochemical analysis with a coefficient of variation of 3.8 using the ADVIA 1800 analyzer (Siemens, Tarrytown, NY, USA).

Statistical analysis

Numerical variables were reported as mean ± standard deviation and categorical variables as proportions. Differences between groups were estimated

using unpaired Student's t-test for numerical variables and the χ^2 test for categorical variables. Multiple logistic regression analysis (adjusted by obesity, diabetes, and hypertension) was performed to assess the association of hypomagnesemia (ordinal variable) and Vitamin D abnormalities (ordinal variables) with SARS-CoV-2 (overall population), severity, and mortality (patients with positive SARS-CoV-2). A 95% confidence interval (95% CI) and $p < 0.05$ were used to establish statistical significance. The data were analyzed with the IBM SPSS Static Version 15.0.

Results

A total of 54 patients, 30 women and 24 men, with a mean age of 53.4 ± 21.8 years were enrolled and allocated into the groups with (n = 27) and without (n = 27) COVID-19.

In the overall population, 78% had low levels of Vitamin D and 55% hypomagnesemia. The most common comorbidities were: diabetes (35%), hypertension (35%), chronic obstructive pulmonary disease 11.1%, liver disease 5%, and asthma 3.7%. However, the distribution of comorbidities between the study groups was similar.

The clinical and biochemical characteristics of the study population are shown in (Table 1). The cases presented a lower oxygen saturation than the controls. There were other significant differences between the study groups.

In addition, a higher percentage of patients with COVID-19 was admitted to the ICU in comparison with the controls (85.1% vs. 33.3%, $p < 0.001$).

Among COVID-19 patients, the multiple logistic regression analysis showed that Vitamin D deficiency (OR = 6.13; 95% CI: 1.32-28.34) and insufficiency (OR = 0.12; 95% CI: 0.02-0.60) are significantly associated with hospitalization (OR = 0.11; 95% CI: 0.02-0.50). However, hypomagnesemia and Vitamin D abnormalities were not associated with mortality (Table 2).

Discussion

Our results suggest that Vitamin D disorders, but not hypomagnesemia, are associated with the severity of SARS-CoV-2.

Previous studies have reported that low magnesium levels are associated to severity and mortality[16,17], which is in disagreement with our findings. This inconsistency could be explained because these studies were retrospective analyses that only included patients with COVID-19 (comparing severe versus non-severe cases), while we conducted a cross-sectional study comparing patients with and without COVID-19. Furthermore, another possible reason is that the frequency of magnesium deficiency in the target population of our study was very high (46.2%) compared to that reported for the adult Mexican population (31%)[18].

Interestingly, most of our study population had Vitamin D deficiency (74.5%); this finding coincides with another Colombian study where it was found that the male gender and the Fitzpatrick IV phototype were associated with an increased risk of Vitamin D deficiency[19]. Besides, a previous systematic review and meta-analysis revealed that low serum Vitamin D levels are associated with an increased risk of COVID-19 infection[20]. Nonetheless, we observed that Vitamin D deficiency is not associated with the presence of SARS-CoV-2. There are several mechanisms involved in the infection of respiratory viruses by Vitamin D deficiency. In this regard, it has been reported that Vitamin D deficiency affects the immune response, particularly innate immune function. Furthermore, low levels of Vitamin D decrease the active Vitamin D synthesis, leading to the mitigation of the antimicrobial and antiviral properties of this vitamin. Furthermore, Vitamin D regulates the expression of cathelicidin and defensin, molecules that induce the expression of antiviral cytokines and chemokines, resulting in the recruitment of T cells, natural killer cells, neutrophils, monocytes, and macrophages. In addition, Vitamin D induces autophagy in monocytes and macrophages through cathelicidin, Beclin 1, and mTOR pathway[21-23]. Furthermore, Vitamin D stimulates PI3KC3 through upregulation of intracellular calcium and nitric oxide, which promotes autophagy[24]. Therefore, the protective actions of Vitamin D may be mitigated by its deficiency, causing a defective response against respiratory viruses, including SARS-CoV-2[25].

It is noteworthy that the results of our study showed that Vitamin D deficiency was not associated with severity and mortality, which is in contrast with several studies. In this regard, it has been reported that advanced age is an important risk factor for the severity and mortality in patients with COVID-19[26]; however, the target population of our study had a mean age < 60 years, which could explain our results. However, in the sub analysis of patients with SARS-CoV-2, Vitamin D deficiency (n = 18) and insufficiency (n = 4) were associated with hospitalization. Nevertheless, it is important to note that these results were obtained from a smaller sample size, which could explain the direct and inverse association of Vitamin D deficiency

Table 1. Clinical and biochemical characteristics of the study population, n = 54

Variables	Overall n = 54	SARS-CoV-2 (+) n = 27	SARS-CoV-2 (−) n = 27	p-value
Age, years	53.4 ± 22.0	52.5 ± 22.4	54.3 ± 21.9	0.77
Women, n (%)	24 (44.4)	14 (51.8)	16 (59.2)	0.78*
Body mass index, kg/m^2	25.3 ± 32.2	26.2 ± 5.8	24.5 ± 5.0	0.23
Systolic blood pressure, mmHg	113.5 ± 32.2	110.1 ± 6.5	116.8 ± 30.3	0.45
Diastolic blood pressure, mmHg	74.0 ± 20.8	71.1 ± 21.9	77.0 ± 19.5	0.29
Oxygen saturation, %	84.7 ± 7.4	81.5 ± 8.7	87.9 ± 3.9	0.001
Magnesium, mg/dL	1.9 ± 0.9	1.9 ± 0.6	1.8 ± 0.4	0.50
Vitamin D, ng/mL	15.8 ± 7.0	15.1 ± 5.0	16.5 ± 8.6	0.48
Days of hospitalization	6.3 ± 5.9	12.3 ± 9.5	11.1 ± 8.9	0.92
Deaths, n (%)	21 (38.8)	13 (48.1)	8 (29.6)	0.16*
APACHE II score	11.9 ± 9.3	12.3 ± 9.5	11.1 ± 8.9	0.81
SOFA score	5.8 ± 3.6	4.8 ± 3.5	6.7 ± 3.5	0.06

Values are mean ± standard deviation. P value estimated with the Student×s t-test. *p-value estimated with the χ^2 test. SARS-CoV-2: severe acute respiratory syndrome coronavirus 2.

Table 2. Multiple logistic regression analysis that evaluates the association between low levels of magnesium and Vitamin D (independent variables) with SARS-CoV-2 and their outcomes (dependent variables). The normal values of magnesium and Vitamin D were used as reference groups

Independent variables	SARS-CoV-2 (+)*	Hospitalization**	ICU admission**	Death**
	OR (95% CI)†	OR (95% CI)†	OR (95% CI)†	OR (95% CI)†
Hypomagnesemia (< 1.8 mg/dL)	0.54 (0.16-1.77)	0.61 (0.16-2.27)	0.78 (0.25-2.37)	1.08 (0.34-3.39)
Vitamin D deficiency (< 20 ng/mL)	2.36 (0.54-10.30)	6.13 (1.32-28.34)	2.79 (0.70-11.13)	2.87 (0.62-13.20)
Vitamin D insufficiency (20 < 30 ng/mL)	0.51 (0.11-2.24)	0.12 (0.02-0.60)	0.27 (0.06-1.14)	0.20 (0.38-1.15)
Magnesium and Vitamin D deficiencies	0.92 (0.25-3.32)	1.29 (0.27-6.12)	2.04 (0.55-7.54)	2.32 (0.65-8.17)

OR: odds ratio; CI: confidence interval; ICU: intensive care unit. *Analysis conducted in the overall population. **Analysis conducted in patients with SARS-CoV-2 (+). †Analysis adjusted by obesity, diabetes, and hypertension. SARS-CoV-2: severe acute respiratory syndrome coronavirus 2.

and insufficiency, respectively. Therefore, these findings could be treated with caution.

A previous meta-analysis revealed that Vitamin D supplementation prevents against acute respiratory tract infection[27]. In this context, a randomized controlled trial showed that a high-dose Vitamin D supplementation turned SARS-CoV-2 RNA negative in Vitamin D-deficient individuals with COVID-19 infection[28]. Another randomized clinical trial suggested that a high dose of Vitamin D improves the clinical course of COVID-19 infection through the suppression of cytokine storms[29]. According to the abovementioned, Vitamin D supplementation may be a promising treatment for COVID-19 in vitamin deficient patients. However, larger randomized controlled trials are mandatory to corroborate the potential beneficial effects of this vitamin on outcomes of COVID-19 infection.

This study has some limitations that should be mentioned. First, taking into account the study design, causality cannot be assured. Second, we recognize the small sample size, which may introduce a potential source of bias. Finally, it is important to note that this study was conducted during the winter, resulting in an increased incidence of respiratory tract infections and reduced sun exposure, which could affect our results.

Conclusion

The results of the present study showed that Vitamin D abnormalities are associated with the severity of

SARS-CoV-2. However, low magnesium and Vitamin D levels are not related with the mortality by COVID-19.

Acknowledgments

The authors would like to thank Q.B.P. Miriam Márquez Córdova and Dr. Rubén Cuevas Martínez of the Hospital General Salvador Zubirán in Chihuahua, Chih. and the collaborators who helped with the measurements of Vitamin D and magnesium levels.

Funding

The authors declare that they have not received funding.

Conflicts of interest

The authors declare no conflicts of interest.

Ethical disclosures

Protection of human and animal subjects. The authors declare that the procedures followed were in accordance with the regulations of the relevant clinical research ethics committee and with those of the Code of Ethics of the World Medical Association (Declaration of Helsinki).

Confidentiality of data. The authors declare that they have followed the protocols of their work center on the publication of patient data.

Right to privacy and informed consent. The authors have obtained approval from the Ethics Committee for analysis and publication of routinely acquired clinical data and informed consent was not required for this retrospective observational study.

Use of artificial intelligence for generating text. The authors declare that they have not used any type of generative artificial intelligence for the writing of this manuscript, nor for the creation of images, graphics, tables, or their corresponding captions.

References

1. Tan CW, Ho LP, Kalimuddin S, Cherng BP, Teh YE, Thien SY, et al. Cohort study to evaluate the effect of vitamin D, magnesium, and vitamin B12 in combination on progression to severe outcomes in older patients with coronavirus (COVID-19). Nutrition. 2020;79-80.:111017.
2. Cooper ID, Crofts CA, DiNicolantonio JJ, Malhotra A, Elliott B, Kyriakidou Y, et al. Relationships between hyperinsulinaemia, magnesium, vitamin D, thrombosis and COVID-19: rationale for clinical management. Open Heart. 2020;7:e001356.
3. Serrano-González SP, Nájera-Reyes JA, Ortiz-Mendoza CM. Changing characteristics of emergency surgery during COVID-19 pandemic: a retrospective cohort study. Cir Cir. 2022;90:13-7.
4. Bozada-Gutiérrez K, Trejo-Ávila M, Moreno-Portillo M. Postoperative complications and predictors of mortality in patients with COVID-19. Cir Cir. 2023;91:344-53.
5. Komiya Y, Runnels LW. TRPM channels and magnesium in early embryonic development. Int J Dev Biol. 2015;59:281-8.
6. Ohyama T. New aspects of magnesium function: a key regulator in nucleosome self-assembly, chromatin folding and phase separation. Int J Mol Sci. 2019;20:4232.
7. Flatman PW. Magnesium transport across cell membranes. J Membr Biol. 1984;80:1-14.
8. Quilliot D, Bonsack O, Jaussaud R, Mazur A. Dysmagnesemia in Covid-19 cohort patients: prevalence and associated factors. Magnes Res. 2020;33:114-22.
9. Tang CF, Ding H, Jiao RQ, Wu XX, Kong LD. Possibility of magnesium supplementation for supportive treatment in patients with COVID-19. Eur J Pharmacol. 2020;886:173546.
10. Liang RY, Wu W, Huang J, Jiang SP, Lin Y. Magnesium affects the cytokine secretion of $CD4^+$ T lymphocytes in acute asthma. J Asthma. 2012;49:1012-5.
11. Iotti S, Wolf F, Mazur A, Maier JA. The COVID-19 pandemic: is there a role for magnesium? Hypotheses and perspectives. Magnes Res. 2020;33:21-7.
12. Dai Q, Zhu X, Manson JA, Song Y, Li X, Franke AA, et al. Magnesium status and supplementation influence vitamin D status and metabolism: results from a randomized trial. Am J Clin Nutr. 2018;108: 1249-58.
13. Mohan M, Cherian JJ, Sharma A. Exploring links between vitamin D deficiency and COVID-19. PLoS Pathog. 2020;16:e1008874.
14. Autier P, Mullie P, Macacu A, Dragomir M, Boniol M, Coppens K, et al. Effect of vitamin D supplementation on non-skeletal disorders: a systematic review of meta-analyses and randomised trials. Lancet Diabetes Endocrinol. 2017;5:986-1004.
15. Arboleda JF, Urcuqui-Inchima S. Vitamin D supplementation: a potential approach for coronavirus/COVID-19 therapeutics? Front Immunol. 2020;11:1523.
16. Alamdari NM, Afaghi S, Rahimi FS, Tarki FE, Tavana S, Zali A, et al. Mortality risk factors among hospitalized COVID-19 patients in a major referral center in Iran. Tohoku J Exp Med. 2020;252:73-84.
17. Zeng HL, Yang Q, Yuan P, Wang X, Cheng L. Associations of essential and toxic metals/metalloids in whole blood with both disease severity and mortality in patients with COVID-19. FASEB J. 2021;35:e21392.
18. Mejía-Rodríguez F, Shamah-Levy T, Villalpando S, García-Guerra A, Humarán IM. Iron, zinc, copper and magnesium deficiencies in Mexican adults from the National Health and Nutrition Survey 2006. Salud Publica Mex. 2013;55:275-84.
19. Daza AM, Casanova ME, Rojas NA, Triana OJ, Ocampo MB. Prevalence and factors associated with vitamin D deficiency in young adults of two higher education institutions in Cali and Bogotá: a crosssectional study. Rev Colomb Endocrinol Diabetes Metab. 2020; 7:12-8.
20. Teshome A, Adane A, Girma B, Mekonnen ZA. The impact of vitamin D level on COVID-19 infection: systematic review and meta-analysis. Front Public Health. 2021;9:624559.
21. Wang J. Beclin 1 bridges autophagy, apoptosis and differentiation. Autophagy. 2008;4:947-8.
22. Jang W, Kim HJ, Li H, Jo KD, Lee MK, Song SH, et al. 1,25-dyhydroxyvitamin D-attenuates rotenone-induced neurotoxicity in SH-SY5Y cells through induction of autophagy. Biochem Biophys Res Commun. 2014;451:142-7.
23. Yuk JM, Shin DM, Lee HM, Yang CS, Jin HS, Kim KK, et al. Vitamin D3 induces autophagy in human monocytes/macrophages via cathelicidin. Cell Host Microbe. 2009;6:231-43.
24. Uberti F, Lattuada D, Morsanuto V, Nava U, Bolis G, Vacca G, et al. Vitamin D protects human endothelial cells from oxidative stress through the autophagic and survival pathways. J Clin Endocrinol Metab. 2014;99:1367-74.
25. Bilezikian JP, Bikle D, Hewison M, Lazaretti-Castro M, Formenti AM, Gupta A, et al. Mechanisms in endocrinology: vitamin D and COVID-19. Eur J Endocrinol. 2020;183:R133-47.
26. Hua W, Xiaofeng L, Zhenqiang B, Jun R, Ban W, Liming L. The epidemiological characteristics of an outbreak of 2019 novel coronavirus diseases (COVID-19) in China. Zhonghua Liu Xing Bing Xue Za Zhi. 2020;41:297-300.
27. Martineau AR, Jolliffe DA, Hooper RL, Greenberg L, Aloia JF, Bergman P, et al. Vitamin D supplementation to prevent acute respiratory tract infections: systematic review and meta-analysis of individual participant data. BMJ. 2017;356:i6583.
28. Rastogi A, Bhansali A, Khare N, Suri V, Yaddanapudi N, Sachdeva N, et al. Short term, high-dose vitamin D supplementation for COVID-19 disease: a randomised, placebo-controlled, study (SHADE study). Postgrad Med J. 2022;98:87-90.
29. Sarhan N, Abou Warda AE, Sarhan RM, Boshra MS, Mostafa-Hedeab G, ALruwaili BF, et al. Evidence for the efficacy of a high dose of vitamin D on the hyperinflammation state in moderate-to-severe COVID-19 patients: a randomized clinical trial. Medicina (Kaunas). 2022;58:1358.

ORIGINAL ARTICLE

Modified extensile calcaneal exposure is safe

La exposición extensible modificada del calcáneo es segura

*Chuansheng Fu[1], Baofu Wei[1], Hongjian Pei[1], Cunyin Xue[1], Jijuan Zhou[2], and Guodong Zhong[2]**

[1]Department of Hand and Foot Surgery, Linyi People's Hospital, Linyi; [2]Academician Gu Yudong Workstation of Heze Bo'ai Hospital, Heze. China

Abstract

Objective: *The objective of this study was to evaluate the effect of open reduction and internal fixation for displaced intra-articular calcaneal fractures through a modified tarsal sinus incision.* **Methods:** *A retrospective review over 3 years of the clinical data of patients with intra-articular calcaneal fractures treated with open reduction and internal fixation through lateral hook curvy incisions. The efficacy of the 25 lateral hook curvy incisions was analyzed.* **Results:** *According to the AOFAS hindfoot function scoring criteria, there were 20 excellent (80%), 2 good (8%), 2 fair (8%), and 1 poor patient outcome. The average pre-operative Bohler's angle was 6.8 ± 8.9°, and the average angle at follow-up was 33.6 ± 5.7°. The average pre-operative Gissane angle was 89.2 ± 20.0°, and the average angle at follow-up was 115.5 ± 5.5°.* **Conclusions:** *A lateral hook curvy incision can expose the posterior articular surface of the calcaneus and the calcaneocuboid joint, reduce stripping and pulling of the soft tissue, and avoid calcaneus valgus caused by the pulling of the peroneus tendon.*

Keywords: *Calcaneal fracture. Hook curvy incision. AOFAS hindfoot function score. Bohler's angle.*

Resumen

Objetivo: *Evaluar el efecto de la reducción abierta y la fijación interna de las fracturas de calcáneo intraarticulares desplazadas a través de una incisión del seno tarsiano modificada.* **Método:** *Revisión retrospectiva de 3 años de los datos clínicos de pacientes con fracturas intraarticulares de calcáneo tratadas con reducción abierta y fijación interna a través de incisiones laterales curvadas en gancho. Se analizó la eficacia de la incisión curvada con 25 ganchos laterales.* **Resultados:** *Según los criterios de puntuación de la función del retropié de la AOFAS, hubo 20 resultados excelentes (80%), 2 buenos (8%), 2 regulares (8%) y 1 pobre. El ángulo de Bohler preoperatorio promedio fue de 6.8 ± 8.9° y el ángulo promedio en el seguimiento fue de 33.6 ± 5.7°. El ángulo de Gissane preoperatorio promedio fue de 89.2 ± 20.0° y el ángulo promedio en el seguimiento fue de 115.5 ± 5.5°.* **Conclusiones:** *Una incisión curvada en gancho lateral puede exponer la superficie articular posterior del calcáneo y la articulación calcaneocuboidea, reducir el desprendimiento y la tracción del tejido blando, y evitar el calcáneo valgo causado por tracción del tendón peroneo.*

Palabras clave: *Fractura de calcáneo. Incisión curvada en gancho. Puntuación AOFAS de función del retropié. Ángulo de Bohler.*

***Correspondence:**
Guodong Zhong
E-mail: zhongguod08@163.com

Date of reception: 13-11-2023
Date of acceptance: 06-03-2024
DOI: 10.24875/CIRU.23000580

Cir Cir. 2024;92(5):608-617
Contents available at PubMed
www.cirugiaycirujanos.com

Introduction

Due to the special anatomical position and irregular stereotypical structure of the calcaneus bone, calcaneal fracture surgeries present difficulties related to exposure, reduction, and fixation and are accompanied by many post-operative complications[1]. The most common complication associated with the surgical treatment of calcaneus fractures is delayed wound healing, likely a reflection of the limited surrounding soft-tissue envelope, as well as the extent of soft-tissue trauma associated with the injury. The most common neurological complication following operative treatment of fractures of the calcaneus is an iatrogenic injury to a sensory cutaneous nerve, particularly the sural nerve, during an extensile lateral approach[2]. Effective treatment of displaced intra-articular calcaneal fractures is challenging for all orthopedic surgeons. Proper incisions can fully reveal the fractured end of the calcaneal bone and the collapsed joint surface, which is conducive to reduction and fixation and reducing incision-related complications. This is a key to the treatment of displaced intra-articular calcaneal fractures. The extensile lateral L-shaped approach to the calcaneus is the method for surgical fixation of displaced intra-articular calcaneus fractures[3,4]. Related complications such as incision infection, non-healing incisions, skin necrosis, and nerve injuries are frequently reported[4,5], and the occurrence of any problem will affect the patient's recovery. Although the sinus tarsi approach and the enlarged sinus tarsi approach can reduce incision-related complications, their application has limitations; mainly for Sanders II and III AB type fractures[6-8]. The coronal view of the calcaneus model was used to demarcate the maximum length of the connection between the talus and calcaneus. This gap between talus and calcaneus is divided into three equal parts through three points: a, b, and c; the lateral point of sustentaculum tali is marked as point c. Based on points a, b, and c, three fracture lines were depicted as A, B, and C according to the Sanders system of classification. The model with double fracture lines (AB, AC, or BC) represented the Sanders Type III (AB, AC, BC) fracture[9].

With the continuous development and progress of minimally invasive technology, modified incision of the tarsal sinus can greatly reduce the incision range but has no impact on the full exposure of the subtalar articular surface. Doctors can also perform fracture reduction under direct vision, and this approach can reduce the damage to the blood supply to the foot and ankle. The purpose of the current study was to describe a modified tarsal sinus incision and evaluate the results of open reduction and internal fixation through the modified tarsal sinus incision as a surgical treatment of displaced intra-articular calcaneal fractures.

Methods

Patients and methods

The clinical data of patients with intra-articular calcaneus fractures treated by open reduction and internal fixation through a lateral hook curvy incision from May 2014 to July 2017 were analyzed retrospectively. The inclusion criteria were acute calcaneal fractures (within 2-3 weeks) involving the joints and Type II and III fractures, based on the Sanders classification[10]. The exclusion criteria were patients with old calcaneal fractures, Type I and IV fractures based on the Sanders classification, extra-articular fractures, and calcaneus fracture of a diabetic foot.

A total of 139 patients with calcaneal fractures admitted to our hospital were retrospectively analyzed. Among them, 13 cases of old calcaneal fractures, 28 cases of Sanders Type I and Type IV fractures, 16 cases of extra-articular fractures, and three cases of diabetic foot were excluded from the study. In 79 patients with calcaneal intra-articular fractures, 25 patients were treated with open reduction and internal fixation using a lateral hook incision.

Among the 25 patients included in this study, 21 were men and four were women. The average age was 44.6 years (range: 25-64 years). The right side was involved in 11 cases, the left side in 10 cases, and bilateral calcaneus fractures were present in four cases. The mechanism of injury was a fall from height in 22 patients and a traffic accident in one case, a heavy pound injury in one case, and falling in one case.

Twenty-five feet had closed fractures, and four cases were open fractures. Two patients had associated lumbar compression fractures and pelvic fractures without surgical treatment. One case had an associated radial fracture with open reduction and internal fixation. One case had an associated lateral malleolar fracture. One patient had an open fracture with a medial soft-tissue defect, and a secondary flap graft was performed to repair the wound.

At the time of admission to the hospital, anteroposterior, lateral, and internal oblique radiographs of the injured foot and an axial radiograph of the fractured calcaneus were taken. A pre-operative CT scan was made for all cases to evaluate the size of the displaced fracture fragments and help the surgeons reduce the displaced fracture fragments. From the plain radiographs, the pre-operative Bohler angle and Gissane angle were measured. The posterior articular surface was divided into three columns by two fracture lines according to the coronal view of CT images. Line C separated the medial fragment from the posterior talar facet of the calcaneus[11,12]. There were 15 cases of Type II fractures, seven Type IIA, and eight Type IIB. Fourteen cases were Type III fractures, 10 were Type IIIAB, one was Type IIIAC, and three were Type IIIAC. In 18 patients with calcaneal fractures, the calcaneocuboid joint surface was involved. If the wrinkle sign was observed at the lateral side of the heel, surgery was performed.

Patients were clinically evaluated using the AOFAS ankle–hindfoot score (best score = 100 points)[6]. This clinical rating system combines subjective scores of pain and function provided by the patient with objective scores based on the surgeon's physical examination of the patient (to assess sagittal motion, hindfoot motion, ankle–hindfoot stability, and alignment of the ankle–hindfoot). The scale includes nine items that can be divided into three subscales (pain, function, and alignment). Pain comprises one item with a maximum score of 40 points, indicating no pain. Function comprises seven items with a maximum score of 50 points, indicating full function. Alignment comprises one item with a maximum score of 10 points, indicating good alignment. The maximum score is 100 points, indicating no symptoms or impairments. The AOFAS score was divided into groups according to the literature: a score of 90-100 was graded as an excellent result, 75-89 as good, 50-74 as fair, and < 49 points was graded as a failure or poor outcome[3].

Anatomical basis and design of the modified tarsal sinus incision

Incision design: an incision was made in the side midline of the calcaneus to open the flap on both sides to render calcaneus exposure and operation easier. Accordingly, the central point of the calcaneocuboid joint was A, and the middle point from the bottom of the sinus tarsus to the metatarsal side of the calcaneus was B. A line was made through A and B. Point C was the intersection point of a 1 cm horizontal line in front of the Achilles tendon and a vertical line to the Achilles tendon from 1 cm above the lateral malleolus. Point D was the intersection of the extension line at a 30° angle between point C and the Achilles tendon and the extension line at two points, A and B. Points C, D, and A were connected into a hook curvy incision, which was extended to both ends through points A and C as required (Fig. 1A). The incision line corresponded to the midline of the lateral wall of the calcaneus, which is the approach for exposing the subtalar joint and the calcaneocuboid joint (Fig. 1B).

Anatomical basis: the blood supply of the lateral calcaneus region derives from the arterial network comprising the lateral calcaneus artery, sinus tarsus artery, lateral tarsal artery, and basolateral plantar artery, and rich vascular chains form in the skin and subcutaneous tissue (Fig. 2A)[13,14]. Although the plantar and lateral skin of the heel is supplied by different angiosomes, this is also the anatomical basis of the laterally expanded L-shaped incision. However, there is an extensive vascular network between the two angiosomes at the lateral side and the plantar skin junction of the heel. Anatomical specimens perfused solely through the anterior tibial artery showed an extensive vascular network between the lateral region and pelma of the heel. The skin below the midline of the calcaneus can also obtain blood supply through the traffic branch of the lateral tarsal artery (Fig. 2B).

The sural nerve is accompanied by a small saphenous vein, wound to the lateral heel below the lateral malleolus, runs parallel to the pelma of the foot, and at the front of the calcaneus, moves obliquely across the peroneus brevis tendon and the peroneus longus tendon to the dorsolateral foot to become the lateral dorsal cutaneous nerve of the foot (Fig. 2C). The sural nerve is a cutaneous nerve. When injured, it mainly causes numbness and paresthesia in the innervated area of the nerve, which can be manifested as numbness in the posterolateral area of the calf, the lateral ankle area, the dorsolateral area of the foot, and the skin of the fourth and fifth toes. The fibular nerve is divided into two-to-three lateral cutaneous nerves behind the lateral malleolus, run downward perpendicular to the foot, and are distributed in the lateral skin of the heel. The proximal part of the sural nerve and the small saphenous vein are included in the flap located proximal to the incision, and the distal part is located in the flap of the distal end of the incision. The

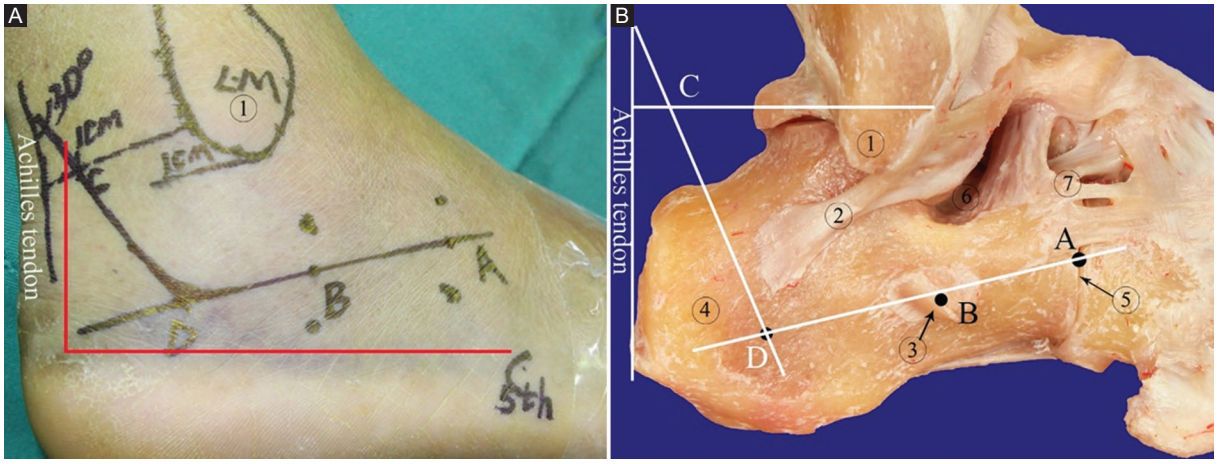

Figure 1. *The design of the modified tarsal sinus incision.* **A:** *the line ABDC is the lateral hook curvy incision.* **B:** *the relationship between the lateral hook curvy incision and calcaneus.* a: *The midpoint of the calcaneocuboid joint.* b: *The calcaneal midpoint at the level of the sinus.* c: *The intersection point of 1 cm horizontal line in front of the Achilles tendon and vertical line to the Achilles tendon from 1 cm above the lateral malleolus.* d: *The intersection point of slash at a 30 less tendon and vertical line to the Achilles tendon f connection.*
1: The lateral malleolus; 2: calcaneofibular ligament; 3: peroneal trochlea; 4: calcaneal tuberosity; 5: Calcaneocuboid joint; 6: Tarsal sinus; 7: Anterior tubercle of calcaneus. The red line is the extended lateral L-shaped approach.

peroneus brevis tendon runs obliquely forward and down the lateral side of the calcaneus, from the back upward and is attached to the lateral calcaneal wall by the inferior peroneal retinaculum (Fig. 2D). The anterior tubercle of the calcaneus and calcaneocuboid joint is located above the front of the peroneal tendon. The peroneal tendon should be pulled down to expose the calcaneocuboid joint and the base of the sinus tarsus. The subtalar articular surface can be clearly exposed through the tarsal sinus, and a Kirschner wire (K-wire) can be inserted to poke the collapsed articular surface through this gap.

Surgical technique

The patients were positioned on the uninjured side with the ankle joint in a neutral position. Surgical pads were folded into squares and placed under the medial malleolus. The heel was slightly inverted in the air. The procedure was performed under a femoral tourniquet. (1) The skin and subcutaneous tissue were cut according to the hook curvy incision line, and the bleeding was carefully stopped (ligation and hemostasis; electric knife used with caution). The peroneal nerve was exposed on the superficial layer of the peroneal tendon, distal to the incision, and was freed and protected (Fig. 3A). (2) At the proximal side of the incision, a cut was made vertically to the periosteum without separation from deep tissue. The lateral calcaneal cutaneous nerve was severed. The lateral calcaneal artery was ligated for hemostasis. A separation was made along the periosteal surface to the malleolar tip, and the calcaneofibular ligament was cut to expose the subtalar articular surface. A separation was made along the surface of the periosteum in the middle of the incision through the deep layer of the peroneus brevis tendon and peroneus longus tendon. An attempt was made to free and protect the peroneus tendon sheath as much as possible to expose the tarsal sinus. A separation was made above the peroneus brevis tendon distal to the incision. The stop point of the extensor digitorum brevis was separated to expose the sinus tarsus, the anterior tubercle of the calcaneus, the calcaneocuboid joint, and the dorsal calcaneocuboid ligament. The proximal peroneus longus tendon was punctured with one-to-two 1.5 K-wires to the external malleolus, the flap was straightened, and the needle was slightly bent to the proximal end. Attention was paid not to squeeze the flap. A 1.5 K-wire was inserted into the talus neck through the front of the peroneus brevis tendon. The flap was straightened and bent medially. As this was necessary, the deep flap was slightly stripped on the surface of the peroneal tendon to reduce flap tension. (3) A large surgical towel was placed under the inner malleolus, and the calcaneus bone was slightly inverted. Slight poking at the subtalar joint with a 3.5 K-wire revealed the posterior articular surface of the calcaneus, and the collapsed posterior articular surface was restored through the sinus tarsal poking using the K-wire for

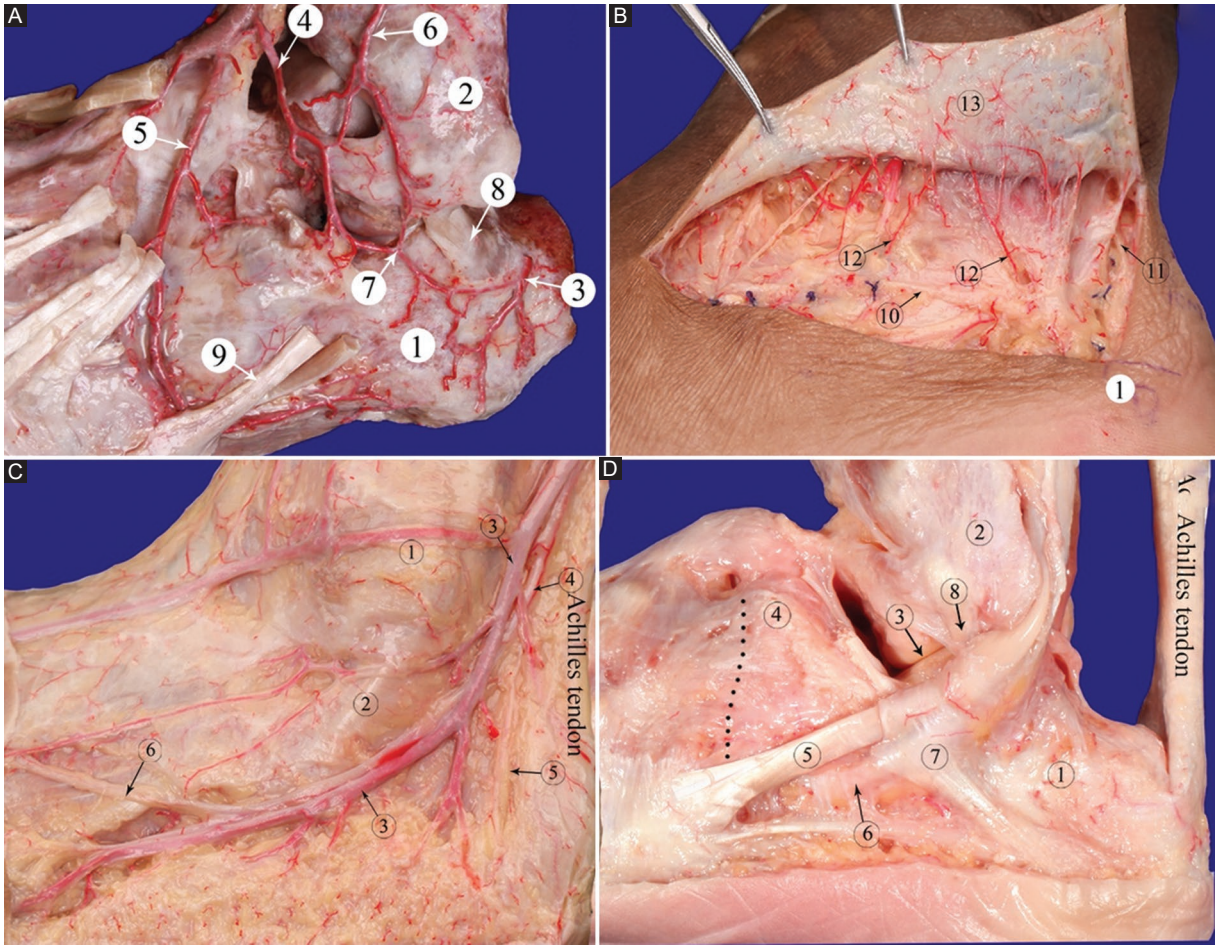

Figure 2. A: *the artery network of the lateral area of the calcaneus.* **B:** *the extensive subcutaneous capillary network in the proximal end of the hook-curvy incision.* **C:** *the sural nerve and less saphenous vein.* **D:** *the lateral wall of the calcaneus and the peroneal tendons.*
1: Calcaneus; 2: lateral malleolus; 3: the lateral calcaneal artery; 4: tarsal sinus artery; 5: lateral tarsal artery; 6: descending branch of external superior malleolus artery; 7: communicating branches; 8: calcaneofibular ligament; 9: tendon of peroneus brevis; 10: the sural nerve; 11: subdermal vascular plexus; 12: Perforating Vessels. c1: the lateral malleolus; c2: tendon of peroneus brevis; c3: the less saphenous vein; c4: the sural nerve; c5: the lateral calcaneal nerve; c6: lateral dorsal cutaneous nerve of foot. d1: calcaneus; d2: lateral malleolus; d3: the subtalar joint; d4: anterior superior tubercle of calcaneus; d5: tendon of peroneus brevis; d6: Peroneus Longus Tendon; d7: retinaculum musculorum peroneorum inferius; d8: calcaneofibular ligament. The black dotted line is the calcaneocuboid joint.

temporary fixation (Figs. 3B and 4). A 3.5 K-wire was placed vertically into the calcaneal tuberosity, which was pulled down slightly to reset. The operator squeezed the calcaneal tuberosity with both hands and turned a K-wire to correct the calcaneus varus. After restoring the joint line of the calcaneal tuberosity, temporary fixation was applied from the calcaneal tuberosity through the posterior articular surface using a K-wire (Fig. 3C). After reduction, one-to-two 2.0 K-wires were temporarily fixed through the calcaneal tubercle to the anterior tubercle of the calcaneus. The calcaneal side and axial radiograph were taken using a C-arm perspective and replaced with the corresponding steel plate/screw fixation (Fig. 3D). (4) The mild valgus position of the heel was maintained, and a negative pressure drainage tube connected with negative pressure drainage was put in place. Subcutaneous intermittent suturing was performed to reduce the incision tension. Loose vertical mattress-type sutures were used for the incision. Soft gauze compressed the lateral wall of the calcaneus.

Post-operative management

We evaluated the peroneal function within 24 h after the patient's surgery, and the injury mainly caused innervation numbness and paresthesia. On the day after surgery, patients can be instructed to perform back extension, plantar flexion, and straight leg elevation exercises under non-weight-bearing ankle

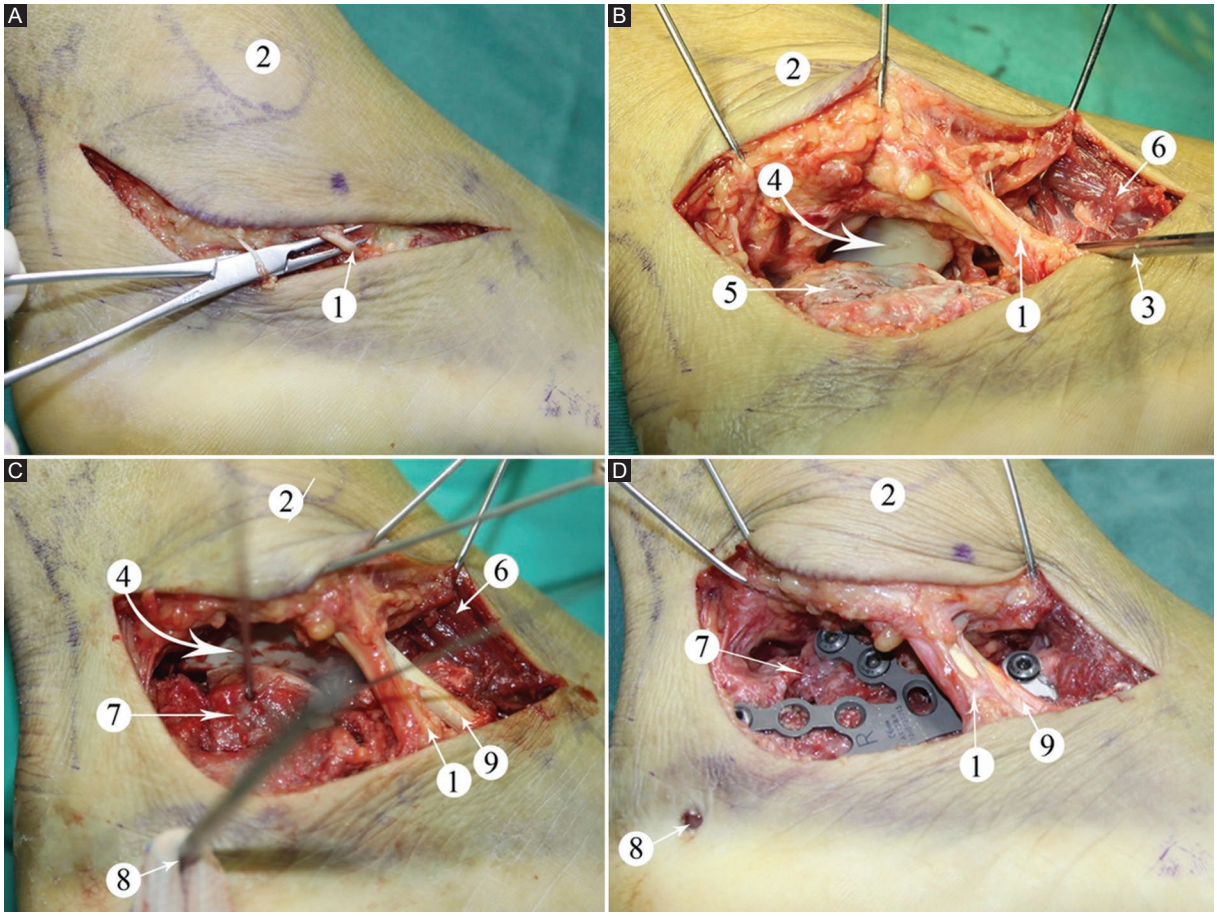

Figure 3. A: *the incision and sural nerve.* **B:** *contactless traction of the Kirschner wire revealed the subtalar joint and the lateral wall of the calcaneus, and the Kirschner wire poke the collapsed articular surface.* **C:** *reduce the articular surface, and temporarily fix with the Kirschner wire.* **D:** *replace with plate fixation and remove temporary Kirschner wire.*
1: sural nerve; 2: lateral malleolus; 3: Kirschner wire poking articular surface; 4: subtalar articular surface; 5: lateral wall of calcaneus; 6: extensor digitorum brevis; 7: reduction of the collapsed fracture block; 8: Kirschner wire for traction of calcaneal tubercle; 9: tendon of peroneus brevis.

joint conditions. Low-molecular-weight heparin calcium anticoagulant therapy was provided after surgery until discharge. Patients were encouraged to carry partial weight on crutches at 4 weeks after surgery and were allowed to carry full weight when signs of bone healing were observed on re-examination X-rays at 6-10 weeks after surgery. The Bohler and Gissane angles were measured by X-ray 6 months after surgery. All patients were followed up for 2 years to assess their recovery.

Results

The modified tarsal sinus incision adequately exposed the posterior facet, the lateral wall of the calcaneus, and the calcaneocuboid joint. A traction valgus of calcaneal tuberosity can correct varus deformity. With the talus articular surface as a reference, the inferior talus' articular surface fracture block was restored through tarsal sinus poking and temporarily fixed with a K-wire (Fig. 4). The articular plane was reduced to squeeze the lateral wall of the calcaneus. Titanium bone plates of appropriate type were selected, trimmed, and shaped according to fracture morphology and then inserted into the lateral calcaneal bone after subperiosteal dissection. After the percutaneous insertion of the guide by the template positioning method, drilling holes and screws were inserted to fix the plate. All 25 cases were followed up for an average of 18.7 (12-24) months. Bone healing was achieved in all patients at 12-month follow-up. The skin incision healed well in all cases without necrosis, infection, or sural nerve damage (Fig. 4). The fracture had healed in all cases after an average period of 8 weeks (6-10 weeks). Due to the different elastic modulus and compositional structure of metal and bone, the stress shielding effect would occur, which could lead to the easy recurrence of fractures

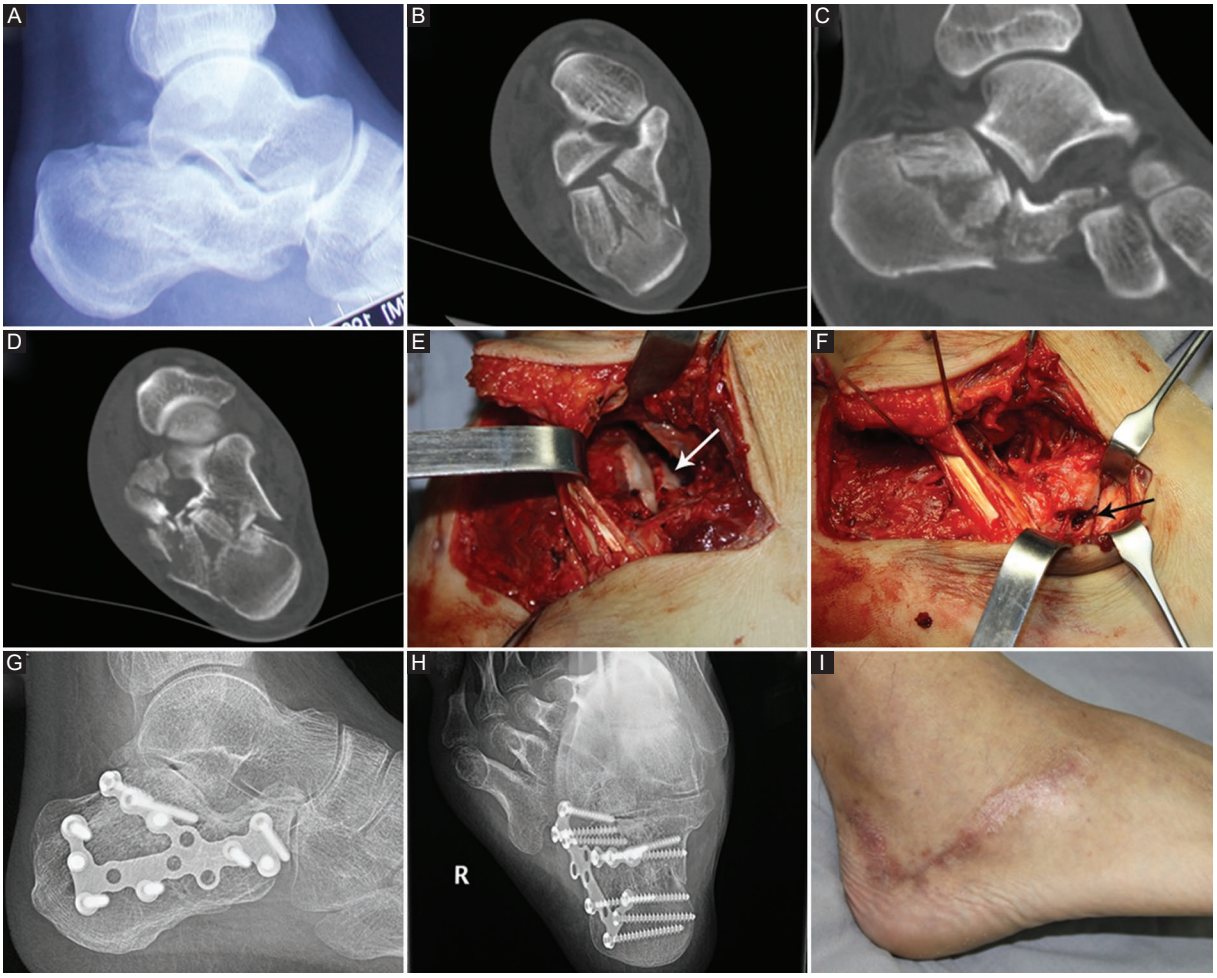

Figure 4. A: *the lateral view of pre-operative radiographs.* **B-D:** *the images of the CT scan, Sanders type IIIBC.* **E:** *the fracture line of the posterior facet of calcaneus (white arrow).* **F:** *the fracture line involved the calcaneocuboid joint (black arrow).* **G** and **H:** *the lateral view and axial view of the post-operative radiographs.* **I:** *the healed lateral hook curvy incision.*

around the fixed object. Accordingly, the plate-screw internal fixers were removed in 12 patients through the original incision 1-3 years after surgery, and all of the incisions had healed well.

According to the AOFAS ankle–hindfoot score, there were 20 excellent (80%), 2 good (8%), 2 fair (8%), and 1 poor patient (4%) outcomes. The 22 excellent and good cases were rated as satisfactory (88%); the three poor and fair cases were rated as unsatisfactory (12%). Pain at the lateral aspect of the heel was the main complaint of the majority of patients, particularly after long walks and heavy work. Six patients complained of feeling sore and uncomfortable in rainy weather; 12 patients (48%) returned to daily activities but could not bear heavy work; 3 cases (12%) felt mild pain when the surgical area was cold. A slight change in posture was observed in one patient (4%) with a bilateral calcaneal fracture. No pain developed related to irritation by the internal plate and screws. No cases of subluxation of peroneal tendons could be detected on follow-up. The one poor case (4%) was a patient with bilateral calcaneal fractures, Sanders IV right and Sanders IIAB left type, with poor post-operative recovery. When walking 100 m, the patient experienced unbearable pain, and foot movement was limited. This patient was found to have hyperplasia of the adjacent joints on X-ray 6 months after surgery. The average pre-operative Bohler's angle was 6.8 ± 8.9°, and the average angle at follow-up was 33.6 ± 5.7°. The average pre-operative Gissane angle was 89.2 ± 20.0°, and the average angle at follow-up was 115.5 ± 5.5°.

Discussion

Calcaneal fractures are the most common tarsal fractures. Due to their irregular morphological

structure and complex biomechanical functions, calcaneal fractures are considered one of the most challenging fractures, particularly displaced intra-articular calcaneal fractures. Restoring the shape of the articular surface, axis, and length and width of the calcaneus is essential for the recovery of the weight-bearing and walking abilities of the foot. In a randomized controlled trial, Buckley et al. found that patients with displaced intra-articular calcaneal fractures who did not receive worker compensation and underwent surgery had significantly higher satisfaction scores compared to non-surgical patients. The key to surgical treatment of displaced intra-articular calcaneal fractures is to fully expose intra-articular fractures to facilitate anatomical reduction and internal fixation. Open reduction and internal fixation through an extended lateral L-shaped approach have been considered the standard treatment[15]. However, the L-shaped incision was made from 3.5 cm below the lateral ankle along the plantar skin junction to the base of the 5th metatarsal bone with this surgical approach, giving rise to disadvantages such as a large dissection range, difficulty exposing the subtalar and calcaneocuboid joint surface, and a high learning curve.

Because the peroneal tendon travels obliquely through the lateral wall of the distal calcaneus, the pulling tendon to the dorsal side indirectly leads to the calcaneus valgus, which is not conducive to the exposure and reduction of the subtalar articular surface. The incidence of complications, such as post-operative incision infection, osteomyelitis, skin margin necrosis, plate exposure, and sural nerve injury is thus high, and the occurrence of complications is inversely correlated with the experience of the surgeon[16].

With the continued development of minimally invasive and rapid rehabilitation concepts, the treatment of calcaneal fractures using a tarsal sinus incision has gradually been recognized in recent years. Some studies found that the incidence of soft-tissue necrosis, infection, and other complications after tarsal sinus incisions had been reduced to some extent[5,13]. However, this method is only suitable for less displaced intra-articular calcaneal fractures, such as Sanders II and IIIAB fracture types[17]. In addition, this incision has limited exposure to the posterior articular surface and a high learning curve, which limits its clinical application[15].

The transverse arm of the lateral enlarged L-shaped incision is located between the blood supply area of the lateral and the plantar angiosomes, enabling the raised skin margin to obtain a sufficient blood supply from the feeding angiosome. Anatomical studies showed the presence of a rich blood supply in the lateral calcaneal region, and its feeding arteries include the lateral calcaneal artery, sinus tarsus artery, and lateral tarsal artery. These arteries have traffic branches that connect to vascular networks. The skin and subcutaneous soft tissue have an extensive vascular network. The lateral region of the heel is also connected to branches of the lateral plantar artery through traffic branches and the vascular network, enabling it to obtain a sufficient blood supply from the pelma area near the plantar region. This is the anatomical basis for the design of the lateral hook curvy incision of the calcaneus. The distal part of the incision can obtain sufficient blood supply from the terminal branches of the plantar and tarsal lateral artery to ensure the survival of the skin margin and significantly reduce the occurrence of complications related to the incision.

Compared with the lateral enlarged L-shaped incision from the metatarsal side of the calcaneus to the proximal end, the lateral hook curvy incision from the midline to the lateral side of the calcaneus is more likely to expose the subtalar joint surface, and the scope of the dissection is small. The hook curvy incision is oblique across the peroneal tendon, and the sinus tarsus and calcaneocuboid joint are exposed above the peroneal tendon, which is more conducive to the reduction and fixation of the fracture when the calcaneocuboid joint is involved. After clearing the tarsal sinus, the collapsed subtalar articular surface can be exposed. With the anterior calcaneus nodule as the fulcrum, a K-wire can be used to poke the collapsed joint surface. At the same time, through the lateral wall extrusion, it is easy to achieve an anatomical reduction of the inferior joint surface and restore the height of the calcaneal bone and the Bohler and the Gissane angles while reducing the dissection of the calcaneal fracture block. The proximal end of the incision may expose the upper edge of the calcaneal tuberosity, facilitating the reduction of the displaced calcaneal tuberosity.

Because the posterior articular surface of the calcaneus is difficult to reveal, and the soft-tissue blood supply of the lateral calcaneus is weak, the selection of appropriate surgical methods is very important for the treatment of calcaneus fractures. The lateral calcaneal L-shape incision is commonly used for the surgical treatment of calcaneal fractures involving the posterior articular surface, as it provides a wide surgical field of view and is firmly fixed with a plate that applies an overall compression force to the calcaneal

bone, thereby restoring calcaneal width and preventing varus and valgus deformities. However, it was reported in the literature that lateral calcaneal L-shaped incision is prone to damaging the lateral calcaneal artery, and the incidence of post-operative soft-tissue necrosis, incision split, exposed plate, and infection is high[18]. In addition, both proximal and distal L-shaped incisions pose a risk of damage to the sural nerve. Therefore, many studies have focused on minimally invasive surgery for calcaneal fractures to minimize soft-tissue damage. The standard tarsal sinus incision is a longitudinal straight incision from the tip of the lateral ankle and extends to the base of the fourth metatarsal bone. As one of the minimally invasive techniques widely used in clinical practice, this approach can directly observe the posterior articular surface, making post-operative incisor-related complications less likely to occur. Li treated 53 cases of calcaneal fracture with incision reduction and internal fixation of the tarsal sinus, and the incidence of post-operative sural nerve injury was 9.6%[19]. The standard tarsal sinus incision is made below the anterior lateral malleolus, exposing the articular surface above the short and long peroneal tendons, where pulling the tendons downward may cause traction injury to the local sural nerve. Scholars conducted anatomical studies on the distribution of the sural nerve in 110 Korean carcasses, and the results showed that 58.8% of the carcasses had isolated a branch of the medial cutaneous nerve of the dorsal foot extending to the sural nerve within the standard tarsal sinus incision[20]. Therefore, a standard tarsal sinus incision may not be able to completely avoid sural nerve injury. A modified tarsal sinus incision can provide sufficient anatomical exposure to complete the reduction and fixation of calcaneal fractures. If it is necessary to extend back to the anterior process of the calcaneus, it will be easier to do so while protecting the long and short peroneal tendons, sural nerve, and accompanying blood vessels. The standard tarsal sinus incision makes it difficult to restore calcaneal width due to the limited exposure of the subtalar articular surface. A modified tarsal sinus incision can be used to reduce the fracture and fix the calcaneal fissure with a shapeable anatomical titanium plate. The location of the screw hole is determined percutaneously using the mold positioning method, after which the locking sleeve is placed. This avoids soft-tissue injury and reduces the possibility of injury to the lateral cutaneous nerve of the foot and subsequently obtains better biomechanical strength.

This study has the following limitations: the included sample size is small, and future studies with larger samples and multiple centers are needed to prove the efficacy of the presented approach. We did not report the effect of injury mechanisms and smoking history on surgical outcomes, which will serve as a limitation of this study and is expected to be explained in future studies. In addition, the researchers did not perform gait or plantar pressure distribution analyses; as such, it is uncertain whether there are significant abnormalities in post-operative gait patterns. Finally, this study did not compare the modified tarsal sinus incision with other surgical methods, and it is anticipated that future studies will be compared by statistical methods to highlight the advantages of the modified tarsal sinus incision.

Conclusion

Despite the limitations of the current study, the modified tarsal sinus incision has shown to be one of the safe methods for the treatment of displaced intra-articular calcaneal fractures. The lateral hook curvy incision can fully expose the subtalar articular surface and the calcaneocuboid joint and avoid ineffective exposure and negative traction reduction, which is conducive to the reduction and healing of the fracture.

Declarations

Ethics approval and consent to participate

This study was conducted in accordance with the Declaration of Helsinki and approved by the ethics committee of Heze Bo'ai Hospital. Written informed consent was obtained from all participants in this study.

Authors' contributions

Conception and design of the work: Fu CS and Wei BF; Data collection: Pei HJ, Xue CY, Zhou JJ, and Zhong GD; Supervision: Fu CS and Wei BF; Analysis and interpretation of the data: Fu CS, Wei BF, Pei HJ, Xue CY, Zhou JJ, and Zhong GD; Statistical analysis: Fu CS, Wei BF, Pei HJ, and Zhong GD; Drafting the manuscript: Fu CS and Wei BF; Critical revision of the manuscript: all authors; Approval of the final manuscript: all authors.

Funding

The authors declare that they have not received funding.

Conflicts of interest

The authors declare no conflicts of interest.

Ethical disclosures

Protection of human and animal subjects. The authors declare that the procedures followed were in accordance with the regulations of the relevant clinical research ethics committee and with those of the Code of Ethics of the World Medical Association (Declaration of Helsinki).

Confidentiality of data. The authors declare that they have followed the protocols of their work center on the publication of patient data.

Right to privacy and informed consent. The authors have obtained the written informed consent of the patients or subjects mentioned in the article. The corresponding author is in possession of this document.

Use of artificial intelligence for generating text. The authors declare that they have not used any type of generative artificial intelligence for the writing of this manuscript nor for the creation of images, graphics, tables, or their corresponding captions.

References

1. Rammelt S, Zwipp H. Fractures of the calcaneus: current treatment strategies. Acta Chir Orthop Traumatol Cech. 2014;81:177-96.
2. Clare MP, Crawford WS. Managing complications of calcaneus fractures. Foot Ankle Clin. 2017;22:105-16.
3. Backes M, Schep NW, Luitse JS, Goslings JC, Schepers T. The effect of postoperative wound infections on functional outcome following intra-articular calcaneal fractures. Arch Orthop Trauma Surg. 2015;135:1045-52.
4. Backes M, Schepers T, Beerekamp MS, Luitse JS, Goslings JC, Schep NW. Wound infections following open reduction and internal fixation of calcaneal fractures with an extended lateral approach. Int Orthop. 2014;38:767-73.
5. Femino JE, Vaseenon T, Levin DA, Yian EH. Modification of the sinus tarsi approach for open reduction and plate fixation of intra-articular calcaneus fractures: the limits of proximal extension based upon the vascular anatomy of the lateral calcaneal artery. Iowa Orthop J. 2010;30:1612-7.
6. Budiman-Mak E, Conrad KJ, Roach KE. The foot function index: a measure of foot pain and disability. J Clin Epidemiol. 1991;44:561-70.
7. Gonzalez TA, Kwon JY. Sinus tarsi approach for calcaneus fractures. Oper Tech Orthop. 2015;25:235-41.
8. Schepers T. The sinus tarsi approach in displaced intra-articular calcaneal fractures: a systematic review. Int Orthop. 2011;35:697-703.
9. He K, Fu S, Liu S, Wang Z, Jin D. Comparisons in finite element analysis of minimally invasive, locking, and non-locking plates systems used in treating calcaneal fractures of sanders type II and type III. Chin Med J (Engl). 2014;127:3894-901.
10. Rao K, Dibbern K, Day M, Glass N, Marsh JL, Anderson DD. Correlation of fracture energy with sanders classification and post-traumatic osteoarthritis after displaced intra-articular calcaneus fractures. J Orthop Trauma. 2019;33:261-6.
11. Sanders R, Fortin P, DiPasquale T, Walling A. Operative treatment in 120 displaced intraarticular calcaneal fractures: results using a prognostic computed tomography scan classification. Clin Orthop Relat Res. 1993;290:87-95.
12. Schepers T, Backes M, Dingemans SA, De Jong VM, Luitse JS. Similar anatomical reduction and lower complication rates with the sinus tarsi approach compared with the extended lateral approach in displaced intra-articular calcaneal fractures. J Orthop Trauma. 2017;31:293-8.
13. Wei BF, Amendola A, Fu CS. Clinical Anatomy and Surgical Altas of the Foot and Ankle. Jinan: Shandong Science and Technology Press Co Ltd.; 2021. p. 178-91.
14. Wei BF, Zhang JZ, Xu XY. Surgical Anatomy Altas of Foot and Ankle. Beijing: People's Military Medical Press Co Ltd.; 2015. p. 187-91.
15. Jansen SC, Bransen J, Van Montfort G, Besselaar AT, Van der Veen AH. Should the extended lateral approach remain part of standard treatment in displaced intra-articular calcaneal fractures? J Foot Ankle Surg. 2018;57:1120-4.
16. Schepers T, Hartog DD, Vogels LM, Van Lieshout EM. Extended lateral approach for intra-articular calcaneal fractures: an inverse relationship between surgeon experience and wound complications. J Foot Ankle Surg. 2013;52:167-71.
17. Piovesana LG, Lopes HC, Pacca DM, Ninomiya AF, Dinato MC, Pagnano RG. Assessment of reproducibility of sanders classification for calcaneal fractures. Acta Ortop Bras. 2016;24:90-3.
18. De Groot R, Frima AJ, Schepers T, Roerdink WH. Complications following the extended lateral approach for calcaneal fractures do not influence mid-to long-term outcome. Injury. 2013;44:1596-600.
19. Li S. Wound and sural nerve complications of the sinus tarsi approach for calcaneus fractures. Foot Ankle Int. 2018;39:1106-12.
20. Jeon SK, Paik DJ, Hwang YI. Variations in sural nerve formation pattern and distribution on the dorsum of the foot. Clin Anat. 2017;30:525-32.

ORIGINAL ARTICLE

Evaluation of hemostatic efficacy and safety of oxidized regenerated cellulose (Pahacel®) in coronary bypass surgery

Evaluación de la eficacia hemostática y de la seguridad de la celulosa regenerada oxidada (Pahacel®) en cirugía de bypass coronario

Hasan A. Keskin

Department of Cardiovascular Surgery, Health Sciences University, Ankara Training and Research Hospital, Ankara, Turkey

Abstract

Objective: *The aim of this study is to evaluate the efficacy and safety of oxidized regenerated cellulose (ORC) in patients who underwent coronary artery bypass grafting (CABG) surgery and to compare the results of patients in whom ORC was used or not used for control of bleeding.* **Method:** *Pre-, intra-, and post-operative demographic and medical parameters of the patients in whom ORC was used or not used were compared. Quantitative data were analyzed with mean and standard deviation. Group differences were assessed with the Mann–Whitney U test.* **Results:** *It was found that the duration of surgery, average numbers of erythrocyte and fresh frozen plasma (FFP) transfusions during surgery, average post-operative FFP transfusion count, duration of intensive care unit stay, and chest tube removal times were lower in the ORC group compared to the control group, and all these differences were statistically significant ($p < 0.05$ for all of these parameters).* **Conclusions:** *The study successfully demonstrated the effective and safe use of topical ORC in controlling bleeding and preventing oozing during CABG surgeries.*

Keywords: *Coronary artery bypass grafting. Oxidized regenerated cellulose. Complications. Hemostat. Hemostasis.*

Resumen

Objetivo: *Evaluar la eficacia y la seguridad de la celulosa regenerada oxidada (CRO) en pacientes sometidos a cirugía de injerto de derivación de arteria coronaria y comparar los resultados de los pacientes en los que se utilizó o no la CRO para el control del sangrado.* **Método:** *Se compararon los parámetros demográficos y médicos pre-, intra- y posoperatorios de los pacientes en los que se utilizó o no CRO. Los datos cuantitativos se analizaron con media y desviación estándar. Las diferencias grupales se evaluaron con la prueba U de Mann Whitney.* **Resultados:** *Se encontró que la duración de la cirugía, el número promedio de transfusiones de eritrocitos y de plasma fresco congelado durante la cirugía, el recuento promedio de transfusiones de plasma fresco congelado posoperatorias, la duración de la estadía en la unidad de cuidados intensivos y los tiempos hasta la extracción del tubo torácico fueron menores en el grupo de CRO en comparación con el grupo control, y todas estas diferencias fueron estadísticamente significativas ($p < 0.05$).* **Conclusiones:** *El estudio demostró con éxito el uso eficaz y seguro de la CRO tópica para controlar el sangrado y prevenir la supuración durante las cirugías de derivación de arteria coronaria.*

Palabras clave: *Cirugía de derivación de arteria coronaria. Celulosa regenerada oxidada. Complicaciones. Hemostático. Hemostasia.*

Correspondence:
Hasan A. Keskin
E-mail: attilakeskin@hotmail.com

Date of reception: 29-10-2023
Date of acceptance: 18-03-2024
DOI: 10.24875/CIRU.23000535

Cir Cir. 2024;92(5):618-625
Contents available at PubMed
www.cirugiaycirujanos.com

Introduction

Bleeding is a common surgical complication which increases post-operative complications, unfavorable transfusion-related events, and the risk of infection, necessitating a longer hospital length of stay (LOS) and greater use of medical resources. When bleeding cannot be controlled during surgery using standard techniques, absorbable hemostatic agents (AHA) have been utilized as adjunctive therapy. When electrocoagulation, ligation, or other conventional techniques of bleeding control are ineffective or impractical, oxidized regenerated cellulose (ORC), a commonly used AHA, can be used in the control of small arterial, venous, and capillary hemorrhage[1]. ORC is a biodegradable, sterile, fibrous substance created by the oxidation of regenerated cellulose. Various forms of ORC are used in surgery for the control of bleeding as an absorbable hemostatic substance[2]. Despite the fact that ORC is widely used worldwide, research on issues relating to the safety and efficacy of this hemostat, as well as its effects on medical costs and surgical outcomes, has been ongoing for years. Many studies have examined its efficacy in numerous specialties, including urology, plastic surgery, obstetrics and gynecology, general surgery, neurology, and cardiovascular surgery[3-7]. Nevertheless, no studies other than two technical descriptions of the use of ORS in cardiac bypass procedures were found in the literature review[8,9]. Despite the fact that 345 coronary artery bypass grafting (CABG) surgeries used one of these techniques, the outcome factors assessed in that study were sparse and not provided in detail[9].

The objective of the present investigation was to conduct a retrospective assessment of the effectiveness and safety of ORC in individuals who underwent coronary bypass surgery, specifically focusing on cases where this hemostatic agent was employed for bleeding control. In addition, the study aimed to compare these outcomes with those of patients in whom the hemostatic agent was not utilized. Numerous hemostatic products are used in medical practice, and the data obtained from this study can serve as a reference for researchers to compare the outcomes of different studies involving various hemostats. Positive findings from this study have the potential to generate interest among surgeons who have not yet utilized ORC in coronary bypass surgeries, encouraging them to use this product and to compare the efficacy and safety of ORC with other hemostats.

Methods

This retrospective, cross-sectional, and observational research included patients who had undergone coronary bypass grafting surgery between September 2022 and March 2023 in the Cardiovascular Surgery Department of Health Sciences University Ankara Training and Research Hospital and in whom ORC was used or not used for control of bleeding. The study was approved by the Ethics Committee of Ankara Training and Research Hospital. The ORC product, used in this study was PAHACEL® standard absorbable hemostat, which is a Class III medical device, and manufactured by Altaylar Medikal, Ankara, Türkiye.

After pre-medication and induction of anesthesia, approximately 300-400 mL of blood was collected from all patients with hemoglobin levels above 12.0 for autotransfusion. All patients underwent the standard conventional cardiopulmonary bypass (CPB) technique. Autologous blood was intravenously administered to the patient after CPB. In the control group, conventional hemostasis was achieved and ORC was not applied. In patients in the ORC group, to ensure hemostasis, ORC product (PAHACEL®) was temporarily applied over the distal and proximal coronary bypass anastomoses, even if the bleeding was minimal, or there was oozing. Following the instructions in the product's user manual, the ORC product was removed once bleeding or leakage was controlled and was not left in the surgical area. After achieving hemostasis, three chest drainage tubes were inserted, one in the left hemithorax and two in the mediastinum. The sternum was approximated using four figure-of-eight wires, and the subcutaneous tissue was closed with PDS sutures, followed by skin closure using staples.

The evaluated parameters regarding the patients and the surgical procedures during the pre-operative, operative process, and post-operative hospital stay were age, gender, body mass index (BMI), American Society of Anesthesiologists (ASA) score, smoking status, additional diseases (diabetes mellitus, hypertension, chronic obstructive pulmonary disease [COPD], etc.), pre-operative thrombocyte, hematocrit, prothrombin time (PT) and pre-, intra-, and post-operative anti-clotting time (ACT) values, operation time, the number of per- and/or post-operative red blood cell or fresh frozen plasma (FFP) transfusions, post-operative platelet transfusion or fibrinogen treatment, the duration of post-operative intensive care

stay, post-operative hospital stay, amount of drainage into the chest tube, the time of chest tube removal, main complications, morbidity, and mortality.

Following standardized protocols, all patients who underwent surgery at the Cardiovascular Surgery Clinic for coronary artery disease were scheduled for a follow-up visit at the outpatient clinic on the 15th day after the operation for examination and removal of sutures were performed. In addition to this regular procedure, patients were informed upon discharge that if they experienced any unexpected signs or symptoms such as severe pain, redness, or discharge at the surgical site, high fever, or difficulty in breathing, they should promptly return to the hospital for immediate evaluation and care.

In line with these principles, during the standard follow-up visit on post-operative day 15 or when patients seek medical attention due to unexpected issues, their current complaints were assessed through questioning, and physical examinations were conducted. If a wound infection was suspected, the wound was drained, and a sample was collected for culture and antibiotic sensitivity testing. In cases where complications were suspected, appropriate tests were carried out and carefully evaluated.

The early complications identified for this study were obtained from patient records during their hospital stay and within the 1st month after the surgery. These complications included seroma, superficial and/or deep wound infections, hematoma, bleeding, tamponade, and pleural effusion. Retrieving information for this retrospective study posed no difficulties since all the parameters evaluated were routine and mandatory data recorded in the hospital's registry system by the attending physician.

Patients with pre-existing chronic liver or kidney dysfunction and those with missing recorded data were excluded from this retrospective analysis. All of the patients had been receiving acetylsalicylic acid preoperatively. Although it had a significant antiaggregant effect, this medication was not stopped, and the patients continued to receive the acetylsalicylic acid treatment.

Results

The study compared a control group of 40 patients, aged 61.05 ± 9.12 (range, 33-78 years), with a group of 52 patients who underwent hemostasis using ORC (ORC group), with an average age of 62.56 ± 9.29 (range, 44-83 years). Table 1 presents the demographic, medical, and pre-operative hematological profiles of the patients. The groups were similar in terms of age, gender, BMI, ASA scores, smoking habits, and most comorbid diseases, except for COPD, as well as pre-operative PT, platelet count, hematocrit, and ACT values. The mean number of vascular grafts was comparable between the control and ORC groups (3.35 ± 1.07 and 3.25 ± 0.91, respectively, $p > 0.05$). All patients in both groups had an ASA III score.

Table 2 outlines the intraoperative parameters. There was a statistically significant difference in the average duration of the operation between the control group (289.17 ± 50.62 min) and the ORC group (265.13 ± 59.45 min) ($p < 0.05$). The ORC group had significantly fewer erythrocyte and FFP transfusions compared to the control group ($p < 0.05$). The mean duration of cardiopulmonary bypass and ACT values did not differ significantly between the groups ($p > 0.05$). LIMA was consistently used as a graft in both groups, with the most common number of grafts being three.

Post-operative parameters in table 3 revealed that in the ORC group, there were significantly fewer FFP transfusions, a shorter mean follow-up time in the intensive care unit, and a shorter mean chest tube removal time compared to the control group ($p < 0.05$). While there was no statistical difference in the total amount of drainage to the chest tube ($p > 0.05$), the mean total drainage was less in the ORC group (1067.31 ± 528.58 mL) than in the control group (1115.00 ± 465.36 mL). ACT, activated partial thromboplastin time, and the mean number of erythrocyte transfusions did not differ significantly between the groups ($p > 0.05$). Although the mean duration of post-operative hospital stay was shorter in the ORC group, there was no significant difference between the groups ($p > 0.05$). Only one patient in the ORC group required a platelet transfusion, and no patients in either group received fibrinogen supplementation.

In the ORC group, eight complications occurred in seven patients, including 3 cases of atrial fibrillation (7.3%), 3 cases of superficial wound infection (7.3%), and 2 cases of pleural effusion (4.9%). The control group experienced 2 sternal wound infections (5.0%) and 4 pleural effusions (10.0%). All complications were effectively addressed during the initial hospitalization period and none of the patients required readmission.

Two patients (3.8%) in ORC and 1 patient (2.5%) in control group required reoperation due to excessive bleeding, which was defined as bleeding exceeding

Table 1. The demographic and medical features and pre-operative hematological profile of the patients

Parameters	Control (n = 40)	ORC group (n = 52)
Age (years) (mean ± SD)	61.05 ± 9.12	62.56 ± 9.29
Gender (number/percentage)		
Male	31 (77.5%)	41 (78.8%)
Female	9 (22.5%)	11 (21.2%)
BMI (kg/m^2) (mean ± SD)	28.05 ± 4.19	28.16 ± 4.73
ASA scores (number/percentage)		
ASA 1	-	-
ASA 2	-	-
ASA 3	40 (100%)	52 (100%)
ASA 4	-	-
Smokers (number/percentage)	12 (30.0%)	13 (25.0%)
Comorbidities (number/percentage)		
HT	23 (57.5%)	32 (61.5%)
DM	24 (60.0%)	30 (57.7%)
COPD	1 (2.5%)	8 (15.4%)
Others	1 (2.5%)	3 (5.7%)
Prothrombin time (s) (mean ± SD)	12.79 ± 1.76	13.72 ± 1.08
Platelet count (×10^3/μL) (mean ± SD)	271.56 ± 56.62	263.96 ± 69.20
Hematocrit (%)	41.01 ± 5.74	40.59 ± 6.47
ACT (s)	135.29 ± 20.09	139.91 ± 20.08

No difference was found between the groups for all parameters ($p > 0.05$); ASA: American Society of Anesthesiologists; BMI: body mass index; COPD: chronic obstructive pulmonary disease; DM: diabetes mellitus; HT: hypertension; ACT: activated clotting time; SD: standard deviation; ORC: oxidized regenerated cellulose.

Table 2. Pre-operative parameters of the patients

Parameters	Control (n = 40)	ORC group (n = 52)
Operation time (min) (mean ± SD)*	289.17 ± 50.62	265.13 ± 59.45
Duration of cardiopulmonary bypass (min)	51.20 ± 14.82	48.64 ± 18.50
Mean number of vascular grafts	3.35 ± 1.07	3.25 ± 0.91
Erythrocyte transfusions (mean ± SD)*	0.38 ± 0.16	0.02 ± 0.01
FFP transfusions* (mean ± SD)	0.40 ± 0.16	0.27 ± 0.12
ACT (s ± SD)	749.54 ± 157.57	709.77 ± 157.26

*Statistically different, $p < 0.05$. FFP: fresh frozen plasma; ACT: activated clotting time; s: seconds; SD: standard deviation; ORC: oxidized regenerated cellulose.

200 cc/h during the early post-operative period. Both patients experienced 200 cc/h bleeding over a period of 5 h, leading to the decision for emergent reoperation. Surgical intervention was performed to achieve local hemostasis since the patients had active surgical bleeding (not oozing) that could not be controlled using hemostatic agents. It was concluded that these two cases of hemorrhage requiring reoperation were not directly associated with the evaluation of ORC's efficacy and safety, which were the aim of the current study. Therefore, these reoperations were not considered in the "discussion" part.

No mortality was observed in the current study.

The Statistical Package for the Social Sciences (SPSS) version 25 (SPSS Inc., Chicago, USA) program was used for statistical analysis. For quantitative data such as age and length of hospital stay, the mean and standard deviation values were used to determine the measure of central trends. Frequency tables and charts were used to present estimated rates of

Table 3. Post-operative parameters of the patients

Parameters	Control (n = 40)	ORC group (n = 52)
Erythrocyte transfusions (mean ± SD)	1.90 ± 1.06	1.71 ± 1.05
FFP transfusions (mean ± SD)*	1.65 ± 1.12	1.23 ± 1.18
Platelet transfusion (number of patients/number of transfused platelet suspension)	0/0	1/1
Fibrinogen supplementation (number of patients/number of transfused fibrinogen suspension)	0/0	0/0
ACT (s ± SD)	119.19 ± 11.64	121.63 ± 13.64
aPTT (s ± SD)	30.50 ± 6.31	28.25 ± 2.73
Follow-up time in intensive care unit (h ± SD)*	102.15 ± 36.79	90.19 ± 45.67
Post-operative hospital stay (days ± SD)	12.54 ± 6.83	10.75 ± 6.86
Total amount of drainage to chest tube (mL ± SD)	1115.00 ± 465.36	1067.31 ± 528.58
Chest tube removal time (h ± SD)*	94.45 ± 37.88	52.29 ± 46.74
Post-operative early complications (number of patients)		
Atrial fibrillation	0 (0%)	3 (5.7%)
Superficial wound infection	0 (0%)	3 (5.7%)
Sternal wound infections	2 (5.0%)	0 (0%)
Reoperation for bleeding	1 (2.5%)	2 (3.8%)
Cardiac tamponade	0 (0%)	0 (0%)
Pleural effusion	4 (10.0%)	3 (5.7%)

*Statistically different, $p < 0.05$. FFP: fresh frozen plasma; ACT: activated clotting time; s: seconds; h: hours; SD: standard deviation; ORC: oxidized regenerated cellulose; aPTT: activated partial thromboplastin time.

qualitative data such as gender and rate of complications. To determine whether there was a difference between the experimental and control groups, it was examined whether the difference between the groups was significant. In this context, since parametric test assumptions were not met, this difference was examined with the Mann–Whitney U test, which is one of the non-parametric tests for the comparison of groups.

Discussion

The disproportion between the blood supply of the myocardium through coronary vessels and the oxygen need of the myocardium leads to ischemic heart disease[10]. Annually, more than 200,000 CABG procedures are carried out in the United States. CABG surgery is frequently regarded as a high-risk procedure with high 30-day morbidity (up to 14.0%) and mortality (up to 2.0%) rates[11]. In the current study, there were no instances of mortality (0%). The morbidity rates, at 15% for the control group and 15.4% for the ORC group, align with existing literature. While the recent adoption of early extubation and fast-track protocols has generally resulted in shorter hospital stays, averaging 5.4 days postoperatively[11], in the current research, longer post-operative LOS, with 12.54 ± 6.83 days for the control group and 10.75 ± 6.86 days for the ORC group, were found. Following CABG surgery, a large number of patients commonly require hospital readmissions (approximately 14%) and emergency department visits (additional 10%) within 30 days after discharge, frequently for complications or complaints linked to the surgery. In all, 7% of patients who have had CABG surgery will require more than one readmission or emergency department visit within 30 days following the procedure[11]. Every complication identified in the present study was successfully addressed during the initial hospitalization period, and there was no necessity for patients to be readmitted after discharge.

Several risk factors contribute to perioperative morbidity and mortality in CABG surgery. Post-operative bleeding is a common complication, impacting approximately 10% of patients and leading to adverse outcomes and higher costs. Definitions of “excessive” bleeding vary but are often based on chest tube drainage. Age, complex operations, pre-operative anemia, cardiac function, cardiopulmonary bypass time, male

sex, and lower BMI contribute to the risk of excessive bleeding, emphasizing the importance of careful management of post-operative bleeding due to its association with increased mortality risk. The risk of bleeding is also associated with surgeon-specific factors such as attention to hemostasis. Pre-operative dual antiplatelet medication (acetylsalicylic acid and clopidogrel, ticagrelor, or prasugrel) may have an approximately 15% risk of bleeding. Although guidelines advise to stop dual antiplatelet treatment 5 days before surgery, this is frequently impossible in emergent operations[12]. In the present study, although all of the patients had been receiving acetylsalicylic acid, which had a significant antiaggregant effect in the pre-operative period, only 2 patients (3.9%) in ORC group and 1 patient (2.5%) had reoperation for bleeding.

Post-operative bleeding, often linked to antiplatelet or anticoagulant use in CABG surgery, remains a constant concern for surgeons. Persistent bleeding from mediastinal drains can lead to sudden cardiopulmonary instability, particularly acute pericardial tamponade, resulting in death. While various sources contribute to bleeding after CABG, oozing from anastomotic suture lines is a primary cause, requiring prompt surgical exploration to prevent adverse outcomes[12].

Traditional surgical methods such as ligation and cauterization may sometimes fail to control bleeding, prompting the use of alternative approaches. Topical hemostatic agents, including ORC, offer a solution. ORC, composed of structured cellulose, stands out for its bioabsorption, biocompatibility, and ease of use. It activates the intrinsic coagulation pathway, forms a gel-like layer, and induces vasoconstriction. ORC's versatility makes it suitable for various surgical sites, ensuring quick adaptation and effective management of local bleeding[1,2,13]. Although ORC is widely used in many surgical fields worldwide, there are only two technical descriptions of the use of ORC in coronary artery bypass surgeries[8,9].

Di Lello et al.[8] employed ORC for sutureless fixation of long aortocoronary saphenous vein grafts (SVG), tailoring an appropriate-sized ORC sheet over the graft segment. While their aim differed from the current study, focusing on graft fixation rather than hemostasis, the technique showcased ORC's versatility.

Canver[9] introduced a method to reduce fatal complications in myocardial revascularization, covering the internal thoracic artery pedicle, distal anastomosis, and SVGs with ORC pieces. Liquid thrombin prevented dislodging, and the chest was closed while monitoring bleeding through flexible suction catheters. In 345 consecutive CABG procedures using this technique, only 0.57% required re-exploration for early post-operative bleeding. No instances of cardiopulmonary collapse or long-term complications were reported, suggesting ORC application might prevent post-operative bleeding and acute graft kinking effectively.

In my opinion, the main limitation of the previous study was the evaluation of a very limited number of outcome parameters, despite the inclusion of a large number of patients. In addition, no other research studies were found in the literature utilizing the same hemostasis technique, suggesting that the results of the study may not have been deemed satisfactory by other researchers. In contrast, the present study evaluated a significant number of outcome parameters. Another difference between the previous study and the current study is that while the previous study applied a liquid thrombin spray on ORC, such an application was not performed in the present study. The final and significant difference of the current study from the previous one is the presence of a control group in the current study.

Given the limited number of studies assessing the hemostatic effects of ORC in CABG surgery, the author conducted the current comparative retrospective analysis. The aim was to compare the pre-, intra-, and post-operative data of patients in whom ORC was used for enhanced hemostasis with those who did not receive any hemostatic agent during CABG surgeries. In summary, when considering various parameters between two groups that exhibited similarities in demographic and medical features, pre-operative hematological profiles, and the number of vascular grafts applied, it was found that the duration of surgery, average numbers of erythrocyte and FFP transfusions during surgery, average post-operative FFP transfusion count, duration of intensive care unit stay, and chest tube removal times were lower in the ORC group compared to the control group, and all these differences were statistically significant. On the other hand, although statistically significant differences were not found, it is noteworthy that the post-operative hospital stay and the total amount of drainage to the chest tube were lower in the ORC group compared to the control group. Given that all these parameters with different values between the groups could be directly or indirectly associated with the patient's hemostatic success and bleeding status, these differences were

interpreted as indicative of the positive contributions of ORC use to hemostasis.

Although some other hemostatic agents such as fibrin sealant[13] and tranexamic acid[14] were used successfully in patients undergoing CABG surgery, there was no studies comparing the effects of these hemostats with ORC in CABG surgeries.

While ORC is widely used and effective, there have been reported adverse effects. In a rare case, ORC residue caused a post-traumatic bronchobiliary fistula, attributed to ORC erosion and diaphragmatic migration[15]. Another case involved a child with pelvic neuroblastoma, where ORC, used for hemostasis, led to a mass mimicking tumor recurrence. Pathological evaluation revealed fibrotic tissue with giant cells, prompting caution about minimizing topical hemostat use and avoiding retention unless essential[16]. Despite ORC's biocompatibility, insufficient absorption can trigger foreign body reactions, mimicking various conditions such as tumor recurrence, granuloma, or abscess[2]. An adverse event occurred with oxidized cellulose (OC) combined with epsilon aminocaproic acid (EACA), leading to acute ischemia. *In vitro* experiments revealed OC's rigid structure in EACA, prompting a cautionary note against their combined use[17].

In addition to these undesirable effects, seroma, allergic skin reactions, or in some cases, abscess formations may develop with the use of ORC[2]. In addition to a case series[18] reporting subhepatic mass formation (five out of 83 patients) after laparoscopic cholecystectomy operations, there are also studies reporting that the use of ORC increases the risk of rehospitalization[19].

Conclusion

The findings of the current study, which utilized topical ORC to achieve hemostasis and prevent oozing at anastomotic sites in CABG surgeries, demonstrated the effective and safe use of ORC with low complication rates. A key aspect of this approach was the removal of ORC after achieving hemostasis, in accordance with the usage guidelines. Although some literature reports have highlighted potential adverse effects associated with ORC usage, none of these effects have been deemed significant enough to hinder the use of ORC. Moreover, the technique described in this manuscript can effectively mitigate most of these undesired adverse events. Conducting studies that compare the outcomes of patients undergoing CABG surgery with or without the use of ORC, along with studies involving a larger number of patients, would provide valuable guidance for surgeons regarding the safety and effectiveness of ORC in achieving hemostasis in these surgeries. In addition, studies comparing ORC with other hemostatic agents in terms of hemostatic success in CABG procedures would contribute to a better understanding of the efficacy and safety of these products.

Acknowledgments

The author thanks Professor Dr. Kemal Kismet and Dr. Kemal Tekin for their dedication and contributions during the preparation of this study.

Funding

The author declares that he has not received funding.

Conflicts of interest

The author declares no conflicts of interest.

Ethical disclosures

Protection of human and animal subjects. The author declares that no experiments were performed on humans or animals for this study.

Confidentiality of data. The author declares that they he has followed the protocols of his work center on the publication of patient data.

Right to privacy and informed consent. The author has obtained approval from the Ethics Committee for analysis and publication of routinely acquired clinical data and informed consent was not required for this retrospective observational study.

Use of artificial intelligence for generating text. The author declares that he has not used any type of generative artificial intelligence for the writing of this manuscript nor for the creation of images, graphics, tables, or their corresponding captions.

References

1. Qian Z, Xiong F, Xia X, Gu P, Wang Q, Wu A, et al. Clinical and economic impact of oxidized regenerated cellulose for surgeries in a Chinese tertiary care hospital. J Comp Eff Res. 2020;9:1079-90.
2. Franceschini G. Internal surgical use of biodegradable carbohydrate polymers. Warning for a conscious and proper use of oxidized regenerated cellulose. Carbohydr Polym. 2019;216:213-6.

3. Shetty DP, Nair HC, Shetty V, Punnen J. A novel treatment for pulmonary hemorrhage during thromboendarterectomy surgery. Ann Thorac Surg. 2015;99:77-8.
4. Keshavarzi S, MacDougall M, Lulic D, Kasasbeh A, Levy M. Clinical experience with the Surgicel family of absorbable hemostats (oxidized regenerated cellulose) in neurosurgical applications: a review. Wounds. 2013;25:160-7.
5. Portilla D, Hernández-Giraldo C, Moreno B, Quijano F, Hoyos LR, Angarita AM, et al. A local hemostatic agent for the management of postpartum hemorrhage due to placenta previa and placenta accreta: a cross-sectional study. Arch Gynecol Obstet. 2013;288:543-9.
6. Morelli L, Morelli J, Palmeri M, D'Isidoro C, Kauffmann EF, Tartaglia D, et al. Robotic surgery and hemostatic agents in partial nephrectomy: a high rate of success without vascular clamping. J Robot Surg. 2015;9:215-22.
7. Sabel M, Stummer W. The use of local agents: surgicel and Surgifoam. Eur Spine J. 2004;13:S97-101.
8. Di Lello F, Mullen DC, Flemma RJ. Sutureless fixation of long aortocoronary saphenous vein grafts with oxidized regenerated cellulose. Ann Thorac Surg. 1989;47:473-4.
9. Canver CC. A draping technique for prevention of coronary bypass graft kinking and suture-line oozing. J Card Surg. 1996;11:408-10.
10. Straus S, Haxhibeqiri-Karabdic I, Grabovica SG, Granov N. A difference in bleeding and use of blood and blood products in patients who were preoperatively on aspirin or dual antiplatelet therapy before coronary artery bypass grafting. Med Arch. 2018;72:31-5.
11. Montrief T, Koyfman A, Long B. Coronary artery bypass graft surgery complications: a review for emergency clinicians. Am J Emerg Med. 2018;36:2289-97.
12. Stephens RS, Whitman GJ. Postoperative critical care of the adult cardiac surgical patient: part II: procedure-specific considerations, management of complications, and quality improvement. Crit Care Med. 2015;43:1995-2014.
13. Wan Y, Lim S, Gao X, Danker WA 3rd, Kocharian R, Gangoli G, et al. Bleeding-related complications and readmission rates associated with fibrin sealant use in patients undergoing coronary artery bypass graft surgery in the United States. J Cardiothorac Vasc Anesth. 2017;31:876-82.
14. De Bonis M, Cavaliere F, Alessandrini F, Lapenna E, Santarelli F, Moscato U, et al. Topical use of tranexamic acid in coronary artery bypass operations: a double-blind, prospective, randomized, placebo-controlled study. J Thorac Cardiovasc Surg. 2000;119:575-80.
15. Seyed-Alagheband SA, Shahmoradi MK, Shekouhi R. Posttraumatic bronchobiliary fistulae due to foreign body remnants after a road traffic injury: a case report. J Med Case Rep. 2021;15:291.
16. Turkyilmaz Z, Karabulut R, Kaya C, Gokce D, Kolay E, Sonmez K. Surgicel mimicking recurrent pelvic neuroblastoma in a 3-year-old boy. Acta Chir Belg. 2022;122:266-8.
17. Alvarez JB, Quiroga JS, Cereijo JM, Lopez LR. Oxidized cellulose as the cause of an acute ischemic event after coronary revascularization. Interact Cardiovasc Thorac Surg. 2010; 11:488-9.
18. Spaziani E, Di Filippo A, Francioni P, Spaziani M, De Cesare A, Picchio M. Subhepatic mass occurrence after using oxidized and regenerated cellulose polymer in laparoscopic cholecystectomy: a case series. Acta Chir Belg. 2018;118:48-51.
19. Arisheh MA, Venturero M, Froom P. Oxidized regenerated cellulose during laparoscopic cholecystectomy increases the risk of rehospitalization. Am Surg. 2020;86:386-8.

ORIGINAL ARTICLE

Acute kidney injury and mortality in patients with critical COVID-19 in Mexico: case–control study

Lesión renal aguda y mortalidad en pacientes con COVID-19 grave en México: estudio de casos y controles

*Ivette Mata-Maqueda[1,2], Juan C. Solís-Sáinz[2], Guadalupe Zaldivar-Lelo de Larrea[2], Ernesto Deloya-Tomas[1,2,3], Jorge López-Fermín[1,2,3], Mª Guadalupe Olvera-Ramos[1,2,3], Gabriela Castillo-Gutiérrez[1,2,3], Jorge D. Carrión-Moya[1,2,3], and Orlando R. Pérez-Nieto[1,2,3]**

[1]Health Services of the State of Queretaro; [2]School of Medicine, Autonomous University of Queretaro; [3]Intensive Care Unit, General Hospital of San Juan del Rio. Queretaro, Mexico*

Abstract

Objective: *We aimed to test the association between acute kidney injury (AKI) and mortality in critically ill patients with Coronavirus disease 2019 (COVID-19).* **Method:** *We conducted a single-center case–control study at the intensive care unit (ICU) of a second-level hospital in Mexico. We included 100 patients with critical COVID-19 from January to December 2021, and collected demographic characteristics, comorbidities, APACHE II, SOFA, NEWS2, and CO-RADS scores at admission, incidence of intrahospital complications, length of hospital and ICU stay, and duration of mechanical ventilation, among others.* **Results***: The median survival of deceased patients was 20 days. After multivariable logistic regression, the following variables were significantly associated to mortality: AKI (adjusted odds ratio [AOR] 6.64, 95% confidence intervals [CI] = 2.1-20.6, p = 0.001), age > 55 years (AOR 5.3, 95% CI = 1.5-18.1, p = 0.007), and arrhythmias (AOR 5.15, 95% CI = 1.3-19.2, p = 0.015). Median survival was shorter in patients with AKI (15 vs. 22 days, p = 0.043), as well as in patients with overweight/obesity (15 vs. 25 days, p = 0.026).* **Conclusion:** *Our findings show that the development of AKI was the main risk factor associated with mortality in critical COVID-19 patients, while other factors such as older age and cardiac arrhythmias were also associated with this outcome. The management of patients with COVID-19 should include renal function screening and staging on admission to the Emergency Department.*

Keywords: *Coronavirus disease 2019. Severe acute respiratory syndrome coronavirus 2. Acute kidney injury. Mortality. Risk factors.*

Resumen

Objetivo: *Probar la asociación entre lesión renal aguda y mortalidad en pacientes con COVID-19 grave.* **Método:** *Realizamos un estudio de casos y controles unicéntrico en la unidad de cuidados intensivos (UCI) de un hospital de segundo nivel en México. Incluimos 100 pacientes con COVID-19 grave de enero a diciembre 2021, recolectando características demográficas, comorbilidad, APACHE II, SOFA, NEWS2 y CO-RADS al ingreso, incidencia de complicaciones intrahospitalarias, duración de la estancia hospitalaria y en la UCI, duración de ventilación mecánica, etc.* **Resultados:** *La mediana de supervivencia de los pacientes que fallecieron fue de 20 días. Al realizar el análisis de regresión logística multivariable, las siguientes variables se asociaron significativamente con la mortalidad: lesión renal aguda (odds ratio ajustada [ORa]: 6.64; intervalo de confianza*

***Correspondence:**
Orlando R. Pérez-Nieto
E-mail: orlando_rpn@hotmail.com

Date of reception: 25-04-2023
Date of acceptance: 25-10-2023
DOI: 10.24875/CIRU.23000207

Cir Cir. 2024;92(5):626-632
Contents available at PubMed
www.cirugiaycirujanos.com

del 95% [IC95%]: 2.1-20.6; p = 0.001), edad > 55 años (ORa: 5.3; IC95%: 1.5-18.1; p = 0.007) y arritmias (ORa: 5.15; IC95%: 1.3-19.2; p = 0.015). La supervivencia fue menor en pacientes con lesión renal aguda (15 vs. 22 días; p = 0,043), así como en pacientes con sobrepeso u obesidad (15 vs. 25 días; p = 0.026). **Conclusiones:** *Nuestros resultados muestran que el desarrollo de lesión renal aguda es el principal factor de riesgo asociado a mortalidad en pacientes con COVID-19 grave, mientras que otros factores, como la edad > 55 años y la presencia de arritmias cardiacas, también se asocian a mortalidad por COVID-19. El manejo de pacientes con COVID-19 debe incluir el tamizaje y la estadificación de la función renal al ingreso a urgencias.*

Palabras clave: *COVID-19. SARS-CoV-2. Lesión renal aguda. Mortalidad. Factores de riesgo.*

Introduction

Coronavirus disease 2019 (COVID-19) is an acute respiratory disease caused by severe acute respiratory syndrome coronavirus 2 (SARS-CoV-2), which was declared a global pandemic on March 11, 2020. As of April 19, 2023, more than 6.9 million deaths have been reported worldwide[1]. This virus mainly affects the respiratory system, producing fever, cough, headache, shortness of breath, sore throat, and chest pain[2]. Nevertheless, it may also cause acute respiratory distress syndrome (ARDS) and multiple organ dysfunction among other severe manifestations of disease. In this regard, acute kidney injury (AKI) has been described as a severe complication of COVID-19, with an incidence ranging from 4.5% and 28%, and a higher prevalence in patients hospitalized in the intensive care unit (ICU)[2,3]. The mechanisms that promote kidney disease have been related to damage induced by cytokines, systemic effects related to mechanical ventilation, and ARDS[4].

AKI is known to increase the severity of illness, duration of hospitalization, and mortality in COVID-19 patients[5]. In fact, AKI has been described as an independent risk factor for mortality in COVID-19 patients hospitalized in the ICU[6]. However, information on kidney disease in patients with COVID-19 is still limited, as the majority of published studies in this respect are case reports and case series[5]. Furthermore, little is known concerning the relationship between AKI and COVID-19 in Hispanic populations, in whom risk factors for disease progression, adverse outcomes, and death from COVID-19 are especially prevalent[7-9].

For the above reasons, in this study, we aimed to test the association between AKI and mortality in critically ill patients with COVID-19 in the ICU of a second-level public hospital in Mexico.

Materials and methods

Setting and patients

We conducted a single-center case–control study at the ICU of the Hospital General de San Juan del Río, part of the Health Services of the State of Queretaro, Mexico (SESEQ), from January to December 2021. Inclusion criteria were all patients with critical COVID-19 (according to the World Health Organization severity definitions[10]) admitted to the ICU during the entire study period. Exclusion criteria were incomplete or missing medical records and patients who were transferred to another medical unit. Consecutive convenience sampling of patients was performed.

In this study, the ethical precepts of the Declaration of Helsinki were followed, and the study protocol was approved in July 2020 by the Research Committee of SESEQ, with the registration number *1201/Subdirección de Enseñanza, Programa de Investigación en Salud/31-07-2020*.

The primary outcome was mortality; hence, cases were defined as patients who died in the ICU, while controls as patients who survived until discharge. Exposures were defined as sex, age, history of comorbidities, APACHE II, SOFA, NEWS2, and CO-RADS scores at ICU admission, the incidence of intrahospital complications (AKI, arrhythmias, and secondary infections), length of hospital and ICU stay, duration of mechanical ventilation, patient-ventilator asynchrony, PaO_2 levels, and static pulmonary compliance. Data were collected by Critical Care Medicine resident physicians and attendings through a review of patients' medical records.

Statistical analysis

Sample size calculations were performed based on the mortality risk by AKI in COVID-19 patients.

Assuming a relative risk of 3.08[11], and a mortality rate of 47%[2], we estimated a minimum of 33 individuals, with an 80% power and alpha of 0.05, allowing for a loss of 20%.

Descriptive statistics were used in qualitative variables. Continuous and categorical variables are presented as means, standard deviations, frequencies, and percentages, where applicable. Differences between categorical variables were evaluated by Fisher's exact test and by analysis of variance for continuous variables. Statistical significance was defined as $p < 0.05$. Normality in the distribution of the variables was tested by the Kolmogorov–Smirnov test. The Mann–Whitney and Kruskal–Wallis tests were used to evaluate the difference between medians, as well as Spearman's one-tailed correlation test for all the non-normally distributed data. Kaplan–Meier analyses were performed to assess survival. Both bivariable and multivariable binary logistic regression analyses were used to identify factors associated with the mortality. Variables with a $p < 0.05$ in the bivariable analysis were fitted into the multivariable logistic regression analysis. Both crude odds ratio and adjusted odds ratio with their corresponding 95% Confidence intervals were calculated to show the strength of the association. In multivariable analysis, variables with a $p < 0.05$ were considered as statistically significant. The fitness of the model was checked by using the Hosmer-Lemeshow goodness-of-fit test. All analyses and figures were performed using IBM SPSS Statistics version 25 (IBM Corp., Armonk, N.Y., USA) and PRISM Software (GraphPad Prism v. 8), respectively.

Results

One hundred and twenty-two potentially eligible patients were screened. After the application of inclusion and exclusion criteria, 100 patients were included in the final analyses (Fig. 1). Table 1 shows the general characteristics of our study population. Fifty patients were male and the mean age was 49 years. Obesity was the most frequent comorbidity (n = 44, 44%). Median APACHE II, SOFA, NEWS2 and CO-RADS scores at admission were 15, 9, 9, and 5, respectively. The incidence of intrahospital complications such as AKI, arrhythmia, ventilator-associated pneumonia, and catheter-related urinary tract infections were 56%, 70%, 67%, and 10%, respectively.

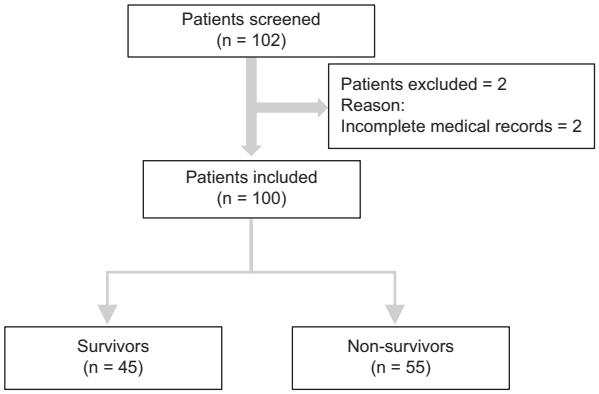

Figure 1. *Patient inclusion flowchart and reasons for exclusion.*

Table 1. General characteristics of our population

Variable	Total sample (n = 100)
Sex*	
Male	50 (50)
Female	50 (50)
Age** (years)	
Male	49.1 (12.2)
Female	49.4 (14.4)
Comorbidities*	
None	22 (22)
Obesity	44 (44)
Overweight	11 (11)
Hypertension	38 (38)
Diabetes mellitus	30 (30)
Patients with two or more comorbidities	35 (35)
Scores***	
APACHE II	15 (12-20)
SOFA	9 (7-11)
NEWS2	9 (7-11)
CORADS	5 (5-5)
Intrahospital complications*	
Acute kidney injury	56 (56)
Arrhythmias (all ventricular extrasystoles)	70 (70)
Ventilator-associated pneumonia	67 (67)
Catheter-related UTI	10 (10)
Days of hospital stay***	14 (10.75-23.25)
Days in ICU***	11 (6-20)
Days on mechanical ventilation***	9 (5-17)
Patient-ventilator asynchrony*	49 (49)
PaO_2 (mmHg)**	63.4 (11.4)
Static pulmonary compliance***	23 (18-26)
Mortality*	55 (55)

*Frequency, (percentage). **Mean, (standard deviation). ***Median, (25^{th}-75^{th} percentiles). ICU: intensive care unit; PaO_2: arterial partial pressure of oxygen; UTI: urinary tract infection.

The median ICU stay was 11 days (interquartile range [IQR] ± 14), while the median days on mechanical ventilation were 9 (IQR ± 12). The mortality rate in our population was 55% (n = 55).

In the bivariable logistic regression, the variables AKI, APACHE score > 25, age > 55, arrhythmias, overweight and obesity, and male sex were positively associated with mortality. However, when the multivariable logistic regression was employed only AKI (AOR 6.64, 95% CI 2.14-20.62, p = 0.001), age >55 years (AOR 5.3, 95% CI 1.57-18.15, p = 0.007), and arrhythmia (AOR 5.15, 95% CI 1.37-19.27, p = 0.015) were significantly associated with mortality (Table 2).

On the other hand, age was significantly higher in deceased patients, compared to survivors (52.9 vs. 44.9 years, using Student's t-test, p = 0.0014; data not shown). Similarly, APACHE II scores were also higher in the non-survivor group, compared to survivors (16 vs. 14, using Mann–Whitney test, p = 0.032; data not shown). In addition, the length of mechanical ventilation was also higher in deceased patients, compared to non-deceased (11 vs. 8 days, using the Mann–Whitney test, p = 0.032; data not shown).

There were no significant differences in the SOFA and NEWS2 scores, length of hospital and ICU stay, number of comorbidities, PaO_2 levels, and static pulmonary compliance between survivors and non-survivors (data not shown). Similarly, there was no correlation between age and length of ICU stay (p = 0.18, Spearman's correlation test; data not shown).

Concerning the deceased patients, the global median survival was 20 days. When comparing the survival of deceased patients with and without overweight and obesity, median survival was 15 and 25 days, respectively (p = 0.026, Fig. 2). Likewise, when comparing the survival of deceased patients with and without AKI, median survival values were 15 and 22 days, respectively (p = 0.043, Fig. 3).

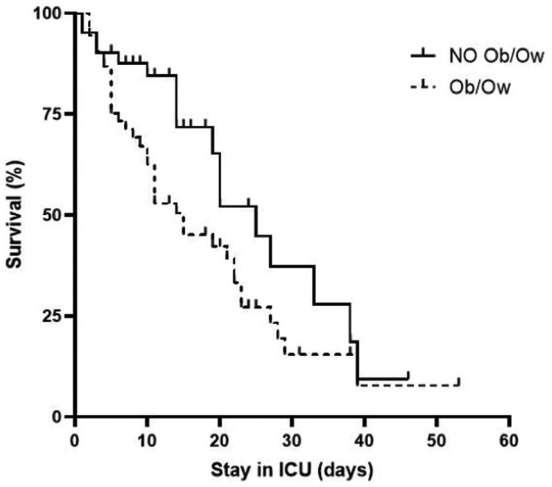

Figure 2. *Kaplan–Meier survival plots in patients with (dashed line) and without (solid line) obesity and overweight (Ob/Ow). Median survival was 15 and 25 days for the group with and without Ob/Ow, respectively. When comparing both curves a significant p = 0.026 was calculated using the Gehan-Breslow-Wilcoxon test.*

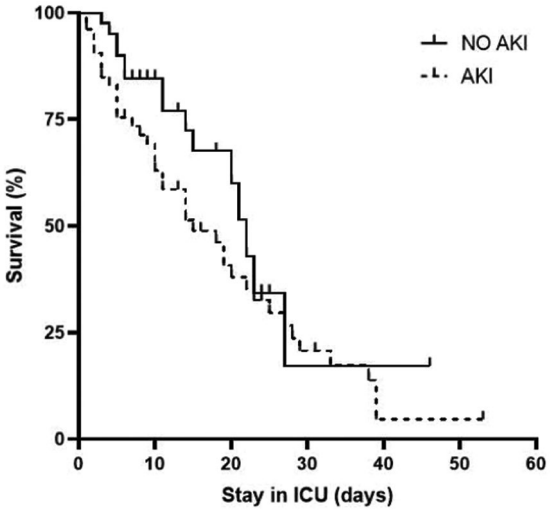

Figure 3. *Kaplan–Meier survival plots in patients with (dashed line) and without (solid line) acute kidney injury (AKI). Median survival was 15 and 22 days for the group with and without AKI, respectively. When comparing both curves a significant p = 0.043 was calculated using the Gehan-Breslow-Wilcoxon test.*

Discussion

In this case–control study conducted in a second-level hospital in Mexico, in accordance with the literature, we found that AKI is an independent risk factor for mortality in critically ill patients with COVID-19, even after adjustment for age and sex. We also found that patients with AKI died earlier than patients without this complication. It has been reported that patients with COVID-19 who develop AKI have a mortality risk 4.5 times higher compared with those who do not[12]. In our study, the incidence of AKI as an intra-hospital complication was 56%, and the patients who developed it showed a 6.6-fold higher risk of dying. The kidney has been identified as a target organ for virus proliferation in patients with severe SARS-CoV-2 infection[13], since a direct SARS-CoV-2 invasion into renal parenchyma has been demonstrated, in addition to microthrombosis, acute tubular necrosis, mitochondrial dysfunction, and arterial occlusion[14]. In addition to direct pathophysiological mechanisms, renal dysfunction in the context of COVID-19 may also occur through the systemic

Table 2. Association of risk factors and mortality in critical COVID-19 patients

Variable	Value n (%)	COR (95% CI; p-value)	AOR (95% CI; p-value)
Acute kidney injury	41 (74.5)	6.2 (2.2-17.6; 0.001)	**6.64 (2.14-20.62; 0.001)**
Age > 55 years	23 (41.8)	4.4 (1.6-12.3; 0.004)	**5.3 (1.57-18.15; 0.007)**
Arrhythmia	46 (83.6)	2.9 (1-8.6; 0.048)	**5.15 (1.37-19.27; 0.015)**
APACHE II score > 25	12 (21.8)	4.9 (1.2-20.1; 0.024)	2.6 (0.47-14.34; 0.271)
Overweight and obesity	37 (67.2)	2.6 (1.15-5.9; 0.021)	2.12 (0.7-6.44; 0.183)
Male sex	34 (61.8)	2.1 (1.2-6.3; 0.013)	0.494 (0.16-1.46; 0.203)
SOFA score > 10	25 (45.4)	1.2 (0.3-1.8; 0.381)	-
NEWS2 score > 10	25 (45.4)	1.31 (0.5-2.9; 0.329)	-
Patient-ventilator asynchrony	17 (30.9)	1.7 (0.6-4.9; 0.177)	-

COR: crude OR (from bivariate regression analysis); AOR: adjusted OR (from multivariable regression analysis). Significant values from multivariable regression are shown in bold. Hosmer-Lemeshow test p = 0.253.

effects of SARS-CoV-2 infection and critical illness[15]. In our study, 74.5% of the deceased patients had AKI, and this was the risk factor with the greatest association with mortality, which is consistent with previously reported data, given that AKI has been pointed out as a marker of severe disease, multiple organ dysfunction, and death from COVID-19[16].

Importantly, 78% of our population had a least one comorbidity, including obesity/overweight, diabetes mellitus, and hypertension. These comorbidities have been identified as significant risk factors for COVID-19-associated AKI[2]. They are characterized by low-grade inflammation and increased immune senescence, although how these specifically impact the kidney in the setting of COVID-19 is still unknown[15]. Of these comorbidities, obesity has been recognized as one of the most important risk factors for disease severity, use of invasive mechanical ventilation, and death, especially in those under 65 years of age[17]. Several mechanisms have been proposed to explain this relationship, including increased angiotensin-converting enzyme 2 (ACE2) expression. Therefore, a greater presence of ACE2 could be a mechanism that increases the risk of disease and death in COVID-19 patients with obesity[18,19]. In our population, mortality was twice as high in patients with overweight and obesity, which is consistent with the literature[20-22]. However, this association was not significant when the multivariable logistic regression was performed.

Increasing age has also been identified as an independent risk factor associated with mortality in COVID-19 patients, and this is certainly the case with the Mexican population[23-25]. Furthermore, increasing age has been associated with an increased risk of presenting with symptoms of severity[26]. In our study, age > 55 years was associated with a 5.3-fold risk of mortality, and age tended to be significantly higher in deceased patients compared to survivors.

In contrast to what has been reported in the literature, in our study, 70% of the patients had ventricular extrasystoles. The cardiac manifestations of COVID-19 include arrhythmias, focal or global myocarditis, necrosis, ventricular dysfunction, heart failure, and thrombosis[27-29]. Atrial arrhythmias are the most frequently observed arrhythmias in patients with severe COVID-19. It has been reported that the overall incidence of atrial fibrillation (AF) ranges from 6.6 to 13% in hospitalized COVID-19 patients without a history of atrial arrhythmia[30,31]. Notably, 83% of our deceased patients presented arrhythmias during their ICU stay, whose presence was associated with a 5.15-fold higher risk of dying.

Finally, we would like to highlight that in our study, the length of mechanical ventilation was higher in non-survivors compared to survivors, which is in line with previously published studies[32].

Limitations of our study include its retrospective nature, as well as potential sampling bias due to convenience sampling, which limits the generalizability of results. In addition, given that this study was conducted in a resource-constrained hospital in Mexico, acute renal replacement therapy strategies (when indicated) were very limited. For instance, slow-continuous renal replacement therapy, the most recommended therapy for hemodynamically unstable critically ill patients, has no

coverage from the state health services, and could therefore not be implemented in our population. Another limitation of our study includes not having the body mass index of the patients due to the impossibility of objectively measuring weight, since hospitalization and ICU beds do not count with digital scales, and therefore, obesity/overweight was ascertained through medical history. Strengths of our study include its sample size, which was adequately powered to detect differences according to the primary outcome. In addition, this study is one of the few to assess the association between AKI and COVID-19 in a Mexican population, along with Casas-Aparicio and colleagues' 2021 study[33]. Esponda-Prado and colleagues also reported on the incidence of AKI among COVID-19 patients, but theirs was a small observational study consisting of solely 22 patients[34].

Conclusion

Our findings show that the development of AKI was the main risk factor associated with mortality in critical COVID-19 patients, while other factors such as age > 55 years and cardiac arrhythmias were also associated with this outcome. The kidney is one of the target organs for SARS-CoV-2 proliferation, and other indirect pathophysiological mechanisms may also cause kidney dysfunction; hence, physicians who evaluate COVID-19 patients at hospital admission should integrate the Kidney Disease: Improving Global Outcomes (KDIGO) classification to determine the kidney function and timely identify the presence of acute or chronic kidney damage. This would allow for early management and avoidance of complications where feasible. The management of patients with COVID-19 should categorically include renal function screening and staging on admission to the Emergency Department.

Funding

The authors declare no funding was received.

Conflicts of interest

The authors declare that they have no conflicts of interest.

Ethical disclosures

Protection of human and animal subjects. The authors declare that the procedures followed were in accordance with the regulations of the relevant clinical research ethics committee and with those of the Code of Ethics of the World Medical Association (Declaration of Helsinki).

Confidentiality of data. The authors declare that they have followed the protocols of their work center on the publication of patient data.

Right to privacy and informed consent. The authors have obtained approval from the Ethics Committee for analysis and publication of routinely acquired clinical data and informed consent was not required for this retrospective observational study.

Use of artificial intelligence for generating text. The authors declare that they have not used any type of generative artificial intelligence for the writing of this manuscript nor for the creation of images, graphics, tables, or their corresponding captions.

References

1. World Health Organization. WHO Coronavirus (COVID-19) Dashboard; 2023. Available from: https://covid19.who.int [Last accessed on 2023 Apr 25].
2. Zhang J, Pang Q, Zhou T, Meng J, Dong X, Wang Z, et al. Risk factors for acute kidney injury in COVID-19 patients: an updated systematic review and meta-analysis. Ren Fail. 2023;45:2170809.
3. Perego AA, Sabiu G, Ottolina D, Colombo R, Casazza G, Gallieni M, et al. Post-mortem renal histopathological findings in 43 COVID-19 patients with acute kidney injury (AKI) deceased in the intensive care unit. J Nephrol. 2023;36:605-8.
4. Ronco C, Reis T. Kidney involvement in COVID-19 and rationale for extracorporeal therapies. Nat Rev Nephrol. 2020;16:308-10.
5. Sabaghian T, Kharazmi AB, Ansari A, Omidi F, Kazemi SN, Hajikhani B, et al. COVID-19 and acute kidney injury: a systematic review. Front Med (Lausanne). 2022;9:705908.
6. Cheng Y, Luo R, Wang K, Zhang M, Wang Z, Dong L, et al. Kidney disease is associated with in-hospital death of patients with COVID-19. Kidney Int. 2020;97:829-38.
7. De Ramos IP, Lazo M, Schnake-Mahl A, Li R, Martinez-Donate AP, Roux AV, et al. COVID-19 outcomes among the hispanic population of 27 large US Cities, 2020–2021. Am J Public Health. 2022;112:1034-44.
8. Ricardo AC, Chen J, Toth-Manikowski SM, Meza N, Joo M, Gupta S, et al. Hispanic ethnicity and mortality among critically ill patients with COVID-19. PLoS One. 2022;17:e0268022.
9. Magesh S, John D, Li WT, Li Y, Mattingly-App A, Jain S, et al. Disparities in COVID-19 outcomes by race, ethnicity, and socioeconomic status. JAMA Netw Open. 2021;4:e2134147.
10. World Health Organization. Therapeutics and COVID-19: Living Guideline; 2023. Available from: https://www.who.int/publications-detail-redirect/WHO-2019-nCoV-therapeutics-2022.4 [Last accessed on 2023 Apr 25].
11. Ali H, Daoud A, Mohamed MM, Salim SA, Yessayan L, Baharani J, et al. Survival rate in acute kidney injury superimposed COVID-19 patients: a systematic review and meta-analysis. Ren Fail. 2020;42:393-7.
12. Puicón-Suárez JB, Zeña-Ñañez S, Failoc-Rojas VE. Association between chronic kidney disease and mortality in patients with a confirmed COVID-19 diagnosis. PeerJ. 2022;10:e13437.
13. Aukland EA, Klepstad P, Aukland SM, Ghavidel FZ, Buanes EA. Acute kidney injury in patients with COVID-19 in the intensive care unit: Evaluation of risk factors and mortality in a national cohort. BMJ Open. 2022;12:e059046.
14. Wishahi M, Kamal NM. Multidisciplinary basic and clinical research of acute kidney injury with COVID-19: pathophysiology, mechanisms, incidence, management and kidney transplantation. World J Nephrol. 2022;11:105-14.
15. Nadim MK, Forni LG, Mehta RL, Connor MJ, Liu KD, Ostermann M, et al. COVID-19-associated acute kidney injury: consensus report of the 25th Acute Disease Quality Initiative (ADQI) Workgroup. Nat Rev Nephrol. 2020;16:747-64.
16. Ronco C, Reis T, Husain-Syed F. Management of acute kidney injury in patients with COVID-19. Lancet Respir Med. 2020;8:738-42.
17. Kompaniyets L, Goodman AB, Belay B, Freedman DS, Sucosky MS, Lange SJ, et al. Body mass index and risk for COVID-19-related hospitalization, intensive care unit admission, invasive mechanical ventilation, and death - United States, March-December 2020. MMWR Morb Mortal Wkly Rep. 2021;70:355-61.

18. Al Heialy S, Hachim MY, Hachim IY, Bin Naeem K, Hannawi H, Lakshmanan J, et al. Combination of obesity and co-morbidities leads to unfavorable outcomes in COVID-19 patients. Saudi J Biol Sci. 2021;28:1445-50.
19. Emilsson V, Gudmundsson EF, Aspelund T, Jonsson BG, Gudjonsson A, Launer LJ, et al. Serum levels of ACE2 are higher in patients with obesity and diabetes. Obes Sci Pract. 2021;7:239-43.
20. Zhou Y, Chi J, Lv W, Wang Y. Obesity and diabetes as high□risk factors for severe coronavirus disease 2019 (<scp>Covid</scp>□19). Diabetes Metab Res Rev. 2021;37:e3377.
21. Pietri L, Giorgi R, Bégu A, Lojou M, Koubi M, Cauchois R, et al. Excess body weight is an independent risk factor for severe forms of COVID-19. Metabolism. 2021;117:154703.
22. Vas P, Hopkins D, Feher M, Rubino F, Whyte M. Diabetes, obesity and COVID-19: a complex interplay. Diabetes Obes Metab. 2020;22:1892-6.
23. Saldías Peñafiel F, PeñAloza Tapia A, Farías Nesvadba D, Farcas Oksenberg K, Reyes Sánchez A, Cortés Meza J, et al. Evaluación de los predictores clínicos de infección respiratoria aguda por coronavirus SARS-CoV-2 en población adulta. Rev Med Chil. 2021;149:1107-18.
24. Parra-Bracamonte GM, Lopez-Villalobos N, Parra-Bracamonte FE. Clinical characteristics and risk factors for mortality of patients with COVID-19 in a large data set from Mexico. Ann Epidemiol. 2020;52:93-8.e2.
25. Salinas-Aguirre JE, Sánchez-García C, Rodríguez-Sanchez R, Rodríguez-Muñoz L, Díaz-Castaño A, Bernal-Gómez R. Características clínicas y comorbilidades asociadas a mortalidad en pacientes con COVID-19 en Coahuila (México). Rev Clín Esp. 2022;222:288-92.
26. Mancilla-Galindo J, Kammar-García A, Martínez-Esteban A, Meza-Comparán HD, Mancilla-Ramírez J, Galindo-Sevilla N. COVID-19 patients with increasing age experience differential time to initial medical care and severity of symptoms. Epidemiol Infect. 2021;149:e230.
27. Bielecka-Dabrowa A, Cichocka-Radwan A, Lewek J, Pawliczak F, Maciejewski M, Banach M. Cardiac manifestations of COVID-19. Rev Cardiovasc Med. 2021;22:365-71.
28. Babapoor-Farrokhran S, Gill D, Walker J, Rasekhi RT, Bozorgnia B, Amanullah A. Myocardial injury and COVID-19: possible mechanisms. Life Sci. 2020;253:117723.
29. Maitz T, Parfianowicz D, Vojtek A, Rajeswaran Y, Vyas AV, Gupta R. COVID-19 cardiovascular connection: a review of cardiac manifestations in COVID-19 infection and treatment modalities. Curr Probl Cardiol. 2022;48:101186.
30. Lavelle MP, Desai AD, Wan EY. Arrhythmias in the COVID-19 patient. Hear Rhythm O2. 2022;3:8-14.
31. Musikantow DR, Turagam MK, Sartori S, Chu E, Kawamura I, Shivamurthy P, et al. Atrial fibrillation in patients hospitalized with COVID-19. JACC Clin Electrophysiol. 2021;7:1120-30.
32. Tanaka C, Tagami T, Nakayama F, Kudo S, Takehara A, Fukuda R, et al. Association between mortality and age among mechanically ventilated COVID-19 patients: a Japanese nationwide COVID-19 database study. Ann Intensive Care. 2021;11:171.
33. Casas-Aparicio GA, León-Rodríguez I, Alvarado-de la Barrera C, González-Navarro M, Peralta-Prado AB, Luna-Villalobos Y, et al. Acute kidney injury in patients with severe COVID-19 in Mexico. PLoS One. 2021;16:e0246595.
34. Esponda Prado JG, Díaz Greene EJ, Padilla Pérez FJ, Vargas González K, Teniza Frias E, Enríquez Barajas A, et al. Lesión renal aguda en pacientes con COVID-19 en la unidad de terapia intensiva del hospital ángeles pedregal. Acta Médi Grup Ángel. 2021;19:229-35.

ORIGINAL ARTICLE

Comparison of US elastography and chemical shift magnetic resonance imaging in multifidus muscle fatty degeneration

Comparación de la elastografía US y la resonancia magnética con codificación de desplazamiento químico en la degeneración grasa del músculo multífido

Fatıh Kırcın[1], Bahar Yanık[2], Erdogan Bulbul[2], Emrah Akay[2], and Gulen Demırpolat[2]*

[1]Radiology Clinic, Afyonkarahisar Sandikli State Hospital, Afyonkarahisar; [2]Department of Radiology, Balikesir University School of Medicine, Balikesir. Turkey

Abstract

Objective: *The purpose of this study was to investigate the feasibility of the use of shear wave elastography (SWE) in comparison to chemical shift encoding (CSE) magnetic resonance imaging (MRI) for the evaluation of multifidus muscle fatty degeneration in patients with chronic low back pain.* **Method:** *Multifidus muscles were evaluated with the CSE-MRI and SWE examinations in control and patient groups. With the in-phase and out-phase sequences in CSE-MRI, signal intensity index (SII), and signal intensity suppression ratio (SISR) values; with the SWE method, shear wave velocity values were determined. Differences in the mean values of these parameters per level and study group were analyzed by Student's t-test.* **Results:** *SWE revealed significantly lower stiffness at the L2-3 level, consistent with the signal index values (SII-SISR) showing increased fatty infiltration on MRI in the patient group. No such relationship was found at the L4-5 level or in control group.* **Conclusions:** *SWE may be a promising method to show muscle fatty infiltration at L2-3 level in patients with chronic low back pain.*

Keywords: *Fatty infiltration. muscle. Opposed-phase. Shear wave elastography. Stiffness. Low back pain. Magnetic resonance imaging. Multifidus.*

Resumen

Objetivo: *Investigar la viabilidad del uso de la elastografía de ondas de corte en comparación con la resonancia magnética con codificación de desplazamiento químico (RM-CDQ) para la evaluación de la degeneración grasa del músculo multífido en pacientes con dolor lumbar crónico.* **Método:** *Los músculos multífidos se evaluaron con RM-CDQ y elastografía de ondas de corte en los grupos de control y de pacientes. Se consideraron las secuencias en fase y fuera de fase en RM-CDQ, y los valores del índice de intensidad de señal y del índice de supresión de intensidad de señal; con el método de elastografía de ondas de corte se determinaron los valores de velocidad de onda de corte. Las diferencias en los valores medios de estos parámetros por nivel y por grupo de estudio se analizaron mediante la prueba t de Student.* **Resultados:** *La elastografía de ondas de corte reveló una rigidez significativamente menor en el nivel L2-3, consistente con los valores de los índices de señal que muestran una mayor infiltración grasa en la RM en el grupo de pacientes. No se encontró tal relación en el nivel L4-5 ni en el grupo de control.* **Conclusiones:** *La elastografía de ondas de corte puede ser un método prometedor para mostrar la infiltración grasa muscular a nivel L2-3 en pacientes con dolor lumbar crónico.*

Palabras clave: *Infiltración grasa. Lumbalgia. Resonancia magnética. Músculo multífido. Fase opuesta. Elastografía de ondas de corte. Rigidez.*

Correspondence:
Erdogan Bulbul
E-mail: drerdoganbulbul@yahoo.com

Date of reception: 22-01-2024
Date of acceptance: 04-04-2024
DOI: 10.24875/CIRU.24000048

Cir Cir. 2024;92(5):633-640
Contents available at PubMed
www.cirugiaycirujanos.com

Introduction

The World Health Organization reports chronic low back pain as one of the leading musculoskeletal problems in the world[1]. Various publications revealed that fatty infiltration of the lumbar multifidus muscle is closely related to low back pain[2-4]. Physical therapy focused on multifidus muscle has been shown to result in regression of fatty infiltration within the muscle, which correlates with functional improvement[5]. Detection of fatty infiltration of lumbar muscles may be highly significant for predicting clinical progression and choosing optimal personalized treatment options[5-8]. Therefore, non-invasive, easily accessible, and reliable imaging techniques are promising tools. Modalities that have been shown useful in the evaluation of intramuscular fatty infiltration include ultrasonography (US), computerized tomography (CT), and magnetic resonance imaging (MRI)[9-13]. Among these different methods, some specific MRI techniques and sequences, such as MR spectroscopy, chemical shift encoded (CSE) imaging stand out[13-15]. CSE MRI is a technique that can show even minimal amounts of fat using different precession frequencies of water and lipid hydrogen protons. Various researchers have shown the feasibility of CSE MR imaging in the evaluation of fatty infiltration of multifidus muscles in individuals with chronic low back pain[16-18].

Sonoelastography which assesses the stiffness of tissues can be performed by US-integrated techniques such as strain elastography and shear-wave elastography (SWE)[19]. The stiffness of tissues can be evaluated by measuring the velocities of shear waves created in soft tissues with the SWE technique[20]. There are various studies examining multifidus muscle stiffness in patients with low back pain using the SWE method[21-23]. To the best of our knowledge, there is only one study evaluating multifidus muscle stiffness and fatty infiltration of lumbar multifidus muscle in the same case group[24].

The primary purpose of this study was to assess whether either technique showed a significant difference between patients with chronic low back pain and control subjects. The secondary purpose of this study was to evaluate the feasibility of the SWE technique in the evaluation of multifidus muscle stiffness as a representative of muscle fatty infiltration, using CSE MRI as a non-invasive quantitative method. In addition, it is aimed to reveal whether fatty infiltration of multifidus muscle can be predicted by SWE measurements by investigating whether there is a correlation between MRI signal index and SWE measurement values in patients with chronic low back pain.

Methods

Study population

Adult patients aged 18-60 years, with chronic low back pain for more than 3 months, who were referred to a tertiary academic center for lumbar MRI examination between September 2020 and April 2021 were prospectively enrolled in this study (n = 305).

Individuals with a history of spinal surgery, any congenital orthopedic pathology other than low back pain, trauma, systemic inflammatory disease, advanced osteodegenerative changes (such as central canal stenosis and nerve root compression), spinal infection, neurological or neoplastic disease, and pregnant women were excluded from the study (Fig. 1). The final patient group consisted of 48 patients with chronic low back pain, 27 were female, and 21 were male, aged 22-59 years. A total of 38 normal control subjects 18 women and 20 men, aged 21-59 years, who did not have low back pain were performed lumbar MRI and did not have the features specified in the exclusion criteria in their history were included. Informed consent was obtained from all participating individuals.

Imaging techniques and image analysis

A 1.5 T MRI scanner (Philips Ingenia, Best, The Netherlands) was used for routine lumbar spinal image acquisition in all participants. In the sagittal plane, T1-weighted images (repetition time [TR]: 430 ms, echo time [TE]: 12 ms, thickness 4 mm, interslice gap 0.4 mm, matrix 240/384r, field of view [FOV] 300 mm, turbo factor [TF] 4, EPI factor 1, and NEX 2) and T2-weighted images (TR: 3000 ms, TE: 120 ms, thickness 4 mm, interslice gap 0.4 mm, matrix 240/384r, FOV 300 mm, TF 17, EPI factor 1, and NEX 2) were obtained. In the axial plane, T2-weighted GRE images (B-FFE) were obtained (TR: 9.6 ms, TE: 4.8 ms, thickness 4 mm, interslice gap 0.4 mm, matrix 148/240r, FOV 160 mm, flip angle (FA) 45°, TF 1, EPI factor 1, and NEX 2). In the control and patient groups who met the criteria, axial images were obtained from the L2-3 and L4-5 levels using an opposed-phase MRI technique, two-point DIXON (mDIXON) sequence

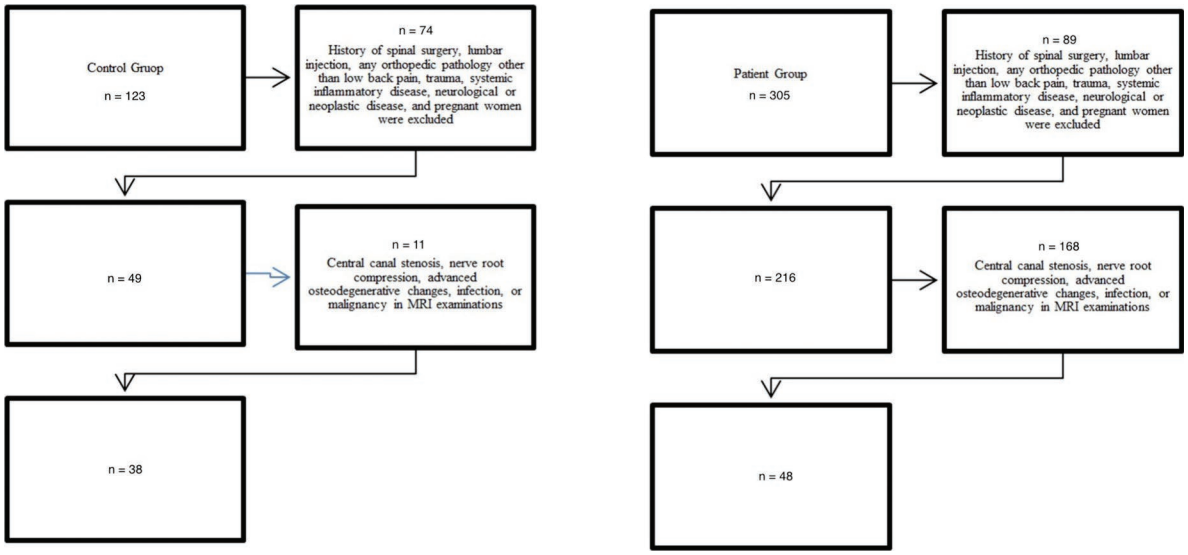

Figure 1. *Flow chart as process illustration for case accumulation and exclusion as performed in this work.*

(TR:5.8 ms, double TE:4.7 ve 2.4 ms, FA 15°, slice thickness 5 mm, interslice gap-2.5 mm, matrix 189/336r, and FOV 400 mm). In-phase and opposed-phase images were obtained from the same anatomical position, and signal intensity (SI) measurements were made at the workstation at both levels. SI measurements were performed with a circular region of interest (ROI) which was manually placed on the central part of the multifidus muscle. Air in the superficial proximity of skin was chosen as a reference region and measurements with the same sized ROI as in the muscle were obtained. Each measurement was acquired 3 times in a single session by the same 5th-year radiology resident. SI index (SII) and SI suppression ratio (SISR) parameters were calculated according to the following formulas using SI values obtained from in and opposed-phase images, as defined in previous articles[17,25];

– The percentage of change in SI of the multifidus muscle:

SII = ([In-phase SI multifidus – Opposed-phase SI multifidus]/[in-phase SI]) × 100

– The percentage of change in SI rate of the multifidus muscle compared with air:

SISR = ([Opposed-phase (SI multifidus/SI air)/In-phase (SI multifidus/SI air)]–1) × 100

Sonoelastography of lumbar multifidus muscles of participants from control and patient groups was performed by a SWE-capable Acuson S2000 US device (Siemens Healthcare, Erlangen, Germany). A 1-6 Mhz broadband convex transducer was used to reduce image noise and provide deep tissue penetration. The same operator performed all ultrasound examinations. Participants were placed in the prone position, and a folded towel was placed under their abdomen to reduce lumbar lordosis. Vertebral levels were defined by sonographic determination of the 12th rib level. Shear wave velocity (SWV) measurements were made in the sagittal plane, at the same anatomical level and side as MRI measurements; approximately 2 cm right side to the midline and parallel to muscle fibers, with the transducer positioned about 10° medialized, without applying any pressure to the probe. SWV measurements were acquired with a ROI of 0.5 cm × 0.6 cm by placing into multifidus muscle from a maximum depth of 5.5 cm. The minimum and maximum SWV values of seven measurements from each examination area were eliminated, and the arithmetic average of the five values was recorded in m/s.

Statistical analysis

Statistical analysis of the obtained data was performed using SPSS for Windows, version 22.0 (IBM Corp, NY, USA). Conformity to the normal distribution of SII, SISR, and SWV values of multifidus muscles at L2-3 and L4-5 levels and other variables were evaluated using analytical methods (Kolmogorov–Smirnov/Shapiro-Wilk tests). The correlation relations between the variables measured at both levels were evaluated

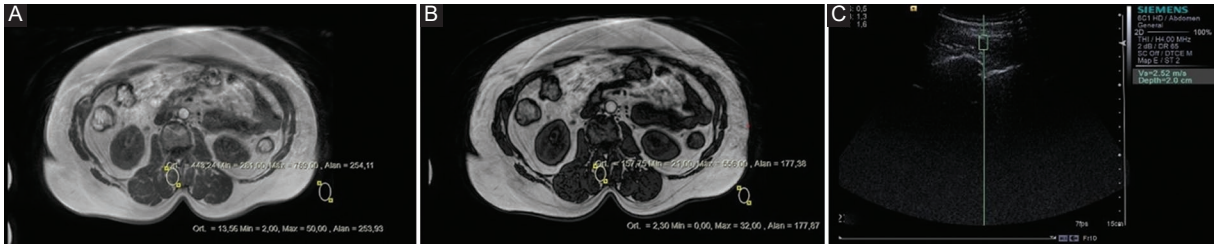

Figure 2. *A 53-year-old female with low back pain.* **A:** *in-phase and* **B:** *opposed-phase images. At the L2-3 level, the SII value and the SISR value are 100.31 and 64.55, respectively.* **C:** *SWV measurement in the multifidus muscle at the same level. The SWV value is 2.52 m/s.*
SII: signal intensity index; SISR: signal intensity suppression rate; SWV: shear wave velocity; **(A-B)** *Ort: mean signal intensity; Min: minimum signal intensity; Max: maximum signal intensity; Alan: Area;* **(C)** *Vs: shear wave velocity.*

by Pearson's correlation test for variables with normal distribution. Group differences for SII, SISR, and SWV values of the multifidus muscles at L2-3 and L4-5 levels were compared using Student's t-test. Cases with a type-1 error level below 5% were interpreted as statistically significant. To investigate intrareader agreement, intraclass correlation coefficients (ICCs) were computed.

Results

The mean age of the control group was 36.16, and the chronic low back pain patient group was 41.79 ($p = 0.019$).

According to the formula, we used in the CSE MRI technique, the semi-quantitative SISR value decreases as the fatty infiltration of the multifidus muscle gradually increases. In the in-phase and out-phase sequences, the fat SI is suppressed, and a higher SII value is obtained according to the formula. In the SWE technique, as the stiffness of tissue decreases, there is a decrease in the SWV value (Figs. 2 and 3). ICCs for SWV, SISR, and SII were 0.73-0.90, 0.80-0.92, and 0.85-0.90, supporting the reproducibility of measurements.

The mean SII and SISR index values obtained from multifidus muscles at L2-3 and L4-5 levels in the control and patient groups by opposed-phase MRI and the mean SWV values measured by SWE from the same levels are given in table 1. There was no statistically significant difference between the control and patient groups regarding SWV, SII, and SISR mean values at L2-3 and L4-5 levels ($p > 0.05$). The correlation between age and multifidus muscle SII, SISR, and SWV values at L2-3 and L4-5 levels in the patient group is shown in table 2. A statistically significant correlation was found between age, and SWV, SII, and SISR values of multifidus muscles at the L2-3 level. As patient age increases, multifidus muscle stiffness decreases, and at MRI, whereas SII increases, SISR decreases, indicating fatty infiltration of the muscle (Fig. 4). At the L4-5 level, no significant correlation between patient age and SWV and SII-SISR index values was noticed.

There was a significant negative correlation between SWV and SII ($r = -0.317$, $p = 0.028$) and a significant positive correlation between SWV and SISR ($r = 0.336$, $p = 0.019$). In other words, as the muscle stiffness decreased, the SII value increased, and the SISR value decreased, indicating fatty infiltration (Fig. 5). No significant correlation was found between SWV and SII ($r = 0.227$, $p = 0.178$) and between SWV and SISR values ($r = -0.174$, $p = 0.236$) for L4-5 level (Table 3).

Discussion

In our study, no statistically significant multifidus muscle stiffness expressing difference was found between the control group and the patient group with low back pain in terms of SWV mean values at L2-3 and L4-5 levels. This result is different from previous studies with the SWE[21-23]. No significant difference was found between the control and patient groups in terms of SWV and signal index values (SII-SISR). In other words, the lack of statistically significant difference between the control and patient groups in SWV values may be due to the similarity of fatty infiltration levels of multifidus muscles in the control and patient groups. It has previously been reported that the multifidus muscle in patients with low back pain was more rigid than the control group, assessed by the SWE method in the prone position and passive state. It has been suggested that this may be caused by increased tonicity, spasm, and fibrotic changes in the multifidus muscle[21,23,26]. Alis et al. reported a significant decrease in

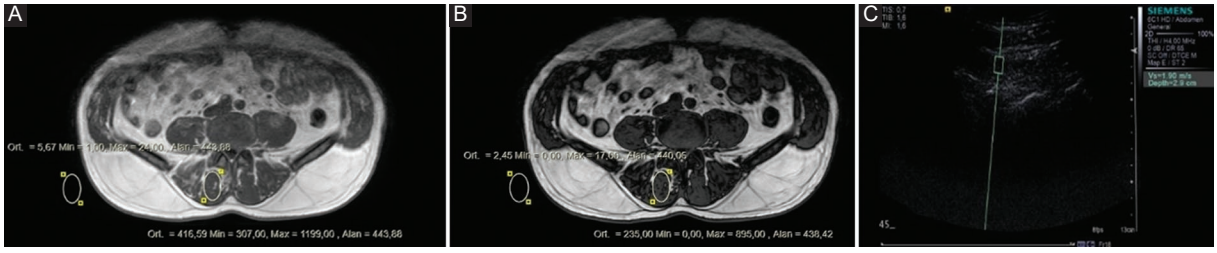

Figure 3. *A 50-year-old male with low back pain.* **A:** *in-phase and* **B:** *opposed-phase images. At the L4-5 level, the SII value and the SISR value are 43.51 and 30.54, respectively.* **C:** *SWV measurement in the multifidus muscle at the same level. The SWV value was 1.90 m/s.*
SII: signal intensity index; SISR: signal intensity suppression rate; SWV: shear wave velocity; **(A-B)** *Ort: mean signal intensity; Min: minimum signal intensity; Max: maximum signal intensity; Alan: Area;* **(C)** *Vs: shear wave velocity.*

Table 1. SWV, SII, and SISR values in the control group and in the patient group

Levels and measurements	Control group mean (± SD)	Patient group mean (± SD)	p-value*
L2-3 level multifidus muscle			
SWV	2.81 (± 0.82)	2.68 (± 0.88)	0.474
SII	31.93 (± 11.51)	33.23 (± 13.88)	0.640
SISR	101.68 (± 73.53)	87.98 (± 72.63)	0.391
L4-5 level multifidus muscle			
SWV	2.76 (± 0.71)	2.52 (± 0.57)	0.097
SII	35.19 (± 12.99)	33.38 (± 10.89)	0.493
SISR	118.18 (± 70.9)	94.87 (± 74.41)	0.147

*Statistically significant P<0.05. SD: standard deviation; SWV: shear wave velocity; SII: signal intensity index; SISR: signal intensity suppression ratio.

Table 2. Correlation results among age and SWV, SII, and SISR values at the L2-3 and L4-5 levels in the patient group

Parameters	L2-3 multifidus muscle		L4-5 multifidus muscle	
	r*	p-value**	r*	p-value**
Age - SWV	–0.305	0.035	–0.228	0.118
Age - SII	0.470	0.001	0.275	0.059
Age - SISR	–0.302	0.037	–0.059	0.692

* r: Pearson correlation coefficient. **Statistically significant p < 0.05. SWV: shear wave velocity; SII: signal intensity index; SISR: signal intensity suppression ratio.

Table 3. Correlation results between SWV and SII values and between SWV and SISR values at the L2-3 and L4-5 levels in the patient group

Levels	SWV-SII		SWV-SISR	
	r*	p**	r*	p**
L2-3 level	–0.317	0.028	0.336	0.019
L4-5 level	0.178	0.227	–0.174	0.236

*r: Pearson correlation coefficient. **statistically significant p < 0.05. SWV: shear wave velocity; SII: signal intensity index; SISR: signal intensity suppression ratio.

the multifidus muscle stiffness at SWE on the same side and at one lower vertebral level in patients with lumbar disc hernia[22]. They suggested that this result may be due to the fatty infiltration of the multifidus muscle. In another study evaluating the stiffness of the lumbar multifidus muscles in patients with chronic low back pain using the strain elastography method and the degree of fatty infiltration was assessed with the B-mode US images, no statistically significant difference was observed between the patients with chronic low back pain and the control group participants in terms of multifidus muscle stiffness in the passive resting state[24]. It has been stated that these different study results may be due to the usage of different sonoelastography methods[21,23]. Since the strain elastography technique is reported to be a user-dependent method, and it's difficult to obtain accurate results, it has been indicated that quantitative results can be achieved with the SWE method, which is a less user-dependent technique[21,23].

It has been previously emphasized in various studies that muscular fatty infiltration may increase depending on age[27-30]. In our study, a decrease in muscle stiffness and an increase in fatty infiltration with increasing age at L2-3 level in the patient group were observed to support this statement. However, no

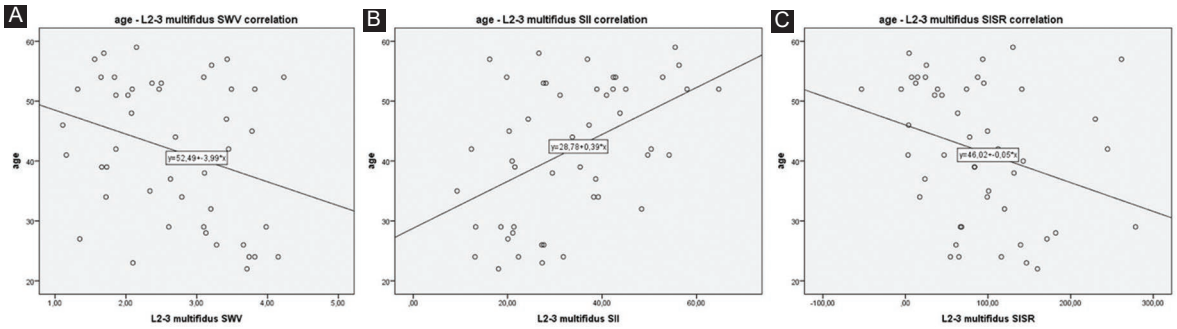

Figure 4. *Point distribution graphics of the L2-3 level.* **A:** *age-SWV,* **B:** *age-SII, and* **C:** *age-SISR correlations have been shown. SII: signal intensity index. SISR: signal intensity suppression rate. SWV: shear wave velocity.*

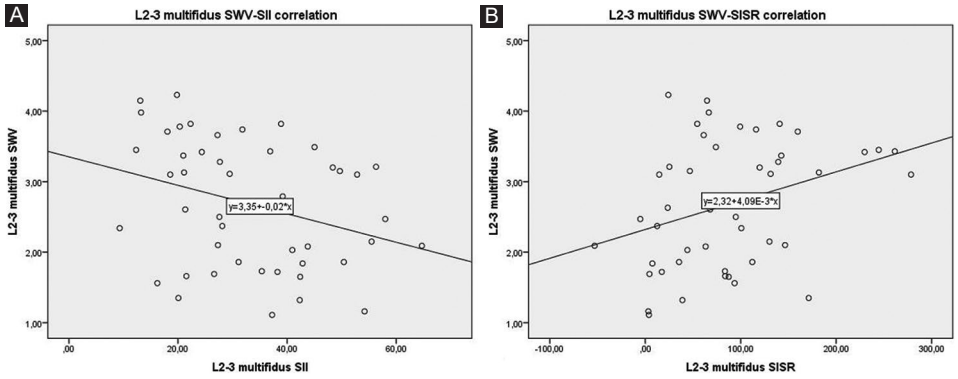

Figure 5. A: *SWV-SII.* **B:** *SWV-SISR point distribution graphics. Correlations of the L2-3 level have been demonstrated. SII: signal intensity index; SISR: signal intensity suppression rate; SWV: shear wave velocity.*

statistically significant correlation was found between age and these parameters at the L4-5 level in the patient group. It was thought that this situation might be due to accompanying fibrotic changes in the muscle, as previously reported in the literature[31,32]. Besides, it might have an adverse effect on the ultrasound waves in the thicker thoracolumbar fascia and subcutaneous fat layer in the caudal part at the L4-5 level[33].

To our knowledge, there is no other study examining the stiffness of multifidus muscles with SWE technique and the muscle fatty infiltration with CSE MRI in the literature. In our study, a correlation was found between SWV values and signals index values indicating that muscle stiffness decreases as fatty infiltration increases in multifidus muscle at the L2-3 level in patients with chronic low back pain. This result is consistent with the knowledge that less rigid sonoelastography values can be detected in muscle tissues with fatty infiltration[31,34]. Our results suggest that SWE may be a promising technique as an alternative method to MRI in detecting muscle fatty infiltration. However, no correlation was found between SWV measurements and CSE MRI signal index values at the L4-5 level. Similarly no statistical correlation between age and these measurement values. This statistical non-significant correlation at the lower lumbar level may be caused by similar factors. One of these factors may be the complex pathophysiological changes at the lower lumbar levels. It has been reported in various studies that different degenerative pathologies such as disc pathologies, spinal stenosis, and spondylolisthesis may cause more intense degeneration in multifidus muscles at lower lumbar vertebral levels[13,35,36]. However, in this study, these pathologies were exclusion criteria. Besides, it has been stated that fibrotic changes also play a role in multifidus muscle degeneration, as this situation causes an increase in stiffness in muscle fibers and bundles and fibrotic proliferation in the connective tissue. This situation can be seen as increased muscle stiffness in sonoelastographic examination[31,32]. It is thought that

another factor that could cause the lack of a statistical correlation between the measurement values at the lower lumbar level could be the lack of a complete methodological standard for sonoelastography examination[21,23,26,37]. There is a large data pool in the literature consisting of different results obtained from various levels and postures in the sonoelastography examination of posterior paraspinal muscles[21,23,26,37]. It is stated that the image is noisier, especially at the L4-5 level, due to the deeper location of the muscle, and a low-frequency transducer is needed. For this reason, we tried to overcome this problem using a low-frequency convex transducer. Moreover, finally, another factor might be the posterior layer of the thoracolumbar fascia which is thicker in the caudal part at the L4-5 level and strongly attenuates ultrasound waves[33].

Our study has some limitations. First, there were the limited number of patients in our control and study groups. Second, since there is no consensus about how to perform the SWE examination of multifidus muscles, our study was based on some application examples in the literature[21,23,26]. Third, our study did not include the participants' body mass index (BMI) values. However, there are studies in the literature reporting no relationship between the fatty infiltration of multifidus muscle and BMI[38,39]. Finally, our study is not supported by the fat fraction measurement, MR spectroscopy data, or histopathological data, which is the gold standard for demonstrating fibrosis and fatty infiltration.

Conclusions

In this study, a statistically significant correlation was found between SWE-assessed muscle stiffness and MRI-assessed fatty infiltration in multifidus muscles at the L2-3 level in the chronic low back pain group but not at the L4-5 level or in control group.

These results suggest that the SWE technique, which is a more practical, easily accessible, and inexpensive method, maybe a promising radiological examination in the detection of multifidus muscle fatty infiltration in symptomatic patients for upper leaves of lumbar paravertebral muscles.

Acknowledgments

The authors would like to thank the ethics committee for the approval of this work.

Compliance with ethical standards

Ethical approval: Informed consent for the study was obtained from all human subjects. The study was approved by the Clinical Research Ethics Committee of our faculty (No. 73023407/604.01.01/37892) and all procedures followed were in accordance with the World Medical Association Declaration of Helsinki: Ethical Principles for Medical Research involving Human Subjects, 2013.

Funding

The authors declare that they have not received funding.

Conflicts of interest

The authors declare no conflicts of interest.

Ethical disclosures

Protection of human and animal subjects. The authors declare that no experiments were performed on humans or animals for this study.

Confidentiality of data. The authors declare that they have followed the protocols of their work center on the publication of patient data.

Right to privacy and informed consent. The authors have obtained approval from the ethics committee for analysis and publication of routinely acquired clinical data and informed consent was not required for this retrospective observational study.

Use of artificial intelligence for generating text. The authors declare that they have not used any type of generative artificial intelligence for the writing of this manuscript nor for the creation of images, graphics, tables, or their corresponding captions.

References

1. Kaplan W, Wirtz V, Mantel A, Béatrice PS. Priority medicines for Europe and the world update 2013 report. Methodology. 2013;2:99-102.
2. Parkkola R, Rytökoski U, Kormano M. Magnetic resonance imaging of the discs and trunk muscles in patients with chronic low back pain and healthy control subjects. Spine (Phila Pa 1976). 1993;18:830-6.
3. Kjaer P, Bendix T, Sorensen JS, Korsholm L, Leboeuf-Yde C. Are MRI-defined fat infiltrations in the multifidus muscles associated with low back pain? BMC Med. 2007;5:1-10.
4. Sollmann N, Bonnheim NB, Joseph GB, Chachad R, Zhou J, Akkaya Z, et al. Paraspinal muscle in chronic low back pain: comparison between standard parameters and chemical shift encoding-based water-fat MRI. J Magn Reson Imaging. 2022;56:1600-8.
5. Woodham M, Woodham A, Skeate JG, Freeman M. Long-term lumbar multifidus muscle atrophy changes documented with magnetic resonance imaging: a case series. J Radiol Case Rep. 2014;8:27.

6. Hebert JJ, Le Cara EC, Koppenhaver SL, Hoffman MD, Marcus RL, Dempsey AR, et al. Predictors of clinical success with stabilization exercise are associated with lower levels of lumbar multifidus intramuscular adipose tissue in patients with low back pain. Disabil Rehabil. 2020;42:679-84.
7. Osorio W, Ceballos C, Moyano J. Effectiveness of acute post-operative pain management by the acute pain service. Cir Cir. 2022;90:197-201.
8. Jermy JE, Copley PC, Poon MT, Demetriades AK. Does pre-operative multifidus morphology on MRI predict clinical outcomes in adults following surgical treatment for degenerative lumbar spine disease? A systematic review. Eur Spine J. 2020;29:1318-27.
9. Flicker PL, Fleckenstein JL, Ferry K, Payne J, Ward C, Mayer T, et al. Lumbar muscle usage in chronic low back pain. Magnetic resonance image evaluation. Spine (Phila Pa 1976). 1993;18:582-6.
10. Hides JA, Stokes MJ, Saide M, Jull GA, Cooper DH. Evidence of lumbar multifidus muscle wasting ipsilateral to symptoms in patients with acute/subacute low back pain. Spine (Phila Pa 1976). 1994;19:165-72.
11. Keller A, Brox JI, Gunderson R, Holm I, Friis A, Reikeras O. Trunk muscle strength, cross-sectional area, and density in patients with chronic lowback pain randomized to lumbar fusion or cognitive intervention and exercises. Spine (Phila Pa 1976). 2004;29:3-8.
12. Hicks GE, Simonsick EM, Harris TB, Newman AB, Weiner DK, Nevitt MA, et al. Cross-sectional associations between trunk muscle composition, back pain, and physical function in the health, aging, and body composition study. J Gerontol A Biol Sci Med Sci. 2005;60:882-7.
13. Kalichman L, Carmeli E, Been E. The association between imaging parameters of the paraspinal muscles, spinal degeneration, and low back pain. Biomed Res Int. 2017;2017:2562957.
14. Takashima H, Takebayashi T, Ogon I, Yoshimoto M, Morita T, Umamura R, et al. Analysis of intra and extramyocellular lipids in the multifidus muscle in patients with chronic low back pain using MR spectroscopy. Br J Radiol. 2018;91:20170536.
15. Han G, Jiang Y, Zhang B, Gong C, Li W. Imaging evaluation of fat infiltration in paraspinal muscles on MRI: a systematic review with a focus on methodology. Orthop Surg. 2021;13:1141-8.
16. Paalanne N, Niinimäki J, Karppinen J, Taimela S, Mutanen P, Takatalo J, et al. Assessment of association between low back pain and paraspinal muscle atrophy using opposed-phase magnetic resonance imaging: a population-based study among young adults. Spine (Phila Pa 1976). 2011;36:1961-8.
17. Yanik B, Keyik B, Conkbayir I. Fatty degeneration of multifidus muscle in patients with chronic low back pain and in asymptomatic volunteers: quantification with chemical shift magnetic resonance imaging. Skeletal Radiol. 2013;42:771-8.
18. Schlaeger S, Inhuber S, Rohrmeier A, Deickmeyer M, Freitag F, Klupp E, et al. Association of paraspinal muscle water-fat MRI-based measurements with isometric strength measurements. Eur Radiol. 2019;29:599-608.
19. Lee SK, Jung JY, Kang YR, Jung JH, Yang JJ. Fat quantification of multifidus muscle using T2-weighted Dixon: which measurement methods are best suited for revealing the relationship between fat infiltration and herniated nucleus pulposus. Skeletal Radiol. 2020;49:263-71.
20. Hug F, Hodges PW, Tucker K. Muscle force cannot be directly inferred from muscle activation: illustrated by the proposed imbalance of force between the vastus medialis and vastus lateralis in people with patellofemoral pain. J Orthop Sports Phys Ther. 2015;45:360-5.
21. Masaki M, Aoyama T, Murakami T, Yanase K, Ji X, Tatehuchi H, et al. Association of low back pain with muscle stiffness and muscle mass of the lumbar back muscles, and sagittal spinal alignment in young and middle-aged medical workers. Clin Biomech (Bristol, Avon). 2017;49:128-33.
22. Alis D, Durmaz ES, Alis C, Erol BC, Okur B, Kizilkilic O, et al. Shear wave elastography of the lumbar multifidus muscle in patients with unilateral lumbar disk herniation. J Ultrasound Med. 2019;38:1695-703.
23. Murillo C, Falla D, Rushton A, Sanderson A, Heneghan NR. Shear wave elastography investigation of multifidus stiffness in individuals with low back pain. J Electromyogr Kinesiol. 2019;47:19-24.
24. Chan ST, Fung PK, Ng NY, Ngan TL, Chong MY, Tang CN, et al. Dynamic changes of elasticity, cross-sectional area, and fat infiltration of multifidus at different postures in men with chronic low back pain. Spine J. 2012;12:381-8.
25. Gokalp G, Yildirim N, Yazici Z, Ercan I. Using chemical-shift MR imaging to quantify fatty degeneration within supraspinatus muscle due to supraspinatus tendon injuries. Skeletal Radiol. 2010;39:1211-7.
26. Koppenhaver S, Gaffney E, Oates A, Eberle L, Young B, Hebert J, et al. Lumbar muscle stiffness is different in individuals with low back pain than asymptomatic controls and is associated with pain and disability, but not common physical examination findings. Musculoskelet Sci Pract. 2020;45:102078.
27. Hadar H, Gadoth N, Heifetz M. Fatty replacement of lower paraspinal muscles: normal and neuromuscular disorders. AJR Am J Roentgenol. 1983;141:895-8.
28. Hebert JJ, Kjaer P, Fritz JM, Walker BF. The relationship of lumbar multifidus muscle morphology to previous, current, and future low back pain: a 9-year population-based prospective cohort study. Spine (Phila Pa 1976). 2014;39:1417-25.
29. Lee SH, Park SW, Kim YB, Nam TK, Lee YS. The fatty degeneration of lumbar paraspinal muscles on computed tomography scan according to age and disc level. Spine J. 2017;17:81-7.
30. Mackintosh S, Young A, Muirhead J, Lee A, Sim JH. A pilot study: can shear wave elastography predict fatty infiltration of the supraspinatus muscle? Sonography. 2020;7:97-109.
31. Brown SH, Gregory DE, Carr JA, Ward SR, Masuda K, Lieber RL. ISSLS prize winner: adaptations to the multifidus muscle in response to experimentally induced intervertebral disc degeneration. Spine. 2011;36:1728-36.
32. Brown E, Yoshitake Y, Shinohara M, Ueda J. Automatic analysis of ultrasound shear-wave elastography in skeletal muscle without non-contractile tissue contamination. Int J Intell Robot Appl. 2018;2:209-25.
33. Moreau B, Vergari C, Gad H, Sandoz B, Skalli W, Laporte S. Non-invasive assessment of human multifidus muscle stiffness using ultrasound shear wave elastography: a feasibility study. Proc Inst Mech Eng H. 2016;230:809-14.
34. Koppenhaver SL, Scutella D, Sorrell BA, Yahalom J, Fernández-de-Las-Peñas C, Childs JD, et al. Normative parameters and anthropometric variability of lumbar muscle stiffness using ultrasound shear-wave elastography. Clin Biomech (Bristol, Avon). 2019;62:113-20.
35. Albert HB, Briggs AM, Kent P, Byrhagen A, Hansen C, Kjaergaard K. The prevalence of MRI-defined spinal pathoanatomies and their association with modic changes in individuals seeking care for low back pain. Eur Spine J. 2011;20:1355-62.
36. Hodges PW, Danneels L. Changes in structure and function of the back muscles in low back pain: different time points, observations, and mechanisms. J Orthop Sports Phys Ther. 2019;49:464-76.
37. Ma CZ, Ren LJ, Cheng CL, Zheng YP. Mapping of back muscle stiffness along spine during standing and lying in young adults: a pilot study on spinal stiffness quantification with ultrasound imaging. Sensors. 2020;20:7317.
38. Mengiardi B, Schmid MR, Boos N, Pfirrmann CWA, Brunner F, Elfering A, et al. Fat content of lumbar paraspinal muscles in patients with chronic low back pain and in asymptomatic volunteers: quantification with MR spectroscopy. Radiology. 2006;240:786-92.
39. Shapiro L, Harish M, Hargreaves B, Staroswiecki E, Gold G. Advances in musculoskeletal MRI: technical considerations. J Magn Reson Imaging. 2012;36:775-87.

ORIGINAL ARTICLE

Morphology of ulnar trochlear notch and defining ideal position for olecranon osteotomy

Morfología de la ulna muesca troclear y definición de la posición ideal para la osteotomía del olecranon

Milan Milinkov[1], Nikola Vučinić[2], Mirko Obradović[3], Nikola Vukosav[3], Milan Tošić[3], and Bojana Krstonošić[2]*

[1]Faculty of Medicine, University of Novi Sad; [2]Department of Anatomy, Faculty of Medicine, University of Novi Sad; [3]Clinic for Orthopedic Surgery and Traumatology, Clinical Center of Vojvodina. Novi Sad, Serbia

Abstract

Objective: *The aim of the study was to calculate the most important parameters of ulna and to determine its gender. Classifying trochlear notch joint surface types and to establish their representation in Serbian population. To determine the ideal position for olecranon osteotomy.* **Material and methods:** *The study included 69 bones. Gender determination was performed using digital scale and photographs of the ulna. The bones weight, maximum and physiological length were measured. The place for the ideal position of olecranon osteotomy (projection of the bare area on its posterior wall) was determined on profile images.* **Results:** *Gender related, 45 (65.21%) bones belonged to males, 24 (34.79%) ulnas belonged to females. Type I of the bare area was present in 38 (55%) ulnas, type II in 20 (29%), whereas type III was present in 11 (16%) bones. The average value for the ideal position of olecranon osteotomy was 23.02 mm. In males' ulnas, it was 23.22 mm, in females, it was 22.59 mm.* **Conclusion:** *Type I of the bare area is the most common type of trochlear notch joint surface in Serbian population. The average value for the ideal position of olecranon osteotomy was 23.02 mm. We believe that a uniform name for the bare area should be established.*

Keywords: *Ulna. Olecranon process. Trochlear notch. Osteotomy. Gender.*

Resumen

Objetivos: *Calcular los parámetros más importantes del cúbito y determinar su género. Clasificar los tipos de superficie de la articulación de la escotadura troclear y establecer su representación en la población serbia. Determinación de la posición ideal para la osteotomía del olécranon.* **Material y métodos:** *El estudio incluyó 69 huesos. La determinación del sexo se realizó mediante escala digital y fotografías del cúbito. Se midió el peso de los huesos, la longitud máxima y fisiológica. El lugar para la posición ideal de la osteotomía del olécranon se determinó en imágenes de perfil.* **Resultados:** *Relacionado con el género, 45 (65.21%) huesos pertenecían a hombres, 24 (34.79%) cúbitos pertenecían a mujeres. El tipo I del área descubierta estuvo presente en 38 (55%) ulna, el tipo II en 20 (29%), mientras que el tipo III estuvo presente en 11 (16%) huesos. El valor medio para la posición ideal de la osteotomía del olécranon fue de 23,02 mm.* **Conclusión:** *El área desnuda tipo I es el tipo más frecuente de superficie articular de muesca troclear en la población serbia. El valor promedio para la posición ideal de la osteotomía del olécranon fue de 23,02 mm. Creemos que se debe establecer un nombre uniforme para el área descubierta.*

***Palabras clave*:** *Ulna. Proceso del olécranon. Escotadura troclear. Osteotomía. Género.*

***Correspondence:**
Milan Milinkov
E-mail: 014293@mf.uns.ac.rs

Date of reception: 22-10-2022
Date of acceptance: 21-03-2023
DOI: 10.24875/CIRU.22000528

Cir Cir. 2024;92(5):641-646
Contents available at PubMed
www.cirugiaycirujanos.com

Introduction

Ulna is one of the bones of the forearm and it is positioned on the medial side of the radius and slightly behind it, in physiological position of supination. According to its shape, ulna belongs to long bones (*ossa longa*) and it is also an even bone. We distinguish the body and two end parts of the bone[1]. There are a trochlear notch, olecranon, and coronoid process on proximal end of ulna. Trochlear notch (*incisura trochlearis*) represents a concave joint surface and it is positioned between coronoid process and olecranon. Bare area divides it into two slopes corresponding to the joint surfaces which articulate with the trochlea of humerus. Olecranon is located at the upper back of the proximal part of the ulna. It tends to have a cube shape, on the front side being recessed into a smooth surface which forms part of the trochlear notch. The triceps attaches to the upper side of the olecranon and its posterior surface is rough and subcutaneous. Coronoid process represents front bottom eminence of the proximal part of ulna. Its shape resembles a four-sided pyramid. Upper side of coronoid process makes the bottom wall of the trochlear notch. On the lateral side, there is a radial notch (*incisura radialis*) which represents joint surface as well[1].

Data about gender affiliation are very important in every anthropological research, although it is not a simple task to determine gender on a single bone[2,3]. There are several ways of determining gender affiliation of ulna in the literature. We assume that authors Reddy and Doshi described optimal parameters[3].

Several classifications of trochlear notch are described regarding shapes of its joint surfaces. They indicate generally present anatomical variation, with certain degree of representation in different populations[4,5].

As fractures of distal humerus are relatively common injuries of the upper extremity, from the clinical point, type of trochlear notch joint surface is significant for performing olecranon osteotomy during operative treatment of the mentioned fractures. Olecranon osteotomy with opened reposition and internal fixation represents widely accepted method of operative treatment for type C fractures of distal humerus (complete intraarticular fracture)[5]. Compared to other surgical approaches to distal humerus, it provides the best approach[6], thus increasing the success of the surgical treatment. Furthermore, the authors suggest the possible impact of variations in trochlear notch joint surfaces on arthroscopic elbow surgeries, design of prostheses for performing elbow arthroplasty, as well as its impact on elbow radiological imaging[5]. Projection of the bare area on posterior wall of ulna represents, "entry point" for performing olecranon osteotomy itself[5,7] as it is well known that the potential joint surface cartilage damage would lead to arthrosis of the affected joint. Besides, current recommendation from AO Foundation for olecranon osteotomy is to perform the chevron osteotomy[8] (Fig. 1). Bare area projection on the back side of the ulna is of crucial importance for such a procedure. Clinical importance of bare area is not supported in current anatomical terminology[9]. In other words, there is no specific name for transverse ridge (bare area) although it significantly morphologically differs from the rest of the trochlear notch[10].

We presume that examining different parameters on ulna, as well as types of trochlear notch joint surfaces regarding their shape will bring important data related to Serbian population. We also believe that the indicative recognition of the bare area projection on the ulnar back wall would contribute to significantly better results in surgical treatment, intraoperatively, as well

Figure 1. *Intraoperative view of the chevron olecranon osteotomy* (Photo from the personal archive of intraoperative photos of co-author Dr. Mirko Obradović).

as postoperatively, resulting in easier recovery and better function of the elbow. Goals of our paper were first to calculate the most important parameters of ulna and to determine its gender, based on the results. Second, the goal was to classify trochlear notch joint surface types and to establish their representation in Serbian population. Third, it was to determine the ideal position for olecranon osteotomy.

Materials and methods

The research was conducted at the Department of Anatomy, Faculty of Medicine, University of Novi Sad. It included 69 bones from the Osteological museum which were of an unknown age. The research exclusion criteria were bone damages and previous fractures. All bones were photographed by *Canon EOS2000D* camera, using a photo stand. During the process, they were on the same distance and under the same angle compared to the camera. Further, photo processing and parameters calculation were done using *ImageJ 1.53K* software. The same person performed both photographing and photo processing.

We classified types of trochlear notch joint surfaces into three types, through direct visualization by the two people, based on the research of Totlis et al.[5].

- Type I – Completely divided olecranon and coronoid process joint surfaces.
- Type II – Connected olecranon and coronoid process joint surfaces with constriction.
- Type III – Connected olecranon and coronoid process joint surfaces without constriction[5] (Fig. 2).

The following parameters were measured to define ulna's gender affiliation, using a digital scale and photographs of ulnas:

- Ulna's weight
- Maximal length – The distance between the highest point of olecranon and the lowest point of ulna's styloid process[3].
- Physiological length – the distance between the most distal points on the coronoid process surface and on the lower surface of ulna distal end part (excluding styloid process)[3].

Location of the ideal position for olecranon osteotomy was defined on bones' profile pictures, by measuring the distance from insertion of triceps on the top of the olecranon to the projection of bare area on the posterior wall of ulna (Fig. 3)[8]. Bones with type III bare area were excluded from the sample (when determining the ideal olecranon osteotomy position). Due to connected joint surfaces, it is not possible to avoid damaging cartilage while performing this procedure. Thus, it is impossible to determine the ideal position for the procedure itself.

The program used for data processing was Statistical Package for the Social Sciences which works under the Microsoft Windows environment. The results are presented using graphs and tables. The descriptive statistics is shown (frequencies and percentages for categorical data, as well as arithmetic means and standard deviations for quantitative data). Since the results of the osteotomy position parameters are expressed quantitatively, it is established that presumption about normal result distribution ($p > 0.05$) was fulfilled using the Shapiro–Wilk test. T-test was used for independent samples to examine differences between male and female ulnas, along with both left and right side of the body in terms of the ideal osteotomy position. χ^2 test was used for categorical data to determine the correlation between male and female ulnas, the side of the body where the bone is located on one side and the frequency of three basic types of trochlear notch joint surfaces on the other side.

The research was approved by the Medical faculty Ethics commission, in Novi Sad (date: 08 December 2021; decision number: 01-39/119/1).

Results

According to the bone gender, 45 (65.21%) were males, while 24 (34.79%) were females. The sample contained 37 (52.62%) right and 32 (46.38%) left bones. Descriptive statistical indicators of the measured parameters are shown in table 1.

Type I bare area was represented by 38 ulnas, type II by 20, whereas type III was represented by 11 bones, out of the total number of ulnas in the sample (Fig. 4).

Numerical representation of trochlear notch joint surfaces regarding gender is shown in figure 5. Type I bare area was present in 62% of male ulnas, and 42% at females, type II was noted in 27% of male and 33% of female ulnas, while type III was noticed in 11% of male and 25% of female bones. Statistically relevant connection was not established between male and female ulnas and the presence of three basic trochlear notch joint surface types. χ^2 (2, N = 69) = 3.335, p = 0.189.

Joint surfaces frequency distribution in the sample showed that 19 ulnas had type I bare area in both left and right bones, type II was noted seven times in left,

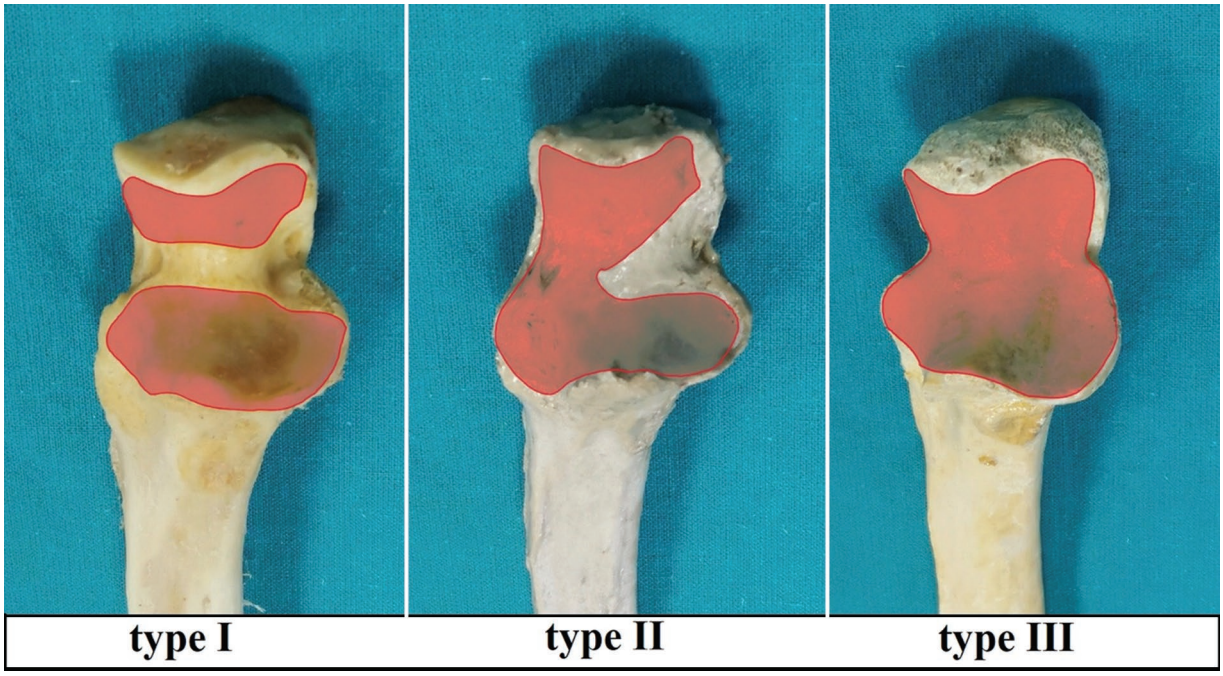

Figure 2. *Representation of basic types of trochlear notch joint surfaces.*

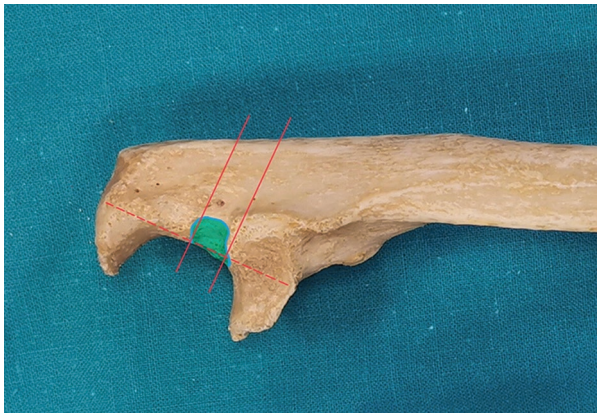

Figure 3. *Representation of the bare area projection on the posterior wall of ulna as an entry point for performing the chevron olecranon osteotomy.*

and 13 times in the sample of right bones, whereas type III was identified six times in left and five times in right bones. Statistically relevant association between left and right side of the body and frequency of three basic types of trochlear notch joint surfaces were not determined. χ^2 (2, N = 69) = 1.537, p = 0.464.

The average value for the ideal position of olecranon osteotomy in the sample (58 bones) was 23.02 mm. In males' ulnas, it was 23.22 mm, while in females, it was 22.59 mm. The results of the t-test indicated that no statistically significant differences were found between male and female ulnas regarding the ideal average position for performing osteotomy (t [56] = 0.619, p = 0.538).

Related to bare area, average value for the ideal position of olecranon osteotomy in type I was 23.31 mm, while in type II it was 22.47 mm. In right ulnas ideal position for performing olecranon osteotomy was 22.61 mm, while in the left bones it was 23.52 mm. The results of the t-test indicated that no statistically significant differences were found between the left and right side of the body in terms of the ideal average position for performing osteotomy (t [56] = 0.976, p = 0.333).

Discussion

Determination of cadaver sex based on skeletal remains certainly belongs to anthropological sciences. Besides gaining anthropological knowledge, it also provides us with significant forensic data[2].

In literature, there are several trochlear notch classifications regarding shapes of its joint surfaces[4,5]. Even though classification on three basic types is described in several research papers[5,11], it is notable that, in anatomical and orthopedics textbooks completely divided, joint surface (type I) is the only one listed[12-14]. We did not find a significant number of scientific papers which included the representation of types of ulnar trochlear notch joint surfaces. Representation of mentioned

Table 1. Representation of descriptive statistical indicators

Parameters	n	Min	Max	M	SD
Weight (g)	69	19	74	47.25	13.53
Maximal length (mm)	69	227.73	304.03	261.87	18.35
Physiological length (mm)	69	195.20	271.38	227.85	16.87
Osteotomy position (mm)	58	14.73	31.18	23.03	3.53

N: number of respondents; Min: minimum; Max: maximum; M: arithmetic mean; SD: standard deviation.

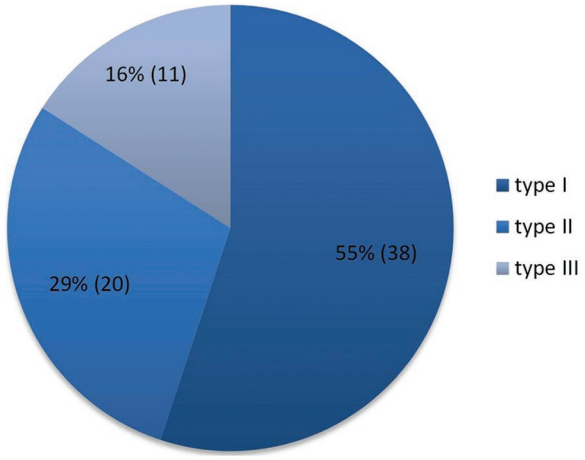

Figure 4. *Representation of trochlear notch joint surface types in our sample.*

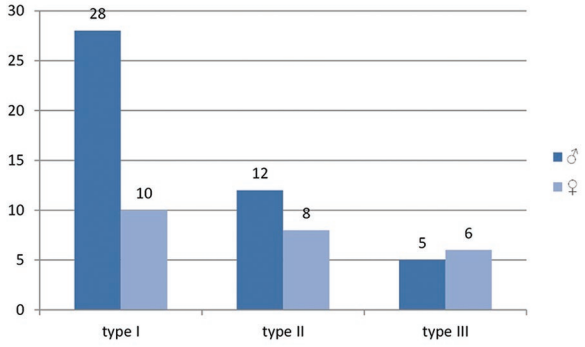

Figure 5. *Representation of trochlear notch joint surfaces types according to gender.*

structure in Serbian population correlates with the results of other European authors[5]. Both in ours and in mentioned research, types I and II are stated as the predominant, with representation of more than 80%. We believe that knowing the projection of the bare area on posterior wall of the ulna is of crucial importance when performing olecranon osteotomy, since it is possible to avoid cartilage damage in mentioned trochlear notch types.

In our study, we decided to use bone weight, maximal length of ulna, and physiological length of ulna when determining bone gender. Other researchers showed that two of three mentioned parameters (bone weight and physiological length of bone) are the most discriminatory variables for determining the cadaver gender related to the ulna, with overall accuracy of 93.2%[3]. Due to the significant differences in male's and female's musculoskeletal system, we feel that determination of bones gender is very useful in our study. Type II bare area is relatively equally represented in males and females in Serbian population. Type I was more common in males, while type III was more frequent in female's ulnas. We attribute different bone representation to non-identical biological development of men and women. This result should be taken with certain amount of constraint due to unequal number of bones of both genders.

Types of trochlear notch articular surfaces have a big role in orthopedics surgery. Some authors state different positions as entry point for performing olecranon osteotomy – at the level of the trochlea of humerus[15,16], then through the trochlear notch itself[17], as well as 3–4 cm from the top of the olecranon[18]. Newer researches cite the projection of bare area on the posterior wall of ulnas entry point for performing olecranon osteotomy[5,8,10] as a part of operative treatment of fractures of the distal end of the humerus. Based on recent research, we determined the ideal position for olecranon osteotomy based on the projection of the bare area on the posterior wall of the ulna. Compared to our results, Chinese authors report a slightly lower value of the ideal position for performing olecranon osteotomy, which is 22 mm[8], and we assume that the difference of approximately 1 mm is insignificant. It is our opinion that determining the average position for olecranon osteotomy brings significant data to orthopedists to avoid damage of the articular surfaces, which would certainly lead to certain postoperative complications.

We often come across authors' hypotheses that different anatomical characteristics can be found among the same bones, on opposite sides of the body (right and left bones)[19]. Yet, there is a relative uniformity of the types of articular surfaces of the trochlear notch between the left and right ulnas in our sample. Six more right bones with the type II trochlear notch are due to the fact that there were more right ulnas in the entire sample. In literature, authors use different names to describe the part of the articular surface

without cartilage, that is, the bare area itself. However, its name does not exist in the official anatomical literature[9]. Based on the anatomical structure of the liver, the *area nuda*, we feel that a uniform name for the bare area should be established. Considering its anatomical appearance and histological structure[14], we suggest the name *area ossea*. The new, specific name would greatly contribute to a better understanding and easier identification of the described structure.

Conclusions

Type I bare area is the most common type of articular surface in Serbian population. The average value for the ideal position of olecranon osteotomy in the sample was 23.02 mm, and no statistically significant differences were found between male and female ulnas regarding the ideal average position for performing osteotomy. Furthermore, no statistically significant differences were found between the left and right side of the body in terms of the ideal average position for performing osteotomy. We believe that knowing the projection of the bare area on posterior wall of the ulna is of crucial importance when performing olecranon osteotomy, since it is possible to avoid cartilage damage in different trochlear notch types. The new special name *area ossea,* which we suggest for the examined structure, would greatly contribute to a better understanding and easier identification.

Funding

The authors declare no funding was received.

Conflicts of interest

All authors declare that they have no conflicts of interest.

Ethical disclosures

Protection of human and animal subjects. The authors declare that the procedures followed were in accordance with the regulations of the relevant clinical research ethics committee and with those of the Code of Ethics of the World Medical Association (Declaration of Helsinki).

Confidentiality of data. The authors declare that they have followed the protocols of their work center on the publication of patient data.

Right to privacy and informed consent. The authors have obtained approval from the Ethics Committee for analysis and publication of routinely acquired clinical data, and informed consent was not required for this retrospective observational study.

References

1. Franco-Valencia M, Torres-González R, Fuentes-Figueroa S. Radiographic measurements of the wrist in healthy Mexicans. Cir Cir. 2006; 74:335-42.
2. Purkait R. Measurements of ulna--a new method for determination of sex. J Forensic Sci. 2001;46:924-7.
3. Reddy BB, Doshi MA. Sex determination from adult human ulna by stepwise discriminant function analysis. Int J Res Med Sci. 2017; 6:5128-31.
4. Yamaguchi B. The bipartient tendency of the articular surface of the trochlear notch in the human ulna. Okajimas Folia Anat Jpn. 1972; 49:23-35.
5. Totlis T, Otountzidis N, Papadopoulos S, Piagkou M, Natsis K. Ulnar trochlear notch articular surface has three morphological patterns: a neglected major anatomical feature. Surg Radiol Anat. 2019;41:1333-6.
6. Luegmair M, Timofiev E, Chirpaz-Cerbat JM. Surgical treatment of AO Type C distal humeral fractures: internal fixation with a Y-shaped reconstruction (Lambda) plate. J Shoulder Elbow Surg. 2008;17:113-20.
7. Wilkinson JM, Stanley D. Posterior surgical approaches to the elbow: a comparative anatomic study. J Shoulder Elbow Surg. 2001;10:380-2.
8. Ao R, Zhang X, Li D, Chen F, Zhou J, Yu B. The bare area of the proximal ulna: an anatomic study with relevance to chevron osteotomy. J Hand Surg Am. 2017;42:471.e1-471.e6.
9. FIPAT. Terminologia Anatomica. 2nd ed. FIPAT.Library.Dal.Ca. Federative International Programme for Anatomical Terminology; 2019.
10. Wang A, Mara M, Hutchinson DT. The proximal ulna: an anatomic study with relevance to olecranon osteotomy and fracture fixation. J Shoulder Elbow Surg. 2003;12:293-6.
11. Milz S, Eckstein F, Putz R. Thickness distribution of the subchondral mineralization zone of the trochlear notch and its correlation with the cartilage thickness: an expression of functional adaptation to mechanical stress acting on the humeroulnar joint. Anat Rec. 1997;248:189-97.
12. Wolfe S, Pederson W, Kozin S, Cohen M. Green's Operative Hand surgery. 8th ed. Philadelphia, PA, USA: Elsevier; 2021.
13. Azar FM, Canale ST, Beaty JH. Campbell's Operative Orthopaedics. 14th ed. Philadelphia, PA, USA: Elsevier.
14. Standring S. Gray's Anatomy. 42th ed. Philadelphia, PA, USA: Elsevier; 2020.
15. Jupiter JB, Neff U, Holzach P, Allgöwer M. Intercondylar fractures of the humerus. An operative approach. J Bone Joint Surg Am. 1985;67:226-39.
16. Müller ME, Perren SM, Allgöwer M, Müller ME, Schneider R, Willenegger H. Manual of Internal Fixation: Techniques Recommended by the AO-ASIF group. 8th ed. Berlin, Germany: Springer Science and Business Media; 1991.
17. Cassebaum WH. Operative treatment of T and Y fractures of the lower end of the humerus. Am J Surg. 1952;83:265-70.
18. Henley MB. Intra-articular distal humeral fractures in adults. Orthop Clin North Am. 1987;18:11-23.
19. Vučinić N, Teofilovski-Parapid G, Erić M, Tubbs RS, Radošević D, Jovančević B. Morphometric analysis of the patterns of calcaneal facets for the talus in Serbian population. PLoS One. 2020;15:e0240818.

ORIGINAL ARTICLE

In total knee arthroplasty surgeries, what is the effective dose of intra-articular tranexamic acid?

En cirugías de artroplastia total de rodilla, ¿cuál es la dosis efectiva de ácido tranexámico intraarticular?

Ismail G. Şahin[1] and Hüsamettin Özdemir[2]*

[1]Department of Orthopaedic and Traumatology, Training and Research Hospital of Muğla Sıtkı Koçman University, Muğla; [2]Department of Orthopaedic and Traumatology, Edirne Sultan 1. Murat State Hospital, Edirne, Turkey

Abstract

Objective: *The aim of our study was to evaluate the effect of different doses of intra-articular (IA) tranexamic acid (TXA) on blood loss in total knee arthroplasty surgeries and compare it to the control group.* **Materials and Methods:** *A total of 160 patients who underwent unilateral total knee arthroplasty surgery at Edirne State Hospital between 2016 and 2020 were divided into four groups. The estimated blood loss and amount of blood loss from drainage, as well as transfusion rates, were compared between the groups based on surgical pre- and post-operative blood parameters to evaluate the dose effectiveness.* **Results:** *In our study, all TXA groups significantly reduced the estimated blood loss and amount of blood loss from drainage compared to the control group. No statistically significant difference was found between the control group and the group receiving 1 g of TXA in terms of transfusion rates (p = 0.062), and no statistically significant difference was found between the groups receiving 2 g and 3 g of TXA.* **Conclusion:** *The use of 2 g of IA TXA is an effective dose for controlling blood loss in total knee arthroplasty surgeries. Lower doses do not have a significant effect on transfusion rates, whereas higher doses do not significantly increase effectiveness.*

Keywords: *Tranexamic acid. Total knee arthroplasty. Intra-articular. Topical. Local. Blood.*

Resumen

Objetivo: *El objetivo de nuestro estudio fue evaluar el efecto de diferentes dosis de ácido tranexámico intraarticular en la pérdida de sangre en cirugías de artroplastia total de rodilla y compararlo con el grupo control.* **Materiales y métodos:** *La pérdida de sangre estimada y la cantidad de sangre perdida por drenaje, así como las tasas de transfusión, se compararon entre los grupos en base a los parámetros sanguíneos preoperatorios y postoperatorios quirúrgicos para evaluar la efectividad de la dosis.* **Resultados:** *En nuestro estudio, todos los grupos de ácido tranexámico redujeron significativamente la pérdida de sangre estimada y la cantidad de sangre perdida por drenaje en comparación con el grupo control. No se encontró diferencia estadísticamente significativa entre el grupo control y el grupo que recibió 1 g de TXA en términos de tasas de transfusión (p = 0.062), y no se encontró diferencia estadísticamente significativa entre los grupos que recibieron 2 g y 3 g de TXA.* **Conclusión:** *El uso de 2 g de ácido tranexámico intraarticular es una dosis efectiva para controlar la pérdida de sangre en cirugías de artroplastia total de rodilla. Las dosis más bajas no tienen un efecto significativo en las tasas de transfusión.*

***Palabras clave*:** *Ácido tranexámico (TXA). Artroplastia total de rodilla (TKA). Intraarticular. Tópico. Local. Sangre.*

***Correspondence:**
Ismail G. Şahin
E-mail: ismailgokhansahin@gmail.com

Date of reception: 01-01-2023
Date of acceptance: 28-07-2023
DOI: 10.24875/CIRU.23000003

Cir Cir. 2024;92(5):647-654
Contents available at PubMed
www.cirugiaycirujanos.com

Introduction

Osteoarthritis is a dynamic process that occurs due to the disruption of the balance between destruction and repair of the joint cartilage and subchondral bone. The goal of treatment is to improve the quality of life by reducing pain and mobility limitations and preserving or improving joint function. When conservative treatment options fail to reduce patient complaints, total knee arthroplasty surgery is currently considered the gold standard surgical treatment method, which is cost-effective and provides long-term survival. Modern total knee arthroplasty surgery began with the development of the tricompartmental total knee prosthesis by Insall and Ranawat in 1973, and the number of surgeries has increased significantly in the past 20 years.

It is reported that the average blood loss during total knee arthroplasty surgery is between 500 and 1500 mL, and the average transfusion rate is 20%, although there are also reports of average blood loss of up to 2000 mL and transfusion rates up to 50%[1-4]. Considering that the average blood volume in the body is approximately 5000 mL and these surgeries are often performed in the geriatric population, blood loss is a significant problem. There are several options to address this problem, including pre-operative iron replacement therapy and erythropoietin therapy; the use of pneumatic tourniquets, hypotensive anesthesia, and autologous blood transfusion during surgery; and following the flexion of the knee after surgery. The most commonly used method to replace this loss is allogeneic blood transfusion. Allogeneic blood transfusion carries the risk of allergic and immunological reactions[2]. There is also a risk of infection, especially in the case of viral diseases during the donor's window period. In addition, according to health-care system data, it is estimated that 2 million total knee arthroplasty surgeries will be performed in the United States in 2030, and the cost of preparing and administering one unit of allogeneic erythrocyte suspension is 250-1000 $ (250 $ in Turkey, 350 $ in France, and 1000 $ in the USA)[3,5-7].

Tranexamic acid (TXA) (cyclohexanecarboxylic acid) (C8H15NO2) is a synthetic derivative of lysine and is an antifibrinolytic drug that inhibits fibrinolysis by binding to the lysine region of plasminogen[4]. It was first described in 1968 and has been used for the control of bleeding in gynecological and hematological diseases, among others, since 1970. It continues to be used in a variety of indications in many fields. It has been included in the World Health Organization's list of essential drugs due to its low cost and cost-effectiveness. TXA, which has been used for the control of bleeding in various fields for many years, has become increasingly popular in the recent years in reducing blood loss associated with total knee and hip arthroplasty[2-4,8-11].

There have been many meta-analyses on the effectiveness of TXA, but a consensus on the optimal dosage and mode of administration has not been reached due to the wide range of dosage and modes of administration. The effectiveness of intra-articular (IA) (topical and local) and systemic (intravenous) use of TXA in orthopedics is still controversial. Different meta-analyses have reported that the use of 1 g or more of TXA IA reduces blood loss and that the use of up to 3 g is effective and safe[2,4,8-11]. In addition, the IA application of TXA is an effective and practical method that allows for standard dosing independent of body weight and offers the opportunity to avoid systemic thrombotic complications (deep vein thrombosis [DVT], pulmonary embolism [PE], and venous thromboembolic event [VTE]) associated with the drug[9,11,12].

There are many studies on the effect of TXA on bleeding in orthopedic prosthetic surgery, and almost all of these studies compare different methods of use with each other or with a control group. The aim of our study is to contribute to the literature by evaluating the effectiveness of IA TXA administration on blood loss and transfusion rates in total knee arthroplasty surgeries, in the same study with different doses (a total of 3 drug and 1 control groups).

Materials and methods

This study includes data from 160 patients who underwent unilateral total knee arthroplasty for primary osteoarthritis at Edirne State Hospital between 2016 and 2020. The effective and safe dose range for IA TXA administration is 1-3 g, so the study groups were formed based on this data[1-4,10-16]. After a power analysis (80%), the study consisted of 40 patients each in 4 groups (IA 1 g, IA 2 g, IA 3 g, and control). Demographic data, estimated blood loss based on pre- and post-surgical blood parameters, drain blood loss, and transfusion data were compared and evaluated. The study included patients with Kellgren–Lawrence Stage 4 primary osteoarthritis, but excluded patients with secondary osteoarthritis (traumatic arthritis, inflammatory arthritis, etc.), a history of

cardiovascular treatment, more than 6 months of anticoagulant use, and a diagnosis or suspicion of thromboembolic events.

Patients were operated on by 2 surgeons. After the surgical drape, the extremity was elevated for 10 min and wrapped with the help of Esmark bandage from distal to proximal and then inflated to 100 mmHg above the patient's systolic blood pressure and a pneumatic tourniquet was used. No patient's tourniquet pressure exceeded 300 mmHg because the surgery of patients with high systolic pressure (> 200 mmHg) was postponed. All surgeries were performed under spinal anesthesia with pneumatic tourniquet[17], using the gap balancing technique[18] to apply a cemented posterior stabilized total knee arthroplasty (PS-TKA) (Total Knee System, Tıpsan, İzmir, Turkey; Knee Prosthesis System, Tıpmed, İzmir, Turkey). After the repair of the patellar tendon, TXA was administered to the TXA groups as a 50 mL solution with TXA (Tranexel 250 mg/5% iv/im injection Solution, Haver Farma İlaç Anonim Şirketi, Istanbul, Turkey) mixed with physiological saline (SF, 0.9% NaCl) and 50 mL SF was administered to the control group IA. After wound closure and dressing, an anti-embolism stocking was applied, and the tourniquet was released about 15 min after IA administration. The drain was clamped for 30 min after tourniquet release and the amount of blood loss from the drain was measured and recorded at 1, 3, 6, 12, 24, and 48 h, postoperatively, with the drain being removed at 48 h.[16] The results of the hemograms were recorded before and after surgery on the 1st, 2nd, and 3rd days. As per American society of anesthesiologists (ASA) criteria, patients with symptomatictic hemoglobin (hgb) levels below 8 g/dL and all patients with hgb levels below 6 g/dL received allogeneic red blood cell suspension transfusions to raise their hgb levels to at least 10 g/dL. The estimated blood loss due to surgery was calculated using the Nadler and Gross formulas[19,20]. According to the Gross formula, 1 unit of red blood cell suspension is considered to be 300 mL for patients who received transfusions, which was added to the estimated blood loss.

All patients were mobilized as soon as possible, within 24 h after surgery, to prevent DVT. The patients were taught bedside foot pump and leg lift exercises and were treated with anticoagulants (0.4 mL enoxaparin and subcutaneous application) and antiembolic stockings for 20 days after surgery. The patients were mobilized and followed up after the surgery with the current rehabilitation protocol[21], and the patients with limited mobility were referred to the physical therapy and rehabilitation unit. After pain control, the patients were discharged from the hospital between the 4th and 6th days after surgery the patients were called to the outpatient clinic on the 20th day after surgery to have their sutures removed and to have their hemogram values checked.

Statistical analysis

Statistical analyses were performed with SPSS v.23.0 software (SPSS Inc., IBM Corporation, Armonk, New York, USA). In the power analysis, it was found that, for the acceptable blood loss amount of 70 units between the treatment groups at 80% power and 5% significance level, and the standard deviation was 100, the sample size that should be included in each group was found to be 40. The groups were analyzed in terms of distribution analysis of the data and homogeneity of variance. Data with normal distribution and homogeneous variance were analyzed with parametric tests (ANOVA), and data that did not comply with normal distribution or did not have homogeneous variance were analyzed with non-parametric tests (Kruskal–Wallis, Mann–Whitney U-test). Chi-square test was used to compare categorical variables. Since there were 6 pairwise comparisons in total, Bonferroni correction was made due to group analysis, and the p-value was calculated as 0.05/6 = 0.0083.

Results

In this study, 160 patients were included, 22 of whom were male (13.75%) and 138 were female (86.25%). In 73 patients (45.63%), the right knee was operated on, and in 87 (54.37%), the left knee was operated on. The groups were compared in terms of age, height, and body weight, and no statistically significant differences were found (Table 1A).

The groups were compared in terms of ASA scores before surgery, joint range of motion measurement, surgical tourniquet time, and discharge times, and no statistically significant differences were found in any parameter (Table 1B).

The groups were compared in terms of hemoglobin (g/dL) before surgery, hematocrit (%), platelets (103/mL), and estimated body blood volume calculated according to the Nadler formula, and no statistically significant differences were found between the groups (Table 1C).

In the evaluation of post-surgical blood loss, the estimated total blood loss volume (PBL) (mL) calculated

Table 1. Whole data of the patients in 5 groups are shown

Section	Parameter	Group 4 (control)	Group 1 (IA 1GR)	Group 2 (IA 2GR)	Group 3 (IA 3GR)	p-values (p < 0.0083)
A	Age (year)	66.38 ± 8.24	66.22 ± 9.28	68.38 ± 5.19	67.32 ± 7.48	0.4332†
	Height (cm)	164.25 ± 7.68	166.18 ± 5.70	161.68 ± 6.01	161.78 ± 6.19	0.0122†
	Weight (kg)	81.33 ± 14.17	79.00 ± 11.35	79.80 ± 10.90	84.38 ± 12.99	0.2283‡
	BMI (kg/m^2)*	30.23 ± 5.44	28.65 ± 4.3	30.60 ± 4.41	29.41 ± 4.23	0.0113‡
	Gender (M/F)	9/31	3/37	6/34	4/36	0.2194§
	Side (right/left)	19/21	18/22	17/23	19/21	0.9394§
B	ASA (I + II/III + IV)	35/5	38/2	35/5	33/7	0.2774§
	Pre-operative ROM**	100 (85-130)	105 (75-125)	105 (70-130)	100 (80-130)	0.6102†
	Tourniquet time (min)	100 (60-120)	100 (60-130)	105 (60-130)	105 (75-120)	0.4472†
	Post-operative discharge day	3 (3-5)	3 (3-4)	3 (3-5)	3 (3-8)	0.1572†
C	Hemoglobin value (g/dL)*	13.30 ± 1.20	12.79 ± 1.36	12.59 ± 1.01	12.62 ± 1.00	0.0232†
	Hematocrit value (%)*	40.32 ± 3.54	39.26 ± 4.15	38.32 ± 2.86	38.37 ± 2.75	0.0283‡
	Platelet count (10^3/mL)*	264.5 (153-439)	278.5 (146-519)	269 (122-512)	257.5 (142-496)	0.8642†
	Body blood volume (l)*	3.54 ± 0.52	3.42 ± 0.39	3.45 ± 0.40	3.59 ± 0.44	0.4714§
D	Blood transfusion (+/-) (%)	9/31 (22.5%)	3/37 (7.5%)	1/39 (2.5%)	1/39 (2.5%)	0.0044§
	Blood transfusion (count)	21	10	2	2	0.0052†
	Blood loss from drain (mL)	649 (250-1195)	475 (200-1100)	389 (120-1100)	343 (100-1155)	0.0012†
	Predictive blood loss (mL)	1147 (457-2533)	793 (144-2199)	729 (198-1834)	622 (129-2048)	0.0012†
	Pbl/drain blood loss ratio	1.61 (0.53-5.03)	1.61 (0.29-5.03)	1.74 (0.3-7.26)	2.02 (0.3-5.07)	0.1332†
E	Hemoglobin value (g/dL)¶	11.00 ± 1.10	10.97 ± 0.91	11.02 ± 1.21	11.11 ± 1.05	0.9803‡
	Hematocrit value (%)¶	33.92 ± 3.45	34.27 ± 2.90	33.72 ± 3.64	33.99 ± 2.91	0.9843†
	Platelet count (10^3/mL)¶	369 (196-679)	246 (239-325)	345 (145-709)	344 (205-882)	0.3512†

*Preoperative.
†Kruskal Wallis.
‡Anova.
§Chi-square.
¶Postoperative 3rd week.
**Range of motion.

using the Gross formula, measurement of blood loss from drains (mL), and transfusion rate (%) were used (Table 1D). In statistical analyses, statistically significant differences were found in terms of estimated blood loss, transfusion rate, and blood loss from drains (p = 0.004/0.001/0.001) (Table 1D).

The relationship between total blood loss and blood loss from drains was examined, and it was found to be 1.61 (0.53-5.07) in the control group, 1.61 (0.29-5.03) in Group 1, 1.74 (0.3-7.26) in Group 2, 2.02 (0.53-4.46) in Group 3, and 1.74 (0.29-7.26) in all patients. In the analysis, no significant difference was found between the groups in terms of total blood loss/blood loss from the drain ratio. (p = 0.133) (Table 1D) (Fig. 1).

On the 20th day after surgery, no significant difference was found between the groups in terms of hemoglobin, hematocrit, and platelet counts (Table 1E). No deep surgical infections, PE, DVT, or VTEs were identified in the included patients.

When the groups were compared two-by-two, it was found that all TXA groups significantly reduced blood loss compared to the control group in terms of PBL (p = 0.001/0.001/0.001) and that there was no statistically significant difference between groups in terms of TXA dose (Table 2).

Table 2. Comparison of groups in terms of predictive blood loss and drainage blood loss

p-values (p < 0.0083)	Group 4 (control)	Group 1 (IA 1GR)	Group 2 (IA 2GR)	Group 3 (IA 3GR)
Group 4	1.000*/1.000†/1.000‡	0.001§/0.001§/0.062	0.001§/0.001§/0.007§	0.001§/0.001§/0.007§
Group 1	0.001§/0.001§/0.062	1.000/1.000/1.000	0.651/0.104/0.308	0.356/0.003*/0.308
Group 2	0.001§/0.001§/0.007§	0.651/0.104/0.308	1.000/1.000/1.000	0.482/0.178/1.000
Group 3	0.001§/0.001§/0.007§	0.356/0.003§/0.308	0.482/0.178/1.000	1.000/1.000/1.000

*Predictive blood loss.
†Drainage blood loss.
‡Allogeneic blood transfusion (%).
§Statistically significant level.

Table 3. Comparison of groups in terms of allogeneic blood transfusion percentage and count

p values (p < 0.0083)	Group 4 (control)	Group 1 (IA 1GR)	Group 2 (IA 2GR)	Group 3 (IA 3GR)
Group 4	1.000*/1.000†	0.062/0.133	0.007‡/0.007‡	0.007‡/0.007‡
Group 1	0.062/0.133	1.000/1.000	0.308/0.165	0.308/0.165
Group 2	0.007‡/0.007‡	0.308/0.165	1.000/1.000	1.000/1.000
Group 3	0.007‡/0.007‡	0.308/0.165	1.000/1.000	1.000/1.000

*Allogeneic blood transfusion (%).
†Allogeneic blood transfusion (count).
‡Statistically significant level.

When the groups were evaluated in terms of transfusion rate (%), 9 patients in the control group (22.5%, 21 patients), 3 patients in the 1st group (7.5%, 10), 1 patient in the 2nd group (2.5%, 2), 1 in the 3rd group. It was determined that the patient (2.5%, 2 units) was transfused (Fig. 2). Group 1 did not create a statistically significant difference in transfusion rates compared to the control group (p = 0.062), Groups 2 and 3 significantly reduced transfusion compared to the control group (p = 0.007/0.007), but there was a statistically significant difference between Groups 2 and 3 (p = 1.000) (Table 3). There was no significant difference between the control group and the first group (p = 0.133) in the double comparisons made after the difference was detected in the comparison of the number of transfusion parameters (p = 0.005). When compared to the control group, the number of transfusions was significantly lower in the 2nd and 3rd groups (p = 0.007/0.007), and no significant difference was found in the two-way comparisons between the drug groups (Table 3) (Figure 3).

When the groups were evaluated in terms of blood loss from drains, it was found that all TXA groups significantly reduced blood loss from drains compared to the control group (p = 0.001/0.001/0.001). In intra-group comparisons, it was found that the application of 3 g of TXA significantly reduced blood loss from drains compared to the application of 1 g of TXA (p = 0.003), but there was no significant difference between the application of 2 g and 3 g of TXA (p = 0.178) (Table 2).

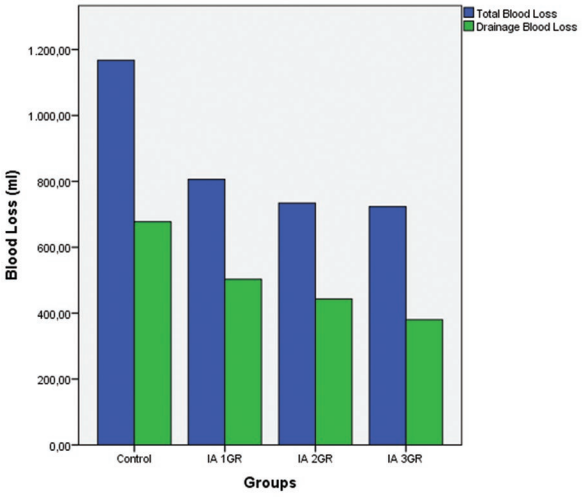

Figure 1. *Blood loss from drainage and total blood loss.*

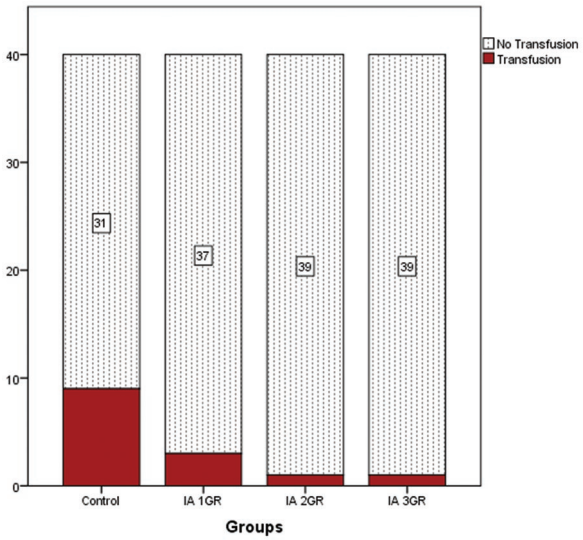

Figure 2. *Allogeneic blood transfusion rates.*

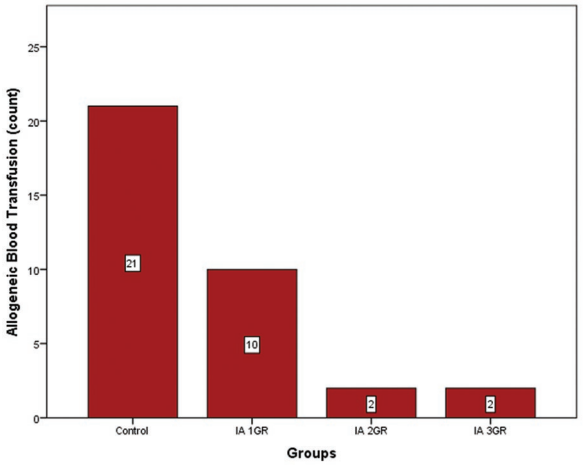

Figure 3. *Allogeneic blood transfusion counts.*

Discussion

TXA is a cost-effective drug that has been used for bleeding control for approximately 50 years. There are many publications and meta-analyses stating that IA applications of TXA start to show its effect at doses of 1 g and above, and its use up to 3 g is effective and safe[1-4,10-16].

A meta-analysis conducted by Xu et al. included 211 publications and found that TXA applications had lower transfusion rates compared to control groups and that IA (topical) use was a safe method in cases with high thrombosis risk[11]. In a study conducted by Kim et al., 0.5, 1, 2, and 3 g IA administration doses of TXA were compared with the control group[14]. In this study, TXA was found to be effective in controlling bleeding at all doses of 1 g and above, and therefore it is recommended to use TXA IA in a 1 g dose. In a study by Sahin et al., the effectiveness and safety of TXA's 2 g IA use was compared with the various combinations and doses of systemic use of TXA, and it was found that IA use of 2 g was effective and safe[1]. In the literature, the effectiveness of TXA in IA applications below 1 g is controversial, and therefore the lowest IA TXA group in our study was taken as 1 g.

In our study, one of the most important parameters was transfusion rates. In a study conducted by Kim et al.,[14] different IA TXA doses were compared to a control group; a 19% transfusion rate was found in the control group, a 9% transfusion rate in the 1 g group, a 10% transfusion rate in the 2 g group, and an 8% transfusion rate in the 3 g group. In another study conducted by Sahin et al.[1], the transfusion rate was found to be 17.64% in the control group and no transfusion was required in the 2 g IA TXA group (0%)[1]. In a study conducted by Georgiadis et al., the transfusion rate in the control group was 8%, whereas the rate in the TXA group was 0%; however, there was no statistically significant difference ($p = 0.118$)[13]. In a study by Lee et al., the transfusion rate in all groups treated with combined IA, IA + intravenous low and high doses of TXA was found to be 0%[15]. In our study, transfusion was performed at a rate of 22.5% in the control group, 7.5% in the 1 g TXA group, and 2.5% in both the 2 and 3 g TXA groups. Unlike the study by Kim et al.,[14] in our study, there was no statistically significant difference in the transfusion rates between the control group and the 1 g TXA group. In addition, there was no statistically significant difference in the transfusion rates between the 2 and 3 g TXA groups. While our transfusion rates seem to be consistent with the literature, according to the meta-analysis conducted by Mi et al., transfusion is performed in 10 g/dL or less in symptomatic patients and in 8 g/dL or less in all patients in the literature, while in our study, transfusion was limited to 8 g/dL or less in symptomatic patients, and 6 g/dL or less in all patients according to the ASA criteria and the decisions of the hospital transfusion committee[2].

In our study, the estimated total blood loss due to surgery was investigated. In a meta-analysis by Moskal and Capps[8], the estimated total blood loss due to surgery was found to be 834.40 mL (640.48-1028.3) in the IA TXA groups and 1195.32 mL (935.63-1455.0)

in the control groups. In a study conducted by Kim et al., TKA surgery was associated with a blood loss of 1503 ± 681 mL in the control group, 1190 ± 379 mL in the 1 g IA TXA group, 1147 ± 432 mL in the 2 g IA TXA group, and 1171 ± 299 mL in the 3 g IA TXA group, and no significant difference was found between the drug groups[14]. In a multicenter randomized controlled study conducted by Stowers et al.[22], the blood loss in the IA 1.5 g TXA application group was 723 mL (620-826), and in the placebo group, it was 1090 mL (923-1257)[21]. In the study conducted by Şahin et al.[1], 832 mL (403-1409) in the 2 g IA TXA group and 1309 mL (408-2119) in the control group were determined. In our study, blood loss was 1147 mL (457-2533) in the control group, 793 mL (144-2199) in the 1 g IA TXA group, 729 mL (198-1834) in the 2 g IA TXA group, and 622 mL (129-2048) in the 3 g IA TXA group. In our study, according with the literature, a significantly lower amount of bleeding was detected in the drug groups compared to the control group. However, no significant difference was found between the drug groups.

In our study, post-surgical drainage blood loss was an important parameter investigated. In a meta-analysis by Moskal and Capps[8], post-operative blood loss from drains was found to be 353.69 mL (279.68-427.70) in the IA-TXA groups and 534.66 mL (410.28-659.05) in the control groups. In the study of Kim et al., 307.4 ± 237.7 mL of drainage blood loss was detected in the control group, 259 ± 163.4 mL in the 1 gr IA TXA group, 261.8 ± 163.9 mL in the 2 g IA TXA group, and 258.0 ± 110.8 mL in the 3 g IA TXA group[14]. In our study, 649 mL (250-1195) of drainage blood loss was detected in the control group, 475 mL (200-1100) in the 1 g group, 389 mL (120-1100) in the 2 g group, and 343 mL (100-1155) in the 3 g group. The relationship between drainage blood loss and total blood loss was investigated and it was determined that the ratio of the amount of drainage blood loss to total blood loss was similar at a level that did not create significant differences between the groups (1.61-2.02).

One of the most significant and serious complications of TXA that has been identified in the literature is that it creates the foundation for thromboembolic events such as DVT, PE, and VTE. A meta-analysis conducted by Moskal and Capps[8] showed that the use of IA TXA does not increase the risk of thromboembolic interactions compared to other modes of use of TXA and that TXA is a cost-effective solution for total knee arthroplasty surgeries in centers with a transfusion rate of more than 25%. A meta-analysis conducted by Xu et al.[11] found that any mode of use of TXA did not increase the risk of thromboembolic events when compared to the control group and that topical TXA application was effective and safer. A meta-analysis conducted by Mi et al.[2], which analyzed the results of a total of 1308 patients showed that intravenous or IA administration of TXA did not increase the risk of thromboembolic events or deep surgical infection. Moskal and Capps[8] found the DVT level between 2.44% and 2.55% for the IA and control groups, and no increased risk associated with the use of TXA was found. In our study, no thromboembolic events or deep surgical infections were observed in the drug groups, consistent with the literature.

Conclusion

In our study, we aimed to contribute to the literature by evaluating the effectiveness of IA TXA application on the amount of blood loss and transfusion rates in total knee arthroplasty surgeries, by comparing different doses proven to be effective in the same study (total of 3 drugs and 1 control group).

In our study, the use of 1 g TXA was not significantly effective when compared to the control group, and the use of 3 g TXA was not superior in any parameter in terms of the preventive effectiveness of blood loss compared to the use of 2 g TXA. According to our study, the use of more than 2 g of TXA IA did not increase the effectiveness of preventing blood loss in total knee replacement surgeries. Therefore, IA use of 2 g TXA is a cost-effective dose in total knee replacement surgeries, and no increase in anti-bleeding efficiency was found with dose increase. We concluded that the cost-effective dose to prevent bleeding in total knee replacement surgeries is 2 g and should be used at this dose.

When the meta-analyses in the literature are examined, the blood transfusion indications and the blood transfusion indications in our study are different for the reasons stated in the publication. Characteristics are an important shortcoming in the evaluation and statistical analysis of transfusion rates. In addition, the relationship between TXA use and returning to daily activities after surgery is important, and the inability to make this comparison in our study is an important shortcoming. Although no significant difference was found between the control and drug groups in terms of blood parameters taken on the 20th day in our study, more comprehensive studies are needed to evaluate the relationship between TXA and activity level in the early postoperative period.

Funding

No financial support was received from any institution or organization during the preparation of this study.

Conflicts of interest

No benefits in any form have been received or will be received from a commercial party related directly or indirectly, financially, or otherwise, to the subject of this article.

Ethical disclosures

Protection of human and animal subjects. The authors declare that no experiments were performed on humans or animals for this study.

Confidentiality of data. The authors declare that they have followed the protocols of their work center on the publication of patient data.

Right to privacy and informed consent. The authors have obtained approval from the Ethics Committee for analysis and publication of routinely acquired clinical data, and informed consent was not required for this retrospective observational study.

References

1. Şahin İG, Akalin Y, Çevik N, Otuzbir A, Özkan Y, Öztürk A. Tranexamic acid in total knee replacement which protocol? Which application form? A prospective randomised study. Acta Orthop Belg. 2019;85:484-93.
2. Mi B, Liu G, Zhou W, Lv H, Liu Y, Zha K, et al. Intra-articular versus intravenous tranexamic acid application in total knee arthroplasty: a meta-analysis of randomized controlled trials. Arch Orthop Trauma Surg. 2017;137:997-1009.
3. Gillette BP, Kremers HM, Duncan CM, Smith HM, Trousdale RT, Pagnano MW. Economic impact of tranexamic acid in healthy patients undergoing primary total hip and knee arthroplasty. J Arthroplasty. 2013;28:137-9.
4. Melvin JS, Stryker LS, Sierra RJ. Tranexamic acid in hip and knee arthroplasty. J Am Acad Orthop Surg. 2015;23:732-40.
5. İndelen C, Uygun Kızmaz Y, Kar A, Shander A, Kırali K. The cost of one unit blood transfusion components and cost-effectiveness analysis results of transfusion improvement program. Turk Gogus Kalp Damar Cerrahisi Derg. 2021;29:150-7.
6. Rigal JC, Riche VP, Tching-Sin M, Fronteau C, Huon JF, Cadiet J, et al. Cost of red blood cell transfusion; evaluation in a French academic hospital. Transfus Clin Biol. 2020;27:222-8.
7. Singh JA, Yu S, Chen L, Cleveland JD. Rates of total joint replacement in the United States: future projections to 2020-2040 using the national inpatient sample. J Rheumatol. 2019;46:1134-40.
8. Moskal JT, Capps SG. Intra-articular tranexamic acid in primary total knee arthroplasty: meta-analysis. J Knee Surg. 2018;31:56-67.
9. Pecold J, Al-Jeabory M, Matuszewski M, Pruc M, Maslyukov A, Krupowies M, et al. Systematic review and meta-analysis of intravenous and topical tranexamic acid in reducing blood loss in knee arthroplasty. Disaster Emerg Med J. 2022;7:166-75.
10. Tan TK, Lee JY, Tay A, Kuster M. Intra-articular versus intravenous administration of tranexamic acid in lower limb total arthroplasty: a systematic review and meta-analysis of randomised clinical trials. Eur J Orthop Surg Traumatol. 2022;33:709.
11. Xu S, Chen JY, Zheng Q, Lo NN, Chia SL, Tay KJ, et al. The safest and most efficacious route of tranexamic acid administration in total joint arthroplasty: a systematic review and network meta-analysis. Thromb Res. 2019;176:61-6.
12. Tammachote N, Raphiphan R, Kanitnate S. High-dose (3 g) topical tranexamic acid has higher potency in reducing blood loss after total knee arthroplasty compared with low dose (500 mg): a double-blind randomized controlled trial. Eur J Orthop Surg Traumatol. 2019;29:1729-35.
13. Georgiadis AG, Muh SJ, Silverton CD, Weir RM, Laker MW. A prospective double-blind placebo controlled trial of topical tranexamic acid in total knee arthroplasty. J Arthroplasty. 2013;28:78-82.
14. Kim JK, Park JY, Lee DY, Ro DH, Han HS, Lee MC. Optimal dose of topical tranexamic acid considering efficacy and safety in total knee arthroplasty: a randomized controlled study. Knee Surg Sports Traumatol Arthrosc. 2021;29:3409-17.
15. Lee SY, Chong S, Balasubramanian D, Na YG, Kim TK. What is the ideal route of administration of tranexamic acid in TKA? A randomized controlled trial. Clin Orthop Relat Res. 2017;475:1987-96.
16. Kim MK, Ko SH, Nam YC, Jeon YS, Kwon DG, Ryu DJ. Optimal release timing of drain clamping to reduce postoperative bleeding after total knee arthroplasty with intraarticular injection of tranexamic acid. Medicina (Kaunas). 2022;58:1226.
17. Arthur JR, Spangehl MJ. Tourniquet use in total knee arthroplasty. J Knee Surg. 2019;32:719-29.
18. Sheth NP, Husain A, Nelson CL. Surgical techniques for total knee arthroplasty: measured resection, gap balancing, and hybrid. J Am Acad Orthop Surg. 2017;25:499-508.
19. Nadler SB, Hidalgo JH, Bloch T. Prediction of blood volume in normal human adults. Surgery. 1962;51:224-32.
20. Gross JB. Estimating allowable blood loss: corrected for dilution. Anesthesiology. 1983;58:277-80.
21. Ekşioğlu E, Gürçay E. Total diz artroplastisi sonrasi rehabilitasyon. J Istanbul Fac Med. 2014;76:16-21.
22. Stowers MD, Aoina J, Vane A, Poutawera V, Hill AG, Munro JT. Tranexamic acid in knee surgery study-a multicentered, randomized, controlled trial. J Arthroplasty. 2017;32:3379-84.

ORIGINAL ARTICLE

Pharyngeal mucosal closure in total laryngectomy: comparison between vertical and T-shaped closure

Cierre de la mucosa faríngea en la laringectomía total: comparación entre cierre vertical y cierre en T

*Adolfo Montemayor-Alatorre, Ruth P. Serna-Vazquez, Karla M. Santos-Santillana, Josefina A. Morales-del Ángel, José R. Córtes-Ponce, and José L. Treviño-González**

Otolaryngology and Head and Neck Surgery Division, School of Medicine and University Hospital "Dr. Jose E. González", Universidad Autónoma de Nuevo León, Monterrey, Nuevo Leon, Mexico

Abstract

Objective: *The objective of this study was to compare the outcomes vertical and T-shaped pharyngoplasty closure techniques after total laryngectomy (TL) and to evaluate the factors associated with the development of pharyngocutaneous fistula.* **Method:** *We performed a retrospective study that included patients with a histopathological diagnosis of laryngeal cancer that underwent TL between 2009 and 2021.* **Results:** *Fifty-seven patients were included in the study. A total of 14 patients underwent a vertical closure of the neopharynx (24.6%), while 43 patients underwent a T-shaped closure (74.4%). Pharyngocutaneous fistula was the most common complication, observed in 40.4% of cases (n = 23). No difference in the rate of complications was observed between groups, with the exception of tracheal dehiscence which was reduced in patients with T-shaped closure (n = 2, 4.7% vs. n = 5, 35.7%, p = 0.002). Diabetes mellitus was more frequently observed in patients with the development of pharyngocutaneous fistula (n = 7, 30.4% vs. n = 3, 8.8%, p = 0.03).* **Conclusions:** *Although complications were lower in the T-shaped closure group, we could not establish the superiority of either technique.*

Keywords: *Laryngectomy. Laryngeal cancer. Wound closure techniques. Fistula. Treatment outcome.*

Resumen

Objetivo: *Evaluar los desenlaces de la técnica vertical en comparación con la técnica en T para el cierre de faringoplastia posterior a una laringectomía total, y evaluar los factores asociados con el desarrollo de fístula faringocutánea.* **Método:** *Estudio retrospectivo de pacientes con diagnóstico de cancer de laringe a quienes se realizó laringectomía total como tratamiento, de 2009 a 2021.* **Resultados:** *Se incluyeron 57 pacientes. A 14 (24.6%) se les realizó una faringoplastia con cierre en T y a 43 (74.4%) un cierre vertical. La fístula faringocutánea fue la complicación más frecuente, presente en el 40.4% de los casos (n = 23). No se observaron diferencias en el desarrollo de complicaciones entre grupos, con excepción de la dehiscencia traqueal, la cual fue menos frecuente en el grupo de cierre en T (n = 2, 4.7% vs. n = 5, 35.7%; p = 0.002). La diabetes mellitus se asoció con el desarrollo de fístula faringocutánea (n = 7, 30.4% vs. n = 3, 8.8%; p = 0.03).* **Conclusiones:** *Aunque se observó una tendencia a una disminución de las complicaciones en el grupo de cierre en T, no se encontró superioridad de una técnica sobre otra.*

Palabras clave: *Laringectomía. Cáncer de laringe. Técnicas de cierre quirúrgico. Fístula. Desenlace de tratamiento.*

***Correspondence:**
José L. Treviño-González
E-mail: jose.trevinog@uanl.mx

Date of reception: 17-06-2022
Date of acceptance: 11-07-2023
DOI: 10.24875/CIRU.22000324

Cir Cir. 2024;92(5):655-659
Contents available at PubMed
www.cirugiaycirujanos.com

Introduction

Total laryngectomy (TL) is the standard treatment for advanced laryngeal cancer and as salvage surgery after chemotherapy or radiotherapy failure[1]. During TL, the closure of the mucosa of the anterior wall of the pharynx is a critical step. The most common pharyngeal closure lines are vertical and T-shaped, using continuous sutures. The selection of the technique is based on the shape and size of the defect, the elasticity of the remaining tissue, and, in great part, to the preferences of the surgeon[2]. Few studies have evaluated the effectivity of different pharyngoplasty techniques and the reported results are controversial[3].

The type of closure technique has been associated with short- and long- term complications[4]. Pharyngocutaneous fistulas (PCF) are the most common complication, with an incidence between 3 and 65%. The development of PCF is due in part to the dehiscence of the pharyngeal sutures and other related risk factors[5]. Dysphagia is also frequently observed in laryngectomized patients. The previous studies have associated the development of dysphagia with vertical pharyngeal closure[6]. However, evidence evaluating the patients' outcomes associated with the type of pharyngeal closure after TL is heterogeneous.

Determining the most effective technique could potentially decrease morbidity, mortality, hospitalization time, and the delay of adjuvant treatment. The objective of this study was to compare the outcomes of both vertical and T-shaped pharyngoplasty closure techniques after TL.

Methods

We performed a retrospective study that included patients with a histopathological diagnosis of laryngeal cancer that underwent TL between 2009 and 2021 at the Otolaryngology and Head and Neck Surgery department at Hospital Universitario "Dr. José E. González". The authors assert that all procedures contributing to this work comply with the ethical standards of the relevant national and institutional guidelines on human experimentation and with the Helsinki Declaration of 1975, as revised in 2008. This study was performed according to the principles stipulated in the Declaration of Helsinki. This project was approved by the Research and Ethics committee of our institution (reference number OT20-00010). The following data were obtained: demographic data, relevant medical history, alcohol and tobacco use, clinical presentation, stage and localization of the tumor, primary closure technique, complications, start of oral feeding, duration of hospitalization, adjuvant treatment, and follow-up.

Subjects

We obtained a sample of subjects over 18 years of age, with histopathological diagnosis of stage 3 or stage 4 pharyngeal carcinoma that underwent TL or salvage laryngectomy with vertical or T-shaped pharyngoplasty. The patients with a diagnosis of extrinsic larynx carcinoma, pharyngeal reconstruction with flap augmentation, a follow-up shorter than a month, presence of distant metastases, or a history of surgery for head and neck cancer were excluded.

Study protocol

The patients were assigned to two different groups based on the surgical closure technique. All surgeries were performed by 2 surgeons (AMA and BGA). In Group 1, the technique consisted of a vertical closure of the mucosa with continuous Connel-Mayo sutures, a second layer of submucosa closure with the same sutures, and a third muscular layer closed with horizontal mattress sutures. All surgeries in group 1 were performed by AMA. In Group 2 —performed by BGA — the technique consisted in a T-shaped mucosa closure with continuous Connel-Mayo sutures, a second layer of submucosa closure with the same sutures, and a third muscular layer closed with horizontal mattress sutures. In both groups, care was taken to close the mucosa without punctures and maintaining inverted edges. In all patients, before closure, a nasogastric tube (NG) was inserted to ensure postoperative feeding and nothing by mouth was indicated.

Statistical analysis

All analyses were performed using SPSS Statistics version 24.0 (SPSS, Inc., Armonk, NY). We obtained the frequencies and percentages for all qualitative variables. We obtained measures of central tendency and the dispersion for quantitative variables. A Pearson's chi-squared test was performed or Fisher Exact test, for 2 × 2 tables. The groups were compared according to pharyngoplasty technique. A value of $p < 0.05$ was considered statistically significant.

Results

Demographic characteristics

Subject characteristics are described in table 1. Fifty-seven patients were included with a mean age of 57 ± 9.3 years. A total of 14 patients underwent a vertical closure of the neopharynx (24.6%), while 43 patients underwent a T-shaped closure (74.4%). Males were the most affected sex (n = 52, 91.2%). A total of 43 (75.4%) and 48 (84.2%) had a history of alcohol consumption and tobacco use, respectively. Biomass exposure was most frequently observed in patients in the vertical closure group compared with T-shaped closure (n = 5, 37.5% vs. n = 2, 4.7%, p = 0.002). Dysphonia was the most common symptom, observed in 54 patients (94.7%). Glottic carcinoma was the most frequently observed (n = 31, 54.4%), followed by transglottic (n = 25, 43.8%), and supraglottic (n = 1, 1.6%) carcinoma. A T4 stage was reported in most patients (n = 40, 70.2%). No patients had distance metastasis. The histopathologic report showed squamous cell carcinoma in 94.7% of the cases. Nodal metastasis was observed in 31.6% of the cases (n = 18) and extracapsular invasion in 3.5% (n = 2). Salvage laryngectomy was performed in 7 patients (12.3%).

Table 1. Demographic characteristics of the studied population

Patients' characteristics	Vertical closure (n = 14)	T-shaped closure (n = 43)	p
Age (mean, SD)	59.5 ± 9.2	59.4 ± 9.5	> 0.05
Female, n (%)	1 (7.1)	4 (9.3)	> 0.05
Alcohol consumption, n (%)	12 (85.7)	31 (72.1)	> 0.05
Alcohol consumption, grams per week	244.7 ± 382.3	368.1 ± 489.6	> 0.05
Tobacco use, n (%)	12 (85.7)	36 (83.7)	> 0.05
Tobacco use, pack year	36.1 ± 26.9	32.7 ± 36.6	> 0.05
Drug use, n (%)	1 (7.1)	5 (11.6)	> 0.05
Biomass exposure, n (%)	5 (35.7)	2 (4.7)	0.002*
Diabetes mellitus, n (%)	4 (28.6)	6 (14)	> 0.05
Hypertension, n (%)	6 (42.9)	12 (27.9)	> 0.05
Symptomatology			
Dysphonia, n (%)	14 (100)	40 (93)	> 0.05
Dyspnea, n (%)	4 (28.6)	21 (48.8)	> 0.05
Dysphagia, n (%)	2 (14.3)	14 (32.6)	> 0.05
Weight loss, n (%)	2 (14.3)	14 (32.6)	> 0.05
Need for urgent trachestomy, n (%)	8 (57.1)	24 (55.8)	> 0.05
T stage			
T3, (%)	3 (21.4)	14 (32.6)	> 0.05
T4, (%)	11 (78.6)	29 (67.4)	> 0.05
N stage			
N0, (%)	10 (71.4)	20 (46.5)	> 0.05
N1, (%)	0 (0)	13 (30.2)	0.01*
N2, (%)	3 (21.4)	7 (16.3)	> 0.05
N3, (%)	1 (7.1)	3 (7.0)	> 0.05
Histological tumor characteristics			
Squamous cell carcinoma, n (%)	13 (92.9)	41 (95.3)	> 0.05
Nodal metastasis, n (%)	1 (7.1)	17 (39.5)	0.02*
Nodal extracapsular extension, n (%)	1 (7.1)	1 (2.3)	> 0.05
Adjuvant radiotherapy, n (%)	7 (50)	14 (32.6)	> 0.05
Adjuvant chemotherapy, n (%)	2 (14.3)	15 (34.9)	> 0.05
Salvage laryngectomy, n (%)	4 (28.6)	3 (7)	> 0.05

*p < 0.05.
SD: standard deviation.

Patients' outcomes associated with closure type

Patients' outcomes are shown in table 2. All patients underwent the insertion of a NG for nutrition. A total of 10 patients (17.5%) required the use of a gastrostomy tube for adequate feeding. Intrahospitalary stay was reduced in patients with T-shaped closure compared with vertical closure, with no statistical significance (12.9 ± 7.9 vs. 17.1 ± 8, p ≥ 0.05). PFC was the most common complication, observed in 40.4% of cases (n = 23). No difference in the rate of complications was observed between groups, with the exception of tracheal dehiscence. Tracheal dehiscence was significantly lower in patients with T-shaped closure (n = 2, 4.7% vs. n = 5, 35.7%, p = 0.002).

Factors associated with the development of PCF

A total of 23 patients developed PCF (40.4%). No differences between alcohol consumption, tobacco, and drug use were observed between groups. Diabetes mellitus was more frequently observed in patients with the development of PCF (n = 7, 30.4% vs. n = 3, 8.8%, p = 0.03). Salvage laryngectomy was performed in 21.7% (n = 5) patients with PCF compared with 5.9% (n = 2) in patients without PCF (p ≥ 0.05). Intrahospitalary stay was significantly higher in patients

Table 2. Patients' outcomes associated with closure type

Outcomes	Vertical closure	T- shaped closure	p
	n = 14	n = 43	
Need for gastrostomy, n (%)	2 (14.3)	8 (18.6)	> 0.05
Initiation of oral diet (days), mean (SD)	37.6 ± 60.6	20.0 ± 19.6	0.04*
Intrahospitalary stay (days), mean (SD)	17.1 ± 8	12.9 ± 7.9	> 0.05
Complications			
PCF, n (%)	7 (50)	16 (37.2)	> 0.05
Day of diagnosis of PCF, mean (SD)	7.6 ± 17.5	3.13 ± 5.7	> 0.05
Tracheal stenosis, n (%)	4 (28.6)	6 (14)	> 0.05
Esophageal stenosis, n (%)	1 (7.1)	1 (2.3)	> 0.05
Dysphagia, n (%)	4 (28.6)	10 (23.3)	> 0.05
Wound infection, n (%)	3 (21.4)	7 (16.3)	> 0.05
Tracheal dehiscence, n (%)	5 (35.7)	2 (4.7)	0.002*

*p<0.05.
SD: standard deviation; PCF: pharyngocutaneous fistulas.

Table 3. Factors associated with pharyngocutaneous fistula formation

Evaluated variables	PCF	Non-PCF	p
	n = 23	n = 34	
Age (mean, SD)	61.1 ± 8.3	58.3 ± 9.9	> 0.05
Female, n (%)	1 (4.3)	4 (11.8)	> 0.05
Alcohol consumption, n (%)	18 (78.3)	25 (73.5)	> 0.05
Tobacco use, n (%)	19 (82.6)	29 (85.3)	> 0.05
Drug use, n (%)	2 (8.7)	4 (11.8)	> 0.05
Biomass exposure, n (%)	2 (8.7)	5 (14.7)	> 0.05
Diabetes mellitus, n (%)	7 (30.4)	3 (8.8)	0.03*
Hypertension, n (%)	10 (43.5)	8 (23.5)	> 0.05
Need for urgent trachestomy, n (%)	14 (60.9)	18 (52.9)	> 0.05
Histological tumor characteristics			
Nodal metastasis, n (%)	6 (26.1)	12 (35.3)	> 0.05
Nodal extracapsular extension, n (%)	1 (4.3)	1 (2.9)	> 0.05
Salvage laryngectomy, n (%)	5 (21.7)	2 (5.9)	> 0.05
Intrahospitalary stay (days), mean (SD)	17.1 ± 11.8	12.1 ± 3.1	0.01
Wound infection, n (%)	7 (30.4)	3 (8.8)	> 0.05
Tracheal dehiscence, n (%)	6 (26.1)	1 (2.9)	0.03*

*p < 0.05.
SD: standard deviation; PCF: pharyngocutaneous fistulas.

with PCF (17.1 ± 11.8 vs. 12.1 ± 3.1, p = 0.01). A higher rate of tracheal dehiscence was observed in patients with PCF (n = 6, 26.1% vs. n = 1, 2.9%, p = 0.03) (Table 3).

Discussion

Surgical closure technique for pharyngoplasty is a determinant factor in the development of post-operative complications. A myriad of closing techniques exists, and yet there is very little literature comparing results between them. This may be due to the fact that the closing technique is not routinely specified in post-operative notes, which would impede analyses of this variable in review articles addressing PCF[7].

We performed a retrospective analysis to compare two techniques of pharyngeal closure: vertical and T-shaped with continuous sutures. We found that both techniques presented similar outcomes. We observed a reduced incidence of PCF and other complications including tracheal stenosis, dysphagia, wound infection, and esophageal stenosis in patients in the T-shaped closure group. However, no statistical significance was found. Tracheal dehiscence was significantly reduced in the T-shaped closure group when compared with vertical closure. In the present study, we found an incidence of PCF similar to previous reported literature. The development of PCF was associated with a history of diabetes mellitus and with a increased postoperative intrahospitalary stay.

Authors, such as Boltes Cecatto et al., Deniz et al., and Avci et al., evaluated the technique by focusing in the comparison of interrupted versus continuous sutures. They found that continuous sutures significantly reduce the incidence of PCF[7-9]. Avci et al. concluded that, aside from the type of suture used, the closing technique is also a critical factor in the development of PCF[7]. Davis et al. observed a higher rate of PCF formation, dysphagia, and strictures in patients in the vertical closure[10]. Walton et al. found that when salvage laryngectomies were excluded from their analysis, T-type closure had a lower fistula rate compared with vertical group, with no difference of postoperative strictures between groups[11]. However, literature remains controversial. The type of closure has been associated with the postoperative development of dysphagia and pseudo-diverticulum. Van der Kamp et al. found a greater incidence of pseudo-diverticulum in patients with vertical closure compared with T-shaped closure[12]. In addition, prolonged surgery time has been associated with the development of PCF; this agrees with a systematic review published by Boltes

Cecatto et al.[8]. Patients that underwent vertical closure had, in average, shorter surgeries and a smaller incidence of PCF.

In our study, most of the salvage laryngectomies developed PCF. In the meta-analysis published by Boltes Cecatto et al., 54% of the analyzed studies showed that pre-operative RT had a significant correlation with the development of PCF[8,13]. Liang et al. reported a greater incidence of PCF in patients that underwent RT (21.2%) compared with patients that did not undergo RT (11.6%)[14].

We observed a 40% overall incidence of PCF with no difference between the closure technique used. The overall incidence of PCF after TL is heterogeneous, being from 11.2% to 34.8% depending on the assessed literature[14,15]. Several risk factors for the development of PCF have been studied, being a history of previous radiotherapy one of the most important[13]. Other associated risk factors include advanced age, history of smoking, preoperative albumin and hemoglobin, T stage, tumor site, and among others[13]. We hypothesize that the tumor size in our population played a major role for high incidence of PCF in patients without a history of radiotherapy. Despite considered T4a in TNM staging and candidates for surgical management, we commonly observed local advanced disease with high tumor burdens which influence at the time of reconstruction and pharyngeal closure.

The main strength of this paper is that each closure technique was performed by a single surgeon, with an identical surgical protocol between the patients of each group. The main limitations are the retrospective aspect of our study, and the relatively small sample size.

Conclusion

The pharyngeal vertical and T-shaped closure techniques using uninterrupted Connel-Mayo sutures show similar efficacy. Although complications were lower in the T-shaped closure group, we could not establish the superiority of either technique. Further studies with larger sample sizes are needed to develop a better understanding of the importance of the closure technique for pharyngoplasty and to find the technique associated with better surgical outcomes.

Funding

The authors declare that they have not received funding.

Conflicts of interest

The authors declare no conflicts of interest.

Ethical disclosures

Protection of humans and animals. The authors declare that no experiments on humans or animals were performed for this research.

Confidentiality of data. The authors declare that they have followed their center's protocols on the publication of patient data.

Right to privacy and informed consent. The authors have obtained the informed consent of the patients and/or subjects referred to in the article. This document is in the possession of the corresponding author.

References

1. Thompson CS, Asimakopoulos P, Evans A, Vernham G, Hay AJ, Nixon IJ. Complications and predisposing factors from a decade of total laryngectomy. J Laryngol Otol. 2020;134:256-62.
2. Rassekh CH, Haughey BH. Total laryngectomy and laryngopharyngectomy. In: Cummings Otolaryngology Head and Neck Surgery. 6th ed. Philadelphia, PA: Saunders Elsevier; 2015. p. 1699-713
3. Haksever M, Akduman D, Aslan S, Solmaz F, Ozmen S. Modified continuous mucosal connell suture for the pharyngeal closure after total laryngectomy: zipper suture. Clin Exp Otorhinolaryngol. 2015;8:281-8.
4. Walton B, Vellucci J, Patel PB, Jennings K, McCammon S, Underbrink MP. Post-laryngectomy stricture and pharyngocutaneous fistula: review of techniques in primary pharyngeal reconstruction in laryngectomy. Clin Otolaryngol. 2018;43(1):109-116.
5. Iglesias-Moreno MC, Gimeno-Hernández J, Gómez-Serrano M, Carricondo F, Gil-Loyzaga P, Poch-Broto J. Pharyngo-cutaneous fistula: an old problem revisited. Acta Otolaryngol. 2011;131:1311-8.
6. Watkinson JC, Gilbert RW. Stell and Maran's Textbook of Head and Neck Surgery and Oncology. 5th ed. Boca Raton: Taylor and Francis Group; 2012.
7. Avci H, Karabulut B. Is it important which suturing technique used for pharyngeal mucosal closure in total laryngectomy? Modified continuous connell suture may decrease pharyngocutaneous fistula. Ear Nose Throat J. 2020;99:664-70.
8. Cecatto SB, Soares MM, Henriques T, Monteiro E, Moura CI. Predictive factors for the postlaryngectomy pharyngocutaneous fistula development: systematic review. Braz J Otorhinolaryngol. 2014;80:167-77.
9. Deniz M, Ciftci Z, Gultekin E. Pharyngoesophageal suturing technique may decrease the incidence of pharyngocutaneous fistula following total laryngectomy. Surg Res Pract. 2015;2015:363640.
10. Davis RK, Vincent ME, Shapshay SM, Strong MS. The anatomy and complications of "T" versus vertical closure of the hypopharynx after laryngectomy. Laryngoscope. 1982;92:16-22.
11. Walton B, Vellucci J, Patel PB, Jennings K, McCammon S, Underbrink MP. Post-laryngectomy stricture and pharyngocutaneous fistula: review of techniques in primary pharyngeal reconstruction in laryngectomy. Clin Otolaryngol. 2018;43:109-16.
12. Van der Kamp MF, Rinkel RN, Eerenstein SE. The influence of closure technique in total laryngectomy on the development of a pseudo-diverticulum and dysphagia. Eur Arch Otorhinolaryngol. 2017;274:1967-73.
13. Wang M, Xun Y, Wang K, Lu L, Yu A, Guan B, et al. Risk factors of pharyngocutaneous fistula after total laryngectomy: a systematic review and meta-analysis. Eur Arch Otorhinolaryngol. 2020;277:585-99.
14. Liang JW, Li ZD, Li SC, Fang FQ, Zhao YJ, Li YG. Pharyngocutaneous fistula after total laryngectomy: a systematic review and meta-analysis of risk factors. Auris Nasus Larynx. 2015;42:353-9.
15. Mattioli F, Bettini M, Molteni G, Piccinini A, Valoriani F, Gabriele S, et al. Analysis of risk factors for pharyngocutaneous fistula after total laryngectomy with particular focus on nutritional status. Acta Otorhinolaryngol Ital. 2015;35:243-8.

ORIGINAL ARTICLE

Does the sonic hedgehog signaling pathway play a role in anti-reflux mechanism of bladder in children?

¿La vía de señalización de sonic hedgehog desempeña un papel en el mecanismo antirreflujo de la vejiga en los niños?

Eda Tokat[1], Mustafa O. Tan[2], and Serhat Gürocak[2]*

[1]Department of Urology, University of Health Sciences, Ankara Research and Training Hospital; [2]Section of Paediatric Urology, Department of Urology, Gazi University School of Medicine. Ankara, Turkey

Abstract

Objective: *A hedgehog family ligand, namely, sonic hedgehog (SHH), was reported to be important in the development of bladder and ureter smooth muscle. In this prospective study, we aimed to determine protein expression of SHH in resected ureterovesical junction (UVJ) segments of children with vesicoureteral reflux (VUR).* **Materials and Methods:** *The study group included 19 children; 12 (63%) girls, 7 (37%) boys, who had ureteroneocystostomy operation; 3 (15.7%) right sided, 7 (36.8%) left sided, 9 (47.3%) bilateral, due to primary VUR between years 2015 and 2018. Totally, 28 UVJ segments were examined for Western Blot analysis to determine related protein expression levels.* **Results:** *The mean Western blot band area of SHH gene pathway related protein was 3880.69 (2059.55-13941.61) while the mean area of β-Actin, the house-keeping gene, was 20180.25 (9530.39-26709.75) (p = 0.001). Correlation analyses between grade of reflux and protein expression of SHH gene pathways revealed no significant relation (p = 0.300). When the UV samples were grouped as low- and high-grade reflux and compared in terms of SHH protein expression levels, no statistically significant difference was found between groups (p = 0.818).* **Conclusion:** *We concluded that SHH signaling molecule which is effective in development of bladder and ureter smooth musculature might also be effective in etiopathology of reflux.*

Keywords: *Sonic hedgehog. Vesicoureteral reflux. Reflux genetics. Bladder development.*

Resumen

Objetivo: *Se ha informado que el ligando sonic hedgehog (SHH) es importante en el desarrollo de los músculos lisos de la vejiga y el uréter. Nuestro objetivo fue determinar la expresión proteica de SHH en los segmentos de la unión ureterovesical de niños con reflujo vesicoureteral (RVU).* **Materiales y Métodos:** *El grupo de estudio incluyó a 19 niños; 12 (63%) niñas, 7 (37%) niños, que tuvieron operación de ureteroneocistostomía (UNC); 3 (15.7%) derecho, 7 (36.8%) izquierdo, 9 (47.3%) bilateral, por RVU primario entre los años 2015-2018. Se examinaron un total de 28 segmentos de la unión ureterovesical para análisis de transferencia Western para determinar los niveles de expresión de proteínas relacionadas en las muestras.* **Resultados:** *El área media de la banda de transferencia Western de la proteína relacionada con la vía del gen SHH fue de 3880.69 (2059.55-13941.61), mientras que el área media de la β-actina, el gen de limpieza, fue de 20180.25 (9530.39-26709.75) (p = 0.001). Los análisis de correlación entre el grado de reflujo y la expresión de proteínas de las vías del gen SHH no revelaron una relación significativa (p = 0.300).* **Conclusión:** *Concluimos que la molécula de señalización SHH también podría ser efectiva en la etiopatología del reflujo vesicoureteral.*

Palabras clave: *Erizo sónico. Reflujo vesicoureteral. Genética del reflujo. Desarrollo de la vejiga.*

***Correspondence:**
Eda Tokat
E-mail: edatokat@gmail.com

Date of reception: 16-12-2022
Date of acceptance: 22-02-2023
DOI: 10.24875/CIRU.22000629

Cir Cir. 2024;92(5):660-664
Contents available at PubMed
www.cirugiaycirujanos.com

Introduction

The non-physiologic retrograde flow of urine from the bladder to kidneys is defined as vesicoureteral reflux (VUR), with 1-2% prevalence and in some children has a genetic predisposition[1]. The triangular region between two ureterovesical junctions (UVJs) and internal ureteral meatus, namely, "the bladder trigone" has a central importance in anti-reflux mechanism and was found to derive mostly from bladder muscle with the contribution of ureteral fibers. This was approved in animal studies by the presentation of two major muscle types in the trigone; detrusor and the muscles associated with the intramural ureter[2]. The cellular morphology of the trigone depends on both its embryological origin and key signaling molecules including sonic hedgehog (SHH) signaling[2,3]. During bladder development, the smooth muscle of bladder differentiates from primitive mesenchyme under the influence of urothelium and a sufficient concentration of SHH was reported to be important in development of bladder smooth musculature[4-7]. Patched (Ptc 1), the membrane bound receptor for SHH is expressed in embryonic bladder mesenchyme. Ptc 1 suppresses the smoothened (Smo) in unbound state and when the SHH binds Ptc 1, this inhibitory effect disappears and initiates the cascade which activates Gli transcription factors (Gli1, Gli 2 and Gli 3) in target cell[8]. Gli1 and Gli 2 are the ones targeting not only the SHH but also Wnt family and bone morphogenic proteins which play role in normal embryonic development and differentiation[5].

The UVJ avoids retrograde flow of urine from the variable pressure bladder to low pressure upper urinary tract (kidney and ureter) depending on the ureteral musculature at the junction particularly. Proper development of ureteral and trigonal musculature ensures this one-way flow. In case a deficiency occurs in trigonal development, some clinical disorders including VUR might occur due to improper muscle formation resulting in a relatively short intramural tunnel[4]. In this regard, we hypothesized that the defective SHH signaling plays a role in development of VUR due to abnormal trigonal/ureteral musculature and aimed to determine protein expression of this gene in resected UVJ segments of children with VUR. In this prospective study, we aimed to determine protein expression of SHH in resected UVJ segments of children with VUR and to our knowledge, this is the first human study trying to highlight the role of SHH protein expression in reflux etiopathogenesis.

Materials and Methods

Study design and sample preparation

This prospective study was approved by the Institutional Ethical Committee and informed consent was obtained from all the patients/parents before their inclusion in the study. (26.02.2018/161).

The study group included 19 children; 12 (63%) girls, 7 (37%) boys, who had ureteroneocystostomy (UNC) operation; 3 (15.7%) right-sided, 7 (36.8%) left-sided, 9 (47.3%) bilateral, due to primary VUR between years 2015 and 2018. The technique of UNC was Cohen in all patients and renal units except one unilateral operation done by the Politano-Leadbetter combined intra and extravesical technique. The hypoplastic and redundant distal ureter was excised and the excised hypoplastic distal segment including the intramural portion was used for the genetic analyses. Finally, a total of 28 UVJ segments were examined for Western Blot analysis to determine related protein expression level of SHH gene signaling pathway in the UVJ specimens. After the appropriate transport of the materials to the laboratory, protein isolation was carried out for each tissue and preserved at –80 for later analysis. Protein concentrations were determined in all samples using Qubit® Protein Assay Kits (Thermo Fisher Scientific, Cat No: Q33211). Western blot band expression levels of housekeeping gene β-Actin and target gene SHH which is thought to be effective in VUR pathogenesis were transformed into numerical data using Image J program (NIH, Bethesda, MD, USA).

Housekeeping genes are known to be expressed in almost all the cells of an organism and generally considered to be the constitutive genes which are essential for the maintenance of the basic cellular functions[9]. In this respect, housekeeping genes are widely used as internal controls for gene expression normalization for analysis as western blotting, northern blotting, RT-PCR, etc.[10]. Therefore, in this study, mean abundance values of SHH protein were calculated and compared with β-actin for each related tissue thus expression levels of Western blot bands were normalized against β-actin. Clinical parameters of the patients enrolled in our study were also retrospectively reviewed.

Western blotting

For protein denaturation, we used 100 μg from each sample and also added 4× NuPAGE LDS sample buffer (thermo fisher scientific, Cat no: NP0004) (5 μL), 10× NuPAGE sample reducing agent (thermo fisher scientific, Cat no: B0004) (2 μL) and distilled water was added to a total volume of 20 μL. This mixture was incubated at 70□ for 10 min and ice cooled for 2 min. 20 μL (100 μg) quantities of prepared protein were loaded and separated by 12% SDS-PAGE (Invitrogen, NuPAGE 4-12% Bis-Tris Gel, Cat: NP0321PK2), then transferred to a polyvinylidene difluoride membrane. Following blocking with 5% bovine serum albumin (5%BSA) in phosphate buffered saline with 0.1% tween 20 (PBS-T), the membrane was incubated overnight at 4℃ with rabbit Anti-SHH Antibody (St. John's Laboratory, Cat: STJ193168) and rabbit anti-β-actin antibody (St. John's laboratory, Cat: STJ91464) as the loading control. Primary antibodies were diluted in 1:500 (anti-SHH) and 1:1000 (anti-β-actin). For the secondary incubation, membranes underwent hybridization with a horseradish peroxidase (HRP)-conjugated goat-anti-rabbit-IgG antibody (1:10000 dilution; advansta, Cat no: R05072-500) for 1 h at room temperature. After washing 3 times in PBS/0.1% tween 20, proteins were visualized in imaging system (ChemiDoc-It^2, UVP) with using 6 ml NZY supreme enhanced chemiluminescent HRP substrate (Nzytech, Cat no: Mb19301) (Fig. 1).

Statistical analysis

Densitometry of the Western Blot protein bands was analyzed using Image J (NIH, Bethesda, MD, USA) software program. Statistical analyses were applied with the (Statistical Package for Social Sciences, Chicago, IL, USA) version 15.0 program. Descriptive analyses were presented as mean ± standard deviation and median (min-max). Normal distribution of data was analyzed using Shapiro–Wilk test ($p \leq 0.05$) and non-parametric tests were used for additional statistics then. Densitometry of the target protein (SHH) band was compared to the house keeping gene, β-actin with Wilcoxon test and groups according to the grade of reflux (low-high), laterality, presence of scar and differential functions (< 40%-≥ 40%) were compared using Mann–Whitney U test. Correlation analyses were applied to test the relation between grade of VUR and protein expression level. $p \leq 0.05$ was considered as statistically significant.

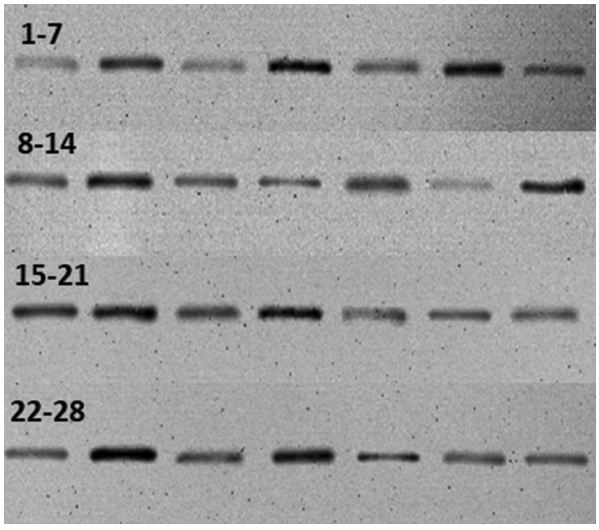

Figure 1: *Sonic hedgehog protein western blot band view of renal units.*

Results

The mean age and follow-up duration of the patients were 88.6 ± 47.7 and 26.76 ± 16.6 months, respectively. According to "International Reflux Grading System" 14 (50%) renal units were grouped as low-grade reflux (Grades 1-3) while 14 (50%) renal units were in high-grade reflux group (Grades 4, 5). No family history of reflux was recorded in the patients included in this study. Of the 19 patients with 28 renal units, six patients with 12 units (42.9%) had bilateral and 9 patients with 9 units (32.1%) had unilateral scar formation on DMSA scintigraphy. Renal units were also grouped according to differential functions (≥ 40% and < 40%) obtained by renal scintigraphy and then compared in terms of protein expressions. In this series, the differential renal function was < 40% in 14 (50%) renal units whereas ≥ 40% in the other 14 (50%).

The mean western blot band area of SHH gene pathway-related protein was 3880.69 (2059.55-13941.61) while the mean area of β-actin, the house-keeping gene, was 20180.25 (9530.39-26709.75) ($p = 0.001$). Correlation analyses between grade of reflux and protein expression of SHH gene pathway revealed no significant relation ($p = 0.30$). When the UV samples were grouped as low- and high-grade reflux and compared in terms of SHH protein expression levels, no statistically significant difference was found between reflux groups ($p = 0.818$). Analysis comparing the specimens according to presence of scar formation revealed no statistically significant difference in terms of SHH protein

Table 1. Sonic hedgehog protein band area calculations according to convenient groups

Classification groups for analysis	Number of contents (renal unit) (%)	SHH protein median western blot band area (min-max)	p-value*
Low-grade reflux	14 (50)	4405.04 (2059.55-12515.64)	0.818
High-grade reflux	14 (50)	3280.69 (2169.98-13941.61)	
Unilateral reflux	10 (35.7)	3284.28 (2169.98-10296.55)	0.314
Bilateral reflux	18 (64.3)	4546.74 (2059.55-13941.61)	
Bilateral scar formation	21 (75)	4296.57 (2059.55-13941.61)	0.915
Unilateral scar formation	7 (25)	3103.74 (2746.96-13941.61)	
≥ 40% differential function	14 (50)	3083.86 (2059.55-13941.61)	1
< 40% differential function	14 (50)	4405.04 (2169.98-12515.64)	

*p ≤ 0.05 is statistically significant.

expression (p=0.915). In addition, there was no statistically significant difference between ≥ 40% and < 40% function groups regarding SHH band area (p = 1). As stated before 9 (47.3%) patients had bilateral reflux whereas 10 (52.7%) had unilateral VUR in this series. In case of the possible impact of bilaterality on the results, the two groups were compared and no statistically difference was found with respect to SHH protein expression between groups (p = 0.314) (Table 1).

Discussion

In the recent study, we found that SHH protein expression levels significantly decreased in the hypoplastic UVJ segments of the patients with VUR. On the other hand, our results did not reveal a relationship between the level of expression and severity of reflux or kidney status.

At the early gestational week 12, the condensate myoblasts of distal ureter convert into smooth muscle fibrils. These longitudinal smooth muscle fibers place at the dorsal wall of the bladder before reaching the orifice. These small diameter muscle fibrils merge the opposite fascicles and create the interureteral muscle and mucosal fold between two ureteric orifices at gestational week 14. The hypothetical function of the intertrigonal muscle is moving the two orifices medially and downward with a periodic contraction and providing a passive antireflux mechanism by the prolongation of intramural ureter[11]. Some studies suggested that the intramural tunnel of ureters compose of bladder muscles and develop independent from the ureters even if in the absence of a ureter, though the mechanism still remains unclear[2,12]. As mentioned above, the muscle development of distal ureteric segments is in mesh with bladder. The development of ureter and trigon musculature is proven to be essential to provide the one-way flow of urine from the ureters into bladder and to prevent the kidneys from reflux of urine or bacteria[4]. Because it is thought that trigon musculature deficiencies result in relatively short intramural tunnel.

A hedgehog family ligand, namely, SHH, controls cell fate, cell differentiation, and proliferation in embryogenesis[7,13]. In the literature, numerous studies have reported the SHH and its downstream signaling molecules produced by the developing bladder epithelium to have a key role in development and patterning of bladder smooth muscle and otherwise cause the bladder development to fail[5-7,14,15]. Histological studies indicated that either SHH or an intact urothelium is necessary to induce smooth muscle differentiation, thus the source of SHH is thought to be the urothelium[8]. When SHH signaling molecule binds with the transmembrane receptor Patched (Ptch), this activation causes depression of Smo and activates the Gli transcription factors in the target cell to involve in bladder development and differentiation[15].

However, several studies reported that high concentrations of SHH inhibit the smooth muscle differentiation while they agreed that lower concentrations induce this process[6,7,16]. Cheng et al. reported that Gli2, one of the target transcription factors of SHH, upregulates the Bmp4 expression and inhibits the smooth muscle differentiation[6]. Another study carried out by Shiroyanagi et al. also supported the information that SHH acts as both an inducer and an inhibitor of bladder smooth muscle differentiation[5].

Our results were in the same direction that SHH is required for normal development of musculature of ureter and trigone and the depressed levels of regarding protein might cause VUR. The insignificant relationship between the severity of reflux and protein expression levels might have occurred due status of other related signaling factors or downstream molecules functionary in this pathway. Furthermore, different expression levels of SHH might cause inhibition or activation and might have varied through years. All the patients were postnatally diagnosed so that there was no investigation about the Shh protein deficiency prenatally through gestational weeks. Although this is the first study in human examining the related protein expression in ureteral specimens, our study has two limitations. First, for ethical reasons, it was not possible to establish a control group to compare the expression levels of Shh protein in normal ureteral tissue. Normal ureteral tissue could be obtained from nephrectomy materials performed with another diagnosis, but this was not possible in our study group because they were pediatric patients. Therefore, further studies with an appropriate control group are needed to address this issue. The second one is relatively small sized study group to generalize our results to overall VUR patients. To the best of our knowledge, our study retains its value to be the first human study aiming to find the effect of SHH signaling pathway in VUR etiopathogenesis.

Conclusions

SHH signaling pathway which is effective in the development of bladder and ureter smooth musculature might also be effective in etiopathology of VUR. Further studies with appropriate control groups will be precious to prove our results and contribute to the diagnosis and treatment of VUR.

Funding

This study is supported by Gazi University Scientific Research Projects Unit with the project coded 01/2019-22.

Conflicts of interest

No potential conflicts of interest were reported by the authors.

Ethical disclosures

Protection of human and animal subjects. The authors declare that the procedures followed were in accordance with the regulations of the relevant clinical research ethics committee and with those of the Code of Ethics of the World Medical Association (Declaration of Helsinki).

Confidentiality of data. The authors declare that they have followed the protocols of their work center on the publication of patient data.

Right to privacy and informed consent. The authors have obtained the written informed consent of the patients or subjects mentioned in the article. The corresponding author is in possession of this document.

References

1. Slabbaert K, Bogaert G. Vesicoureteric reflux (VUR) in children: where are we now. Arch Esp Urol. 2012;65:450-8.
2. Viana R, Batourina E, Huang H, Dressler GR, Kobayashi A, Behringer RR, et al. The development of the bladder trigone, the center of the anti-reflux mechanism. Development. 2007;134:3763-9.
3. Yu J, Carroll TJ, McMahon AP. Sonic hedgehog regulates proliferation and differentiation of mesenchymal cells in the mouse metanephric kidney. Development. 2002;129:5301-12.
4. Liaw A, Cunha GR, Shen J, Cao M, Liu G, Sinclair A, et al. Development of the human bladder and ureterovesical junction. Differentiation. 2018;103:66-73.
5. Shiroyanagi Y, Liu B, Cao M, Agras K, Li J, Hsieh MH, et al. Urothelial sonic hedgehog signaling plays an important role in bladder smooth muscle formation. Differentiation. 2007;75:968-77.
6. Cheng W, Yeung CK, Ng YK, Zhang JR, Hui CC, Kim PC. Sonic hedgehog mediator Gli2 regulates bladder mesenchymal patterning. J Urol. 2008;180:1543-50.
7. Haraguchi R, Motoyama J, Sasaki H, Satoh Y, Miyagawa S, Nakagata N, et al. Molecular analysis of coordinated bladder and urogenital organ formation by Hedgehog signaling. Development. 2007;134: 525-33.
8. Tasian G, Cunha G, Baskin L. Smooth muscle differentiation and patterning in the urinary bladder. Differentiation. 2010;80:106-17.
9. Zhu J, He F, Hu S, Yu J. On the nature of human housekeeping genes. Trends Genet. 2008;24:481-4.
10. Lin J, Redies C. Histological evidence: housekeeping genes beta-actin and GAPDH are of limited value for normalization of gene expression. Dev Genes Evol. 2012;222:369-76.
11. Oswald J, Schwentner C, Lunacek A, Fritsch H, Longato S, Sergi C, et al. Reevaluation of the fetal muscle development of the vesical trigone. J Urol. 2006;176:1166-70.
12. Wang GJ, Brenner-Anantharam A, Vaughan ED, Herzlinger D. Antagonism of BMP4 signaling disrupts smooth muscle investment of the ureter and ureteropelvic junction. J Urol. 2009;181:401-7.
13. Ericson J, Muhr J, Jessell T, Edlund T. Sonic hedgehog: a common signal for ventral patterning along the rostrocaudal axis of the neural tube. Int J Dev Biol. 2003;39:809-16.
14. Jenkins D, Winyard PJ, Woolf AS. Immunohistochemical analysis of Sonic hedgehog signalling in normal human urinary tract development. J Anat. 2007;211:620-9.
15. DeSouza KR, Saha M, Carpenter AR, Scott M, McHugh KM. Analysis of the Sonic hedgehog signaling pathway in normal and abnormal bladder development. PLoS One. 2013;8:e53675.
16. Cao M, Tasian G, Wang MH, Liu B, Cunha G, Baskin L. Urothelium-derived Sonic hedgehog promotes mesenchymal proliferation and induces bladder smooth muscle differentiation. Differentiation. 2010;79: 244-50.

CASO CLÍNICO

Neoplasia sólida pseudopapilar de páncreas: hallazgo incidental cada vez más frecuente

Solid pseudopapillary neoplasia of the pancreas: incidental finding with increased frequency

Inés Cañas-García, Clotilde Moreno-Cortés, Enrique Dabán-Collado y Benito Mirón-Pozo*
Servicio de Cirugía General y Aparato Digestivo, Hospital Clínico San Cecilio, Granada, España

Resumen

En el contexto de las lesiones quísticas del páncreas y su clínica paucisintomática, se presenta el caso de una mujer de 33 años que inicia estudio por epigastralgia y molestias abdominales. Se realizan tomografía computarizada y resonancia magnética, con hallazgo de una lesión a nivel de la cabeza-proceso uncinado del páncreas, compatible con una neoplasia pseudopapilar sólida del páncreas. Se interviene realizando duodenopancreatectomía cefálica de Whipple, que transcurre sin incidencias. Tras 18 meses de seguimiento, persiste libre de enfermedad. Cabe destacar la importancia de las imágenes previas a la planificación terapéutica, por la proximidad de la tumoración al tronco celíaco en la salida de la arteria hepática.

Palabras clave: *Neoplasia. Pseudopapilar. Páncreas.*

Abstract

In the context of cystic lesions of the pancreas and their paucisymptomatic symptoms, we present the case of a 33-year-old woman with epigastric pain and nonspecific abdominal discomfort. Computed tomography and magnetic resonance imaging were performed, with the finding of a lesion at the level of the head-uncinate process of the pancreas, compatible with a solid pseudopapillary neoplasm of the pancreas. The procedure was performed with a cephalic pancreaticoduodenectomy of Whipple, without incident. After 18 months of follow-up, the disease remains free. It is worth highlighting the importance of images prior to therapeutic planning, due to the proximity of the tumor to the celiac artery in the hepatic artery´s origin.

Keywords: *Neoplasia. Pseudopapillary. Pancreas.*

***Correspondencia:**
Inés Cañas-García
E-mail: inescanasgarcia@gmail.com

Fecha de recepción: 23-09-2021
Fecha de aceptación: 07-01-2022
DOI: 10.24875/CIRU.21000735

Cir Cir. 2024;92(5):665-667
Contents available at PubMed
www.cirugiaycirujanos.com

Introducción

Se presenta el caso de una mujer de 33 años con dolor abdominal inespecífico, en la cual los hallazgos radiológicos muestran una tumoración quística del páncreas. Las pruebas complementarias apuntan a una neoplasia sólida pseudopapilar del páncreas. Se trata de una lesión frecuentemente asociada a mujeres jóvenes, de localización preferente en el cuello y la cola pancreáticos, de carácter premaligno, con capacidad para metastatizar hasta en un 15% de los casos[1,2], por lo que un diagnóstico diferencial adecuado es de vital importancia para planificar el tratamiento. La particularidad del caso radica en la infrecuente localización de la lesión en la cabeza del páncreas, así como su relación con las estructuras circundantes (arteria hepática en su salida del tronco celíaco y ampolla de Vater), que determinó la realización de una cirugía agresiva con duodenopancreatectomía cefálica de Whipple.

Caso clínico

Mujer de 33 años sin antecedentes, estudiada por epigastralgia, diarreas, saciedad precoz y distensión abdominal. Se realiza una analítica que reporta marcadores tumores normales. La tomografía computarizada (TC) (Fig. 1) multifásica con contraste y la resonancia magnética (RM) (Fig. 2) evidencian una lesión a nivel de la cabeza-proceso uncinado del páncreas, hipointensa en T1 e hipertensa en T2, de diámetro mayor de 92 mm, sin asociar dilatación de la vía biliar, atrofia distal glandular ni lesiones a distancia. Se sospecha una neoplasia pseudopapilar sólida del páncreas. Es intervenida quirúrgicamente y se evidencia una gran tumoración, cuya enucleación se desestimó por afectación de la papila duodenal, llevándose a cabo una duodenopancreatectomía cefálica de Whipple (Fig. 3). El estudio anatomopatológico confirmó la resección con márgenes sin invasión ganglionar, vascular ni perineural. La paciente completó el posoperatorio sin incidencias y fue dada de alta al noveno día. Tras 18 meses de seguimiento, persiste libre de enfermedad.

Discusión

Distinguir las características clínicas y radiológicas de las neoplasias quísticas del páncreas es fundamental para el diagnóstico diferencial, y puede ayudarnos a adoptar la mejor actitud terapéutica. La incidencia de neoplasias quísticas del páncreas ha aumentado

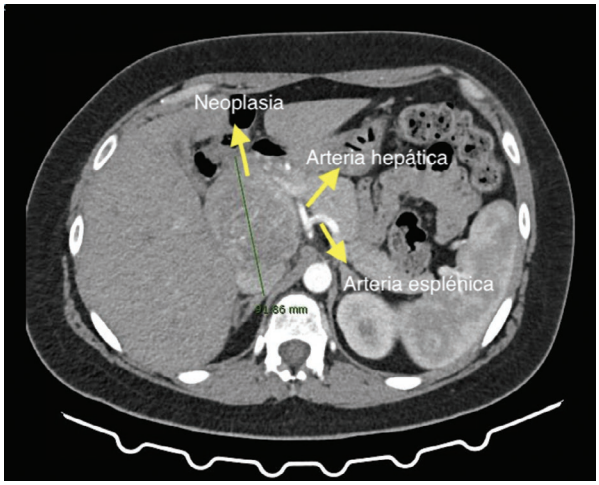

Figura 1. *Se aprecia una masa de 92 mm de diámetro anteroposterior, dependiente de la cabeza pancreática, adyacente al tronco celíaco y la arteria hepática, que rodea sin infiltrar.*

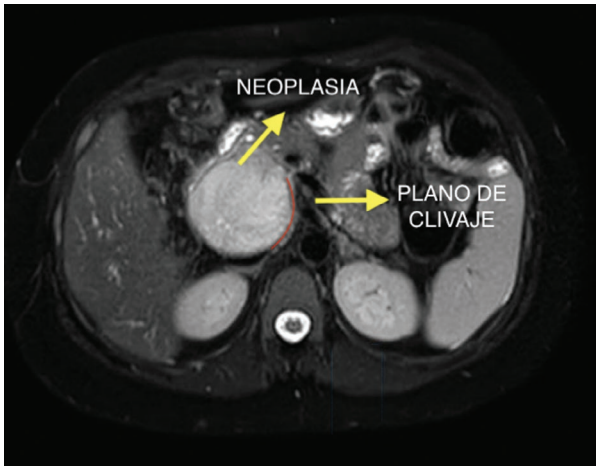

Figura 2. *Resonancia magnética en fase T2 que muestra una masa hiperintensa rodeada de pseudocápsula con plano de separación con las estructuras adyacentes.*

debido al incremento en la realización de pruebas de imagen por otros motivos, pudiendo alcanzar una incidencia del 8% en la población[1]. El diagnóstico diferencial puede tener implicaciones terapéuticas importantes: la anamnesis, valorar la ingesta enólica, la presencia de colelitiasis, los antecedentes de traumatismos abdominales y, sobre todo, la pancreatitis aguda o crónica, son elementos cruciales para sospechar o no neoplasias malignas[2,3]. La TC con contraste intravenoso y la RM con secuencias de colangiopancreatografía son las pruebas de imagen ideales para valorar las características del conducto pancreático, la presencia o no de atrofia glandular y la posible afectación de la

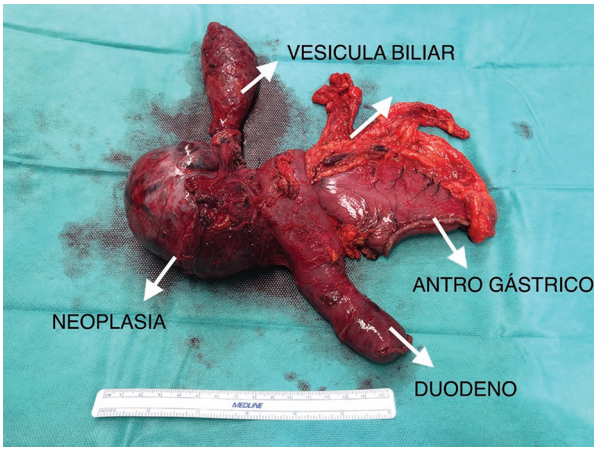

Figura 3. *Pieza quirúrgica. Duodenopancreatectomía cefálica.*

vía biliar, y para la mejor caracterización de las lesiones quísticas[4]. El papel de la ecoendoscopia digestiva radica en la detección de pequeñas lesiones periampulares y pancreáticas con mayor sensibilidad que otras pruebas anteriores. Además, puede valorar las relaciones anatómicas que circundan la lesión. También permite tomar muestras para el estudio anatomopatológico y la determinación de marcadores, como el antígeno carcinoembrionario o la amilasa[5].

La neoplasia sólida pseudopapilar del páncreas afecta preferentemente a mujeres jóvenes. Alcanza una incidencia del 2% según algunas series. En general es asintomática y se detecta por síntomas relacionados con la compresión de órganos vecinos. Suele localizarse en el cuerpo-cola del páncreas[6,7]. Tiene una apariencia típica en las pruebas de imagen (TC y RM); en la RM en fase T2 se muestra como una masa hiperintensa rodeada de una pseudocápsula.

Presenta un crecimiento expansivo, aunque raramente infiltrante. Se la considera *borderline* por su potencial para metastatizar[8]. A pesar de ello, tiene muy buen pronóstico si se reseca en estadios precoces. Por lo tanto, está asentada la indicación de resección quirúrgica una vez establecido el diagnóstico de sospecha, sobre todo en lesiones mayores de 5 cm o cercanas a la zona de la cabeza y el proceso uncinado pancreáticos[9]. Son factores de mal pronóstico la invasión perineural, la invasión vascular y la presencia de metástasis ganglionares o extrapancreáticas (generalmente hepáticas).

Conclusión

La particularidad de este caso radica en la localización de la lesión en la cabeza pancreática y la proximidad a estructuras vasculares y a la papila duodenal, que impidieron una resección conservadora, teniéndose que llevar a cabo una cirugía agresiva para la escisión total de la lesión.

Financiamiento

Los autores declaran no haber recibido financiamiento para la elaboración de este artículo.

Conflicto de intereses

Los autores declaran no tener conflicto de intereses.

Responsabilidades éticas

Protección de personas y animales. Los autores declaran que para esta investigación no se han realizado experimentos en seres humanos ni en animales.

Confidencialidad de los datos. Los autores declaran que han seguido los protocolos de su centro de trabajo sobre la publicación de datos de pacientes.

Derecho a la privacidad y consentimiento informado. Los autores han obtenido el consentimiento informado de los pacientes y/o sujetos referidos en el artículo. Este documento obra en poder del autor de correspondencia.

Uso de inteligencia artificial para generar textos. Los autores declaran que no han utilizado ningún tipo de inteligencia artificial generativa en la redacción de este manuscrito ni para la creación de figuras, gráficos, tablas o sus correspondientes pies o leyendas.

Bibliografía

1. Yamaue H, Tanimura H, Shono Y, Onishi H, Tani M, Yamoto H, et al. Solid and cystic tumor of the pancreas: clinicopathologic and genetic studies of four cases. Int J Pancreatol. 2000;27:69-76.
2. Salinas W, Marani M, Reimondez S, Alcaraz A, Signorini F, Maraschio M, et al. Solid pseudopapilar neoplasm of the pancreas. Cir Cir. 2021;89:263-8.
3. Charville GW, Kao CS. Serous neoplasms of the pancreas. Arch Pathol Lab Med. 2018;142:1134-40.
4. Llatas J, Palomino A, Frisancho O. Tumor de Frantz: neoplasia sólida pseudopapilar de páncreas. Rev Gastroenterol Peru. 2011;31:56-60.
5. Fong ZV, Ferrone CR, Lillemoe D, Fernández del Castillo C. Intraductal papillary mucinous neoplasm of the pancreas. Current state of the art and ongoing controversies. Ann Surg. 2016;263:908-17.
6. Frago R, Fabregat J, Jorba R, García-Borobia F, Altet J, Serrano MT, et al. Solid pseudopapillary tumors of the pancreas: diagnosis and curative treatment. Rev Esp Enferm Dig. 2006;98:809-16.
7. Cienfuegos JA, Rotellar F, Ruiz-Canela M. Neuroendocrine tumors of the pancreas: keys issues in dealing with heterogeneity. Rev Esp Enferm Dig. 2017;109:672.
8. Jorba R, Fabregat J, Borobia FG, Busquets J, Ramos E, Torras J, et al. Neoplasias quísticas del páncreas. Manejo diagnóstico y terapéutico. Cir Esp. 2008;84:296-306.
9. Busquets J, Fabregat J, Jorba R, Borobia FG, Valls C, Serrano T, et al. Indicaciones y resultados de la cirugía conservadora en las lesiones localizadas en la cabeza pancreática. Cir Esp. 2007;82:105-11.

CLINICAL CASE

Report of two cases of high cervical injury: an adequate functional result with timely surgical management

Reporte de dos casos de lesión cervical alta: un resultado funcional adecuado con manejo quirúrgico oportuno

Antonio Sosa-Nájera[1], Abrahan A. Tafur-Grandett[2], Alejandro Ceja-Espinosa[1], Raúl Huato-Reyes[1], and Jórge Ortega-Espino[2]*

[1]Department of Neurosurgery, Grupo Neurológico de Alta Especialidad, Hospital Ángeles Morelia, Morelia, Michoacán; [2]Department of Neurosurgery, Centro Médico "Lic. Adolfo López Mateos", Instituto de Salud del Estado de México, Toluca, Estado de México. Mexico

Abstract

Introduction: *Odontoid fractures correspond to 9-15% of cervical spine fractures. Atlas fracture is rare (3-13%)[8].* **Case presentation:** *Male with Anderson and D´Alonzo Type II Odontoid fracture with unstable fragment treated with occipitocervical fixation with occipital plate, C2-C3 transfacet screws; Female with type E Jefferson fracture + anterolateral atloaxial dislocation, treated with occipitocervical fixation, C2-C3-C4 transfacet screws.* **Discussion:** *Anderson and D'Alonzo Type II fractures and Jefferson type E fractures are a surgical emergency due to instability and neurological deficit.*

Keywords: *Type II odontoid fracture. Jefferson fracture. Spinal cord trauma. Occipitocervical fixation. Posterior cervical instrumented fusión.*

Resumen

Introducción: *Las fracturas odontoideas corresponden del 9-15% de las fracturas de la columna cervical. La fractura del atlas es poco común (3-13%)[8].* **Presentación del caso:** *Masculino con fractura de Odontoides tipo II de Anderson y D´Alonzo con fragmento inestable tratado con fijación occipitocervical con placa occipital, tornillos transfacetarios C2-C3; Femenino con fractura de Jefferson tipo E + luxación atloaxoidea anterolateral, tratada con fijación occipitocervical, tornillos transfacetarios C2-C3-C4.* **Discusión:** *Fracturas tipo II de Anderson y D´Alonzo y fracturas de Jefferson tipo E son una urgencia quirúrgica debido a inestabilidad y déficit neurológico.*

Palabras clave: *Fractura de odontoides tipo II. Fractura de Jefferson. Traumatismo Raquimedular. Fijación occipitocervical. Fusión cervical posterior.*

Correspondence:
Abrahan A. Tafur Grandett
E-mail: atafur.grandett@hotmail.com

Date of reception: 08-09-2021
Date of acceptance: 21-10-2021
DOI: 10.24875/CIRU.21000719

Cir Cir. 2024;92(5):668-673
Contents available at PubMed
www.cirugiaycirujanos.com

Introduction

Odontoid fractures correspond to 9-15% of cervical spine fractures[1]. Of these, the Anderson and D´Alonzo Type II fracture is the most common and occurs in more than 60% of cases[2]. These are usually the result of high energy trauma, such as car accidents or falls from height, most of them are associated with a head injury to the frontal region that indirectly produces an extension injury and predominates in males[3].

According Anderson and D´Alonzo, these fractures can be classified as: Type I: Fracture of the odontoid apex, Type II: Fracture of the odontoid base, Type III: Vertebral body fracture, and Type II odontoid fractures (T II-OF) can be treated surgically or conservatively[1,4].

Various treatments have been proposed for TII-OF with the aim of reducing fracture fragments, stabilizing the fracture, allowing fusion, and reducing pain[5]. In general, the treatment of patients with a fracture of the odontoid process is based on the type of fracture, the age of the patient, the patient's health, the relationship with neurological deficits, and personal preference of the surgeon. Relative indications for surgery include fracture dislocation > 5 mm, angulation > 10 and failed attempts at closed reduction. Surgical treatment may involve anterior odontoid screw fixation or posterior atlantoaxial arthrodesis, resulting in stabilization of the upper cervical spine[5,6].

In cases with indication for surgery for surgery, the purpose of the intervention will be: (A) to release trapped root elements through discectomies, corpectomies, laminectomies, evacuation of collections of expansion of spaces, (B) align vertebral segments by compass or halo traction, manipulation or surgery, (C) stabilize vertebral elements with surgical techniques via anterior, posterior or with double 360° approaches, and (D) stop the clinical-radiological evolution, (E) allow maximum functional recovery[7]. Atlas fracture is rare, accounting for 3-13% of all cervical spine fractures and 1.3-2% of all spinal injuries[8,9]. Unstable atlas fracture is even rare and is mainly caused by vertical falls, traffic accidents and other vertical traumatic forces[9]. Atlas fractures were classified by Jefferson in 1920, into seven types (Table 1)[10].

Jefferson Type E fracture is very dangerous, as displacement of bone blocks can cause spinal cord injury, leading to serious complications such as paraplegia and death.

Therefore, the stability of the atlantoaxial complex must be reconstructed surgically. Treatment is aimed at correcting the dislocation, restoring stability to the atlantoaxial joint, and retaining the maximum degree of motion of the cervical spine[9].

Table 1. Jefferson Classification of Atlas fractures

Type	Anatomical diagnosis
A	Unilateral or bilateral anterior arch fracture
B	Unilateral or bilateral posterior arch fracture
C	Simple fracture of a lateral mass
D	Comminuted lateral mass fracture (the TLA is possibly damaged)
E	True Jefferson fracture in which the anterior and posterior arches of the atlas are fractured bilaterally (unstable atlas fracture)
F	Linear or crossed unilateral anterior arch and posterior arch fractures
G	Isolated TLA break

TLA: transverse ligament of the atlas.

Case presentation

The first case is a 20 years old male who suffers direct head trauma when diving into a pool exerting direct axial force on the cervical spine, refers to paresthesia in upper limbs at the time of trauma, denies loss of alertness, as well as epileptic seizures, 15 points in the Glasgow Coma Scale, motor and sensory system without alterations, global ++/+++ muscle stretch reflexes, intact posterior cords, and multiple SCALP- type cranial vault wounds.

Simple tomography of normal skull and simple crane cervical tomography with 3D reconstruction showing Anderson and D´Alonzo Type II odontoid fracture with unstable left fragment and risk of posterior displacement (Fig. 1). An urgent decision was made to perform a posterior approach for occipitocervical fixation with occipital plate, 4 C2-C3 polyaxial trans facet screws, titanium bars, and Cross Link and subsequent placement of rigid Aspen-type collar (Fig. 2).

The second case is a 29 years old female who has a fall of approximately 6 m in height, exerting vertical force on the cervical spine, refers to a sudden decrease in force in both thoracic limbs, denies other symptoms. To the neurological examination with a 15 points in the Glagow Coma Scale, motor system with force 3/5 on the Daniels scale C5, C6, C7, and C8 myotomes, sensory without alterations, intact posterior cords, global ++/+++ muscle stretch reflexes

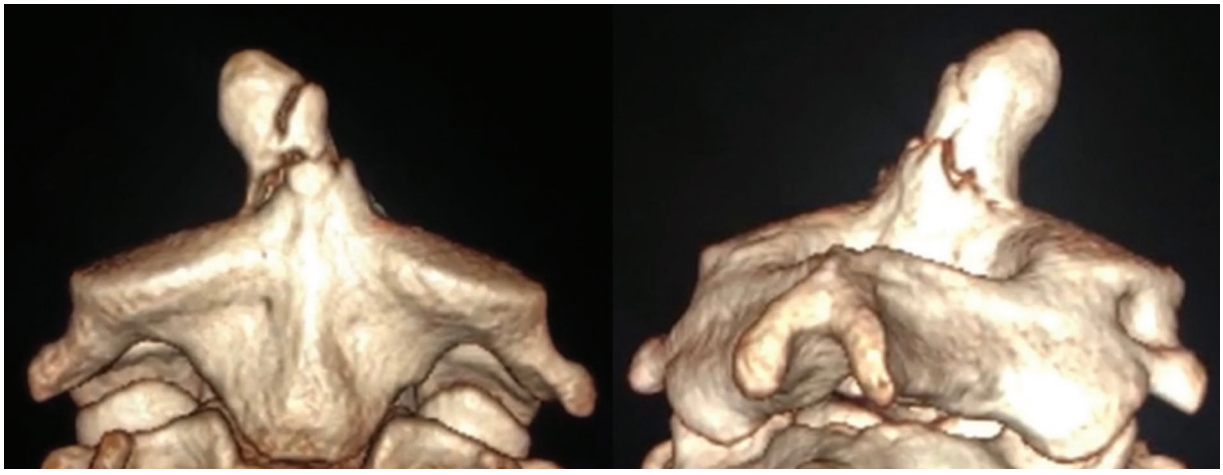

Figure 1. *3D reconstruction of craniocervical CT with Anderson and D´Alonzo Type II odontoid fracture with unstable left fragment and posterior displacement.*

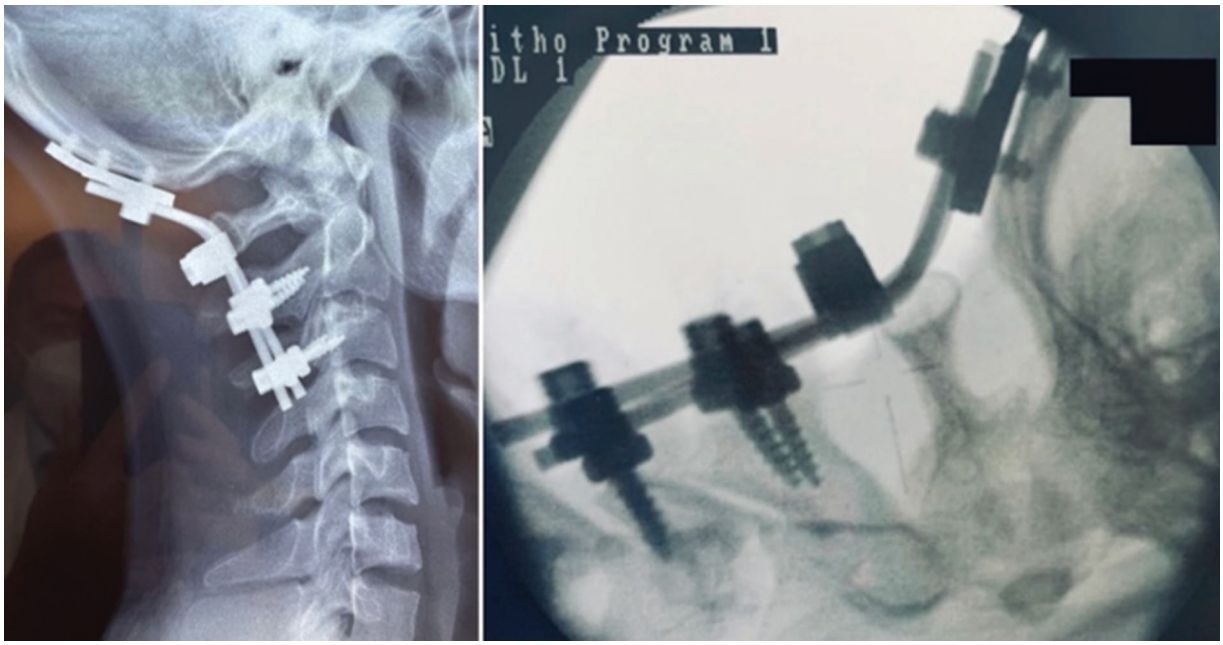

Figure 2. *Occipitocervical fixation with occipital plate, four poly axial trans facet screws C2 C3, titanium bars, and Cross Link.*

craniocervical computerized tomography showing Type E Jefferson fracture + anterolateral atloaxial dislocation (Fig. 3).

It was to decide to perform a posterior approach with occipitocervical fixation with an occipital plate, six polyaxial trans facet screws of C2-C3-C4, titanium bars, and Cross Link and subsequent placement of a rigid Aspen-type collar (Fig. 4).

Both patients in the post-operative period without added neurological deficit, presenting reversal of symptoms on admission, with control radiological studies with adequate placement of prosthetic material, returned home 2 days after the operation (Fig. 5).

Discussion

Odontoid fractures are often caused by high energy trauma, such as fall from a height and traffic accidents[11-13]. Represent 9-15% of all cervical fractures. These injuries are believed to be extremely dangerous due to the potential risk of upper cervical cord injury after traumatic instability. The distribution of odontoid

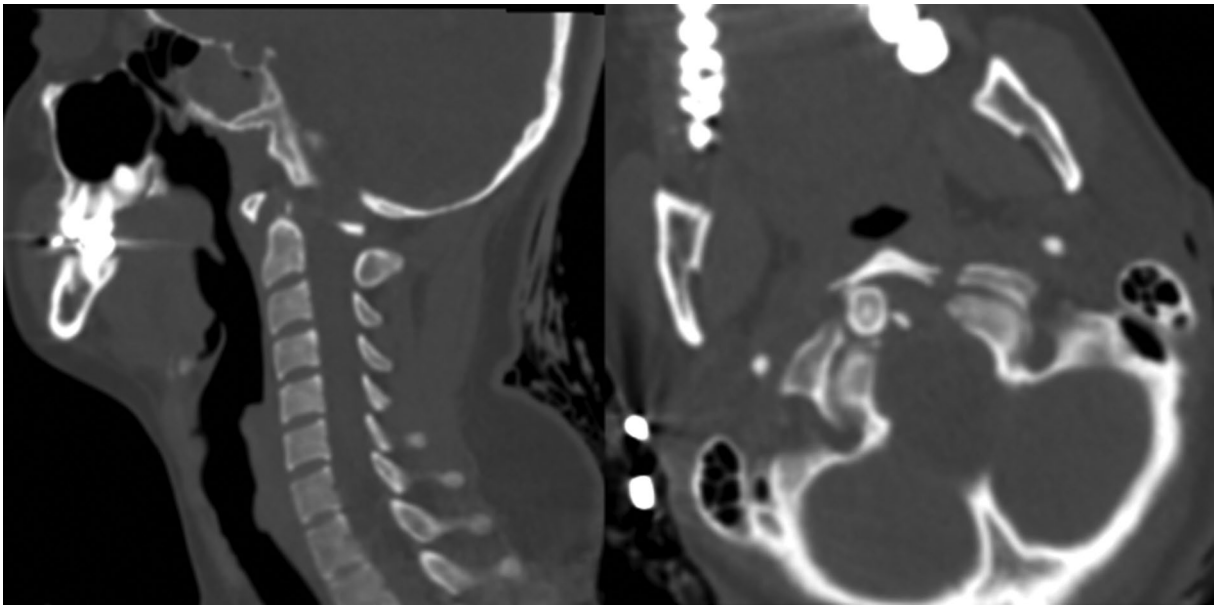

Figure 3. *Craniocervical TC scans showing type E Jefferson fracture + anterolateral atloaxial dislocation.*

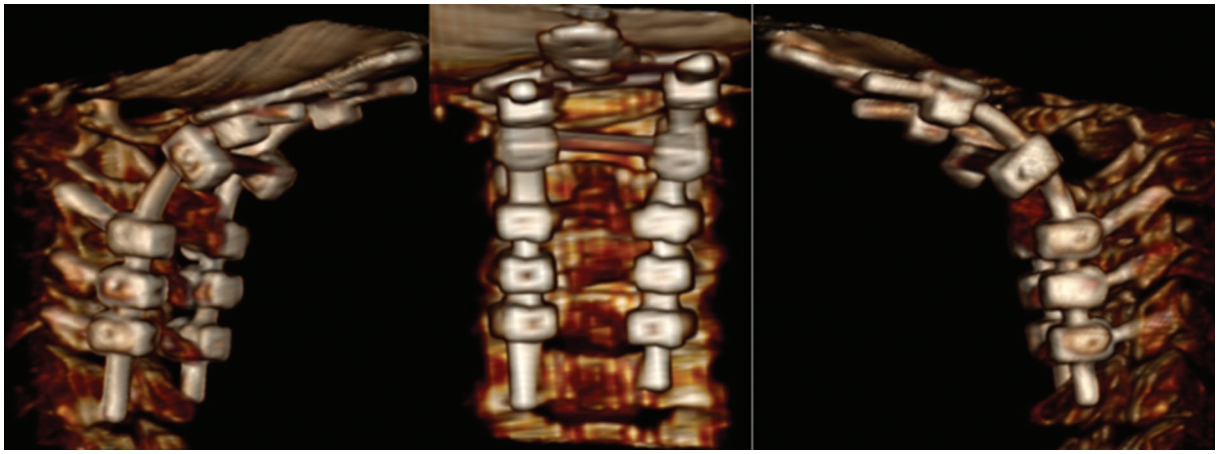

Figure 4. *Occipitocervical fixation with an occipital plate, six polyaxial trans facet screws C2-C3-C4, titanium bars, and Cross Link.*

fractures according to age shows two peaks, one in younger patients (17-30 years), associated with high energy trauma, the other peak occurs in geriatric patients (> 70 years old) and is associated with low energy trauma, such as falls[1,14,15].

Although the majority of patients arriving at the hospital will not have a noticeable neurologic injury, a detailed neurologic evaluation is required, as displaced fracture fragments can compress the spinal cord and lead to cervical myelopathy. In a review of 446 T II-OF, Przybylsky found that 82% of the patients were neurologically intact, 8% had minimal sensory disturbances in the scalp or extremities and 10% had significant neurological deficits[16]. However, in a retrospective analysis of 16 patients with neglected odontoid fractures, Crockard et al.[1] found that all patients had neck pain at 1 year and 69% had clinical signs of myelopathy, including upper extremity weakness and gait disturbances[1,7].

Acceptable options for the initial treatment of all types of odontoid fractures include external cervical immobilization with a hard cervical collar, whereas Type II fractures should be considered for surgical fixation in the context of a 5 mm displacement, communication, Type IIA, and inability to achieve/maintain fracture alignment with external immobilization[3].

Surgeons appear to recognize morbidity as an important factor during the decision-making process and have concluded that morbidity is not an absolute

Figure 5. *Post-surgical result without neurological deficit, with adequate rangers of mobility in cervical flexion and extension, strength 5/5 on the Daniels scale in all four extremities.*

contraindication to surgery. The morbidity that is relevant for surgery is also relevant for non-surgical treatment[1].

Jefferson fractures are associated with other traumatic cervical injuries in up to 50% of cases, most commonly with posteriorly displaced T II-OF[17,18]. Unstable Jefferson fractures are characterized by a tear of the transverse ligament of the atlas (TLA), resulting in lateral displacement of the lateral masses after excessive axial loading[18,19].

At present, the treatment of C1 fractures remains controversial and there are no internationally accepted standards of treatment. For isolated atlas fractures, conservative treatment is the main method, but for unstable atlas fractures, surgical treatment remains the preferred method. It is widely accepted that surgery is indicated for atlas fracture associated with atlantooccipital instability, intraligamentous rupture of the TLA, and for "unstable" atlas fracture[9,20,21].

Anderson and D'Alonzo T II-OF and Jefferson type E fractures are a surgical emergency due to the potential for instability, they present and the secondary neurological deficit for the patient requesting to generate quadriplegia, high cervical injury with ascending spinal cord edema and secondary bulbar injury, cardiorespiratory arrest, and even death, surgical treatment must be individualized for each patient and according to the surgeon's expertise.

The cure rate for T II-OF (with an age range of 18-64 years) treated with posterior atlantoaxial fixation is relatively high[22].

Decision-making for odontoid fracture is challenging and requires careful consideration of many factors related to the nature of the fracture and the patient. The selection of the fixation procedure requires a thorough understanding of the patient´s anatomy and careful preparatory evaluation and planning for successful treatment and favorable clinical outcomes[3].

For Jefferson Type E fractures occipitocervical fixation combined with short-term external immobilization establishes upper cervical stability and prevents further spinal cord injury and damage to nerve function[18].

Occipitocervical fusion with transpedicular fixation has the advantages of reliable fixation, few complications, and high fusion rates[9].

The most important point of treatment for atlantoaxial fracture is to reduce and stabilize the injured segment to prevent further neurological injury. The TLA frequently causes severe instability of the upper cervical spine.

Surgical treatment is always necessary for patients combined with bilateral anterior and posterior arch fractures, and unstable fractures with lesion of the TLA[23,24].

Funding

The authors declare no funding was received.

Conflicts of interest

The authors declare that there are no conflicts of interest.

Ethical disclosures

Protection of human and animal subjects. The authors declare that no experiments were performed on humans or animals for this study.

Confidentiality of data. The authors declare that they have followed the protocols of their work center on the publication of patient data.

Right to privacy and informed consent. The authors have obtained the informed consent of the patients and/or subjects referred to in the article. This document is in the possession of the corresponding author.

References

1. Falavigna A, Righesso O, Da Silva PG, Siri CR, Daniel JW, Veiga JC, et al. Management of Type II odontoid fractures: experience from Latin American spine centers. World Neurosurg. 2017;98:673-81.
2. Fiumara E, Tumbiolo S, Lombardo MC, Maugeri R, Porcaro S, Gioia F, et al. Type II Odontoid Fracture: a case series highlighting the treatment strategies. Acta Neurochir Suppl. 2019;125:317-24.
3. Carvalho AD, Figueiredo J, Schroeder GD, Vaccaro AR, Rodrigues-Pinto R. Odontoid fractures: a critical review of current management and future directions. Clin Spine Surg. 2019;32:313-23.
4. Patel AA, Lindsey R, Bessey JT, Chapman J, Rampersaud R, Spine Trauma Study Group. Surgical treatment of unstable Type II odontoid fractures in skeletally mature individuals. Spine (Phila Pa 1976). 2010;35:S209-18.
5. Clark CR, White AA 3rd. Fractures of the dens. A multicenter study. J Bone Joint Surg Am. 1985;67:1340-8.
6. Grasso G, Leone L, Torregrossa F. Management of odontoid cervical fracture. World Neurosurg. 2019;123:246-7.
7. Ochoa G. Surgical management of odontoid fractures. Injury. 2005;36 Suppl 2:B54-64.
8. Kandziora F, Chapman JR, Vaccaro AR, Schroeder GD, Scholz M. Atlas fractures and atlas osteosynthesis: a comprehensive narrative review. J Orthop Trauma. 2017;31:S81-9.
9. Guo W, Lin Y, Huang J, Hu F, Ding Z, Xiao Z, et al. Treatment strategy of unstable atlas fracture: a retrospective study of 21 patients. Medicine (Baltimore). 2020;99:e20153.
10. Jefferson G. Fracture of the atlas vertebra. Report of four cases and a review of those previously recorded. Br J Surg. 2005;7:407-22.
11. Ni B, Guo Q, Lu X, Xie N, Wang L, Guo X, et al. Posterior reduction and temporary fixation for odontoid fracture: a salvage maneuver to anterior screw fixation. Spine (Phila Pa 1976). 2015;40:E168-74.
12. Ryken TC, Hadley MN, Aarabi B, Dhall SS, Gelb DE, Hurlbert RJ, et al. Management of isolated fractures of the axis in adults. Neurosurgery. 2013;72 Suppl 2:132-50.
13. Hadley MN, Dickman CA, Browner CM, Sonntag VK. Acute axis fractures: a review of 229 cases. J Neurosurg. 1989;71:642-7.
14. Subach BR, Morone MA, Haid RW Jr., McLaughlin MR, Rodts GR, Comey CH. Management of acute odontoid fractures with single-screw anterior fixation. Neurosurgery. 1999;45:812-9; discussion 819-20.
15. Lee PC, Chun SY, Leong JC. Experience of posterior surgery in atlanto-axial instability. Spine (Phila Pa 1976). 1984;9:231-9.
16. Butler JS, Dolan RT, Burbridge M, Hurson CJ, O'Byrne JM, McCormack D, et al. The long-term functional outcome of Type II odontoid fractures managed non-operatively. Eur Spine J. 2010;19:1635-42.
17. Levine AM, Edwards CC. Fractures of the atlas. J Bone Joint Surg Am. 1991;73:680-91.
18. Hu Y, Yuan ZS, Kepler CK, Dong WX, Sun XY, Zhang J. Comparison of occipitocervical and atlantoaxial fusion in treatment of unstable Jefferson fractures. Indian J Orthop. 2017;51:28-35.
19. Kontautas E, Ambrozaitis KV, Kalesinskas RJ, Spakauskas B. Management of acute traumatic atlas fractures. J Spinal Disord Tech. 2005;18:402-5.
20. Hein C, Richter HP, Rath SA. Atlantoaxial screw fixation for the treatment of isolated and combined unstable Jefferson fractures-experiences with 8 patients. Acta Neurochir (Wien). 2002;144:1187-92.
21. Mead LB 2nd, Millhouse PW, Krystal J, Vaccaro AR. C1 fractures: a review of diagnoses, management options, and outcomes. Curr Rev Musculoskelet Med. 2016;9:255-62.
22. Huang DG, Zhang XL, Hao DJ, He BR, Wang XD, Liu TJ. The healing rate of Type II odontoid fractures treated with posterior atlantoaxial screw-rod fixation: a retrospective review of 77 patients. J Am Acad Orthop Surg. 2019;27:e242-8.
23. Cao L, Yang E, Xu J, Lian X, Cai B, Liu X, et al. "Direct vision" operation of posterior atlantoaxial transpedicular screw fixation for unstable atlantoaxial fractures: a retrospective study. Medicine (Baltimore). 2017;96:e7054.
24. Takayasu M, Aoyama M, Joko M, Takeuchi M. Surgical intervention for instability of the craniovertebral junction. Neurol Med Chir (Tokyo). 2016;56:465-75.

CASO CLÍNICO

Carcinoma adenoneuroendocrino mixto: reporte de caso

Mixed adenoneuroendocrine carcinoma: case report

Ángel A. Hernández-Moreno[1], Carlos E. Durón-Gutiérrez[2], Sheyla P. Serrano-González[2], Grettel León-Martínez[3] y José G. Arroyo-Del-Castillo[4]*

[1]Servicio de Cirugía Plástica y Reconstructiva, Hospital Regional Lic. Adolfo López Mateos, Instituto de Seguridad y Servicios Sociales de los Trabajadores del Estado (ISSSTE); [2]Servicio de Cirugía General, Hospital General Tacuba, ISSSTE; [3]Servicio de Anatomía Patológica, Hospital General Tacuba, ISSSTE; [4]Servicio de Neurocirugía, Instituto Nacional de Neurología y Neurocirugía, Secretaría de Salud de la Ciudad de México. Ciudad de México, México

Resumen

Introducción: *El carcinoma adenoneuroendocrino mixto es un tumor raro del tracto gastrointestinal con doble diferenciación en carcinoma adenomatoso y neuroendocrino, cada componente con al menos el 30%.* **Caso clínico:** *Mujer de 60 años con cuadro de dolor abdominal agudo. Se decide tratamiento quirúrgico, encontrando un tumor a nivel de ciego y colon ascendente, y se realizan hemicolectomía derecha e ileostomía.* **Discusión:** *El carcinoma adenoneuroendocrino mixto puede aparecer en diversos órganos. Son tumores muy malignos, con alto riesgo de metástasis.* **Conclusiones:** *Estos tumores no presentan síntomas ni hallazgos radiológicos o de laboratorio específicos; el diagnóstico depende de estudios histopatológicos e inmunohistoquímicos posoperatorios.*

Palabras clave: *Carcinoma adenoneuroendocrino mixto. Diferenciación adenocarcinomatosa. Diferenciación neuroendocrina. Cáncer colorrectal.*

Abstract

Introducción: *Mixed adenoneuroendocrine carcinoma is a rare tumor of the gastrointestinal tract with double differentiation into adenomatous and neuroendocrine carcinoma, each component with at least 30%.* **Case report:** *A 60-year-old female with acute abdominal pain. Surgical treatment was decided, finding a tumor at the level of the cecum and ascending colon, a right hemicolectomy and ileostomy were performed.* **Discussion:** *Mixed adenoneuroendocrine carcinoma can appear in various organs. They are highly malignant tumors, with a high risk of metastasis.* **Conclusions:** *These tumors do not present symptoms or specific radiological or laboratory findings; diagnosis depends on postoperative histopathological and immunohistochemical studies.*

Keywords: *Mixed adenoneuroendocrine carcinoma. Adenocarcinomatous differentiation. Neuroendocrine differentiation. Colorectal cancer.*

***Correspondencia:**
Ángel A. Hernández-Moreno
E-mail: dr.alexhmoreno@gmail.com

Fecha de recepción: 16-09-2021
Fecha de aceptación: 14-03-2022
DOI: 10.24875/CIRU.21000713

Cir Cir. 2024;92(5):674-678
Contents available at PubMed
www.cirugiaycirujanos.com

Introducción

El carcinoma adenoneuroendocrino mixto (MANEC, *mixed adenoneuroendocrine carcinoma*) es un tumor raro del tracto gastrointestinal que consiste en una diferenciación doble adenocarcinomatosa y neuroendocrina, y cada componente representa al menos el 30% del tumor[1]. Aunque no son comunes, estos tumores muestran un comportamiento agresivo y, en general, presagian un mal pronóstico. La estandarización del tratamiento en los MANEC ha sido históricamente difícil por la falta de clasificación histológica diagnóstica. Debido a su rareza, las recomendaciones de tratamiento actuales para el carcinoma mixto adenoneuroendocrino se basan en datos limitados y siguen las pautas generales para el tratamiento de los adenocarcinomas y las neoplasias neuroendocrinas[2]. La incertidumbre sobre la eficacia de las estrategias de tratamiento local y sistémico disponibles es un problema de composición. Incluso aquellos pacientes con enfermedad limitada localmente tienen una esperanza de vida relativamente corta. En 2010, la Organización Mundial de la Salud (OMS) finalmente reconoció esta condición poco común como una entidad específica para el cáncer de colon con la esperanza de especificar mejor las opciones de tratamiento en el futuro[3]. Los MANEC representan el 3-9.6% de todos los cánceres colorrectales y solo se han notificado ocho casos en el ciego hasta la fecha, por lo que el siguiente caso es excepcionalmente raro[4].

Presentamos el caso de una paciente de 60 años, con cuadro clínico de abdomen agudo, quien se sometió a evento quirúrgico encontrando apendicitis aguda y como hallazgo operatorio un tumor de ciego y colon ascendente, notificado posteriormente por el área de patología como MANEC.

Caso clínico

Mujer de 60 años, con antecedentes de diabetes tipo 2 e hipertensión arterial sistémica; niega antecedentes quirúrgicos. Inicia su padecimiento actual un día antes de su valoración con dolor de tipo cólico en el hipocondrio derecho, de intensidad 7/10 en la escala numérica del dolor, irradiado al cuadrante inferior derecho, acompañado de distensión abdominal, náusea llegando al vómito de contenido gastroalimentario en tres ocasiones, sin exacerbantes ni atenuantes; de manera ocasional, en las últimas 12 horas se presentó con dolor

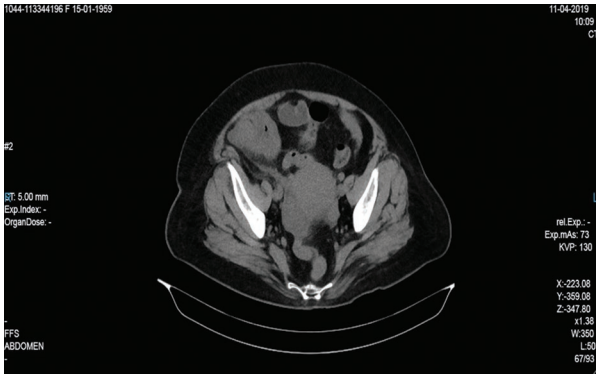

Figura 1. *Tomografía abdominal en fase simple, corte axial, en la que se aprecia una tumoración aparentemente dependiente del ciego (círculo).*

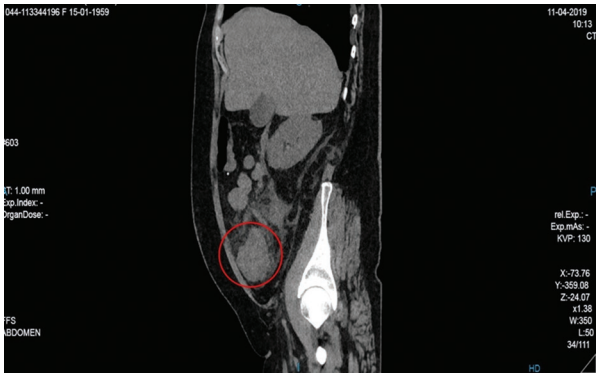

Figura 2. *Tomografía abdominal en fase simple, corte transversal, en la que se aprecia una tumoración aparentemente dependiente del ciego (círculo).*

de tipo punzante, de intensidad 10/10 en la escala numérica del dolor, en la región de la fosa iliaca derecha. En la exploración física, neurológicamente íntegra, cardiopulmonar sin compromiso, abdomen globoso a expensas de panículo adiposo, peristalsis aumentada en intensidad y frecuencia, doloroso a la palpación en hipocondrio derecho y fosa iliaca derecha, Murphy negativo, McBurney positivo, con presencia de masa palpable en la fosa iliaca derecha, de aproximadamente 5 × 5 cm, móvil, no adherida a planos profundos y de consistencia firme; resto sin alteraciones. Laboratorios: leucocitos 12.67 $10^3/\mu l$, hemoglobina 14.1 g/dl, hematocrito 44.2 %, plaquetas 367,103/mm^3, neutrófilos 82%, glucosa 24.2 mg/dl, urea 32.4 mg/dl, BUN 15.0 mg/dl, creatinina 1.0 mg/dl, sodio 137.0 mmol/l, potasio 4.6 mmol/l, cloro 98.8 mmol/l, bilirrubina total 0.18 mg/dl, bilirrubina directa 0.44 mg/dl, bilirrubina indirecta 0.26 mg/dl, DHL 357 U/l, AST 15.5 U/l, ALT 10.5 U/l, fosfatasa alcalina 107 U/l, ACE 2.13 ng/ml,

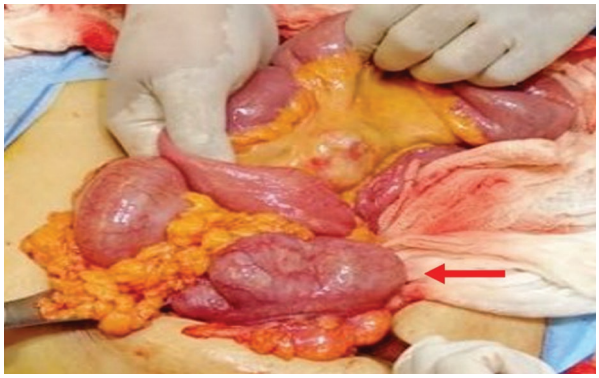

Figura 3. *Tumor dependiente del ciego obtenido por laparotomía exploradora (flecha).*

Figura 4. *Pieza quirúrgica obtenida de hemicolectomía derecha e iliectomía distal.*

C1-125 87.2 U/ml y AFP 3.54 U/ml. Tomografía abdominal en fase simple: imagen sugestiva de apendicitis aguda retrocecal complicada, con acentuados cambios inflamatorios y líquido libre en hueco pélvico, con engrosamiento nodular de la pared del ciego con múltiples ganglios ileocecales y retroperitoneales (paraórticos, intercavoaórticos y retrocrurales), el mayor de 17 mm, que pudieran ser por el proceso inflamatorio por contigüidad sin poder descartar una lesión subyacente del colon (Figs. 1 y 2). Se decide su tratamiento quirúrgico abierto, durante el cual se encuentra una tumoración a nivel de ciego y colon ascendente, de aproximadamente 10 cm, de consistencia firme, con tejido inflamatorio, y perforación a nivel de tercio medio, con salida de material fecal a la cavidad, así como proceso agudo en fase II a nivel apendicular. Se realizan hemicolectomía derecha e ileostomía, y se envía la pieza a patología. Se coloca drenaje de tipo laminar de media pulgada dirigido al hueco pélvico, el cual emerge a nivel del cuadrante inferior derecho (Figs. 3 y 4).

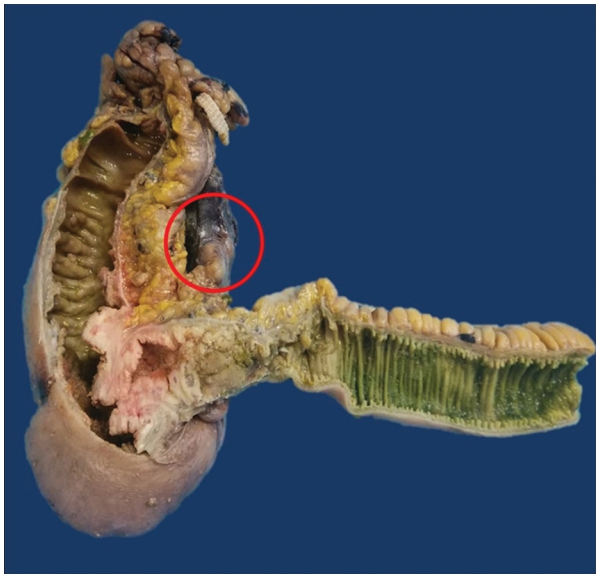

Figura 5. *Producto de hemicolectomía e ileostomía distal, con apéndice posileal (círculo). Se observa una lesión neoplásica en la mucosa del íleon, la válvula ileocecal y el ciego.*

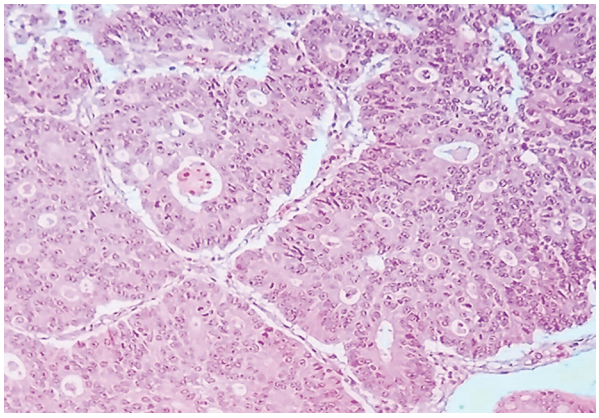

Figura 6. *Proliferación neoplásica con patrón insular, que sugiere diferenciación neuroendocrina.*

Posterior al evento quirúrgico, la paciente es enviada al área de hospitalización a cargo del servicio de cirugía general, donde se mantiene 24 horas en ayuno, con ileostomía funcional y herida quirúrgica sin complicaciones. Es manejada con antibioticoterapia: metronidazol 500 mg intravenoso cada 8 horas durante 14 días y ertapenem 1 g intravenoso cada 24 horas durante 7 días. Se inicia la vía oral, tolerándola adecuadamente, presentando gasto por ileostomía. Reporte de patología: adenocarcinoma moderadamente diferenciado con características histológicas de carcinoma mixto adenoneuroendocrino de grado 2 moderadamente diferenciado; apendicitis aguda ulcerada, abscesada, transmural,

en apéndice posileal (Figs. 5 y 6). Se reporta estudio de inmunohistoquímica: MLH-1 intacto, MSH-6 intacto, CD56 positivo, sinaptofisina positivo, MSH-2 intacto, PMS-2 intacto y cromogranina positivo. Como parte del tratamiento clínico posoperatorio de la paciente se brinda terapia analgésica con base en celecoxib 100 mg por vía oral cada 12 horas por 14 días, así como diclofenaco 100 mg por vía oral cada 12 horas por 7 días. Se añadió tratamiento procinético de tipo cinitaprida 1 mg por vía oral cada 8 horas por 30 días. Igualmente se decide el envío de la paciente al área de oncología médica, donde actualmente continúa en seguimiento y en valoración para el inicio de quimioterapia.

Discusión

Los MANEC en el tracto gastrointestinal pueden aparecer en diversos órganos, como el esófago, el estómago y el colon, pero son más comunes en el recto[5-7]. Independientemente de la localización y del estadio del tumor, los MANEC parecen ser tumores muy malignos, con alto riesgo de metástasis a distancia. La agresividad parece depender del componente endocrino, sea cual sea su proporción[2]. El diagnóstico se basa principalmente en la citología y la arquitectura del tumor, y se completa mediante inmunotinción con marcadores neuroendocrinos específicos, como cromogranina, sinaptofisina y CD56 (para el componente neuroendocrino), combinados con marcadores de diferenciación no endocrina, como queratina 7. No está claro si el MANEC es biológicamente más similar al neuroendocrino o al adenocarcinoma. Sin embargo, es un tumor extremadamente raro, con la mayoría de los casos presentados en reportes aislados[5]. Estos tumores no exhibieron síntomas específicos ni las pruebas radiológicas o de laboratorio específicas de ellos revelaron hallazgos únicos; por lo tanto, el diagnóstico depende de los estudios histopatológicos e inmunohistoquímicos posoperatorios[8]. Debido a su rareza, se conocen pocos aspectos con respecto al origen y a las mejores opciones terapéuticas. Las últimas recomendaciones de la OMS sugieren que los MANEC deben tratarse como un adenocarcinoma; sin embargo, la evidencia reciente, según numerosos autores, indica que el tratamiento debe basarse en el componente histológico más agresivo[9]. Los MANEC requieren un manejo más complejo, incluida la administración de una quimioterapia adaptada al paciente de acuerdo con la histología de su tumor. La única estrategia terapéutica para los MANEC es la resección quirúrgica completa (resección R0) para tumor primario y metástasis. Debido a su naturaleza agresiva y alta tasa de recurrencia, la quimioterapia adyuvante constituye una parte crítica del tratamiento y mejora significativamente la supervivencia[10]. Los MANEC comprenden dos componentes claramente diferentes (adenocarcinomatosos y neuroendocrinos) que tienen distintas respuestas a la quimioterapia. Como resultado, la parte más onerosa y desafiante del tratamiento de los pacientes con MANEC es la elección de la quimioterapia adecuada, tanto para el tumor primario como para las metástasis a distancia[11,12]. En nuestro caso, la paciente presentó datos inespecíficos de abdomen agudo, relacionados principalmente con un padecimiento apendicular agudo, pero en la exploración física se vislumbró una masa aparentemente no dependiente del proceso agudo, y aunado a esto la imagen tomográfica identificó una tumoración que se encontraba proveniente de colon, decidiéndose su tratamiento quirúrgico; sin embargo, fue el estudio histopatológico el que reveló la estirpe tumoral.

Conclusiones

Debido a su rareza, todavía existe un importante debate sobre el tratamiento de los MANEC. Estos tumores no presentan síntomas ni hallazgos radiológicos o de laboratorio específicos; de este modo, el diagnóstico depende de los estudios histopatológicos e inmunohistoquímicos posoperatorios. Debido a los síntomas inespecíficos, la naturaleza altamente agresiva y el potencial metastásico de estos tumores, es vital que los médicos sigan teniendo conocimiento de los MANEC por sus diagnósticos diferenciales. La literatura sobre los MANEC es aún limitada y se basa principalmente en informes de casos únicos. El diagnóstico, el manejo quirúrgico y los criterios de seguimiento de estos tumores aún no están claros.

Financiamiento

Los autores declaran no haber recibido financiamiento.

Conflicto de intereses

Los autores declaran no tener conflicto de intereses.

Responsabilidades éticas

Protección de personas y animales. Los autores declaran que para esta investigación no se han

realizado experimentos en seres humanos ni en animales.

Confidencialidad de los datos. Los autores declaran que han seguido los protocolos de su centro de trabajo sobre la publicación de datos de pacientes.

Derecho a la privacidad y consentimiento informado. Los autores han obtenido el consentimiento informado de los pacientes y/o sujetos referidos en el artículo. Este documento obra en poder del autor de correspondencia.

Bibliografía

1. Paredes MC, Velasco AA, Wong-Achi X. Carcinoma adenoneuroendocrino mixto de la ampolla de Vater: reporte de caso. Rev Cir. 2019;71:261-5.
2. Bosolino A, Ratto R. Tumores neuroendocrinos de colon y recto. Acta Gastroenterol Latinoam. 2019;48:327-37.
3. González González HH, Skrove JL, Sharma R, Sobrado J. A rare case of mixed adenoneuroendocrine carcinoma of the ileocecal valve. Cureus. 2019;11:e3942.
4. Gualdrini Ubaldo A. Cáncer colorrectal en la Argentina: organización, cobertura y calidad de las acciones de prevención y control. Instituto Nacional del Cancer. 2011;1:1-329.
5. Oneda E, Liserre B, Bianchi D, Rota LSavelli G, Zorzi F, et al. Diagnosis of mixed adenoneuroendocrine carcinoma (MANEC) after neoadjuvant chemotherapy for pancreatic and gastric adenocarcinoma: two case reports and a review of the literature. Case Rep Oncol. 2019;12:434-42.
6. Harada K, Sato Y, Ikeda H. Clinicopathologic study of mixed adenoneuroendocrine carcinomas of hepatobiliary organs. Virchows Arch. 2012;460:281-9.
7. Gurzu S, Kadar Z, Bara T, Bara T Jr, Tamasi A, Azamfirei L, et al. Mixed adenoneuroendocrine carcinoma of gastrointestinal tract: report of two cases. World J Gastroenterol. 2015;21:1329-33.
8. Düzköylü Y, Aras O, Bostancı EB, Keklik Temuçin T, Ulaş M. Mixed adeno-neuroendocrine carcinoma; case series of ten patients with review of the literature. Balkan Med J. 2018;35:263-7.
9. La Rosa S, Marando A, Sessa F, Capella C. Mixed adenoneuroendocrine carcinomas (MANECs) of the gastrointestinal tract: an update. Cancers (Basel). 2012;4:11-30.
10. Paspala A, Machairas N, Prodromidou A, Spartalis E, Ioannidis A, Kostakis ID, et al. Management of MANEC of the colon and rectum: a comprehensive review of the literature. Mol Clin Oncol. 2018;9: 219-22.
11. Sato O, Tsuchikawa T, Yamada T, Sato D, Nakanishi Y, Asano T, et al. Metastatic mixed adenoneuroendocrine carcinoma of the liver successfully resected by hepatic trisectionectomy following chemotherapy: a case report. Clin Case Rep. 2019;7:491-6.
12. Nishida T, Blay JY, Hirota S, Kitagawa Y, Kang YK. The standard diagnosis, treatment, and follow-up of gastrointestinal stromal tumors based on guidelines. Gastric Cancer. 2016;19:3-14.

CASO CLÍNICO

GIST en yeyuno proximal asociado a hemorragia masiva de tubo digestivo. Reporte de caso

Proximal jejunal GIST associated with massive gastrointestinal bleeding. Case report

José J. Vargas-Montes[1], Miguel E. Yado-López[1], Pamela L. Huerta-Martínez[1], Barbara I. Rojo-Rodríguez[2] y Antonio Tirado-Motel[3]*

[1]Departamento de Cirugía Digestiva y Endocrina, Centro Médico Nacional del Noreste, Unidad Médica de Alta Especialidad, Hospital de Especialidades No. 25, Instituto Mexicano del Seguro Social (IMSS), Monterrey, Nuevo León; [2]Departamento de Medicina Interna, Centro Médico Nacional del Bajío, IMSS, León, Guanajuato; [3]Departamento de Medicina Interna, Hospital General Regional Dr. Manuel Cárdenas de la Vega, Instituto de Seguridad y Servicios Sociales de los Trabajadores del Estado, Culiacán, Sinaloa. México

Resumen

Introducción: *Los tumores del estroma gastrointestinal (GIST) son poco frecuentes, con una incidencia de 10 a 15 casos por millón de habitantes. Suelen localizarse en el estómago (56%), el intestino delgado (32%), el colon-recto (6%) y el esófago (< 1%). Sus síntomas incluyen náusea, vómito y plenitud abdominal; el 30% son asintomáticos. Es común su hallazgo incidental durante una cirugía abdominal o en estudios de imagen. La resección con márgenes negativos es el tratamiento estándar.* **Caso clínico:** *Mujer de 69 años que debuta con hemorragia masiva de tubo digestivo, requiriendo tratamiento quirúrgico. Se detecta un tumor de yeyuno compatible con GIST.*

Palabras clave: *Tumores del estroma gastrointestinal. Yeyuno. Intestino delgado. Hemorragia. Tumor.*

Abstract

Introduction: *Gastrointestinal stromal tumors (GIST) are rare, reported incidence is between 10 to 15 cases per million of habitants. They are usually located in the stomach (56%), small intestine (32%), colon-rectum (6%), and esophagus (<1%). Its symptoms include nausea, vomiting and abdominal fullness; 30% are asymptomatic. Incidental finding during abdominal surgery or imaging studies is common. Resection with negative margins is the standard treatment.* **Case report:** *A 69-year-old female patient who debuted with massive digestive tract bleeding, requiring surgical treatment. A tumor was detected at jejunum compatible with a GIST.*

Keywords: *Gastrointestinal Stromal Tumors. Jejunum. Small Intestine. Hemorrhage. Tumor.*

***Correspondencia:**
José J. Vargas-Montes
E-mail: josevargasmontes.jv@gmail.com

Fecha de recepción: 13-09-2022
Fecha de aceptación: 03-10-2022
DOI: 10.24875/CIRU.22000464

Cir Cir. 2024;92(5):679-682
Contents available at PubMed
www.cirugiaycirujanos.com

Introducción

Los tumores del estroma gastrointestinal (GIST, *gastrointestinal stromal tumor*) son tumores poco frecuentes del tracto gastrointestinal, de origen mesenquimal[1]. La mayoría de los estudios reportan una incidencia con relevancia clínica de 10-15 casos por millón de habitantes[2].

Los GIST suelen localizarse en el estómago (56%), seguido del intestino delgado (32%), el colon-recto (6%) y el esófago (< 1%). Esporádicamente pueden afectar el omento, el mesenterio y el peritoneo. Sus síntomas iniciales pueden incluir náusea, vómito y plenitud abdominal, aunque el 30% de los casos son asintomáticos; sin embargo, es común la detección de lesiones pequeñas asintomáticas de forma incidental durante una cirugía abdominal o en estudios radiológicos y endoscópicos[1,2].

La tinción inmunohistoquímica para el antígeno CD117 es positiva en el 95% de los GIST y se considera un pilar en el diagnóstico[3].

La resección con márgenes negativos continúa siendo el tratamiento estándar para los pacientes con GIST. La localización anatómica del tumor es un factor pronóstico bien documentado posterior a la cirugía radical. Los tumores en el intestino delgado tienen un peor pronóstico que los gástricos, pero un mejor pronóstico que los colorrectales, siendo los de peor pronóstico los de localización extraintestinal[4].

Caso clínico

Mujer de 69 años con antecedentes de histerectomía total abdominal hace 35 años por miomatosis uterina y resección de quiste renal izquierdo hace 13 años, sin complicaciones aparentes. Refiere múltiples transfusiones de paquetes globulares por anemia de origen desconocido. No presenta otros antecedentes de importancia para el padecimiento actual.

Inicia un cuadro clínico caracterizado por sangrado transrectal sin síntomas acompañantes, motivo por el cual se inicia protocolo diagnóstico. Se realiza colonoscopia en la que se reportan recto y sigmoides con abundantes coágulos y 12 divertículos no complicados localizados en el colon sigmoides; el resto del estudio sin alteraciones. Se diagnostica en ese momento con hemorragia de tubo digestivo bajo secundaria a enfermedad diverticular autolimitada. Sin embargo, la paciente continúa con un cuadro clínico caracterizado por múltiples evacuaciones de características melénicas, ameritando hospitalización a cargo del servicio de gastroenterología para protocolo diagnóstico y terapéutico. Se realizan tránsito intestinal, sin alteraciones, y enteroscopia anterógrada que muestra a nivel del yeyuno proximal una lesión mucosa engrosada de 7 mm con cambio de coloración y otra lesión a 10 cm de esta, sobreelevada, friable, ulcerada, de 20 mm de diámetro. Se realiza toma de biopsias, con posterior sangrado abundante de tipo arterial. Interconsultan a nuestro servicio durante el procedimiento sin ameritar intervención quirúrgica de urgencia por cese del sangrado posterior a la colocación de dos hemoclips, con vigilancia hospitalaria. Durante su estancia presenta otro episodio de sangrado de tubo digestivo bajo, con abundantes evacuaciones sanguinolentas y datos de choque hipovolémico, junto con disminución del nivel de hemoglobina de hasta 4.3 g/dl. Al identificar hemorragia masiva y datos de inestabilidad hemodinamica, se inicia tratamiento a base de transfusión de paquetes globulares y se procede a tratamiento quirúrgico con laparotomía exploradora, durante la cual se identifica un tumor en el yeyuno proximal de 4 × 2 cm de diámetro, hipervascularizado, localizado a 20 cm del ángulo de Treitz, no perforado (Fig. 1), con ausencia de líquido libre, sin otros datos de importancia. Se realiza resección intestinal de 10 cm a 10 cm del ángulo de Treitz y entero-enteroanastomosis latero-lateral mecánica. Se envía la pieza para estudio histopatológico definitivo. Durante el procedimiento quirúrgico se realiza transfusión de paquetes globulares, con reporte de hemoglobina posquirúrgica de 8.4 g/dl.

Posterior a la cirugía, la paciente reingresa a piso dependiente de aminas vasoactivas a base de norepinefrina a dosis de 0.08 μg/kg/min, y se mantiene en observación quedando en manejo conjunto por gastroenterología y cirugía digestiva. Con adecuada evolución clínica y aumento de la hemoglobina a valores normales, se decide su egreso hospitalario 8 días posteriores a la intervención y se cita a la consulta externa para seguimiento.

Acude a la consulta externa de cirugía digestiva con reporte histopatológico que concluye: tumor del estroma gastrointestinal de bajo grado (GIST) de 4 × 3 × 2.5 cm de diámetro, sin presencia de necrosis y bordes libres de neoplasia, con menos de 5 mitosis en 50 campos de alto poder. Se realiza tinción con hematoxilina y eosina (Fig. 2) e inmunohistoquímica, en donde se reportan marcadores DOG1 y CD 117 positivos (Fig. 3); CKAE1/AE3, S100 y actina de músculo liso negativos.

Se solicita valoración por oncología médica, sin ameritar tratamiento adyuvante por resección tumoral

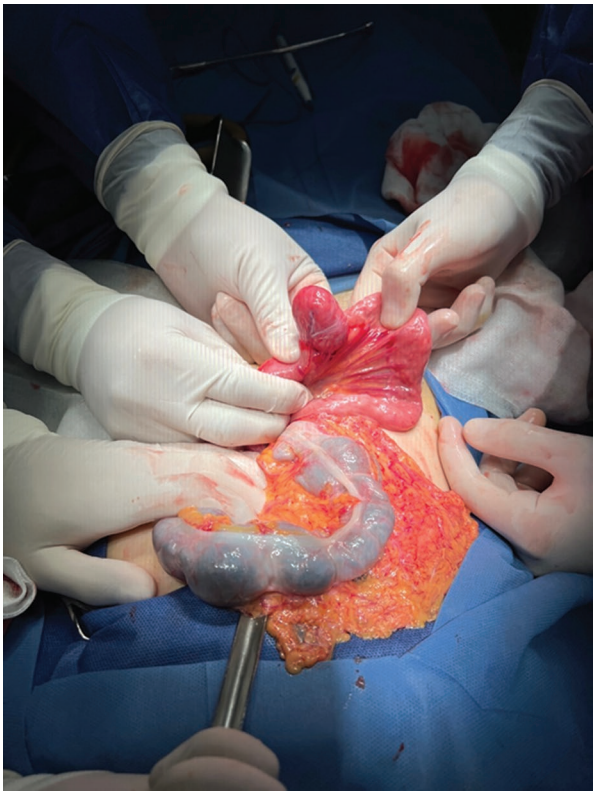

Figura 1. *GIST de yeyuno durante la laparotomía exploradora.*

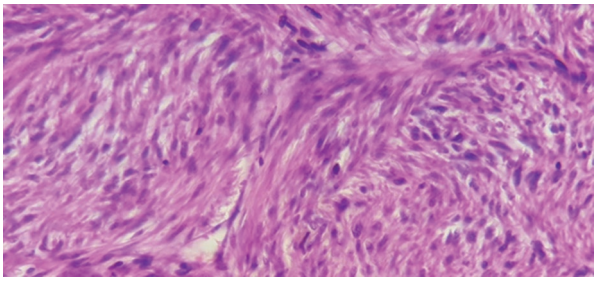

Figura 2. *Tinción de hematoxilina-eosina con ampliación 40×. Células neoplásicas fusocelulares que se disponen en patrón sincitial, núcleo alargado y citoplasma eosinófilo.*

R0 y ausencia de enfermedad metastásica en los estudios de extensión, motivo por el cual se mantiene en vigilancia médica.

Discusión

Los GIST localizados en el yeyuno son poco frecuentes, representando el 0.1-3% de todos los tumores gastrointestinales. Unos pocos casos se presentan con melena, hematemesis y anemia, debido a sangrado recurrente. El sangrado

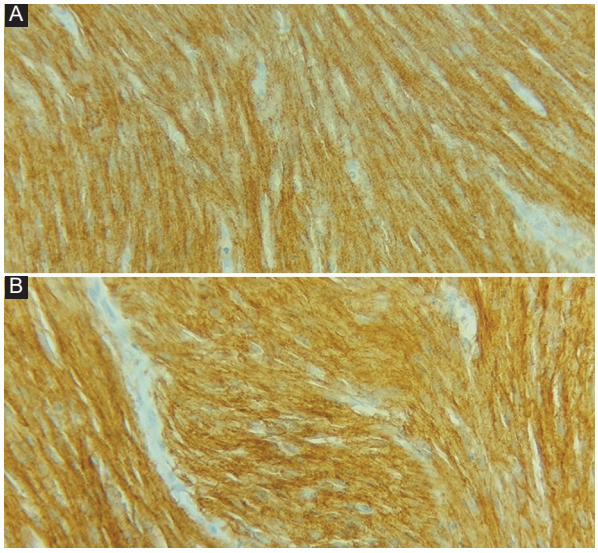

Figura 3. *Inmunohistoquímica en la que se observa positividad para DOG1* **(A)** *y CD117* **(B)**.

gastrointestinal agudo es una presentación común en la práctica médica y puede condicionar una emergencia que amenace la vida[3,5].

Se ha reportado la presentación con hemorragia de tubo digestivo en casi el 25% de los GIST de yeyuno; aun así, es inusual que presenten hemorragia gastrointestinal masiva que requiera una intervención urgente[5,6]. En nuestro caso, la paciente cursa con hemorragia masiva, una presentación poco frecuente de este tumor, y requiere un procedimiento quirúrgico de urgencia en el que se detectado un tumor de yeyuno proximal.

La endoscopia superior e inferior continúa como estudio de primera línea en la hemorragia gastrointestinal. El sangrado derivado del intestino delgado se mantiene como un reto diagnóstico por ser una región poco accesible con endoscopia convencional. Es necesario realizar estudios de imagen complementarios posterior a la ausencia de datos de sangrado en la endoscopia superior e inferior, incluyendo cápsula endoscópica, angiografía por tomografía computarizada (TC), TC con contraste intravenoso o contraste oral, enteroscopia y enterorresonancia magnética[3].

Microscópicamente, la mayoría de los GIST muestran tres subtipos histológicos principales: tipo de células fusiformes (el más común, 70%), tipo epitelioide (20%) y tipo mixto (10%). Para su diferenciación es necesario el estudio con inmunohistoquímica[6,7].

Para el manejo de los GIST se utilizan diversas modalidades de tratamiento, incluyendo resección quirúrgica, terapias médicas dirigidas, quimioterapia y

radioterapia; sin embargo, se prefiere la resección quirúrgica, debido a la respuesta indeseable de otras modalidades[6]. La resección quirúrgica es el tratamiento de elección en cualquier GIST potencialmente resecable con un tamaño mayor de 2 cm, si el tumor está localizado y sintomático o si se cuenta con datos de malignidad en el ultrasonido endoscópico[8]. Se recomienda únicamente vigilancia posquirúrgica si se logró una resección tumoral R0 (márgenes microscópicos negativos)[1]. En nuestro caso se realizó una resección quirúrgica completa de la lesión, con reporte histopatológico de GIST de células fusiformes con bordes libres de tumor, motivo por el cual se consideró como un tratamiento exitoso y la paciente se mantuvo solo en vigilancia.

El pronóstico de los GIST depende del tamaño, la localización anatómica, los hallazgos de imagen, las metástasis y la ruptura del tumor[6]. Numerosos estudios sugieren que la expresión inmunohistoquímica está relacionada con el pronóstico[9]. La estratificación del riesgo de Fletcher es un método establecido para clasificar el riesgo de recurrencia[10].

Los inhibidores de la tirosina cinasa son de utilidad en el tratamiento de los GIST como terapia preoperatoria neoadyuvante durante 6 a 12 meses para la citorreducción tumoral de tumores de gran tamaño para hacerlos operables. Si se considera a los inhibidores de la tirosina cinasa como parte del plan de tratamiento, es altamente recomendable el análisis de mutación tumoral. Las mutaciones del gen KIT se encuentran en aproximadamente el 80% de los GIST[11-13].

Conclusiones

Los GIST representan una afección con una incidencia baja, sobre todo los localizados en el yeyuno y aquellos que debutan con hemorragia gastrointestinal masiva. Debido a su agresividad y su presentación inespecífica, es importante contar con el conocimiento de este tipo de tumores, con la finalidad de establecer un diagnóstico temprano y otorgar un tratamiento oportuno, ya que tras una resección tumoral con márgenes libres se mejorará la supervivencia del paciente.

Agradecimientos

A todos los involucrados en la publicación del artículo.

Financiamiento

Los autores declaran no haber recibido ningún financiamiento.

Conflicto de intereses

Los autores declaran no tener ningún conflicto de intereses.

Responsabilidades éticas

Protección de personas y animales. Los autores declaran que para esta investigación no se han realizado experimentos en seres humanos ni en animales.

Confidencialidad de los datos. Los autores declaran que en este artículo no aparecen datos de pacientes.

Derecho a la privacidad y consentimiento informado. Los autores declaran que en este artículo no aparecen datos de pacientes.

Uso de inteligencia artificial para generar textos. Los autores declaran que no han utilizado ningún tipo de inteligencia artificial generativa en la redacción de este manuscrito ni para la creación de figuras, gráficos, tablas o sus correspondientes pies o leyendas.

Bibliografía

1. Liu H, Santanello A, Jiménez M, Kumthekar N. Jejunal gastrointestinal stromal tumor (GIST) as a rare cause of GI bleed: a case report. Cureus. 2022;14:e24272.
2. Sánchez-Hidalgo JM, Durán-Martínez M, Molero-Payan R, Rufián-Peña S, Arjona-Sánchez A, Casado-Adam A, et al. Gastrointestinal stromal tumors: a multidisciplinary challenge. World J Gastroenterol. 2018;24:1925-41.
3. Mahmoud S, Salman H. Massive bleeding of a jejunal gastrointestinal stromal tumour: a rare case of a life-threatening presentation. J Surg Case Rep. 2020;2020:rjaa355.
4. Zhang Q, Shou CH, Yu JR, Yang WL, Liu XS, Yu H, et al. Prognostic characteristics of duodenal gastrointestinal stromal tumours. Br J Surg. 2015;102:959-64.
5. Mohamed AA, al Zahrani SM, Mohamed SA, Qureshi AS. Massive gastrointestinal haemorrhage unusual presentation of gastrointestinal stromal tumors of the jejunum: case report and literature review. Cureus. 2021;13:e14266.
6. Azimi B, Shahrbaf MA, Iranshahi M, Parsaeian F. A case of jejunal GIST revealed by hematemesis: unusual situation. Int J Surg Case Rep. 2022;94:107146.
7. Villafuerte Quimíz WL, Ostaiza Véliz IV, Williams Vargas LN, Palomeque Salazar X. Tumores del estroma gastrointestinal: revisión y manejo multidisciplinario. J Am Health. 2021;4:26-35.
8. Lim KT. Current surgical management of duodenal gastrointestinal stromal tumors. World J Gastrointest Surg. 2021;13:1166-79.
9. Qu H, Xu Z, Ren Y, Gong Z, Ju RH, Zhang F, et al. The analysis of prognostic factors of primary small intestinal gastrointestinal stromal tumors with R0 resection. Medicine. 2022;101:e29487.
10. Ito T, Kushida T, Sakurada M, Tanaka K, Sato K, Maekawa H. Complete wedge resection for duodenal gastrointestinal stromal tumour: a case series of three patients. Int J Surg Case Rep. 2022;90:106674.
11. El-Menyar A, Mekkodathil A, Al-Thani H. Diagnosis and management of gastrointestinal stromal tumors: an up-to-date literature review. J Cancer Res Ther. 2017;13:889-900.
12. Blay JY, Kang YK, Nishida T, Von Mehren M. Gastrointestinal stromal tumours. Nat Rev Dis Primers. 2021 Mar 18;7(1):22.
13. Serrano C, George S. Gastrointestinal stromal tumor: challenges and opportunities for a new decade. Clin Cancer Res. 2020;26:5078-85.

CASO CLÍNICO

Técnica tridente modificada para el abordaje de un lipoma facial

Modified trident technique for surgical approach to facial lipoma

*Nancy Trujillo-García[1], Irma Y. Castillo-López[2], Carmen A. Carrillo-López[1] y Diana P. Mariscal-Arellano[3]**

[1]Departamento de Cirugía Maxilofacial, Hospital General Regional 46, Instituto Mexicano del Seguro Social (IMSS); [2]Departamento de Otorrinolaringología y Cirugía de Cabeza y Cuello, Hospital General Regional 46, IMSS; [3]Departamento de Otorrinolaringología y Cirugía de Cabeza y Cuello, Centro Médico Nacional de Occidente, IMSS. Guadalajara, Jalisco, México

Resumen

Introducción: *Los lipomas son los tumores de origen mesenquimatoso más comunes en todo el cuerpo. Aunque tienen una baja incidencia en la cavidad oral, su abordaje quirúrgico puede ser un enorme reto.* **Caso clínico:** *Varón de 10 años con un lipoma gigante del espacio geniano y masticador resecado mediante abordaje intraoral modificado de la técnica descrita por Ramírez-Oropeza.* **Discusión:** *Se describen las principales ventajas y limitaciones de un abordaje intraoral.* **Conclusiones:** *Se seleccionó este abordaje intraoral por la menor posibilidad de lesionar el nervio facial, los mejores resultados estéticos y ser menos invasivo, obteniendo excelentes resultados.*

***Palabras clave*:** *Bichectomía. Lipoma. Espacio masticador. Abordaje intraoral.*

Abstract

Introduction: *Lipomas are the most common tumors of mesenchymal origin throughout the body. Although they have low incidence in the oral cavity, they surgical approach can be challenging.* **Case report:** *10-year-old male with a giant lipoma in the buccal and masticator space, an intraoral surgical approach was chosen using by modifying trident technique of Ramírez-Oropeza.* **Discussion:** *The main advantages and limitations of this intraoral approach are examined.* **Conclusions:** *An intraoral approach was selected because of less possibility of injuring the facial nerve, better esthetic results and less invasive, obtaining excellent results.*

***Keywords*:** *Bichectomy. Lipoma. Masticator space. Intraoral approach.*

***Correspondencia:**
Diana P. Mariscal-Arellano
E-mail: prismariscal@hotmail.com

Fecha de recepción: 08-05-2022
Fecha de aceptación: 09-07-2022
DOI: 10.24875/CIRU.22000254

Cir Cir. 2024;92(5):683-688
Contents available at PubMed
www.cirugiaycirujanos.com

Introducción

Los lipomas están compuestos por adipocitos maduros rodeados por una fina cápsula fibrosa[1] y en general se desarrollan superficialmente en el tejido subcutáneo. Son blandos, indoloros y varían en tamaño de 1 a > 10 cm. La transformación maligna a liposarcoma es rara[2].

Son los tumores de origen mesenquimatoso más comunes en todo el cuerpo, pero suelen ser muy raros en la cavidad oral, con una incidencia del 1-4%[3]. En el estudio realizado por Studart-Soares et al.[4] se revisaron 450 lipomas intraorales y se encontró que el sitio más común era la mucosa bucal (38.7%), seguida del vestíbulo (7.8%), el área retromolar (4.7%) y otros lugares (48.8%). No se encontraron diferencias significativas entre hombres y mujeres (el 52.2% eran hombres y el 47.8% eran mujeres). Puede aparecer a cualquier edad, pero se ha visto predilección por la cuarta a sexta décadas de la vida[5].

Aunque su etiología precisa permanece desconocida, las principales teorías orientan a que se encuentran involucrados factores como la herencia, la degeneración grasa, cambios hormonales, infección, acúmulo de células embriogénicas lipoblásticas en el sitio de origen e irritación crónica[6].

El diagnóstico primeramente se realiza por la clínica, y los estudios de imagen ayudarán a hacer el diagnostico diferencial; con ultrasonido se puede diferenciar un lipoma de un quiste epidermoide o ganglionar[7], y la resonancia magnética es muy específica para valorar la extensión y sus interrelaciones con estructuras anatómicas clave. El diagnóstico diferencial de los lipomas puede ser entre diferentes condiciones, como quistes epidermoides, hematomas, paniculitis y otras formas de tumores adipocíticos[7,8]. Si un lipoma causa síntomas, como dolor o restricción de movimiento, o tiene características de malignidad (p. ej., rápido crecimiento o cambios durante la vigilancia), está indicada una biopsia con histopatología para el diagnóstico definitivo[2].

El tratamiento principal es la cirugía, cuyos riesgos generales incluyen formación de cicatrices, seroma y hematoma[9]. Algunas alternativas son la liposuccion[10] y las inyecciones con bajas concentraciones de desoxicolato, usado con éxito en un estudio de seis pacientes[11]; sin embargo, se necesitan más estudios antes de que pueda recomendarse de manera sistemática.

Existen diferentes tipos de abordajes quirúrgicos para los tumores en la región de la cara y el cuello. El criterio médico, basándose en las características particulares de cada caso, será determinante para seleccionar la técnica a emplear.

En la literatura se han descrito diferentes abordajes para tumores que se encuentran afectando el espacio masticatorio. Por mencionar algunos, existen la cirugía endoscópica, los abordajes submaseterino ampliado, transmandibular y transoral, e incluso la combinación de varios de estos abordajes en tumores que lo ameriten[12-16].

Algunos aspectos relevantes que deben considerarse al seleccionar un abordaje son el tamaño del tumor y el involucro de estructuras adyacentes, pero sobre todo la naturaleza del tumor. En el caso de un lipoma, siempre se deberá tomar en cuenta el origen benigno de la lesión, por lo cual no justifica una cirugía que cause grandes secuelas estéticas o funcionales.

Caso clínico

Varón de 10 años con obesidad infantil como único antecedente patológico relevante (relación peso/talla + 5 desviaciones estándar). Acudió a nuestra consulta por un aumento de volumen masticatorio izquierdo de 7 meses de evolución, el cual inició de manera lenta, progresiva, indolora y sin aparente involucro de estructuras adyacentes.

En la exploración física presentaba acantosis *nigricans,* ginecomastia y tumor en la región masticatoria izquierda, de consistencia blanda, bordes bien delimitados, no doloroso, móvil, no adherido a planos profundos y sin cambios tróficos en la piel (Fig. 1).

La tomografía computarizada simple de cabeza y cuello evidenció asimetría de la hemicara izquierda a expensas de tejidos blandos, correspondiente a una masa delimitada por una cápsula inmediatamente debajo del músculo buccinador, con una atenuación de −99 UH correspondiente a densidad de tejido graso. Sus límites abarcaban anteriormente hasta el músculo depresor del ángulo de la boca, interiormente el borde inferior de la mandíbula, lateralmente se ubicaba sobre el músculo masetero, extendiéndose anteriormente hasta el arco cigomático. Se observa una ramificación hacia la fosa infratemporal, rodeando el músculo pterigoideo lateral. Sus diámetros máximos eran de 53 × 44 × 46 mm (Fig. 2).

Figura 1. *Paciente con tumor en la región masticatoria izquierda.*

Figura 2. *Tomografía computarizada simple, corte coronal. Se observa la extensión infratemporal del lipoma.*

Optamos por un abordaje intraoral modificado de la técnica en tridente[1]. Como preparación prequirúrgica solo se realizaron enjuagues con clorhexidina bucofaríngea. Previa orointubación y anestesia general balanceada, se colocaron separadores tipo Minnesota en la mejilla para la exposición adecuada del sitio quirúrgico. Se utilizó lidocaína con epinefrina para anestesia y vasoconstricción local, con el fin de mejorar la hemostasia; se realizó bloqueo cigomático alto izquierdo, troncular mandibular izquierdo y ramo C2 izquierdo.

En todas las técnicas se utilizó lidocaína con epinefrina al 2% en cartucho dental. El bloqueo cigomático alto izquierdo se realizó con una jeringa para carpule dirigiéndose oblicuamente de delante atrás y de abajo arriba en el fondo de saco vestibular en la región del segundo molar superior y la tuberosidad maxilar izquierda. En cuanto a la troncular mandibular izquierda, se utilizó una aguja corta en la zona de la espina de Spix mandibular izquierda, en dirección oblicua anteroposterior. Por último, para la región maseterina y C2 se utilizó medio cartucho en presentación dental en la zona del fondo de saco vestibular hacia el ángulo mandibular izquierdo, y se depositó en el músculo masetero y la zona de ángulo mandibular homolateral.

A continuación se identificaron los límites anatómicos: papila del conducto de Stenon y línea alba de la mordida en el carrillo. Se realizó una incisión de 1 cm en el punto intermedio de estas dos estructuras utilizando una hoja de bisturí del n.º 15 (Fig. 3); para lograr una mejor visualización se amplió la incisión anteriormente hasta alcanzar los 4 cm de longitud, lo que permitió la visualización del espacio bucal y masticatorio. A continuación, se realizó disección roma hasta visualizar el músculo buccinador, para continuar con la disección a través de este, separando el tumor del espacio bucal, pterigoideo e infratemporal izquierdo (Fig. 4).

Se obtuvo un tumor lipomatoso completo (Fig. 5), dentro de su cápsula. Al final de la cirugía se optó por sutura con puntos simples con Vycril 3-0 desde planos profundos, dejando una única herida quirúrgica en la pared lateral izquierda del vestíbulo de la cavidad oral (Fig. 6).

Discusión

El espacio masticador es un área virtual que puede ser dividida en tres subsecciones: masetérica, pterigomandibular y temporal[17]. Dentro de este espacio se encuentran contenidos los músculos de la masticación, vasos sanguíneos y, de suma importancia, los ramos terminales del nervio facial cigomático y bucal[18].

Hay múltiples lesiones que pueden afectar este espacio, ya sea por contigüidad, originadas directamente en este sitio o incluso como metástasis de tumores

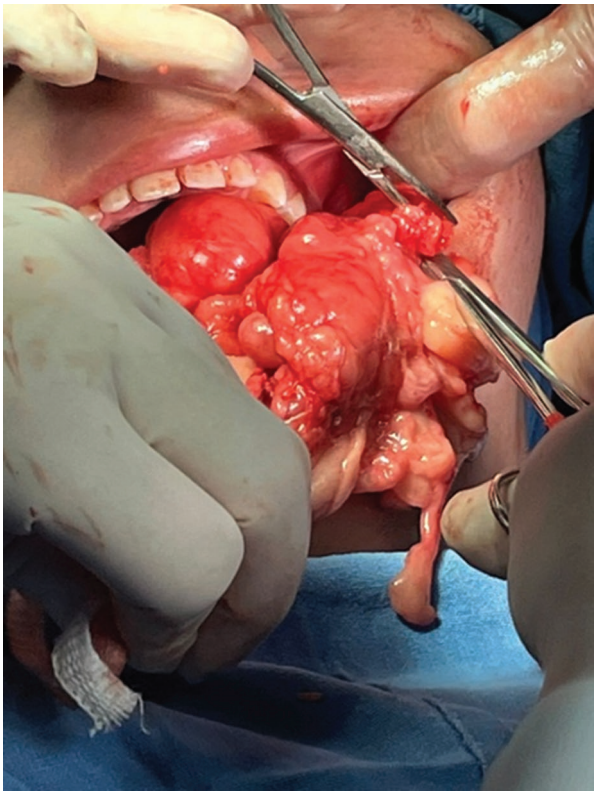

Figura 3. *Disección roma hasta llegar a visualizar el musculo buccinador para continuar la disección a través de él.*

Figura 5. *Sutura con puntos simples de Vycril 4-0.*

Figura 4. *Tumoración extraída por completo, con su cápsula intacta.*

malignos localizados en un lugar distante[19-21]. De los tumores lipomatosos en todo el cuerpo, cerca del 13% aparecen en la cabeza y el cuello, resultando los tumores benignos más comunes en esta zona[22]. No obstante, pueden estar tan adheridos a las estructuras adyacentes que incluso resulte necesaria la resección de parte de los músculos masticatorios para su completa extirpación[23].

Aquí proponemos un abordaje intraoral como una excelente opción, ya que provee resultados rápidos y eficientes, y es una opción segura para la escisión quirúrgica. Además, tiene buena funcionalidad y mejores resultados estéticos[24].

Cabe agregar que durante el transquirúrgico se debe identificar y delimitar adecuadamente el conducto de Stenon para facilitar su preservación funcional y minimizar el riesgo de desarrollar sialoceles o fístulas salivales como complicación. El primero es una pseudocápsula inflamatoria que contiene secreciones salivales dentro de los tejidos blandos de la mejilla, sin un drenaje adecuado[25]. Clínicamente se presenta como un aumento de volumen, doloroso, firme, pero no indurado, en la región parotídea, lo que es el resultado de la acción lítica de los componentes salivales que impiden la cicatrización. Es muy importante la vigilancia posquirúrgica para descartar esta complicación. Actualmente, las inyecciones de toxina botulínica se pueden realizar como tratamiento de

Figura 6. *Paciente en el posquirúrgico inmediato, con simetría facial.*

primera línea para estas complicaciones, o incluso un tratamiento conservador mediante vendajes compresivos y punción percutánea suele lograr una evolución favorable[26].

También se debe tomar en cuenta suturar adecuadamente los colgajos para evitar traumatismos, porque la masa de crecimiento lento crea un área más grande de mucosa que, si no se sujeta bien con la sutura, puede caerse y lesionarse al masticar[27].

Conclusiones

La principal limitación del abordaje intraoral es el reducido campo quirúrgico, así como la potencial contaminación por la microbiota intraoral, por lo que generalmente se suele preferir el abordaje extraoral[28] aunque existe mucho más riesgo de lesionar el nervio facial y deja una cicatriz visible.

Al poner en una balanza los riesgos y la seguridad de la cirugía junto a los términos estéticos, decidimos usar un abordaje intraoral. Al ampliar la incisión anteriormente y completar 4 cm de longitud se pudo ampliar la visualización del campo quirúrgico. La disección digital y roma con gasa nos ayudó a desprender el tumor logrando un campo quirúrgico limpio. Con esto se logró la resección completa de la tumoración, con su cápsula intacta (Fig. 6) y con óptimos resultados estéticos y ninguna complicación.

A pesar de que el abordaje extraoral es uno de los más utilizados para tumoraciones en el espacio masticador, si las características anatómicas permiten un abordaje intraoral es una excelente opción que siempre debe considerarse. Recomendamos este abordaje siempre y cuando se tenga experiencia y la certeza de que, a pesar del campo quirúrgico limitado, se podrá acceder adecuadamente a la zona donde se delimita el tumor.

Concluimos que en casos similares a este, refiriéndonos a un tumor bien delimitado y de fácil acceso, es mucho mejor el abordaje intraoral por tener mejores resultados estéticos, preservar la funcionalidad, la cicatrizacion de la herida es más rápida, eficiente y es una alternativa segura[29].

Agradecimientos

Los autores agradecen al servicio de otorrinolaringología del Hospital General Regional 46 del Instituto Mexicano del Seguro Social.

Financiamiento

Los autores declaran no haber recibido financiamiento para este estudio.

Conflicto de intereses

Los autores declaran no tener conflicto de intereses.

Responsabilidades éticas

Protección de personas y animales. Los autores declaran que para esta investigación no se han realizado experimentos en seres humanos ni en animales.

Confidencialidad de los datos. Los autores declaran que han seguido los protocolos de su centro de trabajo sobre la publicación de datos de pacientes.

Derecho a la privacidad y consentimiento informado. Los autores han obtenido el consentimiento informado de los pacientes y/o sujetos referidos en el artículo. Este documento obra en poder del autor de correspondencia.

Uso de inteligencia artificial para generar textos. Los autores declaran que no han utilizado ningún

tipo de inteligencia artificial generativa en la redacción de este manuscrito ni para la creación de figuras, gráficos, tablas o sus correspondientes pies o leyendas.

Bibliografía

1. Brito-Vera JP, Gómez-Barajas LD, Santana-Montes DR, Ramírez Oropeza F. Bichectomía: técnica del tridente, presentación de una nueva técnica quirúrgica. An Orl Mex. 2020;65:37-42.
2. Goldstein A. Overview of benign lesions of the skin. En: Lee S, editor. UpToDate: Waltham, Mass., 2022. Disponible en: https://www.uptodate.com.
3. Alharbi AS. Intraoral lipoma of the cheek — a case report with a one-year follow-up and review of literature. Cureus. 2020;12:e10537.
4. Studart-Soares EC, Costa FW, Sousa FB, Negreiros-Nunes Alves, AP, Lima-Verde Osterne R. Oral lipomas in a Brazilian population: a 10-year study and analysis of 450 cases reported in the literature. Med Oral Patol Oral Cir Bucal. 2010;15:e691-6.
5. Taira Y, Yasukawa K, Yamamori I, Iino M. Oral lipoma extending superiorly from mandibular gingivobuccal fold to gingiva: a case report and analysis of 207 patients with oral lipoma in Japan. Odontology. 2012;100:104-8.
6. Furlong MA, Fanburg-Smith JC, Childers EL. Lipoma of the oral and maxillofacial region: site and subclassification of 125 cases. Oral Surg Oral Med Oral Pathol Oral Radiol Endod. 2004;98:441-50.
7. Rahmani G, McCarthy P, Bergin D. The diagnostic accuracy of ultrasonography for soft tissue lipomas: a systematic review. Acta Radiol Open. 2017;6:2058460117716704.
8. Berenguer B, Lorca-García C, Lancharro A, De Tomás E. Pediatric tumors of the buccal fat pad: lipoma and hemangioma. Acta Chir Belg. 2019;120:341-3.
9. Chandawarkar RY, Rodríguez P, Roussalis J, Tantri MD. Minimal-scar segmental extraction of lipomas: study of 122 consecutive procedures. Dermatol Surg. 2005;31:59.
10. Wilhelmi BJ, Blackwell SJ, Mancoll JS, Phillips LG. Another indication for liposuction: small facial lipomas. Plast Reconstr Surg. 1999;103:1864.
11. Rotunda AM, Ablon G, Kolodney MS. Lipomas treated with subcutaneous deoxycholate injections. J Am Acad Dermatol. 2005;53:973.
12. Iwai T, Sugiyama S, Hirota M, Mitsudo K. Endoscopically assisted intraoral resection of lipoma in the masticator space. Ear Nose Throat J. 2022;101:33-5.
13. Ferbeyre-Binelfa L. Abordaje submaseterino ampliado para la resección de lipoma del espacio masticatorio: nota anatomoquirúrgica y reporte de un caso. Gac Mex Oncol. 2015;14:125-31.
14. Almeida-Parra F, Bueno -De Vicente A, Ranz-Colio A, Leyva-Moreno P, Núñez Paredes J, Picón Molina M, et al. Transmandibular approach in head and neck oncological surgery. Chin J Dent Res. 2020;23:257-64.
15. Lao WP, Han PS, Lee NH, Gilde JE, Inman JC. Transoral excision of parapharyngeal tumors. Ear Nose Throat J. 2021;100):NP454-8.
16. Noguchi T, Sugiura Y, Okada N, Tsuchiya Y, Hyasaka JI, Sasaguri KI, et al. A modified preauricular and transmandibular approach for surgical management of osteosarcoma of the mandibular condyle within the masticator space and infratemporal fossa: a case report. J Med Case Rep. 2019;13:58.
17. Chughtai S, Chughtai KA, Montoya S, Bhatt AA. Radiographic review of anatomy and pathology of the masticator space: what the emergency radiologist needs to know. Emerg Radiol. 2020;27:329-39.
18. Fernandes T, Lobo JC, Castro R, Oliveira MI, Som PM. Anatomy and pathology of the masticator space. Insights Imaging. 2013;4:605-16.
19. Baddour HM, Ochsner MC, Patel MR, Switchenko JM, Beitler JJ, Magliocca K, et al. Surgical resection is justifiable for oral T4b squamous cell cancers with masticator space invasion. Laryngoscope. 2021;131:E466-72.
20. Gordon JS, Mandel L. Masseteric intramuscular hemangioma: case report. J Oral Maxillofac Surg. 2014;72:2192-6.
21. Frade-Porto N, Delgado-Fernández J, García-Pallero MLA, Penanes-Cuesta JR, Pulido Rivas P, Gil Simoes R. Subcutaneous tissue metastasis from glioblastoma multiforme: a case report and review of the literature. Neucirugia (Astur: Engl Ed). 2019;30:149-54.
22. Morales-Cadena M, Acosta-Domínguez A, Hope-Guerreo JA. Lipoma del espacio parafaríngeo. An ORL Mex. 2007;52:3.
23. Tsumuraya G, Yamada H, Shimizu H, Hamada Y. Intramuscular lipoma in the masseter muscle: a case report. Br J Oral Maxillofac Surg. 2014;52:e21-3.
24. Coelho RCP, Oliveira EM, Silva GCC, Aguiar EG, Moreira AN, Souza LN. Intraoral excision of a huge cheek lipoma. J Craniofac Surg. 2018;29:e96-7.
25. Kalmar CL, Patel VA, Slonimsky G. Transoral floor of mouth lipoma resection: a technical multimedia analysis. Am J Otolaryngol. 2020;41:102572.
26. Aloua R, Slimani F. Salivary parotid cyst as an occurred complication of subangulomandibular approach of mandibular subcondylar fracture: a case report. Ann Med Surg (Lond). 2020;60:673-4.
27. De Sanctis CM. An unusual intraoral lipoma: a case report and literature review. Am J Case Rep. 2020;21:e923503-1-5.
28. Navaneetham A, Rao A, Gandhi A, Jeevan CA. Lipoma involving the masticator space. Ann Maxillofac Surg. 2011;1:93-4.
29. Tahim A, Ali S, Cheng L. An intra-oral approach to facial skin lumps — a move towards scarless surgery. Oral Maxillofac Surg. 2018;22:285-8.

Vaccination during the COVID-19 pandemic: correspondence

Vacunación durante la pandemia de COVID-19: correspondencia

Rujittika Mungmunpuntipantip[1] and Viroj Wiwanitkit[2]*

[1]Private Academic Consultant, Bangkok Thailand; [2]Department of Biological Science, Joseph Ayobabalola University, Ikeji-Arakeji, Nigeria

Dear Editor,

We would like to discuss the article entitled "Vacunación durante la pandemia de COVID-19: ¿cómo abordar la complejidad del fenómeno?[1]." Caycho-Rodriguez and others The social sciences play a crucial role in ensuring vaccination success and providing accurate information on benefits, hazards, and supply. To enhance vaccination rates, strategies such as aggressive communication, eradicating disinformation, and establishing independent authorities to monitor and report on the process have been proposed[1]. The main issue at hand right now is still how widely people are accepting the COVID-19 vaccine. Regarding vaccination acceptance, the global public health sector continues to encounter substantial obstacles. One study found a connection between vaccine fear and mistrust of the local health-care system[2]. People may turn to public health solutions more or less frequently during a crisis, depending on how much faith they have in their local public health administration. How confident the public is in their local public health response will determine how well public health initiatives perform during the crisis. The public's faith in their local public health crisis response will have a significant impact on how successfully public health programs work during the COVID-19 pandemic[3]. Public trust in authorities, professionals, and scientists must strengthen to boost immunization rates and win over doubters. Studies, for instance, have connected anti-vaccine sentiments to a lack of trust in the local health-care system. Public trust in authorities, professionals, and scientists must strengthen to boost immunization rates and win over doubters. For instance, studies have shown a connection between anti-vaccine beliefs and mistrust of the local health-care system[2,3]. How confident someone is in their ability to implement public health measures during a crisis will determine how prepared they are.

Editor, nos gustaría comentar un artículo titulado "Vacunación durante la pandemia de COVID-19: ¿cómo abordar la complejidad del fenómeno?[1]." Caycho-Rodrguez y otros El valor de las ciencias sociales como clave para el éxito de la vacunación, la información adecuada sobre las ventajas, los riesgos y el suministro de vacunas, la comunicación asertiva, la erradicación de la desinformación y el establecimiento de organismos independientes para monitorear e informar sobre el proceso de vacunación pública son solo algunos de los métodos sugeridos para aumentar las tasas de vacunación[1]. El principal problema en este momento sigue siendo qué tan ampliamente acepta la gente la vacuna contra el COVID-19. En cuanto a la aceptación de la vacunación, el sector de la salud pública mundial sigue encontrando obstáculos importantes. Un estudio encontró una conexión entre el miedo a las vacunas y la desconfianza en el sistema de salud local[2]. Las personas pueden recurrir a soluciones de salud pública con mayor o menor frecuencia durante una crisis, según la confianza que tengan en la administración local de salud pública. La confianza del público en su respuesta local de salud pública determinará el desempeño de las iniciativas de salud pública durante la crisis. La fe del público en su respuesta local a la crisis de salud pública tendrá un impacto significativo en el éxito del

***Correspondence:**
Rujittika Mungmunpuntipantip
E-mail: rujittika@gmail.com

Date of reception: 08-12-2022
Date of acceptance: 20-12-2022
DOI: 10.24875/CIRU.22000617

Cir Cir. 2024;92(5):689-690
Contents available at PubMed
www.cirugiaycirujanos.com

funcionamiento de los programas de salud pública durante la pandemia de COVID-19[3]. La confianza pública en las autoridades, los profesionales y los científicos debe fortalecerse para aumentar las tasas de inmunización y ganarse a los escépticos. Los estudios, por ejemplo, han relacionado los sentimientos contra las vacunas con la falta de confianza en el sistema de salud local. La confianza pública en las autoridades, los profesionales y los científicos debe fortalecerse para aumentar las tasas de inmunización y ganarse a los escépticos. Por ejemplo, los estudios han demostrado una conexión entre las creencias antivacunas y la desconfianza en el sistema de salud local[2,3]. La confianza de alguien en su capacidad para implementar medidas de salud pública durante una crisis determinará qué tan preparado está.

Funding

The authors declare that they have not received funding for this study.

Conflicts of interest

The authors declare that they have no conflicts of interest.

Ethical disclosures

Protection of humans and animals. The authors declare that no experiments on humans or animals have been performed for this research.

Confidentiality of data. The authors declare that no patient data appear in this article.

Right to privacy and informed consent. The authors declare that no patient data appear in this article.

References

1. Caycho-Rodríguez T, Gallegos M. Vacunación durante la pandemia de COVID-19: ¿cómo abordar la complejidad del fenómeno? Cir Cir. 2022;90:860-1.
2. Sookaromdee P, Wiwanitkit V. Factors influencing COVID-19 vaccine acceptance and hesitancy: correspondence. Hum Vaccin Immunother. 2022;18:2085471.
3. Mungmunpuntipantip R, Wiwanitkit V. COVID-19 vaccination hesitancy. Recenti Prog Med. 2021;112:596.

Subvariantes BQ.1.1 y XBB de ómicron: un problema global y estrategias de manejo

Omicron's BQ.1.1 and XBB sub-variants: a global problem and management strategies

*Sergio A. Ramírez-García[1], Diana García-Cruz[2] y Carlos E. Cabrera-Pivaral[3,4]**

[1]Facultad de Ciencias Químicas, Universidad Autónoma Benito Juárez de Oaxaca, Oaxaca, Oax.; [2]Departamento de Consulta Externa, Servicios Médicos Particulares de Genética Médica, A.C, Guadalajara, Jal.; [3]Departamento de Salud Pública, Centro Universitario de Ciencias de la Salud, Universidad de Guadalajara, Guadalajara, Jal.; [4]Dirección de Investigación, Centro Dermatológico Me Piel, Guadalajara, Jal. México

Señor editor:

Ante la declaración del Technical Advisory Group on SARS-CoV-2 Virus Evolution (TAG-VE) de la Organización Mundial de la Salud para el caso de todas las variantes «sopa» actuales, BQ.1.1 y XBB, sobre las implicaciones para la salud[1-3], los estudios publicados son limitados, pero destacan tres trabajos en los que se menciona que la variante BQ.1.1 es descendiente de la subvariante ómicron BA.5 y BQ.1. La BQ.1.1 tiene uno de los números más altos de mutaciones inmunoevasoras en regiones que codifican para sitios antigénicos clave de la proteína Spike, como son p.K444T, p.N460K y p.R346T. Esta cepa tiene una tasa global del 65% (GISAID)[1-3]. La subvariante XBB*, por otra parte, es una recombinación de los sublinajes BA.2.10.1 y BA.2.75, y tiene una prevalencia global del 1.3%. Se trata de una subvariante híbrida con siete mutaciones clave para evadir la inmunidad[1-3]. En clínica no reportan sus características distintivas.

Con estas consideraciones, y retomando la identificación clínica temprana para reducir la mortalidad, esta se puede realizar con una revisión de la cavidad oral, la cual ha permitido distinguir muchas de las variantes del SARS-CoV-2, incluso las subvariantes de ómicron, que cada una presentan diferencias[4]. Ante nuevas variantes que evaden el sistema inmunitario hay que reactivar la inmunidad entrenada, y para ello tenemos el inmunorregulador OM85, el cual favorece la fagocitosis y disminuye la expresión viral, y ha sido base del manejo de ómicron en la Sierra Sur de Oaxaca.[4] En el caso de la variante XBB, sugerimos el dobesilato de calcio, que bloquea la unión del heparán sulfato a ACE2, o la pirdenidona LP, que regula negativamente ACE2[5], lo que inhibe la entrada a la célula del SARS-CoV-2. Actualmente hay nuevos receptores virales que abordar, como GPR78, exotoxinas y las xilosil transferasas que por *docking* interactúan con el SARS-CoV-2[6]. El carboplatino y la gemcitabina son efectivos en tales situaciones. Lejos de ver un problema global de salud, es necesario retomar tratamientos novedosos, pero sobre basados en el diagnóstico temprano.

Financiamiento

Los autores declaran no haber recibido financiamiento para este estudio.

Conflicto de intereses

Los autores declaran no tener conflicto de intereses.

Responsabilidades éticas

Protección de personas y animales. Los autores declaran que para esta investigación no se han realizado experimentos en seres humanos ni en animales.

***Correspondencia:**
Carlos E. Cabrera-Pivaral
E-mail: carlos.pivaral@academicos.udg.mx.

Fecha de recepción: 21-11-2022
Fecha de aceptación: 20-12-2022
DOI: 10.24875/CIRU.22000591

Cir Cir. 2024;92(5):691-692
Contents available at PubMed
www.cirugiaycirujanos.com

Confidencialidad de los datos. Los autores declaran que en este artículo no aparecen datos de pacientes. Además, los autores han reconocido y seguido las recomendaciones según las guías SAGER dependiendo del tipo y naturaleza del estudio.

Derecho a la privacidad y consentimiento informado. Los autores declaran que en este artículo no aparecen datos de pacientes.

Uso de inteligencia artificial para generar textos. Los autores declaran que no han utilizado ningún tipo de inteligencia artificial generativa en la redacción de este manuscrito ni para la creación de figuras, gráficos, tablas o sus correspondientes pies o leyendas.

Bibliografía

1. World Health Organization. TAG-VE statement on Omicron sublineages BQ.1.1 and XBB. (Consultado el 20-11-2022.) Disponible en: https://www.who.int/news/item/27-10-2022-tag-ve-statement-on-omicron-sublineages-bq.1-and-xbb.
2. Wong C. Subvariant 'soup' may drive wave. New Sci. 2022;256:11.
3. Callaway E. COVID 'variant soup' is making winter surges hard to predict. Nature. 2022;611:213-4.
4. Domínguez-Rodas J, López de la Mora DA, Dávalos NO, Ramírez-García SA, Rincón AR, Guzmán LR, et al. Detección clínica y descripción de las características socio-demográficas de la variante SARS-COV-2 omicron en población de la sierra sur de Oaxaca. Cir Cir 2022;90:567-472.
5. Seifirad S. Pirfenidone: a novel hypothetical treatment for COVID-19. Med Hypotheses. 2020;144:110005.
6. Achom A, Das R, Pakray P. An improved Fuzzy based GWO algorithm for predicting the potential host receptor of COVID-19 infection. Comput Biol Med. 2022;151:106050.

CARTA AL EDITOR

Estrategias de manejo en la triplidemia por virus respiratorios y la importancia social del algoritmo de diagnóstico clínico-genético de SARS-COV2

Management guidelines in triplidemia due to respiratory viruses and the social importance of the clinical-genetic diagnosis algorithm of SARS-COV2

Sergio A. Ramírez-García[1], Carlos E. Cabrera-Pivaral[2], José Domínguez-Rodas[3], David A. López-de la Mora[4], Sabina López-Toledo[1], Felicitas Ortiz-García[1], Reyna M. Hernández-Vásquez[1] y Diego A. Cáceres-Gutiérrez[4]*

[1]Instituto de Nutrición y Estudios Municipales, Universidad de la Sierra Sur, Miahuatlán de Porfirio Díaz, Oaxaca, Oax.; [2]Departamento de Salud Pública, Centro Universitario de Ciencias de la Salud, Universidad de Guadalajara, Guadalajara, Jal.; [3]Unidad de Investigación de Medicina Traslacional y Medicina de Precisión, Servicios Médicos Profesionales, Particulares, A.C., Miahuatlán de Porfirio Díaz, Oaxaca, Oax.; [4]Departamento de Ciencias Biomédicas, Centro Universitario Tonalá, Universidad de Guadalajara, Guadalajara, Jal. México

Señor Editor:

Retomamos el artículo de Ramírez-García[1] publicado recientemente, el cual nos muestra cómo detectar los diferentes tipos de variantes de SARS-CoV-2 sin realizar estudio molecular (Tabla 1) mediante la exploración de la cavidad oral. Desde un punto de vista social esto es muy importante porque permite abordar más rápido un problema de salud global como es la triplidemia por infección simultánea por SARS-CoV-2 ómicron variante BQ.1.1, virus de la influenza H2N3 y virus sinscitial respiratorio (VSR), facilitando el diagnóstico diferencial y el inicio de tratamiento temprano, lo cual puede reducir la mortalidad. En este sentido, un blanco es fortalecer la inmunidad entrenada, por lo cual se puede retomar el uso de OM-85 que favorece la producción de alfa defensinas que opsonizan a los patógenos respiratorios como el SARS-CoV-2, el VSR y el virus influenza, entre otros[2], además de que tiene un efecto antiviral contra el SARS-CoV-2 para reducir los RNA de los marcos de lectura y de otros genes. Otros adyuvantes que valdría la pena retomar en la triplidemia son la pirfenidona de liberación prolongada, el Vita Deyun® y la S-adenosil-metionina[3,4], por ser antiinflamatorios, antioxidantes y con actividad antiviral para COVID-19, ya que al silenciar la expresión de ACE2 evitan el ingreso del SARS-CoV-2 y simultáneamente bloquean la tormenta de citocinas. En el caso de la S-adenosil-metionina, parece tener su efecto en el control del estrés oxidativo mitocondrial durante una infección de vías respiratorias, particularmente en el acúmulo de ADN mitocondrial circulante mutado, que recientemente se ha reportado en la COVID-19[5]. Por último, habría que retomar el uso del dobesilato de calcio, el cual bloquea la unión sistema APOE-heparán sulfato a ACE2, bloqueando la entrada del SARS-CoV-2, muy útil sobre todo en las variantes de ómicron, que ha mostrado una gran variabilidad genética en la proteína *spike*. En el abordaje de la triplidemia en el ámbito hospitalario privado y público se debe identificar clínicamente la variante de COVID-19 e iniciar tratamiento específico en los primeros 2 a 4 días, para reducir la mortalidad y morbilidad, a la par con antivirales específicos para influenza y VSR. De esta manera, se propone considerar como alternativas los inhibidores de la fusión viral a la membrana, como

***Correspondencia:**
Carlos E. Cabrera-Pivaral
E-mail: carlos.pivaral@academicos.udg.mx

Fecha de recepción: 18-11-2022
Fecha de aceptación: 04-12-2022
DOI: 10.24875/CIRU.22000584

Cir Cir. 2024;92(5):693-695
Contents available at PubMed
www.cirugiaycirujanos.com

Tabla 1. Algoritmo clínico-genético para la identificación de las variantes de SARS-CoV-2

Linaje o variante genética de SARS-CoV-2	Características de la cavidad oral	Motivo de consulta
Ómicron (linajes BQ.1.1), conocida como «perro del infierno»	Enantema palatofaríngeo difuso con petequias, telangiectasias, con incremento de vasos sanguíneos en el paladar, paladar posterior exudativo y anterior violáceo	Exantema macular y papular en la región del tórax, espalda y zona plantar
Ómicron (linaje BA2.75, p.G446S y p.R493Q en el gen para la proteína ***spike***), conocida como «centauros»	Paladar eritematoso, con hiperproliferación de vasos sanguíneos	Neuropatía periférica con cuadro respiratorio moderado
Ómicron (linajes BA.5, BA.4, BA.1)	Vasculitis del paladar con efélides, enantema serpentiforme en el paladar posterior	Neuropatía periférica proximal y distal
Linajes delta AY.4/ómicron BA.1 (deltacrom)	Enantema vesicular palatofaríngeo en patrón de racimos, con hiperproliferación de vasos y microefélides, paladar con coloración salmón	Neuropatía, insuficiencia venosa, telangiectasias oculares y en piel
Ómicron (linajes BA.2.12 y BA.2.9	Paladar con orofaringe exudativa ulcerativa y presencia de petequias	Macroangiopatía
Ómicron (linajes BA.2 y BA.2.12.1)	Petequias en la orofaringe acompañadas de enantema vesicular difuso en el arco faríngeo y la base de la lengua	Cuadro gripal leve
Ómicron (linajes BA.2, BA.3, BA.4 y BA.5)	Paladar posterior violáceo, enantema vesicular palatofaríngeo difuso, hiperproliferación de vasos sanguíneos	Neuropatía periférica
Ómicron (linajes B.1.1.529)	Telangiectasia única y vasculitis en forma de microefélides, paladar anterior con coloración salmón o rosa pálido	Neuropatía periférica
Ómicron (linajes B.1.1.529)	Telangiectasia única y vasculitis en forma de microefélides, paladar anterior con coloración salmón o rosa pálido	Neuropatía periférica
Ómicron (linajes B.1.1.529)	Telangiectasia única y vasculitis en forma de microefélides, paladar anterior con coloración salmón o rosa pálido	Neuropatía periférica
Ómicron (linajes BA.1, BA.1.1)	Hiperproliferación de vasos sanguíneos, microefélides, paladar color salmón o rosa pálido	Neuropatía periférica y diarrea
Linajes alfa Q Beta linaje B1.1351 Gamma (linajes P. 1) Épsilon (B.1.43 y B.1.43)	Enantema vesicular palatofaríngeo, mucosa del paladar posterior color salmón o amarillo, hipertrofia de los corpúsculos gustativos	Cuadro respiratorio grave
Alfa, linaje B.1.1.7, clado GR	Mucosa palatina de color salmón o amarillo, sin enantemas	Cuadro respiratorio grave
Delta (linaje B1.617.2)	Enantema vesicular palatofaríngeo en patrón racemoso y difuso, hematomas palatinos	Epistaxis espontánea
Delta (linajes AY)	Enantema palatofaríngeo en patrón racemoso y/o difuso, orofaringe exudativa y con grietas	Epistaxis espontánea
Mu (B.1.621, B.1.621.1)	Faringe posterior con enantema vesicular herpetiforme con hematomas palatofaríngeos	Cuadro respiratorio moderado
COVID-19 prolongada, COVID-19 subaguda	Fibrosis central palatina, paladar anterior y posterior color rosa pálido, violeta claro o salmón	Neuropatía periférica, miopatía

OM-85, dobesilato de calcio, pirfenidona de liberación prolongada y Vita Deyun®, así como antagonistas de los radicales libres como la S-adenosil-metionina. En el medio clínico privado en México hay medicamentos con los que afrontar la triplidemia, por lo que se propone que debe ser acuñado como política pública.

Agradecimientos

Los autores agradecen al CB-Xpert Laboratorio de Patología Clínica, Miahuatlán de Porfirio Díaz, Oaxaca.

Financiamiento

Los autores declaran no haber recibido financiamiento.

Conflicto de intereses

Los autores declaran no tener ningún conflicto de intereses.

Responsabilidades éticas

Protección de personas y animales. Los autores declaran que los procedimientos seguidos se conformaron a las normas éticas del comité de experimentación humana responsable y de acuerdo con la Asociación Médica Mundial y la Declaración de Helsinki.

Confidencialidad de los datos. Los autores declaran que han seguido los protocolos de su centro de trabajo sobre la publicación de datos de pacientes.

Derecho a la privacidad y consentimiento informado. Los autores han obtenido el consentimiento informado de los pacientes y/o sujetos referidos en el artículo. Este documento obra en poder del autor de correspondencia.

Uso de inteligencia artificial para generar textos. Los autores declaran que no han utilizado ningún tipo de inteligencia artificial generativa en la redacción de este manuscrito ni para la creación de figuras, gráficos, tablas o sus correspondientes pies o leyendas.

Bibliografía

1. Ramírez-García SA. Palato-pharyngeal enanthem in the genetic variants of the COVID-19 and its sensitivity. Cir Cir. 2022;90:429-30.
2. Domínguez-Rodas J, Ramírez-García SA, Rincón-Sánchez AR, Dávalos-Rodríguez NO, Juárez-Pérez MH, Cabrera-Pivaral CE. COVID-19 pandemic experience of the management of outpatient rural population from the Sierra Sur de Oaxaca, Mexico. Cir Cir. 2022;90:133-4.
3. Cabrera Pivaral CE, Rincón Sánchez AR, Dávalos Rodríguez NO, Ramírez García SA. Parsonage Turner syndrome associated with COVID-19: about two family cases. Neurologia. 2022 Feb 3. Online ahead of print.
4. Aguilar-Lemarroy A, López-Uribe A, Sánchez-Corona J, Jave-Suárez LF. Severe acute respiratory syndrome coronavirus 2 ORF3a induces the expression of ACE2 in oral and pulmonary epithelial cells and the food supplement Vita Deyun® diminishes this effect. Exp Ther Med. 2021;21:485.
5. Scozzi D, Cano M, Ma L, Zhou D, Zhu JH, O'Halloran JA, et al. Circulating mitochondrial DNA is an early indicator of severe illness and mortality from COVID-19. JCI Insight. 2021;6:e143299.